Entropy Generation Minimization for Enhancing the Fluid Recovery and Energy Efficiency in Petroleum Reservoirs

by

© Murtada A. Elhaj

A Thesis submitted to the School of Graduate Studies

in partial fulfillment of the requirement for the degree of

Doctor of Philosophy

Faculty of Engineering and Applied Science

Memorial University of Newfoundland

May 2021

St. John's, Newfoundland and Labrador

Canada

Abstract

Hydrocarbon reservoir fluids usually contain a significant amount of mechanical energy that depends on the distribution of temperature and pressure throughout the reservoir. A fraction of the fluid's useful energy is lost during the irreversible processes that occur throughout the production life of the reservoir. Entropy generation (or production) can characterize this loss of useful energy in petroleum reservoirs.

A petroleum engineer can develop an appropriate production strategy that minimizes entropy production in a reservoir to promote the efficient use of the reservoir energy. The design of a poor reservoir production system might result in a short-lived production well, low reservoir recovery factor, and inefficient use of available resources. Such an issue would not only result in the loss of a valuable portion of the reservoir's useful energy but also financial benefits.

Various forms of energy exchange occur during hydrocarbon production in reservoirs, e.g., fluid and rock expansion, fluid flow, gravity drainage, and compaction of poorly consolidated rocks. During a reservoir's production lifetime, irreversible processes (e.g., fluid friction and heat transfer) lead to waste of energy, reducing the overall system's operational efficiency. Therefore, there is a desire to select an appropriate design that minimizes the entropy generation. In this thesis, we investigate the effect of essential factors such as reservoir formation, reservoir fluids, and production rate on entropy generation. The ultimate goal is to design a reservoir production strategy using the entropy generation analysis such that the production efficiency can be maximized.

To simulate the fluid flow behavior of a reservoir system, a pseudo-steady flow state is developed in this thesis for single-phase (dry gas) and two-phase (oil-water) flow models in both the wellbore and reservoir. The effect of the wellbore conditions on the single-phase models is investigated and analyzed. One-dimensional flow is assumed in the wellbore, whereas radial flow occurs in the reservoir. Mass, momentum, energy, and entropy balance equations, including a method of Entropy Generation Minimization (EGM), are used to address the fluid flow behavior and energy loss in wellbore and reservoir systems. For a single-phase flow, the near-wellbore region is investigated and considered to be a separate zone for model development, which allows flexibility in modelling skin effects near the wellbore.

Numerical methods are used to solve the fluid flow and entropy equations. The models are solved by a numerical scheme programmed in the MATLAB environment with an appropriate algorithm. For validation purposes, a commercial simulator, Computer Modeling Group (CMG), is used to verify the predicted results.

A new production performance criterion called the Coefficient Of Performance (COP) is introduced. The COP integrates the recovery factor with entropy generation and provides a quantitative measure to optimize reservoir production. The models are used to conduct a parametric sensitivity analysis that includes the effects of fluid and rock parameters, such as permeability, porosity, viscosity, skin factor, Bottom Hole Pressure (BHP), wettability, and temperature on the total entropy production. The COP is used to optimize the operating conditions of the reservoir, such as the production rates and BHP. It is found that permeability and BHP have the most impact on the total entropy production for single-

phase models. Concurrently, temperature and wettability are essential factors for two-phase flow models.

This thesis enhances the understanding of reservoir energy analysis and provides more accurate models for calculating the optimum production rate of a given reservoir. In particular, the results presented in this thesis will impact production history calculations and reservoir simulation results. Furthermore, this research provides practitioners and engineers in the petroleum industry with a useful alternative approach for maximizing recovery efficiency by minimizing entropy generation.

Dedication

To my father, Abdein A. Elhaj, who always encouraged me to get the highest education and be a man. He never saw this adventure. I deeply missed you.

To my mother, Shadia M. Saeed. Without your support and endless love, this work would never see the light. To all my siblings, I love you to the moon and back.

To my beloved wife, Tasnim, my daughter, Shahd, and sons, Hammam and Eyad, without whom this dissertation would have been completed in less than three years.

To every teacher who taught me during my academic life. To all my friends who gave me the strength to overcome my challenges.

Acknowledgments

I would like to acknowledge and thank the following special people sincerely without whom this study would never be achieved.

To my former supervisor, Dr. Enamul Hossain, who believed in me when others did not and gave me the opportunity to study at Memorial University and for his guidance and mentorship. To my co-supervisors, Dr. Greg F. Naterer, Dr. Syed A. Imtiaz, and Dr. Sohrab Zendehboudi, I cannot find words that express my sincere gratitude for the spectacular insights and vision that kept me going throughout this study. I am greatly indebted to them for providing positive input and encouragement towards my research. I gratefully acknowledge and appreciate their technical expertise, critical thinking, and valuable comments on research, publications, and dissertation.

To my beloved wife, none of this work would be possible without your patience. To my mother, who never stopped supporting me in my entire life and has been a constant source of love, concern, strength, and support.

The financial assistance offered by Equinor (formerly Statoil) Canada, Memorial University (NL, Canada), Natural Sciences and Engineering Research Council of Canada (NSERC), and InnovateNL (formerly RDC) is greatly acknowledged.

Last but not least, I thank my Lord, who provided for me full and limitless support and assistance.

Table of Contents

List of Tables

List of Figures

Nomenclature

Acronyms

BHP	Bottom Hole Pressure	(Pa)
CMG	Computer Modelling Group	
COP	Coefficient of Performance	
FV	Future Value	(USD)
RF	Recovery Factor	
NPV	Net Present Value	(USD)
PVT	Pressure-Volume-Temperature	

Variables

B	Formation Volume Factor	$\left(\frac{m^3}{m^3}\right)$
C	Integration Constant	
C_T	Total Effective Compressibility	(Pa^{-1})
D	Wellbore Diameter	(m)
E_{vp}	Rate of Dissipation in Porous Media	$(\frac{J}{m^3\ s})$
F^{Dr}	Interpolating Functions for Drainage Capillary Pressure	
F^{Im}	Interpolating Functions for Imbibition Capillary Pressure	
F^*	Interpolating Functions for Scanning Curves Capillary Pressure	
f_M	Moody Friction Factor	
f_p	Porous Media Friction Factor	
G_i	Initial Gas In Place	(m^3)
H	Well Depth	(m)
h	Formation Thickness	(m)

k	Absolute Permeability	(m^2)
k_o	Oil Effective Permeability	(m^2)
k_w	Water Effective Permeability	(m^2)
k_{ro}	Oil Relative Permeability	
k_{rw}	Water Relative Permeability	
L	Well Length	(m)
n	Number of Years	
P	Pressure	(Pa)
P_i	Initial Pressure	(Pa)
P_f	Final Pressure	(Pa)
$\overline{P}$	Average Pressure	(Pa)
$\overline{P}_{fd}$	Final Average Pressure in Damaged Region	(Pa)
$\overline{P}_{id}$	Initial Average Pressure in Damaged Region	(Pa)
$\overline{P}_{fu}$	Final Average Pressure in Undamaged Region	(Pa)
$\overline{P}_{iu}$	Initial Average Pressure in Undamaged Region	(Pa)
P_c	Capillary Pressure	(Pa)
p_d	Displacement (Entry) Pressure	(Pa)
P_w	Wetting Pressure	(Pa)
P_{nw}	Non-Wetting Pressure	(Pa)
P_{neg}	Maximum Negative Capillary Pressure	(Pa)
P_c^{Dr}	Drainage Capillary Pressure	(Pa)
P_c^{Im}	Imbibition Capillary Pressure (Bounding	(Pa)
P_c^{DI}	Capillary Pressure at Reversal from Main Drainage	(Pa)
q	Flow Rate	$(\frac{m^3}{s})$
q_o	Oil Flow Rate	$(\frac{m^3}{s})$

q_w	Water Flow Rate	$(\frac{m^3}{s})$
Q	Flow Rate (Field Conditions)	$(\frac{MMbbl}{year})$
r	Radius	(m)
r_w	Wellbore Radius	(m)
r_e	Reservoir Radius	(m)
$\dot{S}$	Entropy Production Rate	$\left(\frac{J}{Km^3s}\right)$
S_T	Total Entropy Production	$\left(\frac{J}{K}\right)$
s_{wc}	Connate Water Saturation	
s_{or}	Residual Oil Saturation	
s_{wi}	Initial Water Saturation	
s_{oi}	Initial oil Saturation	
s_e	Effective Saturation	
s	Skin Factor	
S_w^*	Saturation (Wetting) At Which a Reversal in The Direction of Saturation Change	
S_{gr}^{max}	Maximum Residual Gas Saturation	
$\overline{S_w}^I$	Effective Water Saturation	
$\overline{S_w}^{ID}$	Apparent Water Saturation at The Most Recent Reversal from Drainage to Imbibition	
$\overline{\overline{S^D}}_w$	Apparent Water Saturation Under Drainage Conditions	
$\overline{\overline{S^I}}_w$	Apparent Water Saturation Under Imbibition Conditions	
S_w^{Hys}	Wetting-Phase Saturation Used for The Generation of Scanning Curves	
S_w^{Max}	Maximum Possible Wetting Saturation	
S_{g1}	Initial Gas Saturation	
S_{g2}	Final Gas Saturation	

S_{IF}	Liquid-Solid Interfacial Areas of Contact Along with the Liquid-Solid Interfaces	
S_{SI}	Solid-Liquid Interfacial Areas of Contact Along with the Solid-Liquid Interfaces	
T	Temperature	(K)
t	Time	(sec)
t_f	Final Time	(s)
t_i	Initial Time	(s)
u	Volumetric Flux	$(m^3/(m^2/s))$
V	Volume	(m^3)
V_b	Bulk Volume	(m^3)
V_p	Pore Volume	(m^3)
v	Velocity	(m/s)
w	Work	(J)

Greek letters

β	Non-Darcy Coefficient	
μ	Viscosity	$(Pa.s)$
ρ	Density	$\left(\frac{Kg}{m^3}\right)$
ϕ	Porosity	
ℓ	Length	(m)
θ_{hys}	Contact Angle Hysteresis	
ϵ	Curvature Parameter for Capillary-Pressure Scanning Curves	
α	Curve Shape Parameter	
λ	Exponent for Analytical Imbibition Nonwetting Phase Relative Permeabilities	
G	Surfaces Free Energy	

n	Curve Shape Parameter
m	Curve Shape Parameter
τ	Non-Equilibrium Coefficient

Subscripts

i	Interest Rate
θ	Inclination Angle

Chapter 1: Introduction

At present, the known world oil reserves are estimated to be at least 1,672 billion barrels, and Canada possesses 10% of these total worldwide oil reserves. Along with a production capacity of 4.6 million barrels of oil per day, these vast reserves place Canada as a primary petroleum supplier both now and into the foreseeable future (Natural Resources Canada, 2019). A majority (almost 97%) of Canadian oil production occurs in three provinces: Alberta (81.8%), Saskatchewan (10.8%), and Newfoundland and Labrador (5.1%) (Natural Resources Canada, 2019). With such a high percentage of the reserves and hydrocarbon production, accurate and advanced technologies that boost the recovery factor and efficiency of recovering the primary reservoir energy are desirable.

1.1. Overview

The use of thermodynamics principles in the petroleum industry has been widely pursued in recent decades. Since thermodynamics is the study of energy conservation (Sangi and Müller, 2019), the first and second laws of thermodynamics can be used to investigate the primary hydrocarbon reservoir energy and entropy processes. In general, entropy is a measure of the molecular configuration probability of a system, or the ability of a system to perform useful work (Bennett, 1982; Naterer and Camberos, 2008).

Various forms of energy exchange occur during hydrocarbon transport in reservoirs (e.g., fluid and rock expansion, fluid flow, gravity drainage, and compaction of poorly consolidated rocks). During the production lifetime, irreversible processes such as fluid friction and heat transfer reduce the overall system's operational efficiency. This thesis

focuses on the energy that exists in the hydrocarbon reservoir, and the energy that results from fluid expansion in particular. From a hydrocarbon production point of view, the primary reservoir energy plays a vital role in fluid production (Sarathi and Tiab, 1981). Production rate, reservoir pressure, and skin factor have been recognized to strongly influence the reservoir energy and consequently the production of reservoir fluids (Civan and Tiab, 1989; M. Elhaj et al., 2020; Tiab et al., 1980). This thesis investigates these factors, along with other reservoir and operating characteristics.

Because of the increasing value and discovery of petroleum and the growing challenges of climate change, better production strategies with improved efficiency are needed. A significant shift in the views on reservoir energy lost during production processes has taken place in recent years (Bejan, 1996; Bidi et al., 2010; Mohsen Torabi et al., 2017a). Petroleum engineers and researchers can develop an appropriate production strategy that minimizes entropy production in a reservoir to promote more efficient use of natural reservoir energy. A poor design of a reservoir production system might result in a short-lived production well and a low reservoir recovery factor. Such an issue would not only result in the loss of a valuable portion of a reservoir's useful energy but also financial investment loss.

The friction that occurs due to fluid motion within a reservoir and from the movement of the fluid relative to the interior of the pipe wall as well as due to energy exchange between the reservoir and environment are causes of reservoir useful energy loss. To decrease this lost reservoir energy, essential production-related factors, including reservoir formation, reservoir fluids, and production rate, are needed for more effective design and maintenance.

Thus, it will be useful to use Entropy Generation Minimization (EGM) and the associated properties of the second law of thermodynamics for the fluid and reservoir.

The development of mathematical models to establish these correlations is one of the objectives of this study. The mathematical models are developed for three regions: (i) the reservoir, (ii) wellbore, and (iii) near-wellbore zones. Various laws and equations (e.g., continuity equation, energy equation, and the first and second thermodynamics laws) are used to develop the mathematical models. In this study, EGM is used as a design tool (or controlling parameter) to optimize the operating parameters and enhance the recovery factor while concurrently consuming the least amount of available energy.

1.2. Hydrocarbon Production and Recovery

This section provides a brief overview of the methodologies employed by production and reservoir engineers in hydrocarbon reservoirs. It also attempts to shed light on the value of the current research in the economy of Newfoundland and Labrador and Canada in general.

Crude oil, natural gas, and water are the substances of main utility to petroleum engineering. These substances are sometimes found at lower temperatures and pressures, like paraffin, gas-hydrates, ice, or high pour-point crudes. At the reservoir and wellbore, these substances occur mainly as fluids, either in the vapor (gaseous) or in the liquid phase, or both. In many cases, the state or phase in the reservoir is totally unrelated to the fluid state at the surface.

As early as 1928, petroleum engineers were giving serious consideration to gas-energy relationship and recognized the need for more precise information concerning physical

conditions in wells and porous media. It was acknowledged earlier that for an accurate estimation for original and gas in place, the change of physical properties of reservoir's samples with pressure would be required (Schilthuis, 1936). Coleman et al. (1930) presented an equation described the relationship between the reservoir pressure, quantity of oil and gas produced, and reservoir fluid properties. This equations and other reservoir mathematical modelling and simulation that defined this relationship were reviewed by Craft and Hawkins (1991). With the development of these techniques, equations, and concepts, unseen actions down in the reservoir became possible to predict and recognize. Reservoir and production engineering became a powerful and well-defined branch of petroleum engineering.

There is a minor difference between a field located beneath land or water in the basic physics and mathematics that describe the phenomena. The primary difference in field development is in decision making. The other difference is that on offshore fields, there are usually two distinct phases: appraisal, under static conditions, followed by dynamic developments. For onshore fields, there is usually no distinction between these two phases; they intend to be one, which is a dynamic development.

In general, a reservoir is defined as an accumulation of hydrocarbon in porous and permeable sedimentary rocks. The accumulation, which has reached a fluid pressure equilibrium throughout its pore volume at the time of discovery, is also sometimes known as a pool. A hydrocarbon field may comprise several reservoirs at different stratigraphic horizons or in different pressure regimes. In terms of a well, there are three main types of conventional wells. The most common well is an oil well with its associated gas. Natural

gas wells are wells drilled specifically for natural gas and contain little or no oil. Condensate wells are wells that contain natural gas, as well as a liquid condensate.

For a petroleum reservoir to exist, there are three main requirements: source rock, reservoir rock, and hydrocarbon trap. The difference between the source and reservoir rock is that the source rock is where the organic material was deposited. On the other hand, the reservoir rock is the rock in which the hydrocarbon can be stored and from which it can be produced.

The initial production of hydrocarbons from an underground reservoir is accomplished using the natural reservoir energy, known as primary recovery. Once the hydrocarbon reaches the wellbore, it is transferred through pipes to surface production facilities. For large fields, the production facilities contain wellhead, manifold/gathering, separation, gas composition, and storage and export facilities. For the small reservoirs, oil is collected in a holding tank and collected at regular intervals by a tanker truck or railcar to be processed at a refinery. **Figure 1.1** gives a simplified schematic of the typical hydrocarbon production process.

The main task of production facilities is to separate the product from the well to the users and dispose of the rest in an environmentally friendly manner. Once the hydrocarbon arrives at the wellhead, the fluid enters separation, where oil, gas, and water are separated. After free water is removed from the fluid by the water treatment facility, it will go to the disposal unit/section. Gas is delivered to users directly after compression, while the oil will be directed to a refinery for more processing and refinement.

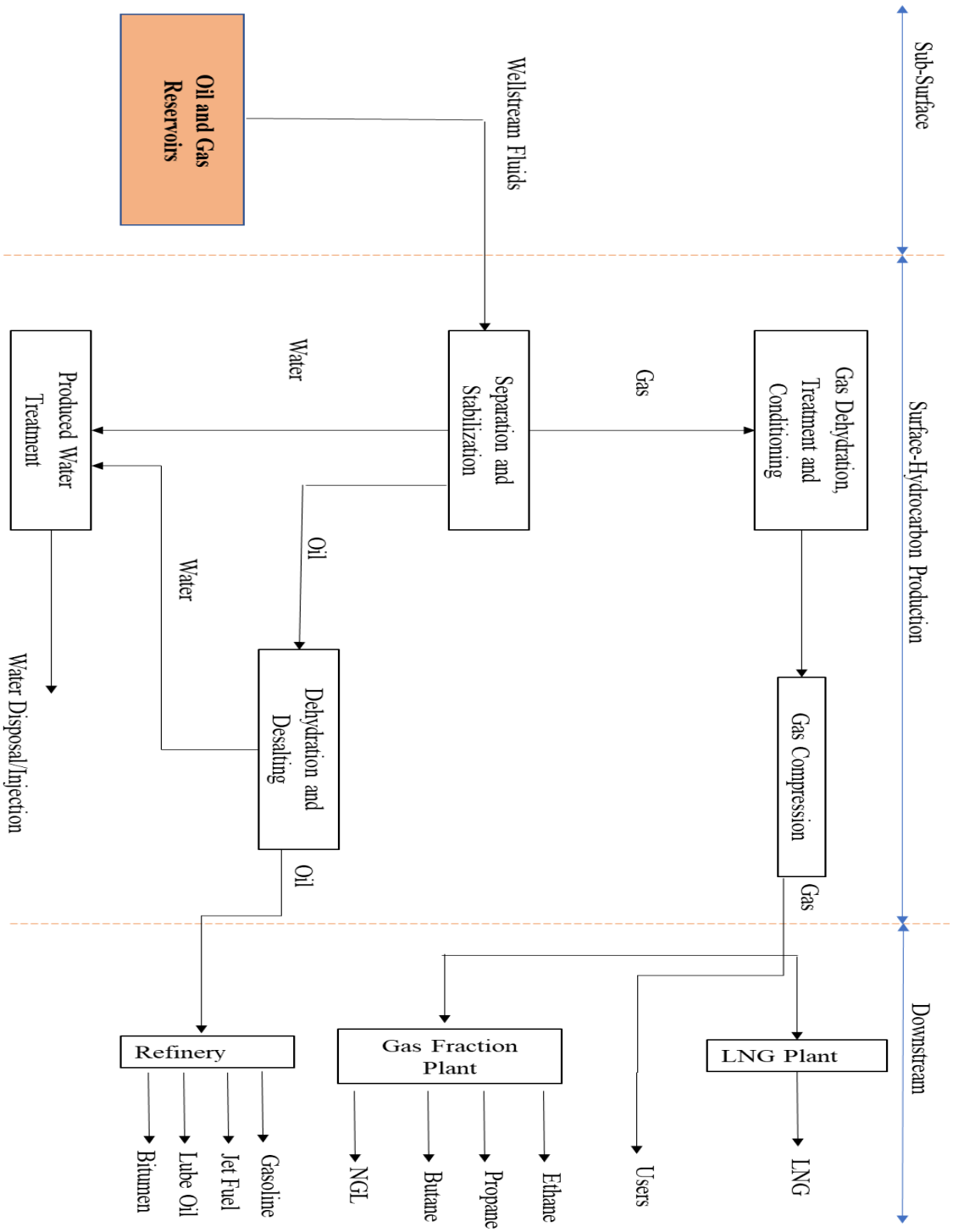

Figure 1. 1. Schematic of hydrocarbon production process

There are three phases of hydrocarbon recovery techniques: primary, secondary, and tertiary. Primary recovery is oil recovery by natural drive mechanisms: solution gas, water influx, gas cap drives, or gravity drainage. The secondary phase comes after initial recovery, and it refers to water or gas injection to increase the reservoir pressure. Tertiary refers to any techniques that are applied after the secondary recovery. **Figure 1.2** illustrates hydrocarbon recovery strategies. This thesis will focus on the primary recovery strategy because it deals directly with the natural reservoir energy, as well as at initial condition. The reservoir pressure is considerably higher than the bottomhole pressure inside the wellbore.

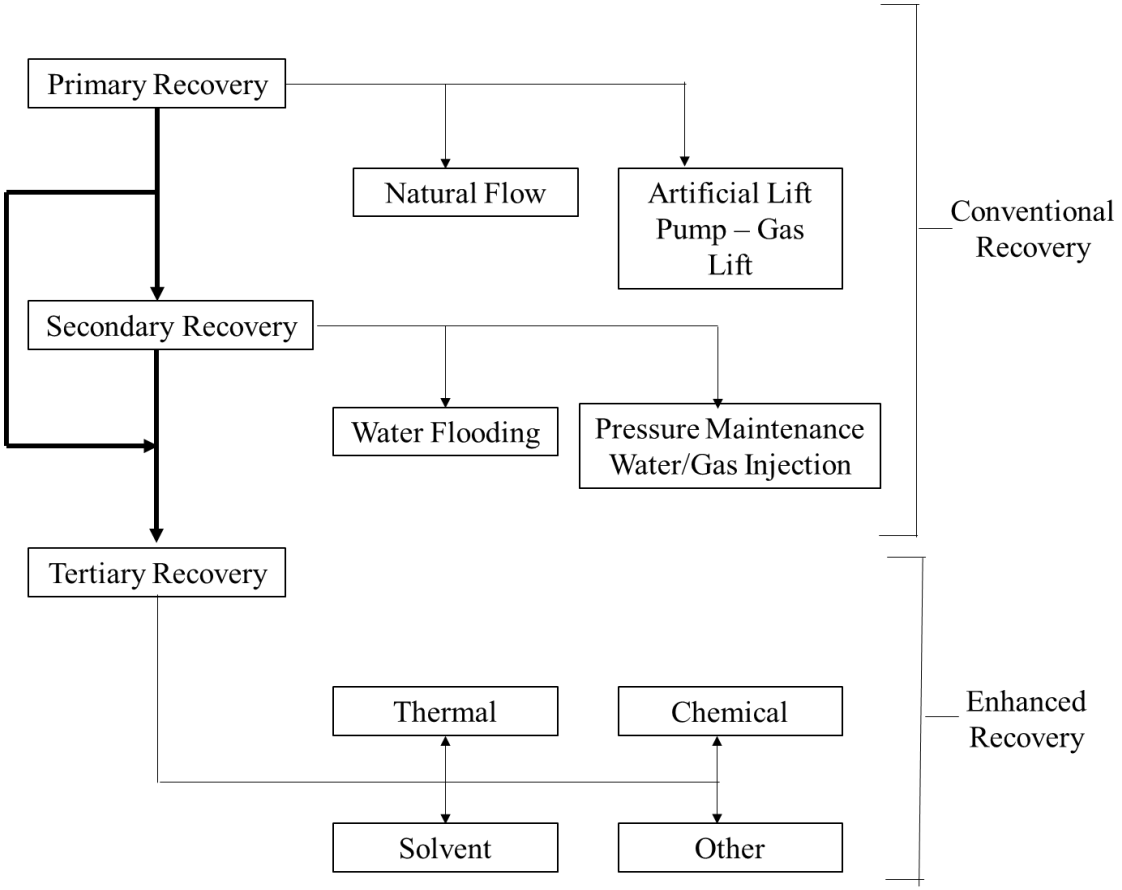

Figure 1. 2. Hydrocarbon recovery classifications

Canada has abundant energy resources and the country is one of the largest and most diverse suppliers of energy in the world. As a country, Canada is ranked third globally in terms of energy resources because of its large oil and natural gas reserves (Natural Resources Canada, 2019). As stated earlier, Newfoundland and Labrador (NL) contributes more than 5% of Canada's hydrocarbon production. There are four fields in NL producing an average of 240,000 barrels per day, and the fifth field, Hebron started oil production from November 2017.

The reservoir simulators that are available today cannot estimate the available energy losses during production operations with high accuracy. Thus, the development of models that can consider the reservoir energy loss would be an asset. Accurate and reliable models that can help to reduce the natural reservoir energy would lengthen the reservoir production life. Therefore, the models verified in this thesis will augment the accuracy of reservoir simulation, enhancing reservoir analysis and management practices.

Another benefit of this study will be developing two-phase flow mathematical models for reservoir energy loss that can be implemented in various commercial simulators for modelling/simulation of production processes in Canadian petroleum reserves.

Finally, the study will enhance the research capabilities of Memorial's faculty and students, strengthen the scientific exchange between Memorial faculty and leading international experts in the field, and present an alternative/suitable approach for reservoir energy modelling.

1.3. Research Objectives

This research aims to show how EGM can serve as a useful design tool for investigating reservoir energy loss under various processes and thermodynamic conditions, eventually achieving higher oil recovery and overall energy efficiency. The method of entropy generation minimization is applied to three sections: the reservoir, wellbore, and around the wellbore. The main objectives of the research are stated below.

Civan and Tiab (1989) investigated the loss of primary reservoir energy. However, the assumptions of a constant total compressibility and density for dry gas reservoirs and unknown gas composition for single-phase models reduce the model's accuracy and render it inapplicable to many practical cases. This research aims to develop a more accurate and reliable model that can be used for estimating the primary reservoir energy loss. Subsequently, the model will be validated using a high-fidelity reservoir simulation model (e.g., CMG).

Most previously reported studies have focused on EGM in the reservoir system, well system, or both systems (reservoir and well). However, the near wellbore skin effect has not been dealt with explicitly in these models despite that this region can be a significant contributor to entropy generation. This thesis will study the skin effect on entropy generation comprehensively. It will extend the reservoir-production system's entropy calculation by incorporating a near well-bore region in the model. It is also intended to use the enhanced model to investigate the effect of wellbore skin conditions (stimulation or damage) on the pressure drop and, consequently, the total entropy production.

Pressure profiles for both the wellbore and reservoir are crucial in calculating the total entropy generation. Therefore, performing a sensitivity analysis by investigating the effect of rock and fluid characteristics on the pressure profile is essential. The sensitivity analysis identifies the most important properties that play a vital role in the total entropy generation minimization.

The development of an optimization strategy for reducing the reservoir energy loss and consequently for obtaining a high recovery factor is a key motivation for conducting this research. Furthermore, finding optimal petroleum reservoir conditions under the primary production mechanism, based on the entropy concept, recovery factor, and economic perspective, is another primary goal.

Development of a comprehensive model that can handle single and two-phase flow (oil – water) systems is also sought in this thesis. Thus, it is important to extend the calculation of entropy for a reservoir and production system from a one-phase fluid flow to two-phase flow in a one-dimensional system.

Applying these modifications to Civan and Tiab's (1989) model will lead to the introduction of more accurate and realistic models for entropy generation in the sub-surface and surface systems of hydrocarbon reservoirs.

1.4. Research Contributions

Although previous studies have investigated EGM, this research is intended to fill in the knowledge gaps of past literature. Moreover, this research can widen our understanding of

the primary reservoir energy losses over production. The contributions of this thesis are briefly described below.

A model for the reservoir and production system model will be developed that calculates the total entropy production in the three sections of the reservoir, wellbore, and near-wellbore. Numerical solutions, using MATLAB, are used to solve the developed mathematical models. In addition, corrections are made to enhance Civan and Tiab's (1989) model to give more accurate and reliable results. This is considered as one of the main contributions of this study. Moreover, verifying the developed models with Civan and Tiab's (1989) model and a high fidelity CMG model highlights this study's achievement.

The effect of wellbore conditions was studied by Civan and Tiab (1989); however, no detailed discussions were made on this aspect. The researchers used an empirical equation to investigate the influence of the skin factor on recovery performance. In the current study, a region around the wellbore is added to give the model more flexibility in simulating the wellbore effect. The permeability of the region around the wellbore (either damaged or stimulated) is different from that of the reservoir. To the best of our knowledge, most of the research studies available in past literature use the Hawkins formula (Hawkins, 1956) for the skin factor to understand the influence of wellbore conditions on entropy production and recovery factor.

Some studies in the literature have developed two-phase flow models in pipelines using thermodynamic concepts to assess the performance of a flowing wellbore (Duruewuru, 1985; Tiab and Duruewuru, 1988). Highlighting another novel aspect of this research, the

present study uses two-phase flow models (oil-water) for the first time to investigate the energy losses in both wellbore (pipeline) and reservoir systems (porous media) using EGM.

Another contribution of this thesis is to determine the optimum conditions that allow a high recovery factor with a minimum available energy loss. A new performance criterion called the Coefficient Of Performance (COP) is introduced. The COP integrates the recovery factor with entropy generation and provides a quantitative measure to optimize reservoir production. Moreover, the COP is used to optimize the operating conditions of the reservoir, such as the production rates and BHP. The Net Present Value (NPV) and Future Value (FV) are used to validate the results obtained from COP. A comparison between the results from NPV and COP shows that COP gives accurate results for calculating the optimum conditions. However, the results are more generic as they do not require cost data (Elhaj et al., 2020). Because the optimum production rate is an essential parameter in reservoir management, a better production strategy is chosen by identifying the effects of different key parameters on the production rate. In this thesis, three main factors are considered for estimating the optimum production rate: (i) recovery factor, (ii) entropy generation, and (iii) economic prospect.

The effects of fluid and rock properties on total entropy production are investigated and discussed. The outcomes of this aspect of the study are constructive for researchers working to identify the most critical factors affecting total entropy production.

1.5. Organization of the Thesis

This thesis consists of seven chapters, and the organization of this dissertation is outlined as follows. **Chapter 1** gives an overview and introduction of the EGM and how it will be used as a tool to better design the optimum operating conditions for reservoir and wellbore systems. In the next chapter, **Chapter 2**, a literature review briefly discusses the prior studies with a focus on the applications of thermodynamics in single-phase and two-phase fluid flows in both porous media and pipelines. **Chapter 3** presents an overview of the effect of the hysteresis phenomenon on EGM by comprehensively reviewing selected fluid and rock properties. **Chapter 4** covers the step-by-step procedure of developing the mathematical formulation of pressure profiles, as well as total entropy production followed by a solution procedure. In addition, this chapter highlights the optimization procedure of the production rate and introduces a new performance parameter named the COP. **Chapter 5** shows the calculations used to develop the pressure and entropy production models for a two-phase flow in a wellbore and porous medium; afterwards, a solution is described. **Chapter 6** provides the results of the models, followed by a detailed discussion. Conclusions and future recommendations are presented in C**hapter 7.**

Chapter 2: Literature Review

2.1. Overview

It is important to design and operate energy systems efficiently to reduce emissions that lead to climate change. The need to have more efficient systems has led engineers to study the best use of available energy resources and to shed light on thermodynamic irreversibilities (Alemayehu et al., 2015). As per the second law of thermodynamics, any operating system is associated with energy loss due to dissipation; this loss is unavoidable (Hatsopoulos et al., 1966).

Carnot (1786) was the first who pointed out that the loss of available energy for an operating system is inevitable. He stated that any moving system has energy loss due to friction and "violent moment," including mechanical and thermodynamic causes (Carnot, 1803, 1786). Sadi, Carnot's son, carried out his father's legacy and pointed out the concept of ideal and real operating systems (Carnot, 1824). It was proved that the ideal system's efficiency is a function of the heat reservoir's temperature. Later, Gibbs (1948) presented a mathematical formula representing the second law of thermodynamics, which originated from Carnot's work.

Entropy Generation Minimization (EGM) has been applied to various engineering disciplines, especially in mechanical and chemical engineering (Duruewuru, 1985). The laws of thermodynamics, especially the second law, permit engineers and researchers to estimate a system's efficiency. In this chapter, two main fluid flow regimes are discussed and critically reviewed: single-phase flow and two-phase flow.

It was found that the entropy generation rate is proportional to the destruction of available work as per the "Gouy-Stodola" theorem (Stodola, 1898). It was proven based on the Gouy-Stodola theorem that if a system's efficiency is to be increased, the entropy generation should be minimized. Therefore, the method of identification and reduction of thermodynamic irreversibilities is known as Entropy Generation Analysis (EGA), while minimizing the losses of a system is called Entropy Generation Minimization (EGM). Although the Gouy-Stodola theorem well covers the relationship between the loss of energy and entropy, the methodology of EGA and EGM was further expanded by Bejan (1996, 1995).

EGA is an important tool for illustrating the influence of irreversibilities within a system on the required energy input. EGA is based on a heuristic approach (Giangaspero and Sciubba, 2013; Sciacovelli et al., 2015). The initial configuration of the system is subsequently improved by introducing possible design modifications. Applying EGA in a system involves steps to be followed, starting by defining the system followed by creating the initial design for the system. Constructing the mathematical model is the next step. Then evaluation and critical analysis of EGA is performed. Modify the design as suggested by a critical inspection of the EGA is the pre-final step. Finally, repeat the computation and iterate until a feasible and acceptable "minimum" of EGA is obtained.

Giangaspero and Sciubba (2013) concluded that the adopted procedure for "optimizing" a design is not a proper optimization, rather a heuristic design approach, essentially based on a thermodynamically sound trial-and-error procedure. Ogulata and Doba (1998) conducted experimental studies on the entropy generation of a cross-flow heat exchanger by

considering the exchanger's irreversibility due to heat transfer and friction resistance. Wang et al. (2018) found that the EGA of material with large thermal diffusivity contributes to obtaining better behavior of the heater during the transient processes when the metal thickness is fixed.

EGM is a deterministic approach (Giangaspero and Sciubba, 2013; Sciacovelli et al., 2015). The fundamental characteristic of the deterministic approach is the analytical definition of the global rate of entropy generation as a function of critical design parameters, like geometry, dimensions and working conditions. A lumped-sum parameter procedure is followed to minimize the energy loss in a system. These steps start to define the initial design variables. Then, develop the mathematical models and equations followed by entropy generation rate evaluation and critical analysis. Afterwards, an optimization algorithm is created to test the optimal factor of the system. In case the minimum entropy generation rate is achieved, the optimal design of the system is finalized and ready; if not, then a new design variable is needed.

Different analytical and empirical techniques were described in past studies for generation minimization problems for engineering systems (Bejan, 1996, 1995; Naterer and Camberos, 2008). Past studies have started re-investigating porous systems from the second law perspective, rather than the first law. These investigations have been extended from thermal to chemical and thermochemical systems (Torabi et al., 2017a). Although many studies have focused on entropy generation minimization in porous media, other systems did not receive attention. For example, systems that have extra physicochemical effects had limited study.

Early discussion/analysis of reservoir energy changes over the reservoir production lifetime emerged during the 1930s when Versluys and Schilthuis showed a strong link between the reservoir energy, production rate, and cumulative production (Schilthuis, 1936; Versluys, 1934). According to Schilthuis' study, an imaginary thermodynamic engine can represent a petroleum reservoir (Schilthuis, 1936). In particular, the study considered the net energy change in this imaginary engine similar to that in the petroleum reservoir. Schilthuis' study did not consider the loss of fluid energy, nor did the approach apply to microscopic-level phenomena (e.g., velocity and position of gas molecules) and non-volumetric reservoirs.

2.2. Reservoir Drive Mechanisms

Newfoundland and Labrador (NL) is one of the main oil producing provinces in Canada. NL's oil and gas industry is considered, historically, relatively new, as the first reserves were discovered in 1979, with the first oil produced in 1997. Currently, the province has mainly four fields: Hibernia, Terra Nova, White Rose, and Hebron, produced an average of 240,000 barrels per day. The NL reservoir fields, like any other reservoir that starts initially using the natural reservoir energy as a production mechanism, have a limited period of time. In this section, different reservoir mechanisms will be discussed and reviewed over the past few decades.

The reservoir drive mechanism, also called natural drive, can be defined as a natural force in the reservoir displaces hydrocarbons out of the subsurface ground into a wellbore and up to the surface. There are five common drive mechanisms: water drive, gas expansion,

solution gas, rock or compaction and fluid drive, and gravity drainage. One type of these drives usually dominates; however, it can also be a combination of two or more drives in one reservoir. Depending on the drive mechanism, characteristic recovery efficiencies can be expected for a given reservoir. However, the water drive is the most efficient drive mechanism, followed by gas drives (gas expansion and solution gas) and gravity drainage. **Figure 2.1** details the reservoir mechanisms. Historically, it is known that reservoir drive mechanisms recover only about 10% of the oil below the surface.

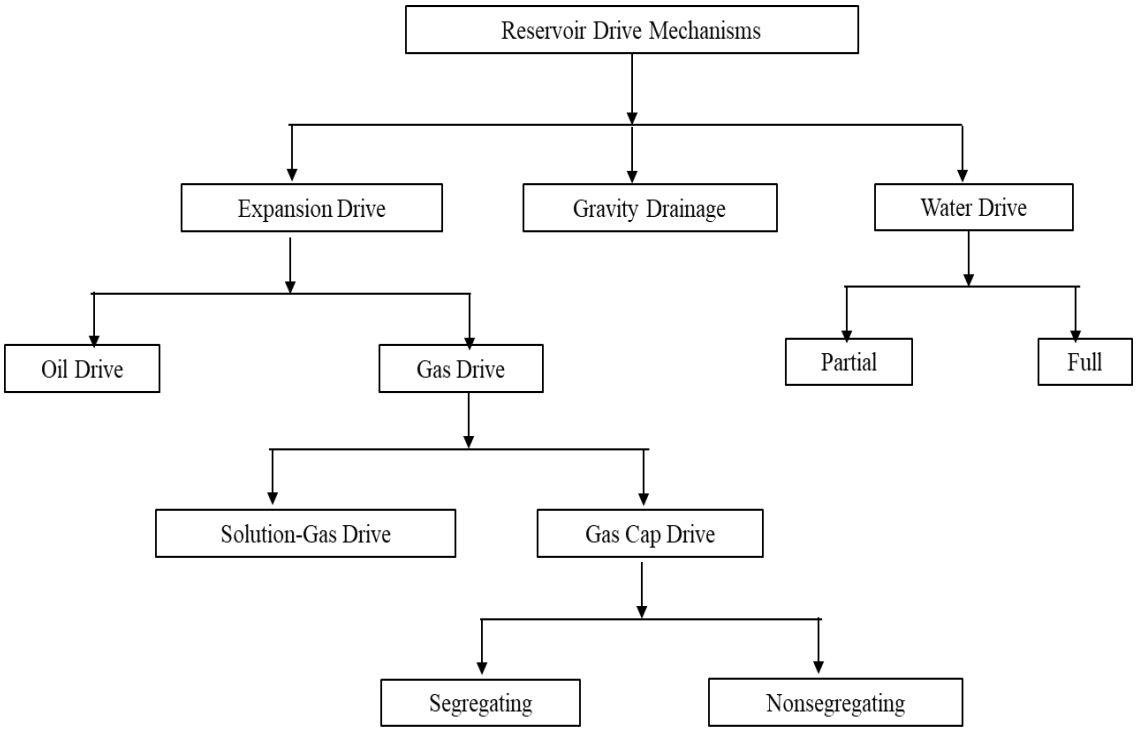

Figure 2. 1. Reservoir Drive Mechanisms

Coleman et al. (1930) were the first to investigate reservoir pressure decline due to hydrocarbon production. They presented an equation that describes the relationship between the reservoir pressure, the amount of the hydrocarbon produced, the hydrocarbon content of the reservoir, and the properties of reservoir fluids. Unfortunately, at that time,

there were no data available to permit the application of a detailed model. Schilthuis (1936) modified the work of Coleman et al. (1930) by deriving models for calculating the reservoir energy changes that occur during production.

In the water drive reservoirs, the oil zone is in contact with an aquifer beneath it that provides the bulk of the reservoir's drive energy. Several past studies have investigated the pressure-production behavior of water drive. For example, Hicks et al. (1959) were among the first who used computer modelling in describing a technique for predicting the future behavior of a water drive reservoir. The diffusivity equation was used to address the effect of permeability and porosity of the rock on the water drive mechanism. This study was limited to the undersaturated reservoirs with constant compressibility. Ogolo et al. (2014) compared the effect of full and partial water drive on gas reservoir recovery. They found that about 70 – 80% of gas can be produced in a partial water drive reservoir compared to 50 – 60% for a full water drive reservoir. They justified this by stating that as long as the reservoir is under a strong aquifer influence, there is a larger residual gas saturation, which leads to a lower recovery factor.

Charles and Crawford (1975) investigated the effect of different factors, including oil production rate and permeability, on oil recovery in reservoirs under the solution gas mechanism. In this investigation, numerical schemes were used for a radial three-phase (oil-water-gas) flow and two-dimensional reservoir model. The study concluded that at low production rates, gas is segregated to the top of the reservoir and produced rapidly, which depleted the reservoir energy. Furthermore, gas solution drive is sensitive in a reservoir with vertical permeability; the highest oil production rates yield higher recovery.

An experimental study focused on the solution gas drive mechanism and indicated that gas mobility in heavy oil is much less than in light oil, leading to improved recovery factor (Pooladi-Darvish and Firoozabadi, 1999). They reported that about 14% of the original oil in place could be produced using the solution gas drive mechanism, which is the average percentage of the recovery achieved by solution gas drive; usually range between 5% to 30%. One of the important conclusions of this study was that formation of gas bubbles takes time, and then the separation from the oil lowers the oil pressure dramatically.

As known in the literature, the solution gas drive described the parallel flow of oil and gas when gravity effects are neglected. Under the gravity influence, the gas that dissolves in oil will migrate upward, where the gas will accumulate at the top of the formation, where, if not originally present, a gas cap is formed. Dumore (1970) conducted an experiment to investigate the gas saturation development and parameters on which this development depends on the gas-cap drive mechanism. The tests showed that gas migration from the bottom of the formation to the top depends mainly on capillary pressure. At low capillary pressure, a conical shape through which the gas migrated to the top, while at high capillary pressure, only one gas channel developed. These two conditions of capillary pressure are called dispersion and non-dispersion. In reservoirs that initially have gas-cap, the gas-cap expansion as the pressure drops is considered the primary energy source in a reservoir. Additional energy is provided by the expansion of solution gas released from the oil. Less significant drive contributions are provided by the expansion of the rock and its associated water.

As the reservoir pressure starts dropping, the under compacted rock matrix and fluid must assume more and more of the overburden load. The resulting deformation of the rock and fluid reduced the total pore volume, which maintains the reservoir pressure and drives additional fluid out of the formation (Garg and Pritchett, 1977). The increased pressure between the grains will cause the reservoir to compact, leading to subsidence at the surface. Various previous studies (Dake, 1998; Garg and Pritchett, 1977) showed that compaction depends mainly on the difference between overburden pressure and fluid pressure. This makes it easier for researchers to measure compaction in the laboratory by increasing overburden pressure on the rock sample, while the fluid pressure in the core is constant.

Gravity drainage or some references call this 'gravity segregation' (Archer and Wall, 1986). It has an important role in several aspects of reservoir behavior, such as the phase movement. Hall (1961) recommended that a number of factors must be considered when dealing with the reservoir under gravity drainage influence. Some of these factors include production rate, well productivity, and the economic advantage of pressure maintenance. The author presented a general method for calculating the performance of a gravity-drainage reservoir. The method is made to take into account variations throughout the reservoir configuration, change in permeability and fluid composition. The proposed method's results were in good agreement with field history data.

As a summary of reservoir drive mechanisms, **Table 2.1** shows the energy sources and ultimate recovery ranges of the major drive mechanisms (Bull-D-14, 1984).

Table 2. 1. Energy sources and recovery factor of reservoir drive mechanisms.

Drive Mechanism	Energy source	Recovery
Solution gas drive	Evolved solution gas expansion	10 – 25%
Water drive	Aquifer expansion	15 – 60%
Gravity drainage drive	Gravity	5 – 20%
Gas-cap drive without gravity drainage	Gas cap expansion	15 – 40%
Gas-cap drive with gravity drainage	Gas cap and evolved solution gas expansion	15 – 80%

2.3. Entropy Generation in Reservoirs, Wellbore, and Non-Porous Media

Past studies have provided valuable information on using the concept of the maximum reversible work function as a tool for investigating the influence of the production rate on the primary reservoir energy (Chen et al., 1999; Duruewuru, 1985; Osoba et al., 1951; Tillero et al., 2011). The influence of gas gravity on reservoir energy is one of the valuable pieces of information extracted by the maximum reversible work function. Furthermore, the similarity in the behavior of volumetric gas condensate and dry gas reservoirs on the change in process/operational conditions is another important factor that previous studies provided by using the concept of the maximum reversible work function.

2.3.1. Entropy Generation in Reservoirs and Wellbore

The importance of production rate on a reservoir's energy and well has been highlighted in numerous studies (Alemayehu et al., 2015; Civan and Tiab, 1989; Mukherjee et al., 1987; Naterer and Camberos, 2008; Sarathi and Tiab, 1981; Slattery, 1972). In the study of Civan and Tiab (1989), entropy production was calculated in both the reservoir and wellbore.

Based on the value of entropy production, the optimal conditions with a high recovery factor were identified. The researchers also concluded that the pressure and non-Darcy coefficient significantly influence the total entropy production.

Previous studies have shown that the laws of thermodynamics can be applied to fluids flowing through pipes or porous media by using key properties, such as heating content, specific volume, and entropy in the flowing well (Sage and Lacey, 1935). In the study by Sage and Lacey (1935), it was found that the loss of energy as a result of frictional effects is not an essential factor when considering the flow of fluids in the tube. In addition, the authors carried out experimental work to analyze the relationship between the flow rate in the wellbore tubing and system energy.

Energy efficiency, availability function, work, and entropy generation were further investigated in petroleum production systems by Tillero et al. (2011). An extensive review of entropy generation modelling in porous media was presented by Torabi et al. (2017). The review reported how local thermal non-equilibrium effects in porous media impact the energy and exergy efficiencies of a given system. Several studies have investigated entropy generation in reservoir systems, including both the reservoir and well. Civan and Tiab (1989) calculated the entropy production in both reservoir and wellbore regions. Their results were used as a criterion for selecting the operating conditions that lead to a high recovery factor. In Civan and Tiab (1989), the damage to the near-wellbore was discussed. The skin factor was changed to take into account any change in the near-wellbore region.

Past researchers developed a numerical transient multiphase flow model with finite-difference approximations in a well (Miller et al., 1998; Miller, 1979). Initially, the model was developed under the condition of the homogenous flow of one component at thermodynamic equilibrium. However, the extension of the model included slip and a finite rate of evaporation. Mass, momentum, energy, and thermodynamic equations were used in model development. The resulting model was only applicable for use in flowing wells, limiting its use in reservoir systems.

A Representative Elementary Volume (REV) averaging technique was used to develop balance equations for two-phase flows in porous media (Gray, 1982). Gray (1982) used the technique to derive vertically averaged balance equations of mass, momentum, energy, and entropy. In the past, the entropy equation for porous media has often been neglected. However, Gray (1982) included it in the derivations, showing that the entropy equation is important when studying fluid flow in porous media. It was concluded that the balance equations are valid for applications in vapor, liquid, or solid phases.

Another important thermodynamic property is known as the "availability function." It can be used to calculate the thermodynamic efficiency of two-phase flowing well cases, including energy loss due to irreversibility (Duruewuru, 1985; Tiab and Duruewuru, 1988). The benefit of using the availability function is that it could estimate the thermodynamic efficiency of a system even if no work (production or consumption) has been done on the targeted system. In addition, the availability function has the potential to compare different processes, which may lead to enhanced knowledge of improvement possibilities for a given system.

2.3.2. Entropy Generation in Non-Porous Media

For a natural circulating loop system, Goudarzi and Talebi (2015) developed an entropy model for single-phase flow under steady and pseudo-steady state conditions. They concluded that as more frictional losses occur, entropy generation increases within the loop. An increase in the Reynolds number leads to an increase in the entropy production rate (Pal, 2014). At a constant Reynolds number, an inverse relationship exists between the entropy production rate and pipe diameter (Bidi et al., 2010b). The method of EGM can be used to find relationships between system parameters to optimize a given system (Bejan, 1996, 1995; Myat et al., 2012; Naterer and Camberos, 2008; Saghi and Lakzian, 2017).

A thermo-fluid dynamic model for a separated two-phase flow was developed by Kocamustafaogullari (1971). The two-fluid model was formulated by considering each phase separately. Therefore, the formulation was expressed in terms of two sets (one for each phase) of conservation equations. In addition to the continuity, momentum, and energy equations, the enthalpy equations were derived with appropriate conditions to formulate the two-phase system's thermo-fluid model. In this study, a stability theory for a general separated two-phase flow system was developed using the thermo-fluid model. It is worth mentioning that the model cannot be applied in porous media; however, its fundamental concepts can be used in porous media (Gray, 1982).

2.3.3. Experimental Investigation of Entropy Generation

The EGM approach includes fluid mechanics, heat transfer, material constraints, and geometry to establish a correlation between the entropy and the optimal conditions for any

system (Bejan, 1996, 1995; Naterer and Camberos, 2008). Past studies extended the analytical EGM methods to numerical and experimental methods. It has been shown that EGM can be used mathematically to stabilize and optimize the use of energy in porous media (Bidi et al., 2010a).

Previous studies have experimentally investigated the thermal performance of a system and its entropy generation (Tharayil et al., 2017). They investigated fluids with different concentrations and their effect on the efficiency based on the second law of thermodynamics. Their results indicated a good match between the model and experiments. Another experimental study examined the influence of vapor quality and nanofluid concentrations on entropy generation and exergy loss nano-refrigerant (Sheikholeslami et al., 2018). It was shown that increasing the concentration leads to an increase in the frictional entropy generation. Rahbara et al. (2018) proposed two new empirical correlations to predict water productivity, leading to lower entropy generation in triangular and tubular solar stills.

2.4. Entropy Generation in Porous Thermal Systems

A porous medium plays a vital role in heat absorption and uniform temperature distribution, which can result in increasing the heat transfer coefficient and eventually decreasing the temperature of a system (Torabi et al., 2017). Generally, two methods can be used to calculate entropy in a thermofluid system: direct or indirect. The direct method applies to laminar flow, and analytical solutions can be used. In contrast, the indirect method is used for turbulent flow, and partial differential equations should be solved

numerically (Herwig and Kock, 2007). Some of the important parameters that affect entropy generation in porous media are discussed hereafter.

2.4.1. Viscosity Effects

In many cases, viscous dissipation is neglected when a fluid flows through a channel (Bejan, 1995). However, for high viscous flow, internal heat generation should be added to the energy equation due to the friction. Darcy's equation can be used to describe the case when viscous dissipation is neglected, while the Brinkman approach in porous media is used when viscous dissipation is considered (Nield, 2007).

Three strategies can be used to visualize the viscous dissipation in porous media: the Local Thermal Equilibrium (LTE) approach, the Local Thermal Non-Equilibrium (LTNE) approach, and Pore Scale Modelling (PSM) approach (Torabi et al., 2017; Nield, 2007). In LTE, the viscous dissipation term is considered in the energy equation without heat generation and steady-state conditions. For the LTNE approach, two energy equations are used to visualize the temperature fields in both fluid and solid porous media phases. If the PSM approach is used, the entropy generation equation will not have a velocity impact, and all of the corresponding fluid friction is calculated via shear stress tensors (Torabi et al., 2017, 2016). Overall, viscous dissipation plays an important role in entropy generation calculations, velocity, viscosity, and fluid temperature.

2.4.2. Radiative Effects

At high temperatures (over 1000 K), previous studies showed that radiative heat transfer is significant in porous media (Bidi et al., 2010; Howell et al., 1996). Many past studies

considered the effect of radiation in porous media, such as in combustion and solar collectors, in thermal modelling (Bidi et al., 2010; Hirasawa et al., 2013).

It has been reported that radiative heat transfer can be simplified by incorporating the radiative effects to the thermal conductivity of the solid phase of porous media. This will affect the heat transfer rate, leading to a decrease in the system's temperature. Few previous research investigations confirmed that as the radiative effect increases, the entropy generation increases as well. However, there is still a knowledge gap of how the radiative effect and the LTNE conditions affect the entropy generation in porous media.

2.4.3. Velocity Slip and Temperature Effects

It was shown that for macro-channels, the continuum conditions at the edge are valid; however, this is not true for microchannels (Sun et al., 2009). The Knudson number is the parameter that can differentiate between slip effects for micro and macro channels. When the Knudson number is less than 0.01, the length scale of the systems is dominant, and the continuum assumption can be used. However, if this ratio is higher than 0.01, the mean free path of the fluid molecules is large enough so that the velocity slip and temperature jump boundary conditions at the interface of the solid walls and the fluid should be considered (Lv et al., 2013; Torabi et al., 2017, 2017).

There are mainly two effects that velocity slip and temperature jump have on the entropy generations in porous media. There is a direct and indirect influence. The direct impact occurs when there is a difference in temperatures between the fluid and the wall. However,

the indirect impact happens due to modification in a system temperature, which ultimately impacts the entropy generation (Torabi et al., 2017).

2.5. Entropy Generation in Porous Systems with Chemical Reactions

Porous media can be affected chemically by reactions due to the large surface area to volume ratio as well as the transport of energy and mass (Vafai, 2015). Porous media chemical reactions can occur in either a fluid or solid phase. An example of a solid chemical reaction in porous media is catalytic porous reactors. Another case can be combustion processes (Howell et al., 1996). The existence of chemical reactions in porous media might complicate the entropy analysis due to the thermodynamic equilibrium assumption (Vafai, 2015).

2.5.1. Modelling of Entropy Generation in Reactive Porous Media

Modelling of entropy generation in reactive porous media requires replacing the assumption of thermal equilibrium with chemical kinetics to represent the chemical activities that occur in porous media (Bidi et al., 2010).

Recent studies have shown that the energy term in the entropy generation equation could lead to a significant deviation from thermal equilibrium conditions, resulting in a significant error in calculations. Thus, the entropy generation calculations should consider the irreversibility of interphase heat transfer set by exothermicity or endothermicity of the

chemical reactions (Torabi et al., 2015a). It implies that analytical approaches would not solve such equations; however, numerical methods could be employed.

A research study investigated the solid-gas porous reactor that was optimized analytically by minimizing the entropy generation (Azoumah et al., 2006). In this study, fluid flow behaviour, conduction, and convection were included in modelling processes under chemical equilibrium. To calculate the total entropy generation, irreversible thermodynamics was involved. Bidi et al. (2010) investigated entropy generation in a premixed, porous burner. The authors modelled fluid flow through a modified version of the steady-state Navier-Stokes equations and used a two-equation model of heat transfer. Based on the literature, entropy generation due to chemical reactions, in particular combustion, may account for more than one-third of the overall thermodynamic irreversibility radiative effects (Alemayehu et al., 2015).

2.5.2. Mass Transfer, Chemical Reactions, and Other Transport Phenomena

Humidifiers, dehumidifiers, cooling towers, and chemical reactors are typical examples of this type of system. To optimize these systems, Entropy Generation Analysis (EGA) has been used. In previous studies, variations in the inlet pipeline length, valve opening time, and overlap period can minimize the entropy production rate (Alemayehu et al., 2015).

Alemayehu et al. (2015) presented a critical review on the theory of entropy generation and its application to different engineering and science cases for design and optimization purposes. Their study focused on the differentiation of the EGA technique from that of

EGM, as well as the level of analysis (local or global). It was found that EGA is related to the identification and reduction of thermodynamic irreversibility, while EGM aims to minimize the energy losses of a system.

Few researchers attempted to include mass transfer and the second thermodynamic law to optimize non-reacting multi-species mixtures (San et al., 1985; Sciacovelli et al., 2015). Using the second law of thermodynamics in such studies can capture mass transfer at a global level and the mass transfer, in this case, was due to evaporation and/or condensation. Bejan (1996) provided several examples for calculations in such devices when the mass transfer occurs in evaporation form. It was concluded that useful work is lost when the system does not attain equilibrium with the environment.

2.6. Mathematical Methods for Entropy Generation

Generally, EGM calculations in a flowing well and reservoir require a solution of one or more challenging partial differential equations (PDE). Therefore, assumptions to simplify such equations are required. Sometimes, it is also necessary to convert the PDE to ordinary differential equations (ODE). However, due to some nonlinearities in the equations, converting a PDF to ODE may not be readily solvable. The general solution of PDEs can be divided into four main categories: analytical, semi-analytical, analytical-numerical, and numerical (Torabi et al., 2016).

Different strategies/methods are used to find a solution for entropy generation problems, including but not limited to the general solution of PDEs and finite difference

approximations. The literature also includes other methods. A brief discussion of some common methods is presented.

2.6.1. Exact Analytical Methods

Sometimes, an exact analytical solution can be found. However, considering the assumptions, this solution might lack viability (Torabi et al., 2016). An exact analytical solution helps to understand the behavior of the system better. It would be easy to visualize system behavior using analytical solutions. It can also be used for the validation of numerical tools. The analytical solutions have been used before in many entropy generation calculations, such as entropy generation in porous media, entropy generation in conjugate conduction-convection systems, heat transfer, and entropy generation within convective fins (Aziz and Khan, 2012).

2.6.2. Semi-Analytical Methods

In conduction and convection problems, the governing equations of entropy generation problems will be nonlinear if the material is temperature dependent or power-law dependent. For radiation problems, two terms contain nonlinearities – one due to the Stefan–Boltzmann law of radiation, and the second because the surface emissivity is a function of temperature. Under these circumstances, the exact analytical solution will not be able to solve such problems. However, several non-exact solution procedures can be followed to address this type of problem. These methods can be considered as approximate analytical techniques. These methods convert the nonlinear parts to a series of an infinite number of simpler differential equations, which can be solved analytically. As several

equations are transformed into differential equations that are solved analytically, and their results are added together, some equations are neglected, leading to accumulated errors. A common approach used to calculate the total EGM is the differential transformation method (DTM) (Lin et al., 2017). DTM is mainly based on Tayler's series; it can give accurate results when used in convective-radiative boundary heat loss problems.

2.6.3. Analytical-Numerical Methods

In these methods, analytical and numerical methods are applied as a solution simultaneously. In some parts of problems, the solution can be found analytically, while the other part cannot be solved analytically. For example, in radiation problems, numerical methods are used as a part of a solution due to complex boundary conditions. As this method uses a combination of analytical and numerical solutions, it has received much attention lately as it can be employed in many problems (Torabi et al., 2015b). Commercial packages, such as Maple and Mathematica, can be used in these problems as they can use analytical and numerical solutions simultaneously.

2.6.4. Numerical Methods

The numerical methods are often utilized in complicated geometry and/or energy equations that contain strong nonlinear equations. Furthermore, numerical solutions are used when momentum and energy balance equations are needed to be solved simultaneously to obtain a solution of entropy generation problems (Mahdavi et al., 2014). There are mainly two numerical approaches that can be followed to obtain the solution of entropy generation. One method is the use of commercial software, such as ANSYS Fluent and COMSOL

Multiphysics. The other technique is to develop a programming code such as a MATLAB code. By adopting numerical approaches, Makhanlall and Liu (2010) provided local and total entropy generation and exergy destruction.

2.6.5. Finite-Difference Approximations

The finite-difference approximation is one of the numerical approaches that can be used in entropy generation cases (Duruewuru, 1985; Tiab and Duruewuru, 1988; Torabi et al., 2017). The basic concept is to replace the original problem with another problem that is easier to solve; the achieved solution is generally close to the original problem's solution (Aziz and Settari, 2002).

The differential equation is replaced by a set of algebraic equations relating the target values for each grid-point. These equations are called the 'finite-difference equations,' and the differential problem is reduced to an algebraic problem. The process of obtaining finite-difference equations that approximate a given differential equation is called 'discretization.'

Generally, there are two types of discretization: (i) discretization in space and (ii) discretization in time. For discretization in space, there are three methods available for the discretization of any given system: (i) the Tayler series method, (ii) the integral method, and (iii) the variational method (Ahmed, 2019; Aziz and Settari, 2002). All these methods can be either (i) explicit or (ii) implicit. It is worth noting that there are two methods of grid construction points distributed and block-centered grids.

Duruewuru (1985) used the finite-difference approximation by employing the block distribution grid system and a point distribution system in the reservoir spatial domain. The time domain is also divided into several time steps during which the system of linear equations is solved to obtain new values of dependent variables.

2.7. Limitations on Modelling of Entropy Generation in Porous Media

In the current literature, there are knowledge gaps that should be filled in entropy generation modelling; some are highlighted in this section. Most of the previous studies have focused on calculating the entropy generation in one system, either a reservoir (porous medium) or wellbore (pipeline). Limited studies have estimated the entropy generation on both systems at the same time.

Another limitation is none of the previous studies have investigated the effect of the zone around the wellbore on the entropy generation or recovery factor. Moreover, previous studies have used outdated techniques to estimate the optimum operation conditions for a system. However, modern methods such as COP have never been employed before to obtain the optimum conditions for hydrocarbon reservoirs.

As in the literature, all previously developed mathematical models representing entropy generation in porous media were either for single or two-phase flow. None of the previous studies have developed a set of equations and models that can be applied for both cases – single and two-phase flow systems. Furthermore, most of the previously developed models for two-phase flow are suitable for oil-gas systems. Thus, oil-water flow systems have not

been investigated. Most of the past entropy modelling studies focused on steady-state conditions. The entropy generation is thus rarely used to address semi-transient operation conditions in porous media.

Chapter 3: Hysteresis in Porous Media Flow

3.1. Background

This chapter examines the hysteresis phenomenon in fluid and rock properties. The research on hysteresis was done under the supervision of my former supervisor, Dr. Enamul Hossain, who left Memorial University part-way through my Ph.D. program. The aim of the topic – hysteresis – was to develop mathematical or empirical models that describe the hysteresis phenomenon in selected rock and fluid properties. The initial stage was to conduct a comprehensive literature review on the most important fluid and rock properties in petroleum engineering, theoretically and experimentally. As a result, four review articles covered the most influential properties in oil and gas engineering were published. The effect of hysteresis on the EGM can be investigated in future work after the fundamental concept is highlighted in this thesis. An overview of the hysteresis phenomenon and its selected properties is highlighted hereafter.

Hysteresis has a significant role in characterizing the hydrocarbon recovery, as well as giving a better understanding of fluid flow and energy availability in porous media. Therefore, an accurate estimation of hysteresis measurement is essential. This also plays a vital role in Entropy Generation Minimization (EGM) calculations in porous media. Numerous previous studies have focused on the effect of hysteresis on EGM. For example, Odukoya et al. (2011) developed a model to determine entropy production due to thermal and fluid irreversibilities in a microchannel. In this model, the hysteresis phenomenon was considered during the start-up of the droplet motion. The model included the surface

tension hysteresis along with the influences of friction and pressure. Another modelling study regarding hysteresis in entropy generation was conducted by Li et al. (2017). In their study, they observed a hysteresis characteristic in the hump region in pump-turbines. It was found that the hysteresis characteristic is orginated from the Euler momentum and hydraulic loss; the latter accounts for a major portion of the hysteresis characteristic.

Figure 3.1 displays a general hysteresis loop for any system. Path A represents the track of the first process for any parameter (in most cases, it is an increasing direction), while path B represents the second process track (often, it is a decreasing direction). The hysteresis characteristic in the hump region can be analyzed for turbomachinery through entropy production. It was found that the hump characteristic and the accompanying hysteresis phenomenon are caused by backflow at the runner inlet and the presence of separation vortices close to the hub and the shroud in the stay/guide vanes, which is dependent on the direction of discharge. Past studies have focused on the hysteresis effect on various rock and fluid properties, such as relative permeability, porosity and permeability, and wettability (Elhaj et al., 2018a, 2018b, 2020).

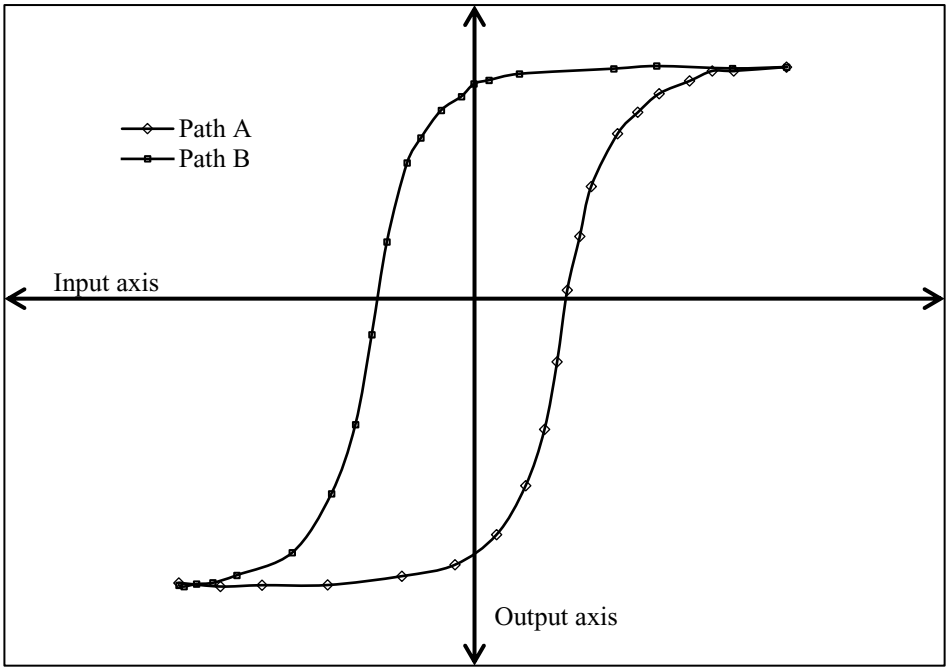

Figure 3. 1. Schematic of hysteresis loop for a system

3.2. Hysteresis in Capillary Pressure

Capillary pressure plays an important role in enhanced oil recovery methods (EOR) (Evans and Geurrero, 1979; Moore and Slobod, 1956; Stegemeier, 1977, 1974) and multiphase flow (Bouchard and Hawkins, 1992; Wang and Alvarado, 2016a). Stegemeier (1977, 1974) and Moore and Slobod (1956) highlighted that by increasing the capillary forces in a reservoir (decreasing the radius curvature), the trapped oil could be produced or prevented from being trapped. In addition, capillary pressure helps to explain the multiphase flow in porous media as well as fluid distributions. This will give a better understanding and establish connections with fluid movement in the reservoir (Bouchard and Hawkins, 1992; Wang and Alvarado, 2016a).

Knowledge of hysteresis in capillary pressure is important for a better understanding of the distribution of saturation in the reservoir. An accurate estimation of capillary pressure is also required, especially in vertical movements, such as in steam-assisted gravity drainage SAGD (Dernaika et al., 2011a; Salter, 1990). Generally, the impact of hysteresis in a reservoir can be observed in well coning attitude (Cutler and Rees, 1970; Killough, 1976), gas storage reservoir systems and water coning (Evrenos, 1969), the redistribution of water after initial infiltration (Talsma, 1970), and the cumulative residual curve (disconnected phases) during displacement (Keelan and Pugh, 1975; Land, 1968; Melrose and Brander, 1974; Morrow, 1970; Pickell et al., 1966; Wardlaw and Taylor, 1976).

In this section, the hysteresis of the capillary pressure in different reservoir rock types along with different variables such as saturation (Brown, 1951) and pore structure (Dullien, 1992; Salter, 1990; Wardlaw and Taylor, 1976), and resistivity index (RI) (Dernaika et al., 2011b) will be discussed. Furthermore, methods and techniques that are used to investigate hystereses such as the porous plate method (Brown, 1951; Kleppe et al., 1997), centrifuge (Hassler and Brunner, 1945; Masalmeh, 2001), static methods (Wang and Alvarado, 2016a), X-Ray CT (Wang and Alvarado, 2016b), Nuclear Magnetic Resonance (NMR) (Green et al., 2008), Capillary Pressure and Resistivity Index by Continuous Injection (CPRICI) (Kokkedee and Boutkan, 1995), and Papillary pressure Probe (Wunnik; et al., 1999) will also be examined.

3.2.1. Modelling of Hysteresis in Capillary Pressure

Due to the time–consuming nature, inaccuracy, and cost limitations for experimental techniques, several studies have attempted to develop a mathematical model that is

complete, consistent, and accurate to describe the hysteresis phenomenon in capillary pressure. In addition, most of the experimental studies were conducted for a water-wet system (Masalmeh, 2001). Therefore, there is a need for a mathematical model that applies to more than one system. In addition, a hysteresis model allows physical plausibility in the problem (Killough, 1976). In this section, the most important models used in the oil and gas industry will be highlighted and discussed in detail.

According to past literature, the relationship between capillary pressure and saturation, which causes the hysteresis phenomenon, does not follow a unique functional relationship (Morrow, 1970). Hysteresis in capillary pressure is described by bounding imbibition and drainage curves and intermediate scanning curves (Killough, 1976; Morrow, 1990), as shown in **Figure 3.2**.

Mathematical models for hysteresis have a long history since 1935 when Preisach (1935) developed the first mathematical model that described the hysteresis phenomena, but not in capillary pressure cases. It was in the area of magnetic fields. The most common mathematical model used for hysteresis in capillary pressure was empirically developed by Killough (1976), which can reproduce the hysteresis curves by remembering the history of saturation.

The main assumption of this model was that capillary pressures should lie initially on one of the bounding imbibition or drainage curves. Accordingly, the model was developed for two main cases: (i) drainage to the imbibition scanning loop and (ii) imbibition to the drainage scanning loop. This model appears in the following form:

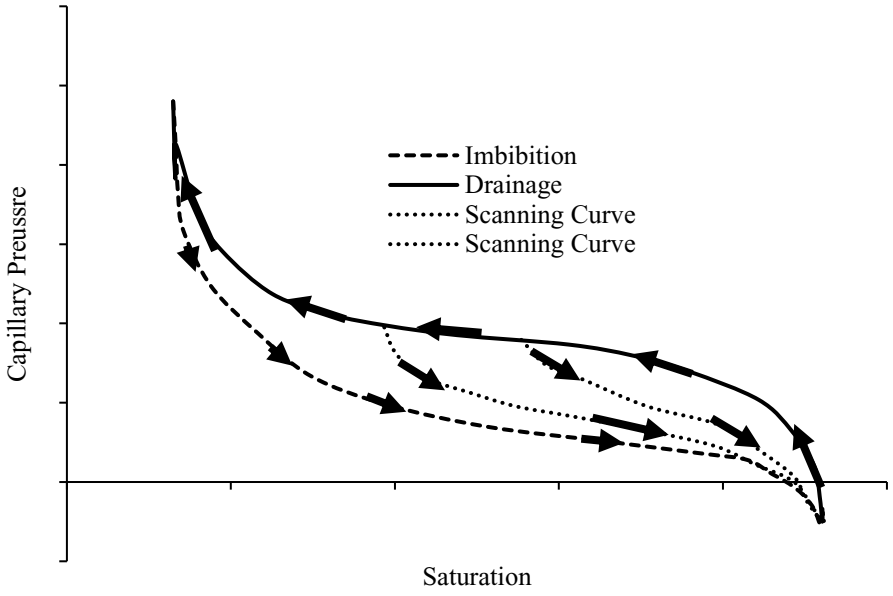

Figure 3. 2. Capillary pressure hysteresis characteristic (Killough, 1976)

$$P_c(S_w) = P_c^{Dr/Im}(S_w) - F^{Dr/Im}.[P_c^{Dr}(S_w) - P_c^{Im}(S_w)] \tag{3.1}$$

where

$$F^{Dr} = \frac{\frac{1}{S_w - S_w^{Hys} + \epsilon} - \frac{1}{\epsilon}}{\frac{1}{S_w^{Max} - S_w^{Hys} + \epsilon} - \frac{1}{\epsilon}} \tag{3.2}$$

$$F^{Im} = \frac{\frac{1}{S_w^{Hys} - S_w + \epsilon} - \frac{1}{\epsilon}}{\frac{1}{S_w^{Hys} - S_{wr} + \epsilon} - \frac{1}{\epsilon}} \tag{3.3}$$

For the scanning curves at turnaround saturation, the equations are given below:

$$P_c(S_w^*) = P_c^{Dr/Im}(S_w^*) - F^{*(Dr/Im)} * [P_c^{Dr}(S_w^*) - P_c^{Im}(S_w^*)] \tag{3.4}$$

where

$$F^{*Dr} = \frac{\frac{1}{S_w^* - S_w^{*Hys} + \epsilon} - \frac{1}{\epsilon}}{\frac{1}{S_w^{Hys} - S_w^{*Hys} + \epsilon} - \frac{1}{\epsilon}} \tag{3.5}$$

$$F^{*Im} = \frac{\frac{1}{S_w^{*Hys} - S_w^* + \epsilon} - \frac{1}{\epsilon}}{\frac{1}{S_w^{*Hys} - S_{wr} + \epsilon} - \frac{1}{\epsilon}} \tag{3.6}$$

To obtain the unknown S_w^{*Hys}, Killough proposed the following equation:

$$1 - F^{Dr/Im} = F^{*(Dr/Im)} \tag{3.7}$$

The above equations confirmed that the hysteresis phenomenon could be explained in terms of a mathematical formula. Using this model in reservoir simulation, it is possible to save time and use only limited storage compared to other simulators (Killough, 1976). However, this model is more effective and accurate compared to others. However, still, it cannot be used without experiments to obtain the parameter ϵ. Artificial techniques might be needed to eliminate some noise in the data, especially when multiple reversals take place on scanning curves (Killough, 1976; Kossack, 2000). Another drawback of this model is that it does not have a simple geometric interpretation (Kossack, 2000). In addition, although the majority of oil reservoirs are mixed-wet (Morrow, 1990), this model is developed only for strong water-wet porous media (Delshad et al., 2003), which may limit its utilization.

Another model that mathematically described hysteresis in capillary pressure was developed by a Brooks and Corey function (Brooks and Corey, 1966; Delshad et al., 2003). The main ideas of this model are to (i) develop the main drainage curve using a Brooks and

Corey function, (ii) model the scanning curves by using an S-shaped function (Lenhard, 1992; Van Genuchten, 1980), and (iii) compute residual oil saturation accurately by taking into account the size of the pores that are oil-wet. This model was tested against experimental data for two-phase flow in mixed-wet rock capillary pressure data; the results were qualitatively confirmed.

The main drainage capillary pressure is modelled using the following equation:

$$\mathrm{P_c} = \mathrm{p_d}(\mathrm{S^n_w})^{-\frac{1}{\lambda}} \tag{3.8}$$

where p_d is displacement (entry) pressure; n refers to a curve-shaped parameter, and λ is the pore-size distribution index. This model considers the pore-size distribution in the rock as a factor that plays a key role in the hysteresis in capillary pressure.

For the main imbibition curve, the proposed model can be generated by a reversal from the main drainage using scanning-path saturation relations developed by Lenhard and Oostrom (Delshad et al., 2003). The proposed equation is given below:

$$\overline{\mathrm{S_w}}(\mathrm{P_c}) = 1 + \frac{\left[\overline{\mathrm{S_w}}^{\mathrm{I}}(\mathrm{P_c}) - 1\right]\left(\overline{\mathrm{S_w}}^{\mathrm{ID}} - 1\right)}{\overline{\mathrm{S_w}}^{\mathrm{I}}(\mathrm{P_c^{DI}}) - 1} \tag{3.9}$$

where P_c^{DI} is the capillary pressure at a reversal from the main drainage; $\overline{S_w}^{I}(P_c)$ and $\overline{S_w}^{I}(P_c^{DI})$ introduce the effective water saturation at the capillary pressure and capillary pressure at the reversal point, respectively.

As mentioned earlier, the scanning curves are modelled by using an S-shaped function,

which is also known as van Genuchten's function (Lenhard, 1992; Van Genuchten, 1980) as follows:

$$P_c = P_{neg} + \frac{1}{\alpha}\left[\frac{1}{(\bar{S}_w)^{\frac{1}{m}}} - 1\right]^{1/n} \tag{3.10}$$

where

$$\bar{S}_w = \frac{S_w - S_{iw}}{1 - S_{iw} - S_{or}} \tag{3.11}$$

Here P_{neg} is the maximum negative capillary pressure when saturation reaches a maximum value on the main imbibition curve, and $\alpha, n,$ and m are the model fitting parameters. The assumptions of n and m for drainage and imbibition follow the investigations of Kool and Parker (1987).

The model was tested against experimental data for mixed-wet rocks from past literature. Another feature of this model is the consideration of pore size distribution in the mathematical calculations for hysteresis in capillary pressure. The model involves parameters such as λ, $\alpha, n,$ and m, which need to be calibrated using both experimental and mathematical modelling. Compared to simulations that do not consider hysteresis, this model requires more memory storage (Delshad et al., 2003).

Models of Killough (1976) and Delshad et al. (2003) focused on two-phase systems. Leverett (1941) suggested for the first time that two-phase capillary pressure and saturation relationships can be extended to three-phase systems (Miller et al., 1998). Based on the

Leveret assumption, a model to represent hysteresis mathematically up to three immiscible fluid phases was proposed by Parker and Lenhard (1987a). The model is able to use water saturation versus air-water capillary pressure in two-phase flow systems and the total liquid saturation versus air-oil water capillary pressure in three-phase systems. The model generates the mathematical equations that represent hysteresis by assuming a scaled saturation-capillary head function $S^*(h^*)$ that may be obtained for a porous medium (Parker and Lenhard, 1987b).

It is known that in three-phase systems, the average water saturation ($\bar{S}_w$) is a function of the only oil-water capillary head (h_{ow}), and the average trapped saturation ($\bar{S}_t$) is a function of air-oil capillary head (h_{ao}) in the absence of fluid entrapment (Brooks and Corey, 1966; Leverett, 1941; Parker and Lenhard, 1987a). Using this assumption, the fluid entrapment effects can be ignored. Moreover, $\bar{S}_w(h_{ow})$ and $\bar{S}_t(h_{ao})$ can be assumed as independent hysteretis functions.

Using van Genuchten's function (Van Genuchten, 1980), the main imbibition and drainage curves of the scaled function for $h^* \geq 0$ can be described by the following expression:

$$\mathrm{S^*(h^*)_i} = (1 + (\propto_{\mathrm{i}} \mathrm{h^*})^{\mathrm{n}})^{-\mathrm{m}} \tag{3.12}$$

$$\mathrm{S^*(h^*)_d} = (1 + (\propto_{\mathrm{d}} \mathrm{h^*})^{\mathrm{n}})^{-\mathrm{m}} \tag{3.13}$$

where *i* and *d* refer to the imbibition and drainage, respectively. Also $\propto, n,$ and m are curved shape parameters. In the case of $h^* < 0$, the following expression is valid.

$$\mathrm{S^*(h^*)_i} = \mathrm{S^*(h^*)_d} = 1 \tag{3.14}$$

For modelling the scanning curves, the model follows the same procedures that Kool and Parker (1987) followed, except the assumption of the closure of scanning curves. The following equations describe scanning curves for the imbibition and drainage, respectively:

$$S^*(h^*) = \{[S^*(h^*)_i - S^*(h_{id}{}^*)_i][S_{di}{}^* - S_{id}{}^*]\} * \{S^*(h_{di}{}^*)_i - S^*(h_{id}{}^*)_i\}^{-1} + S_{id}{}^* \quad (3.15)$$

where $S^*(h_{id}{}^*)_i$ and $S^*(h_{di}{}^*)_i$ are values of $S^*(h^*)_i$ as given in Equation (3.12), *id* refers to the drainage to imbibition, and di refers to the imbibition to drainage. Then

$$S^*(h^*) = \{[S^*(h^*)_d - S^*(h_{di}{}^*)_d][S_{id}{}^* - S_{di}{}^*]\} * \{S^*(h_{id}{}^*)_d - S^*(h_{di}{}^*)_d\}^{-1} + S_{di}{}^* \quad (3.16)$$

where $S^*(h_{id}{}^*)_d$ and $S^*(h_{di}{}^*)_d$ are values of $S^*(h^*)_d$ given in Equation (2.13).

When comparing the model results to experimental data, the results show close agreement, especially for scanning paths (Lenhard, 1992). Despite this model's accuracy for two-phase and even three-phase systems, the model's scaling factors, which were determined through regression analysis, were different when the model was used in two different porous media (Lenhard, 1992). Therefore, this model should consider the contact angle effect and experimental uncertainty if it needs to be applied for three-phase systems. When using this mathematical model for different porous media, an accurate approach to estimate the scaling factors (not scaling paths) is required, which can be obtained by the ratio of interfacial tensions of these media (Delshad et al., 2003; Parker and Lenhard, 1987b, 1987a).

Modelling of hysteresis in capillary pressure can be divided into two categories: (i) mathematical base and (ii) simulation base. In this section, the applications of hysteresis in terms of the simulation aspect are discussed. **Table 3.1** presents the basic and widely used

models that describe the hysteresis phenomenon in two and three-phase flow systems. Fundamentally, these models characterize the role of each factor in determining the hysteresis behaviour (Dullien, 1992; Miller et al., 1998).

Table 3. 1. Hysteresis models for capillary pressure systems

Reference	Mathematical Formula	System	Analysis
Two-Phase Systems			
(Brooks and Corey, 1966; Miller et al., 1998)	$\bar{S}_w = (\epsilon P_c)^{-\lambda} \quad (\epsilon P_c) > 1$	Air-Water	(i) Applicable for isotropic and anisotropic media
	$\bar{S}_w = 1 \quad (\epsilon P_c) \leq 1$		(ii) For main drainage curve
(Killough, 1976)	$P_c(S_w) = P_c^{Dr/Im}(S_w) - F^{Dr/Im} * [P_c^{Dr}(S_w) - P_c^{Im}(S_w)]$	Water-Oil and Gas-Oil	(i) Applicable for imbibition, drainage, and scanning curves
	$F^{*Dr} = \frac{\frac{1}{S_w^* - S_w^{*Hys} + \epsilon} - \frac{1}{\epsilon}}{\frac{1}{S_w^{Hys} - S_w^{*Hys} + \epsilon} - \frac{1}{\epsilon}}$ $F^{*Im} = \frac{\frac{1}{S_w^{*Hys} - S_w^* + \epsilon} - \frac{1}{\epsilon}}{\frac{1}{S_w^{*Hys} - S_{wr} + \epsilon} - \frac{1}{\epsilon}}$		(ii) Minimum time and small memory storage
(Van Genuchten, 1980)	$\bar{S}_w = \left[\frac{1}{1+(\propto P_c)^n}\right]^m (m = 1 - \frac{1}{n}) \quad P_c > 0$	Soil-Water	(i) Simple compared to others
	$\bar{S}_w = 1 \quad P_c \leq 0$		(ii) For the main drainage curve
(Delshad et al., 2003)	$P_c = p_d(S^n{}_w)^{-\frac{1}{\lambda}} \quad P_c \geq p_d$	Mixed-wet	(i) Used S-shape and Van Genuchten's function (Parker and Lenhard, 1987a; Van Genuchten, 1980)
	$S^n{}_w = \frac{S_w - S_{wr}}{1 - S_{wr}}$		(ii) Applicable for imbibition, drainage, and scanning curves
(Lenhard and	$\overline{\overline{S^D}}_w = [1 + \{\alpha_d(P_c - P_{max})\}^{n_s}]^{-m_s} \quad P_c \geq P_{max}$	Mixed-wet	(i) Modified from Van Genuchten's model (Van

Oostrom, 1998)			Genuchten, 1980) to be used in mixed-wet media.
	$\bar{\bar{S}}^{I}_{w} = [1 + \{\alpha_i(P_c - P_{max})\}^{n_s}]^{-m_s} \quad P_c \geq P_{max}$		(ii) Applicable for imbibition, drainage, and scanning curves
(Wang and Alvarado, 2016a)	$P_{nw} - P_w = P_c - \tau \frac{\partial S_w}{\partial t} \quad 10^4 \leq \tau \leq 10^7$	Low salinity water-oil	(i) Mainly developed for dynamic systems
	$\tau = \frac{\alpha \emptyset \mu}{k\lambda}\left(\frac{P_e}{\rho_g}\right)^2$		(ii) Applicable for imbibition and drainage
(Kleppe et al., 1997)	$S_g = S_{gr}^{max} + \left[\frac{S_g(P_c - P_{c1}) - S_{gr}^{max}}{S_{g1} - S_{g2}}\right](S_g - S_{g2})$	Gas-Oil	(i) Modified for Killough model
	$S_{g1} \geq S_g \leq S_{g2}$		(ii) Applicable for imbibition, drainage, and scanning curves
	$P_c = P_c^{Dr/Im} - F^{Dr/Im} * [P_c^{Dr} - P_c^{Im}]$		
	$F^{Dr} = \frac{\frac{1}{\overline{S_{g1} - S_g + \epsilon}} - \frac{1}{\epsilon}}{\frac{1}{S_{g1} - S_{gr}^{max} + \epsilon} - \frac{1}{\epsilon}}$		
Three-Phase Systems			
(Miller et al., 1998; Parker and Lenhard, 1987a)	$(\bar{S})_i = (1 + (\propto_i P_c)^n)^{-m} \quad P_c > 0$ $(P_c)_i = 1 \quad P_c \leq 0$ $(\bar{S})_i = \frac{S_i - S_r}{1 - S_r}$	Aqueous phase wetting	(i) Contact angle effects should be considered
	$(\bar{S})_d = (1 + (\propto_d h^*)^n)^{-m} \quad P_c > 0$ $(\bar{S})_i = 1 \quad P_c \leq 0$ $(\bar{S})_d = \frac{S_d - S_r}{1 - S_r}$		(ii) Applicable for imbibition, drainage, and scanning curves
(Lenhard et al., 1989; Miller et al., 1998)	$\tilde{S}_w(P_c) = \frac{\left(\tilde{S}^{I}_{w}(P_c) - \tilde{S}^{I}_{w}(P^{ID}{}_c)\right)\left(\tilde{S}^{DI}_{w} - \tilde{S}^{ID}_{w}\right)}{\tilde{S}^{I}_{w}(P^{DI}{}_c) - \tilde{S}^{I}_{w}(P^{ID}{}_c)} + \tilde{S}^{ID}_{w}$	Aqueous phase wetting	(i) Modified of Van Genuchten's model (Van Genuchten, 1980) to be used in simulation
	$\tilde{S}_w = \bar{S}_w + \frac{S_{nwt}}{1 - S_{rw}}$		(ii) Applicable for imbibition, drainage, and scanning curves

3.2.2. Experimental Observations of Hysteresis in Capillary Pressure

Experimental validation of the existence of hysteresis in capillary pressure has been studied previously (Killough, 1976; Morrow, 1970; Szabo, 1974). The most common method to test hysteresis in capillary pressure is the bi-stability of an interface in a non-uniform tube (Morrow, 1970). This experiment was used to explain the principles of hysteresis in capillary pressure in porous media (Crawford and Hoover, 1966; Haines, 1930; Morrow, 1970). During the intrusion of pore spaces by a fluid, small fluctuations in pressure happen because of the instability of interface configurations, which cause hysteresis in the capillary pressure (Haines, 1930; Morrow, 1970).

One of the static methods to investigate hysteresis in capillary pressure is called mercury injection (Brown, 1951; Nooruddin et al., 2014; Pickell et al., 1966; Purcell, 1950, 1949; Wardlaw and Taylor, 1976). The mercury injection method is relatively simple, fast, and low cost compared to other methods. Moreover, it is used to interpret the size and shape of the pores and throats in porous media (Dumore and Schols, 1974; Greder et al., 1997; Wardlaw and Taylor, 1976). However, mercury injection techniques, at high capillary pressure values, may underestimate water saturation compared to oil/brine outcomes (Greder et al., 1997). During the hysteresis in capillary pressure using the mercury injection technique, several authors showed that the capillary pressure estimations are dependent on the structure of porous media but also on rock and fluid interactions, temperature, and confinement and pore pressure, which indicates the necessity of measuring hysteresis under reservoir conditions (Greder et al., 1997).

The other main static method is to restore state technique of Leverett (Leverett, 1941) and Bruce *et al.* (Bruce and Welge, 1947; Rose and Bruce, 1949). This method is more representative than mercury injection because it considers reservoir conditions (Greder et al., 1997). Moreover, it is suitable for unconsolidated reservoir systems. However, this technique is relatively costly, very slow, and cannot be applied to a large number of cores (Greder et al., 1997). Both mercury injection and restore state methods give similar capillary pressure results if the proper conversion factors are chosen (Brown, 1951).

A similar technique to the restore state method is the centrifuge technique of Hassler and Brunner (1945). One of their assumptions was that as the sample is far away from the rotation axis, the saturation region always reaches 100% (Wunderlich, 1985). This technique is faster compared to the restore state method because equilibrium is obtained more quickly due to the gravity effect (Evans and Geurrero, 1979). Many authors (Cano Barrita et al., 2008; Green et al., 2008; Omoregle, 1988) referred to the equilibrium in centrifuge technique as hydraulic equilibrium, not thermodynamic equilibrium as suggested by Morrow (1970), which cannot be achieved in the laboratory or the reservoir (Omoregle, 1988). Although the centrifuge technique is widely used in the oil and gas industry to measure capillary pressure (Omoregle, 1988), it is limited to test hysteresis phenomena in capillary pressure because of its lack of ability to measure the imbibition cycle (Evans and Geurrero, 1979; Hassler and Brunner, 1945) and the equilibrium state in the centrifuge environment is not well defined (Wunderlich, 1985). Moreover, the data must be smoothed before calculations (Hassler and Brunner, 1945).

Another popular technique that is used to investigate hysteresis in capillary pressure is the

porous–plate method, which was originally proposed by Omoregle (1988) and later developed by McCullough et al. (1944) and others (Bruce and Welge, 1947; Rose and Bruce, 1949; Thornton and Marshall, 1947). This technique uses a highly hydrophilic capillary diaphragm placed at the bottom of the sample and can restore conditions close to reservoir conditions (Longeron et al., 1989b). The porous plate is a technique considered to be the most direct and accurate method to test hysteresis in capillary pressure (Cano Barrita et al., 2008; Green et al., 2008). The equilibrium can be controlled not only by the rock properties but also by the porous plate's properties and the contact between the plate and the sample (Omoregle, 1988). This method also can be applied to unconsolidated samples (Greder et al., 1997). Although it is direct and accurate, many authors reported that it is time-consuming, which usually takes weeks or months to reach the equilibrium state for each capillary pressure point (Cano Barrita et al., 2008; Green et al., 2008). Moreover, this technique is costly, cannot be applied to a large set of samples, and gives large errors for capillary pressure hysteresis values beyond 10 bars (Greder et al., 1997).

The dynamic capillary pressure measurement technique is one method that can be used to investigate hysteresis in capillary pressure. Brown (1951) first proposed this technique by using the measurements taken by the Hassler and Brunner technique (Hassler and Brunner, 1945). In this method, two fluids are allowed to flow through the sample simultaneously, and once the equilibrium state is reached, both liquids continue to flow, but their saturation does not change (Brown, 1951). The apparatus of this technique consists of two end plates; one of them is a disc diaphragm, which controls the pressure in the oil phase, and the other is a ring diaphragm, which allows the oil to flow through (Hassler and Brunner, 1945).

An experimental method that can measure the hysteresis in capillary pressure was introduced by Kleppe et al. (1997). The main idea of this method is the scaling of the data that is obtained from the drainage and imbibition of capillary pressure to saturation ranges, which make it suitable for usage in simulation models. This method gives accurate measurements that can be used to construct the hysteresis curves for the capillary pressure. This method gave a better explanation for computing hysteresis; by using scaled data, compared to that proposed in simulations by Killough (1976). However, the Killough method assumes that the drainage and imbibition curves meet at the residual saturation, which is not always the case (Tan, 1990).

More recently, some advanced experimental techniques have been developed to measure capillary pressure, for example, X-Ray CT (Dernaika et al., 2011b; Wang and Alvarado, 2016b), Nuclear Magnetic Resonance (NMR) (Green et al., 2008), Magnetic-Resonance-Imaging (MRI) (Cano Barrita et al., 2008), Capillary Pressure and Resistivity Index by Continuous Injection (CPRICI) (Kokkedee and Boutkan, 1995; Masalmeh, 2001), and a Capillary pressure Probe (Wunnik; et al., 1999). These advanced methods can overcome some of the limitations of conventional techniques; for example, the use of MRI can lower the time requirement (Cano Barrita et al., 2008; Green et al., 2008). Also, the methods can give a better explanation of hysteresis phenomena in capillary pressure. In addition, these recent techniques are designed to take measurements under reservoir conditions (Kokkedee and Boutkan, 1995).

To compare these techniques and their effectiveness in investigating the hysteresis phenomenon, several authors conducted experimental studies. The literature shows that

restore state and mercury injection methods gave nearly identical curves when plotted within an appropriate scale (Brown, 1951; Purcell, 1950, 1949). Another comparison between static methods and the dynamic method showed that the results were almost similar, which indicates that the static techniques are valid in dynamic systems (Brown, 1951). Good agreement was also found between the centrifuge technique and the porous–plate method in low water saturation (Greder et al., 1997; Melrose, 1990; Sabatier, 1994). One study was conducted to compare mercury injection and porous–plate techniques; again, a match was found but not for all tested samples (Sabatier, 1994).

On the other hand, under reservoir conditions, mercury injection and the porous–plate method did not give a good match when different fluid pairs were used (Bouvier and Maquignon, 1991; Longeron et al., 1989a). This difference was due to two reasons: the first was due to effective stress, and the second was due to a lack of equilibrium in the test (Greder et al., 1997; Swanson, 1985). Another study pointed out that the mercury injection technique gave low values when fluid pairs were used, such as oil – brine and gas – brine (Hamon, G., & Pellerin, 1997; Sabatier, 1994).

Most studies that investigate the hysteresis in capillary pressure were conducted for the two-phase system either with oil – brine, gas – brine, or oil – gas; only a few recent studies were done on a three-phase system of water – gas – oil (Habte et al., 2015; Kantzas et al., 1998). There is an opportunity for researchers and investigators to explore further.

3.3. Hysteresis in Permeability and Porosity

In Petroleum and Geomechanics Engineering, understanding the hysteresis phenomenon on porosity and absolute permeability is required for hydrocarbon production in a reservoir. Hysteresis has a significant role in porous media and depends on several physical and mechanical properties.

3.3.1. Modelling of Hysteresis in Porosity

There are two primary types of equations that can be used to describe the relationship between confining pressure and porosity: 1) exponential (Hoholick et al., 1984), and 2) power-law (David et al., 1994). For the exponential relationship, the following equation can be used for shale, sandstone and carbonate formation (Dong et al., 2010):

$$\phi = \phi_o \exp\left(-\beta(P_e - P_o)\right) \tag{3.17}$$

where ϕ is the porosity under the effective confining pressure, ϕ_o is porosity under atmospheric pressure, β is a material constant.

For the power law:

$$\phi = \phi_o \left(\frac{P_e}{P_o}\right)^{-q} \tag{3.18}$$

where q = a material constant.

Dong et al. (2010) used these two equations to investigate the hysteresis phenomenon mathematically, using experimental data, under the influence of: i) a deformation mechanism, ii) stress range and maximum overburden, iii) sample anisotropy and sample

length and iv) using gas as a fluid on the stress dependency of permeability. Their work indicated that power-law and exponential methods described the relationship between hysteresis and confining pressure almost identically for all tested formations (sandstone and shale). In addition, after applying Klinkenberg correction, the exponential hysteresis of porosity for sandstone was close to theoretical values, while much higher in shale. Few recommendations were suggested in this study to improve the work quality, such as using an explicit form of the power-law model that must be incorporated to give more accurate results when specific storage is included.

Another recent study carried by Civan (2017) used the expression of effective stress, which is the difference between the confining pressure and pore fluid, to build up the mathematical model.

$$\sigma_{eff} = P_c - XP_e \tag{3.19}$$

where X is the Biot coefficient (Biot, 1941).

Civan showed that one relationship for porosity and effective stress for shale formations could not be used for the whole range of effective stress data. The reason was slope discontinuities were observed in both cases, loading and uploading. Moreover, the study referred to reasons for hysteresis due to the many variables, such as elastic and plastic deformation shearing, grain fracture and material ageing. Furthermore, in this study, a mathematical model was proposed for the whole range of effective stress data. This can be shown as:

$$\phi = \phi_\infty + (\phi_0 - \phi_\infty)\left(\frac{\sigma_{\text{eff}} - \sigma_{\text{cr}}}{\sigma_{\text{eff},0} - \sigma_{\text{cr}}}\right)^{A_2(c_0 - c_\infty)} \quad (3.20)$$

where ϕ = total porosity, σ_{eff} = effective stress, $\sigma_{eff,0}$ = initial effective stress, σ_{cr} = critical effective stress, c_0 and c_∞ = represent the coefficients of compressibility at zero and infinite effective stresses.

The outcome of this study agreed with Dong et al. (2010), which correlated the whole range of effective stress data with one equation that would lead to incorrect results and predictions. Instead, the data must be correlated separately before and after the critical effective shear stress. The reason for is the relative contribution of fracture changes by transition across the effective critical stress.

3.3.2. Modelling of Hysteresis in Permeability

Material properties, such as permeability, can be altered by effective stress in the mathematical expression of Warpinski and Teufel (1992),

$$X = F(\sigma - \propto p) \quad (3.21)$$

where X = property or process of the material such as permeability, porosity, or deformation, and F = generalized function.

Equation 3.21 is a general function that describes the relationship between any property of the material (e.g., permeability) and the effects of stress. Numerous studies used this formula to investigate what kind of expression correlates the relationship. For example, Jones and Owens (1980) presented the relationship between permeability and effective stress as

$$\left(\frac{k}{k_o}\right)^{1/3} = \log\left(\sigma - \propto p\right) \tag{3.22}$$

where k and k_0 are permeabilities at a given net stress and a minimum applied net stress, respectively.

Similarly, Teklu et al. (2016b) found the same relationship, a cubic root of permeability of tight formation with the net stress, from experimental work. In the conclusion of the Teklu et al. (2016b) study, a mathematical model was proposed for representing the hysteresis phenomenon in permeability,

$$k = \frac{\mu(p_{avg})c_g(p_{avg})Vl}{A} \frac{\Delta \ln\left(\frac{p^2_{upstream-}p^2_{initial}}{p^2_{upstream-}p^2(l,t)}\right)}{\Delta t} \tag{3.23}$$

where k, l and A are permeability, core length and cross-section area, respectively. Also, V is downstream volume, and μ and c are gas viscosity and compressibility at an average pore pressure p and over a time interval Δt.

The three studies of Teklu et al. (2016b) used the same correlation for permeability to investigate the hysteresis. As results of these studies, it was reported that: i) the hysteresis of permeability in fractured cores was more noticeable than in the matrix, ii) the hysteresis during the second and third cycles of effective stress was undistinguished; therefore, it was negligible, while it was observed in the fracture cores during the second and third cycle. The reason was the increase of the effective permeability in the fracture cores in which the loading and unloading opened new paths and connected the fractures.

Similar to Equation (3.17), an exponential equation was suggested by David et al. (1994) to correlate the net stress and the permeability,

$$k = k_o \exp\left(-\gamma(P_e - P_o)\right) \tag{3.24}$$

where γ is the material constant (γ = 9.81 - 18.1x10^3 MPa^{-1}).

On the other hand, Shi and Wang (1986) suggested a power-law relationship instead of exponential,

$$k = k_o \left[\frac{P_e}{P_o}\right]^{-p} \tag{3.25}$$

where p is an experimentally determined constant.

A comparison between these two relationships, power-law and exponential, was reported in the study of Dong et al. (2010). In general, the hysteresis behaviour was more observable when using power-law than the exponential relationship in most of the tested rocks. The exponential formula underestimated the permeabilities when the effective pressure was low or high.

In the study of Civan (2017), a new mathematical formula was proposed. The compressibility of the matrix, solid and fracture was incorporated in this model. The final form of this model is presented in Equation (3.26) below,

$$k = k_\infty + (k_0 - k_\infty)\left(\frac{\sigma_{eff} - \sigma_{cr}}{\sigma_{eff,0} - \sigma_{cr}}\right)^{A_2(c_0 - c_\infty)} \tag{3.26}$$

The same conclusion as the porosity was also highlighted in the permeability (Dong et al., 2010) to represent the whole data set. Instead, the proposed model in Equation (3.26) can

represent the data without giving a discontinuity in the plots. Equation (3.26) was modelled based on analyzing and correlating the experimental data of Dong et al. (2010) and Heller et al. (2014).

3.3.3. Experimental Observations of Hysteresis in Permeability and Porosity

Teklu et al. (2016b) investigated the permeability and porosity hysteresis in a low permeability formation (see **Figure 3.3**). They found that both permeability and porosity were inversely proportional to net stress. In their study, nano, micro, and milliDarcy core samples were used to measure the porosity and permeability hysteresis with net stress. Permeability was measured in broken cores using the Gas Research Institute (GRI) method (see Cui et al., 2009; Institute, 1998; Luffel et al., 1993; Luffel and Guidry, 1992; Profice et al., 2011; Tinni et al., 2012)). Teklu et al. (2016b) used a GRI method to measure porosity. Permeability values ranged from 0.000037mD to 3.029mD. The porosity ranged from 4.8% to 18.13%, the net stress was between 500 to 1000 psi, and the temperature effect on permeability showed a direct relationship that when permeability increases, temperature increases as well. This behaviour between permeability and temperature is different than what has been reported by Sinha et al. (2013). Teklu et al. (2016b) demonstrated the phenomenon of hysteresis in permeability and porosity in loading and unloading for net stress. Generally, the outcomes followed many past studies that reported the empirical models of permeability and net stress.

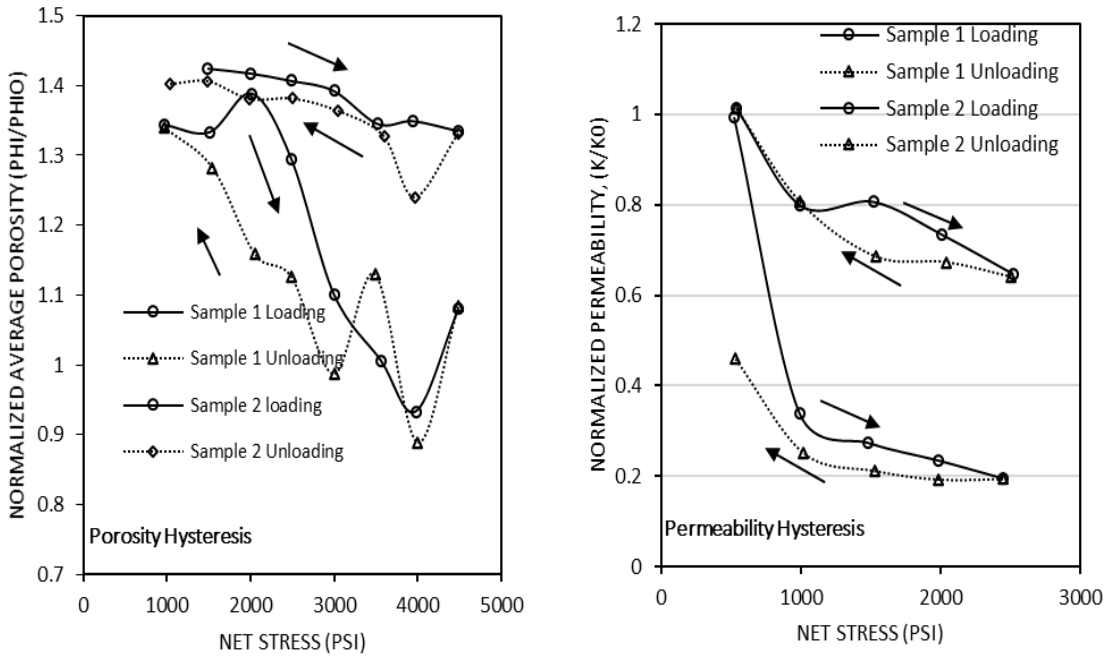

Figure 3. 3. Porosity and Permeability – Net Stress Hysteresis for Low Permeability Formation (Teklu et al., 2016b).

Another study by Teklu et al. (2016c) investigated the hysteresis behaviour on cyclic (three times) permeability-porosity and net stress for carbonate rocks from Middle East reservoirs. During the cyclic permeability and porosity versus net stress, some unusual behaviour of carbonate samples was observed. One of the samples showed a fluctuation in its trend in cyclic permeability values compared to the general observation. The reason for this behaviour is microcracks. These were noticed during the experiment as it was closed at some stress conditions and opened at other stress conditions. This observation indicated that cyclic injection could improve the techniques of hydraulic fractures in tight reservoirs. Although there is some conflict in a few samples, the general trend for carbonate samples is the same for shale samples in the first study (Teklu et al., 2016b). It was concluded that both permeability and porosity increase with a decrease of net stress, and hysteresis values

in the first cycle were followed by the second were considered while in the third cycle, it was neglected. Also, it was concluded that cyclic hysteresis could be used mostly in low formation reservoirs.

Another study by Teklu et al. (2016a) highlighted the cyclic matrix permeability hysteresis during stress loading and unloading on tight reservoirs. Many studies focused on the hysteresis phenomenon during loading and unloading stress versus cyclic fracture and matrix permeability for different formations, such as Nelson and Handin (1977), Kranzz et al. (1979), Witherspoon et al. (1980), Bernabe (1987), Morita et al. (1992), and Selvadurai (2015). However, this study observed that matrix and fracture permeability hysteresis have different behaviour during loading and unloading of the net stress. When the matrix permeability increases with a decrease in net stress, the fracture permeability can sometimes decrease with a decrease in net stress (Nelson and Handin, 1977). Both pore pressure and confining stress effects on permeability were investigated in this study for a tight reservoir at 250^0 F. Samples that were used in this study have a 1-inch diameter, 2-inch length, 0.0419 to 0.0963 matrix porosity, 0.0846 to 0.103 fracture porosity, 71.7 to 314 nano-Darcy matrix permeability, and 0.257 to 398 mDarcy fracture permeability. The Nitrogen pressure in this study varied from 500psi to 5000psi. It was found that fracturing during hysteresis can improve the permeability from nanoDarcy to millieDarcy levels, especially at a high stress of 5000psi. At this pressure, porosity is negligible. Also, matrix permeabilities were found to be less stress dependent than fracture permeabilities.

Figure 3.4 shows a diagram of a Formation Response Tester (FRT), which was used by Teklu et al. (2016a-c). This device is designed to measure the permeability change of the

samples during the flooding of different fluids. It can handle three paths forward, backward, and across the face direction up to a 177^0 C temperature. Teklu *et al.* (2016a-c) used this device as a steady-state method for determining the permeability.

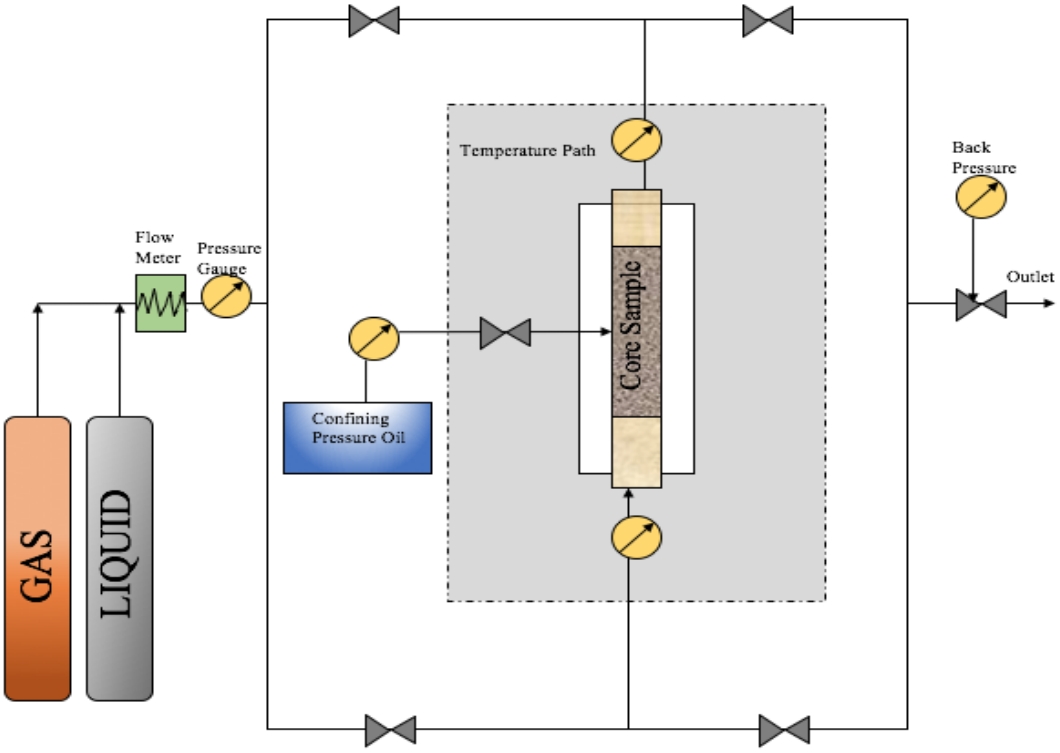

Figure 3. 4. Diagram of the Formation Response Tester (FRT) (Chandlereng, 2017)

Maiti et al. (2008) distinguished the role of hysteresis of particle porosity in trickle-bed reactors (TBRs) by selecting particles of different pore density materials. This type of reactor is mostly used in the oil refinery and petrochemical industry (Larachi et al., 1998; Maiti and Nigam, 2007; Nigam; et al., 2011). Although this study did not focus on porous media but rather TBRs, it showed how the hysteresis behaviour is important in particle porosity. From the same material, particles of three different pore densities (nonporous, semi-porous, porous) were used to investigate the hysteresis phenomenon. All three types

of particles were used under dry and wet-bed conditions to determine the pressure drop hysteresis. From their study, the pores played a significant role in hysteresis of TBRs.

In the dry-bed case, open loop hysteresis was observed during the first cycle of operation, and hysteresis increases with an increase of pore density for the particles. On the other hand, in the wet-bed case, open loop hysteresis is hardly noticeable, but the behavior of hysteresis with a pore density of the particles is the same as the dry-bed case. Comparing the three types of particles, porous particles showed the highest amount of hysteresis in the wet-bed procedure.

Other past studies investigated the hysteresis behaviour for porosity and permeability in non-porous media. Bendix et al. (2016) investigated the hysteresis due to the change of porosity of Silicone binder-based zeolite coatings for temperature and mechanical stability. Another study by Potter et al. (2008) examined the magnetic and hysteresis measurements and their effects on several petrophysical properties. Other related studies can be found in past studies of Ivakhnenko and Potter (2008, 2004) and Potter (2007).

3.4. Hysteresis in Relative Permeability

Among the rock properties, relative permeability was most widely investigated experimentally for hysteresis. Relative permeability is a key parameter in two-phase flow in porous media (Kadet and Galechyan, 2014; Wang and Alvarado, 2016a). **Figure 3.5** depicts an example of relative permeability hysteresis.

3.4.1. Modelling of Hysteresis in Relative Permeability

The mathematical hysteresis models of relative permeability have been developed to

investigate complex recovery scenarios and production plans, especially in reservoir simulators (Killough, 1976).

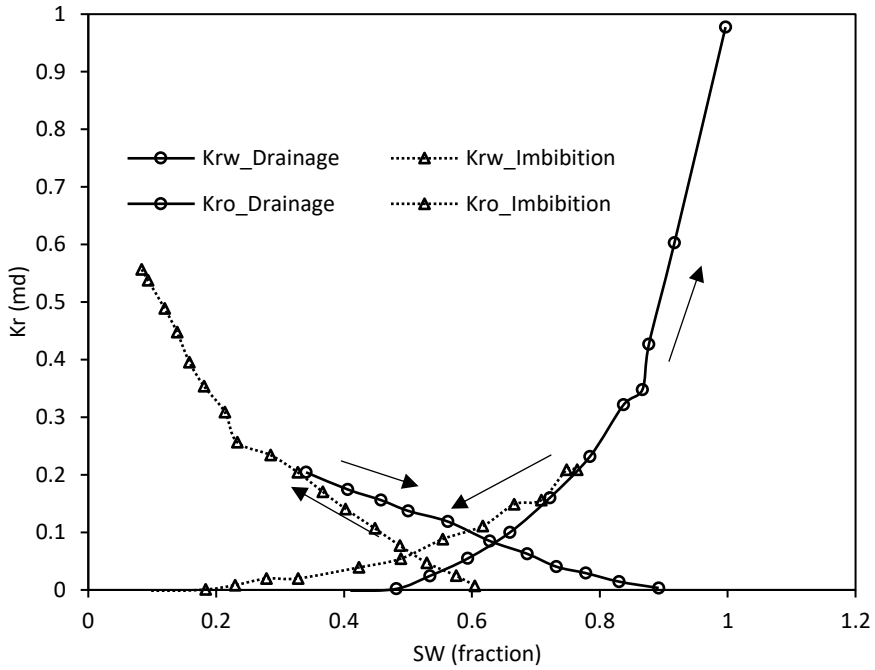

Figure 3. 5. Relative Permeability – Saturation Hysteresis (Kadet and Galechyan, 2014)

Furthermore, experiments have some limitations, such as time-consuming, cost, limitation in one system (water-wet or oil-wet) and machine errors. Therefore, there is a need for a mathematical model that is accurate and applicable to more than one system. To that extent, several studies attempted to develop a mathematical model that is complete, consistent and accurate to describe the hysteresis phenomenon in relative permeability.

Generally, mathematical models for hysteresis have a long history since 1935 when Preisach (1935) developed the first model that described the hysteresis phenomena but not related to relative permeability; it was in the area of magnetic fields. The most widely used mathematical model for hysteresis in relative permeability was developed empirically by

Land (1968) and modified by Killough (1976), which can reproduce the hysteresis curves by remembering the history of saturation. The main assumption of this model was that relative permeability must lie initially on one of the bounding imbibition or drainage curves. Accordingly, the model was developed for two main cases: drainage to an imbibition scanning loop and imbibition to a drainage scanning loop; as well as scanning curves at the turnaround saturation, where the hysteresis's saturation is unknown. This model can be described using the following equations:

$$K_{rN}^{Im}(S_N) = K_{rN}^{Dr}(S_N^{Hyst}).\left[\frac{K_{rN}^{Exp}(S_N^{Norm}) - K_{rN}^{Exp}(S_{Nr}^{Max})}{K_{rN}^{Exp}(S_N^{Max}) - K_{rN}^{Exp}(S_{Nr}^{Max})}\right] \quad (3.27)$$

where

$$S_{Nr} = \frac{S_N^{Hyst}}{1 + C * S_N^{Hyst}} \quad (3.28)$$

$$C = \frac{1}{S_{Nr}^{Max}} - \frac{1}{S_N^{Max}} \quad (3.29)$$

Here S_N^{Max} = Maximum trapped saturation; S_N = Trapped nonwetting saturation; K_{rN}^{Im} = Imbibition nonwetting-phase relative permeability; K_{rN}^{Dr} = Drainage nonwetting-phase relative permeability; K_{rN}^{Exp} = Experimental nonwetting-phase relative permeability; and = Normalized nonwetting-phase saturation.

This series of equations showed that the hysteresis phenomena could be explained in terms of a mathematical formula, which will lead to better understanding. By using this model in reservoir simulation, it appears to save time and use only limited storage compared to other

simulators (Killough, 1976; Kossack, 2000). Although this model is more effective and accurate compared to others, still it cannot be used without experiments to find parameters such as K_{rN}^{Exp}.

Pore size distribution is also considered one of the most important factors that affect relative permeability, the same as saturation (Burdine, 1953). Burdine used the pore size distribution data to measure relative permeability by using a mathematical formula driven by fluid flow law in porous media. Lenhard and Oostrom (1998) used Burdine's mathematical formula and Brooks-Corey main drainage capillary pressure function (Delshad et al., 2003) to develop a mathematical model that can predict the hysteresis phenomenon of relative permeability as follows,

For $\bar{S}_w \leq \bar{M}_{ow}$

$$K_{rw} = \bar{S}_w^{(2+3\lambda)/\lambda} \tag{3.30}$$

$$K_{ro} = (1 - \bar{S}_w)^2 . \left[1 - \bar{S}_w^{\frac{2+3\lambda}{\lambda}}\right] \tag{3.31}$$

For $\bar{S}_w \geq \bar{M}_{ow}$

$$K_{rw} = S_w^2 \left[1 + \bar{M}_{ow}^{\frac{2+\lambda}{\lambda}} - \Omega^{\frac{2+\lambda}{\lambda}}\right] \tag{3.32}$$

$$K_{ro} = (1 - \bar{S}_w)^2 . \left[\Omega^{\frac{2+\lambda}{\lambda}} - \bar{M}_{ow}^{\frac{2+\lambda}{\lambda}}\right] \tag{3.33}$$

where $\Omega = \bar{M}_{ow} + \bar{S}_o$

$$\bar{S}_o = \frac{S_o - S_{or}}{1 - S_{iw} - S_{or}} \tag{3.34}$$

Also λ = Pore-size distribution index.

The model was tested against experimental data for mixed-wet rocks from past literature and showed acceptable agreement. Another good feature of this model is the consideration of pore size distribution in the mathematical calculations for hysteresis. A series of studies were conducted in the same area of this study for drainage-imbibition and imbibition-drainage reversals that can be found, for example, in past literature (Delshad et al., 2003; Lenhard, 1992; Lenhard et al., 1989; Parker and Lenhard, 1987a, 1987b).

Table 3.2 presents the most widely used models that describe the hysteresis phenomenon in two and three flow systems. Fundamentally, these models characterize the role that each factor plays in determining the hysteresis behaviour (Dullien, 1992; Miller et al., 1998).

Table 3. 2. Hysteresis Models for Relative Permeability Hysteresis

Reference	Mathematical Formula	System	Analysis
(Miller et al., 1998)	$K_{rw} = \left(\frac{S - S_r}{1 - S_r}\right)^2 \frac{\int_0^s \frac{ds}{P_c^2}}{\int_0^1 \frac{ds}{P_c^2}}$ $K_{rnw} = \left(1 - \frac{S - S_r}{S_c - S_r}\right)^2 \frac{\int_0^s \frac{ds}{P_c^2}}{\int_0^1 \frac{ds}{P_c^2}}$	Air-Water	(iii) Applicable for isotropic and anisotropic media (iv) For main Drainage curve
(Lenhard and Oostrom, 1998)	$K_{rw} = \bar{S}_w^{\frac{1}{2}} \left\{1 - \left[1 - \bar{S}_w^{\frac{1}{m}}\right]^m\right\}^2$	Mixed-wet	(iii) Modified from Van Genuchten's model (Van Genuchten, 1980) to be used in mixed-wet media. (iv) Applicable for imbibition, drainage,

	$K_{rw} = (\bar{S}_t - \bar{S}_w)^{\frac{1}{2}}\left\{1 - \left[1 - \bar{S}_w^{\frac{1}{m}}\right]^m - \left[1 - \bar{S}_t^{\frac{1}{m}}\right]^m\right\}^2$		and scanning curves
(Wang and Alvarado, 2016a)	$K_{rw} = K_{rwiro}\left(\frac{S_w - S_{wcrit}}{1 - S_{wcrit} - S_{oirw}}\right)^{N_w}$ $K_{row} = K_{rocw}\left(\frac{1 - S_w - S_{orw}}{1 - S_{wcon} - S_{orw}}\right)^{N_w}$	Low salinity water-oil	(iii) Mainly developed for Dynamic systems (iv) Applicable for imbibition and drainage
(Corey, 1954)	$K_{rw} = \bar{S}_w^4$ $K_{rnw} = (1 - \bar{S}_w)^2(1 - \bar{S}_w^2)$	Aqueous phase wetting	(iii) Contact angel effects should be considered (iv) Applicable for imbibition, drainage, and scanning curves
(Lenhard et al., 1989)	$K_{rw} = \bar{S}_w^{l+1+2/\lambda}$ $K_{rnw} = (1 - \bar{S}_w)^l\left(1 - \bar{S}_w^{1+2/\lambda}\right)$	Aqueous phase wetting	(iii) Modified of Van Genuchten's model (Van Genuchten, 1980) to be used in simulation (iv) Applicable for imbibition, drainage, and scanning curves

3.4.2. Experimental Observations of Hysteresis in Relative Permeability

Colonna et al. (1972) conducted an experimental study on the effects of alternate displacement of water and gas on the hydrocarbon behaviour of rocks. The evolution of the gas relative permeability and capillary pressure has been measured simultaneously for sandstone samples. The hysteresis for both was observed versus saturation. A theoretical model that can predict the hysteresis of underground gas storage facilities was presented.

Two types of relative permeability hysteresis – flooding phase-dependent and cycle-dependent – were reported by Bouchard and Hawkins (1992). The magnitude of this hysteresis depends on three main factors: fluid type, the structure of the pore, and wettability. Using water as a flooding fluid gives different results than oil flooding, called flooding phase-dependent hysteresis. Using the same phase, which refers to cycle-dependent hysteresis, yields different results for sequential floods. Their study focused on using oil and brine as a fluid flooding system. With oil and water flooding, different values in water relative permeability have been noticed during the experimental results for oil-wet rock, which is consistent with past literature (Amaefule and Handy, 1982; Batycky et al., 1981; Braun and Blackwell, 1981; Chierici, 1984; Jr. et al., 1985; Torabzadeh and Handy, 1984; Van Spronsen, 1982). Torabzadeh and Handy (1984) obtained the same results as Bouchard and Hawkins (1992) for cycle-dependent hysteresis for oil flooding cases. Evrenos (1969) showed the results for both oil and water flooding in both steady and unsteady conditions. Bouchard and Hawkins (1992) highlighted the importance of the second cycle relative permeability hysteresis of oil flooding in simulating Enhanced Oil Recovery (EOR).

Braun and Holland (1995) measured the relative permeability for water-wet samples. The oil phase and the water phase were used in this study. Results showed the difference between the imbibition and drainage in the water phase is less observed compared to the oil phase case. Two types of rocks were used in this study: outcrops and reservoir samples. For outcrops, the results showed little hysteresis in water relative permeability compared to oil relative permeability, which showed a considerably different trend for imbibition and

drainage curves by almost 5% PV separation. For reservoir samples, the separation space between drainage and imbibition curves for oil relative permeability was 15% PV. For the water relative permeability, hysteresis was noticed only for low water saturation. The outcomes of the study can be summarized as the main cause of oil relative permeability hysteresis is a more noticeable process than water relative permeability due to the wide range of contact angles in mixed wet conditions rather than in water-wet rock. The second outcome, using the experimental procedure by Braun and Holland (1995) provides scanning curves and can be used in fluid flow modelling.

Obtaining the relative permeability curves is a challenging and time-consuming process (Wang and Alvarado, 2016a). Overall, the two main methods used to determine the relative permeability curves are for steady and unsteady state conditions. The unsteady state is more accurate but time-consuming compared to the steady-state method. The study confirmed that high-quality capillary pressure data at the reservoir condition enhanced the accuracy of relative permeability drainage and imbibition curves obtained from unsteady state experiments. Using steady and unsteady state experiments at reservoir conditions gave an accurate estimation for the relative permeability hysteresis.

A summary of a list of articles from past literature that focused on relative permeability hysteresis is shown in **Table 3.3**. Types of fluids used in a study, as well as whether that study dealt with simulation and modelling along with the experimental study are main points in **Table 3.3** for comparisons between published articles.

Table 3. 3. Overview of past publications on relative permeability hysteresis

Authors	**Rock Type**	**Flooding Phase**	**Critical Analysis**
(Evrenos, 1969)	Consolidated ceramic tiles and unconsolidated ground glass	Gas-Oil	Mathematical models of hysteresis
(Colonna et al., 1972)	Unconsolidated of glass beads	Gas	Compared the experimental results with qualitative trends
(Carlson, 1981)	NA	Water	Algorithm proposed for determining hysteresis
. (Batycky et al., 1981)	Berea Sandstone	Oil-Water	-Unsteady state displacement method. -Measuring relative permeability without consideration for capillary pressure will lead to a major error
(Jr. et al., 1985)	Berea Sandstone	Oil-Water	-Oil relative permeability is a function of IFT and viscosity -Water relative permeability is a function of capillary number
(Denoyelle and Lemonnier, 1987)	Sandstone	Gas-Water	-Numerical model was used in this study -Gas relative permeability hysteresis has more influence in producing oil than water
(Bouchard and Hawkins, 1992)	Berea Sandstone	Oil-Brine	-Cycle-dependent and flooding phase-dependent relative permeability hysteresis was observed

			-The centrifuge method has been used to measure relative permeability curves
(Braun and Holland, 1995)	Outcrop of Berea Sandstone	Water-Oil	-Hysteresis in oil relative permeability is weaker than hysteresis of water relative permeability -Applications of relative permeability hysteresis in EOR
(Dixit et al., 1997)	Sand packs	Crude oil-Brine-rock	-Water wet sample used in this study -3-D model was proposed to determine relative hysteresis
(Christensen et al., 1998)	Heterogeneous sandstone	Water-Alteration-Gas (WAG)	-Data from field used in simulation to investigate the hysteresis -Model was compared to the standard two-phase Killough and Carson hysteresis model (Killough, 1976)
(Masalmeh, 2001)	Both Carbonate and Sandstone	water	-Conceptual hysteresis model was presented in this study -For oil-wet samples, oil relative permeability hysteresis is clearly noticeable
(Spiteri et al., 2005)	Berea Sandstone	Gas-Water	-New model for relative permeability was proposed -Model tested for relative permeability hysteresis in the context of CO2 sequestration in saline aquifers

(Zhang et al., 2010)	NA	Gas-Water	-Implicit pressure and explicit saturation (IMPES) approach used in this study to determine the hysteresis -Under transient condition, the hysteresis was tested
(Akbarabadi and Piri, 2013)	Sandstone	CO2-brain	Trapped CO2 saturation (S_{co2r}) to initial saturation of CO2 was very significant
(Parvazdavani et al., 2014)	Sandstone	Oil-water	-Nano silica particles were used in this study -Hysteresis decrease as the dispersed nano-silica particles used
(Wang and Alvarado, 2016a)	Sandstone	Crude oil and synthetic brine	-High salinity and low salinity brine were used in this study -Complexity and time consumption are the main factors when measuring relative permeability hysteresis

3.5. Hysteresis in Wettability

The wettability of rocks is a crucial property in many aspects, such as controlling the location, flow, and distribution of fluids in the reservoir (Anderson, 1986a). Moreover, studies have shown the effect of wettability in the electrical properties of porous media (Anderson, 1986b; Elhaj et al., 2018a), capillary pressure (Anderson, 1987a), waterflood behaviour (Anderson, 1987b), relative permeability (Anderson, 1987c; Elhaj et al., 2018b), dispersion (Wang, 1988), simulated tertiary recovery (Anderson, 1986a), irreducible water saturation (Anderson, 1987c), and residual oil saturation (Anderson, 1987a; Hirasakl, 1991). As it is known, wettability can be measured by the contact angle (Yuan and Lee,

2013; Zisman, 1964), which can indicate the wetting phase's angle to the solid. As the contact angle is a characteristic of the rock wettability, and it is considered only an indication of rock wettability, this means a contact angle with much less than (90°) indicates high wettability. In contrast, the contact angle with a much larger angle than (90°) indicates low wettability.

There are two types of contact angles: (i) static or (ii) dynamic, based on the movement or the stationary location of the fluid and solid while the measurement takes place (Johnson Jr et al., 1977). Most studies refer to wettability by the degree of contact angles (Bartell and Cardwell, 1942; Cassie and Baxter, 1944; Michaels and Lummis, 1959). In this thesis, term “contact angle” shall refer to wettability.

The hysteresis of wettability has a long history in the oil and gas industry (Benner et al., 1942; Haines, 1930; Melrose, 1965). It was found in a previous study that the hysteresis that occurred with a contact angle was akin to similar hysteresis that existed in petroleum engineering, such as capillary pressure hysteresis and relative permeability hysteresis (Johnson et al., 1977). Therefore, when the interface of oil-water, for an instant, gave two angles for a reservoir rock, at advancing and receding points of the water, this phenomenon of exciting two angles for one system is well known as hysteresis of contact angle (Benner et al., 1942). Other authors refer to the hysteresis term in wettability to the difference between these two angles (advancing and receding) (Extrand, 2004, 2003, 2002; Gao and McCarthy, 2006).

Three cases can happen for a reservoir rock (Benner et al., 1942), shown graphically in **Figure 3.6** below. In the first case, the two different angles were less than 90°; the reservoir rock would be water-wet, and there would be a continuous movement of water forcing the oil out of the rock. In the second case, the two different angles were higher than 90°; the reservoir rock would be oil-wet, and there would be a continuous movement of oil, forcing the water out of the rock. In the third case, the two different angles were on opposite sides (one was less than 90°, and the other was greater than 90°), there would be no liquid movement in either direction.

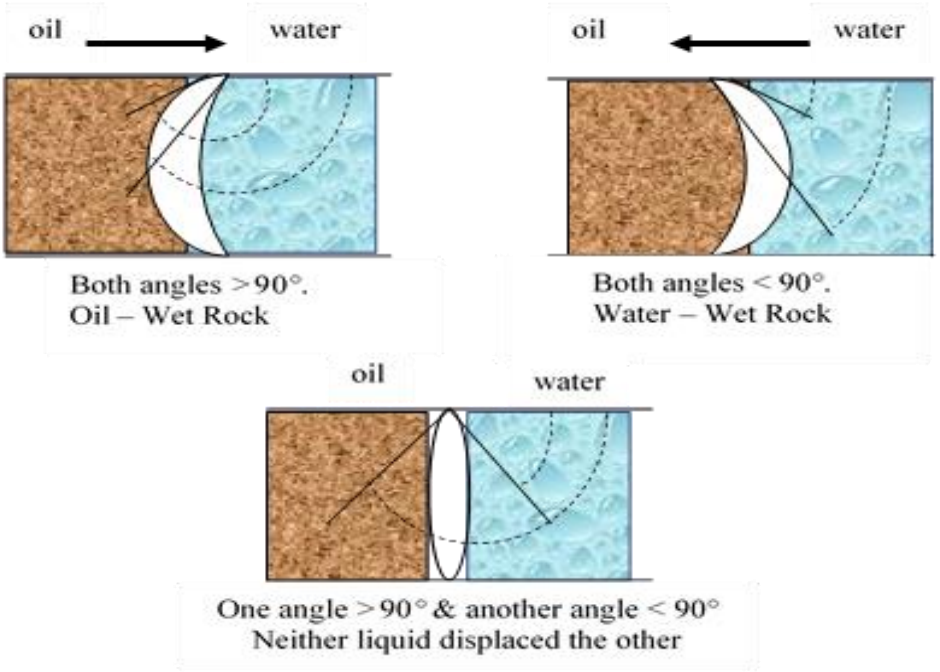

Figure 3. 6. Schematic of Three Scenarios of Hysteresis Phenomenon in Wettability

Despite the extensive studies that focused on investigating contact angle hysteresis, the fundamental reasons for this phenomenon are not entirely understood (Extrand and Kumagai, 1997). It is often referred to as surface heterogeneity (Good, 1952; Pease, 1945;

Ruch and Bartell, 1960), roughness (Eick et al., 1975; Huh and Mason, 1977; Shuttleworth and Bailey, 1948), overturning of molecular segments at the surface (Hansen and Miotto, 1957; Langmuir, 1938), adsorption and desorption (Vergelati et al., 1994), inter-diffusion (Good and Kotsidas, 1979; Timmons and Zisman, 1966), and or surface deformation (Bikerman, 1950; Lester, 1961). In the next two sections, essential experimental and theoretical techniques will be highlighted and discussed.

3.5.1. Modelling of Hysteresis in Wettability

As discussed in previous sections, hysteresis can be referred to as the difference between advancing $\boldsymbol{\theta_a}$ and receding $\boldsymbol{\theta_r}$ angles, which can be mathematically formulated as $\boldsymbol{\theta_{hys}}$:

$$\theta_{hys} = \theta_a - \theta_r \tag{3.35}$$

Past literature on contact angle hysteresis has highlighted several mathematical models. As Extrand (2003) reported that the first model was developed (Cassie, 1948; Cassie and Baxter, 1944) and applied to heterogeneous surfaces. It can estimate the values of advancing and receding angles as:

$$\cos\theta_i = \alpha_1 \cos\theta_{i,1} + \alpha_2 \cos\theta_{i,2} \tag{3.36}$$

where i refers to either advancing or receding, 1 and 2 for material type, and α_1, and α_2 are the fractional areas of material 1 and material 2:

$$\alpha_1 + \alpha_2 = 1 \tag{3.37}$$

The model developed by Cassie is relatively simple and straightforward, and the primary assumption of this model is that the fluid will change the model surfaces. But this model

and other models that originated from it failed to predict contact angle correctly (Brockway and Jones., 1964; Dettre and Johnson Jr, 1965; Gaines, 1960). All of these models assumed that the apparent contact angle is controlled by the interfacial contact area between liquid and solid. Several studies have suggested that contact angles can be estimated by the interactions that occur at the contact line (Extrand, 2003, 2002).

More advanced models have been developed (Good, 1952; Johnson Jr and Dettre, 1964; Marmur, 1994; Neumann and Good, 1972; Öpik, 2000). Most of these models employed geometry as a function; moreover, the surface roughness was also included. The effect of surface roughness and chemical non-uniformities on the wettability hysteresis were investigated mathematically. In these mathematical models, the geometries were assumed to be regular, such as the form of parallel stripes (Öpik, 2000). A previously published study that dealt with this assumption can be found in Marmur (1994). The reader may also refer to the study by de Genes for more details (De Gennes, 1985).

An interesting study conducted by Brandon et al. (1997) modelled and simulated hysteresis phenomena of three-dimensional sessile drops in equilibrium with a chemically heterogeneous smooth solid surface in which the energy is spatially periodic. The main assumptions of this model are: (i) the fluid and liquid are mutually immiscible, (ii) the gravity effect is neglected, and (iii) contact angle is assumed to vary along the surface. To achieve stability, the dimensionless free energy of the system is given by:

$$G = S_{IF} - \left[\iint \cos\theta_i\,(x,y)dxdy\right]_{S_{SI}} \tag{3.38}$$

where G is free energy, x and y spatial coordinates, S interfacial area, and $\cos\theta_i\ (x, y)$ can be defined by Young's equation:

$$\cos\theta_i\ (x, y) = \frac{\sigma_{sf}(x, y) - \sigma_{sl}(x, y)}{\sigma_{lf}} \tag{3.39}$$

Here $\sigma_{sf}(x, y)$ and $\sigma_{sl}(x, y)$ are solid-liquid and solid-fluid interfacial tension, respectively. As a conclusion for this result, the hysteresis was found to have existed in both the average contact angle (as a function of volume) and liquid-fluid interfacial curvature. Another conclusion of this study was a good agreement in calculating the drop shapes in three-dimensional space with the Young and Young-Laplace equations. Although this study showed good results as well as a better understanding in three-dimensions, it had limitations, such as the software that was used failed to include a large size of a bubble, similar to the study that dealt with a two-dimensional sessile drop (Brandon and Marmur, 1996). Several studies also considered the surface free energy of wetting as a function in the mathematical models (Cheng et al., 2016; Extrand, 2004, 2003, 2002, 1998; Extrand and Kumagai, 1997).

3.5.2. Experimental Observations of Hysteresis in Wettability

Many experimental techniques and methods were developed during the past few decades to investigate and measure the hysteresis phenomenon in contact angles. These techniques can be divided into techniques measured on flat solid surfaces and others on different geometries (non-ideal surfaces), such as plates, fibres, and powders (Chau, 2009). In another perspective, these techniques can be categorized in terms of static and dynamic conditions depending on the liquid situation during measurements (Ralston and

Newcombe, 1992; Yuan and Lee, 2013). In this section, both perspectives, movement type and surface type, will be discussed briefly.

The most common method that is used to describe and measure the contact angle depends on observing the image of the drop by low-magnification optical devices (Chau, 2009). It is challenging to determine the degree of wettability with the low-magnification device. Additionally, keeping a surface clean in an open-air laboratory is difficult. An advantageous technique to keep surfaces clean and uncontaminated is by abrasion and polishing underwater using scrupulously controlled conditions (Wark and Cox, 1932).

A well-known technique that is used to measure the tangent angle of the contact angle known as "telescope-goniometer" is used to determine the contact angles (Bigelow et al., 1946) on a flat solid surface, as shown in **Figure 3.7**. The same method was designed and modified by Zisman (1968). The eyepiece was used to measure the tangent of the drop and the surface contact point. Over the years, enhancements and improvements were made to improve the accuracy of angle measurements, such as magnifying (up to 50 times) the intersection profile allowed for better assessment and a camera instead (A and Smithwich, 1988; Leja and Poling, 1960). Another study proved the sessile drop's angle could be measured up to an accuracy of ±2° when the contact angle is higher than 20°(Hunter, 2001). A motor-driven syringe is employed in the experimental set-up to control the liquid rate when measuring the dynamic contact angle (Kwok et al., 1996). The advantages of this method can be (1) the simplicity of this method, (2) a small surface, and a small amount of liquid are required to conduct this experiment.

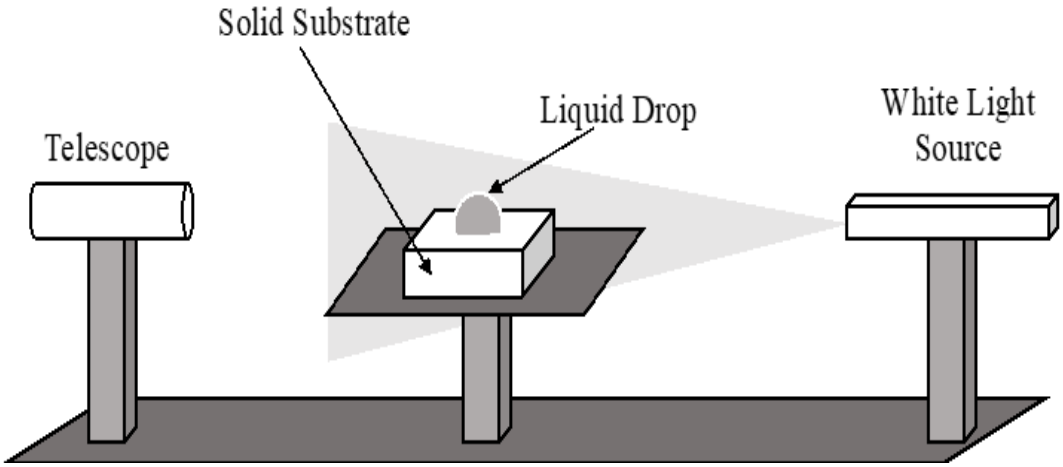

Figure 3. 7. Telescope-goniometer technique for contact angle measurement (Salim et al., 2008)

On the other hand, when the liquid size and surface are small, there is a possibility of the existence of impurities, which may affect the reading of the angle, likely to be high (Chau, 2009; Yuan and Lee, 2013). This method entirely depends on measuring the tangent line's angle that leads to significant inaccurate measurements if a minor error occurs (Yuan and Lee, 2013). The focus of the camera is toward the most significant drops (Chau, 2009; Yuan and Lee, 2013). Variations of contact angle measurements happen when the flat surface is either heterogeneous or rough (Chau, 2009). Finally, the small size of the droplet leads to difficulties in measuring the contact angle (Brandon et al., 2003; Letellier et al., 2007).

Another popular method that is used for investigating hysteresis is a "tilted plate" or "inclined plate" introduced in the 1940s (Macdougall and Ockrent, 1942). **Figure 3.8** depicts a schematic of the inclined plate method. This technique is a modified version of the "telescope-goniometer" technique. The same method was used to study contact angle hysteresis on various polymer surfaces, such as silicon wafers and elastometric surfaces

(Extrand and Kumagai, 1997, 1995). This technique used a recorded video camera and videotape to measure both angles using a protractor. When the drop started moving, the tape was stopped. Measurements of these two angles must be determined carefully because, most of the time, they can be different (Krasovitski and Marmur, 2005; Pierce et al., 2008).

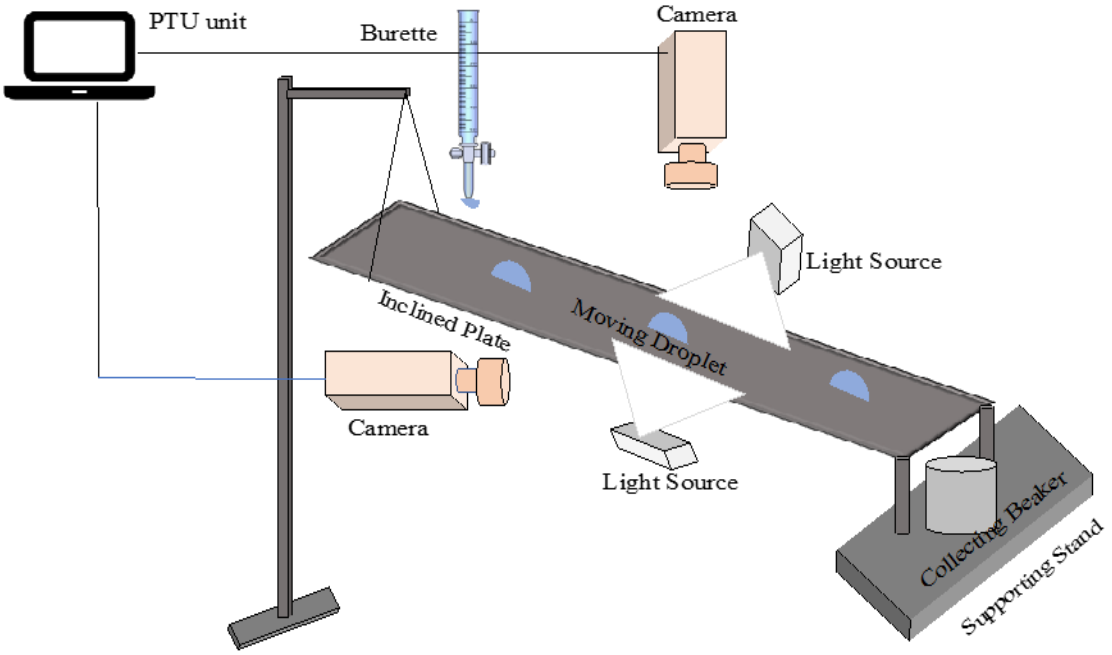

Figure 3. 8. Inclined plate technique for contact angle measurement (Puthenveettil et al., 2013).

In the early history of contact angle measurement, a platinum wire was used to measure contact angle hysteresis by forming sessile drops on a solid surface (Zisman, 1968). The drops were created by heating the wire and then putting it in a fluid to form the drops. The drop gently and slowly puts on a surface, building a sessile drop (Yuan and Lee, 2013). Despite the accuracy of reproducing the sessile drop that was be claimed (±2°) (Spelt et al., 1986), some concerns about moving the drop from the wire to the surface may cause some kinetic energy from the flowing, which may lead to metastable contact angles

(Derjaguin, 1946; Eick et al., 1975; Johnson Jr and Dettre, 1966; Neumann and Good, 1972).

The Tangentometer method is also known for measuring contact angle hysteresis, which uses a mirror seated at the droplet's baseline (Phillips and Riddiford, 1972; Yuan and Lee, 2013). The role of the mirror is to rotate until the full curve of the drop is formed, and with its reflection image, the protractor adhered to the mirror can be used to measure the tangent line's angle. This method has the problem of measurement errors because of the inherent subjectivity of tangentometers (Fenrick, 1964). The specular reflection from the drop surface by using a light source is another technique that can be applied to estimate the hysteresis of the contact angle (Langmuir and Schaefer, 1937). The light source is rotated around the droplet until it is reflected from the drop dies; afterwards, the contact angle can be read from the degree of the rotation. The accuracy of this method is (±1°) and it can be used for both sessile drops and menisci (Johnson and Shah, 1985).

For the other types of surfaces, non-ideal or different geometry, **Table 3.4** summarizes, discusses, and analyses the techniques used to measure contact angle hysteresis. In a general comparison between these techniques, the most widely used technique that can be applied for most cases is the Wilhelmy balance method (Wilhelmy, 1863) because it can be used in static and dynamic contact angle measurements as well as its simplicity. In addition, most of the other techniques primarily originated from its fundamentals. Other studies considered temperature dependency on measuring the contact angle hysteresis, such as the captive bubble method (Taggart et al., 1930) and capillary rise at a vertical plate

method (Budziak and Neumann, 1990; Kwok et al., 1995; Neumann, 1964; Shimokawa and Takamura, 1973). Some studies give low error possibility, and others provide large error values under exceptional circumstances, such as capillary rise at a vertical plate method and individual fibre method (Schwartz and Minor, 1959), respectively. For more details about these techniques to estimate the contact angle, see **Table 3.4** below.

Table 3. 4. Nonideal geometry surface techniques for contact angle hysteresis

Technique	Principles	Advantages	Disadvantages	Ref.
Captive Bubble Technique	• Creating an air bubble below a solid surface by injecting air into a fluid. • A needle is used to keep the bubble from drifting.	• The surface is in contact with a saturated atmosphere. • Contaminated and clean surface. • Easy to study temperature-dependence	• It requires more liquid. • Liquid causes the sabotage of the film	(Taggart et al., 1930)
Tilting Plate Method	• a meniscus created on both sides of the plate due to immersing a plate into a liquid • the position of the meniscus to the plate must be horizontal. • The contact angle is the angle between the plate and the horizontal.	• Simple and does not depend on the operator's subjectivity • Less error compared to others (only ±5°).	• The disturbance of the liquid during the measurement is considered to be a significant problem.	(Zhang et al., 1989)
Wilhelmy Balance Method	• Moving flat plate up and down for	• Simplest methods. • Accurate contact	• A high sensitivity electro balance is	(Lund et al., 2019; Rohmer et

	measuring the contact angle. • Depends on surface tension calculations	angle values. • It is used for dynamic contact angle measurement.	needed. • The plate must have a constant perimeter • The sample must have the same composition and topography on all sides.	al., 2017; Santoso et al., 2019; Wilhelmy, 1863)
Capillary Rise at a Vertical Plate	• Capillary height determined by the integration of the Laplace equation • Capillary height can be used to determine the contact angle.	• Accuracy up to (±0.1°) can be obtained. • The surface tension and contact angle can be measured at the same time • the temperature versus contact angles can be measured.	• The surface tension should be known. • Inaccurate values if the liquid contains the surface-active agent.	(Budziak and Neumann, 1990; Kwok et al., 1995; Neumann, 1964; Shimokawa and Takamura, 1973)
Individual Fiber	• Putting a fibre in a horizontal position in the field of microscopic. • A goniometer eyepiece is a tool to estimate the contact angles.	• The zero contact angle can be measured. • The homogeneity of the fibre surface can be tested.	• Significant errors occurred due to the small dimensions of the drop curvature. • Practically it is difficult to get accurate values when the depth of immersion is relatively small.	(Schwartz and Minor, 1959)
Capillary penetration methods for particles	• Monitoring the rate at a liquid penetrates • A flat cake created by compressing the powders. • The contact angle is	• It gives better correlation results than the captive bubble technique. • It can handle the presence of a porous architecture.	• The method depends on determining the effective capillary radius, which difficult to measure accurately. • The critical	(Lerk et al., 1977; Washburn, 1921; Zografi and Tam, 1976)

	measured from the liquid drops.		surface tension should always be higher than the surface tension. • The packing powder must be obtained in the capillary tubes.	

3.6. Hysteresis in Viscosity

The oil viscosity is one of the essential reservoir fluid properties that is used in different petroleum engineering calculations such as hydraulic calculations for surface facilities, sub-surface simulations, pipeline systems, hydrocarbon reserves, enhanced oil recovery methods, process simulations, and fluid flow through porous media (Kulchanyavivat, 2005; Lindeloff et al., 2004; Monnery et al., 1995; Quiñones-Cisneros, 2000). Many factors affect oil viscosity, for instance, oil composition, temperature, pressure, and density (Santos et al., 2017).

The term “hysteresis in viscosity” is not well documented in the literature, but recently, some studies have investigated the hysteresis behavior of viscosity in nanofluids (Maïga et al., 2006; Murshed and Estellé, 2017; Nguyen et al., 2008, 2007). A nanofluid is a fluid that contains a very small size of particles, called ultrafine practices, in a conventional base fluid, which helps in enhancing the conventional base fluid’s characteristics (Buongiorno, 2005; Daungthongsuk and Wongwises, 2007; Taylor et al., 2013). Nanofluids have several applications in different fields such as in polymer flooding, advanced heat transfer or cooling techniques, energy harvesting, microelectronics, micro-electromechanical systems, microfluidics, transportation, medical, and numerous thermal management

systems (Murshed et al., 2008; Murshed and Estellé, 2017; Saidur et al., 2011). Different nanofluids were tested for hysteresis at various conditions such as nanoparticle concentration, particle size, temperature, and shearing time (Aladag et al., 2012; Nguyen et al., 2007). Due to the lack of information on hysteresis in conventional oil fluid viscosity, this section will only focus on nanofluid viscosity.

3.6.1. Modelling of Hysteresis in Viscosity

There are few studies in the literature in this area; thus, no comprehensive hysteretic model has been proposed for nanofluid viscosity. The lack of studies in hysteresis of the viscosity of nanofluids in past literature might encourage researchers to investigate and shed light on the hysteresis phenomenon in the viscosity of nanofluids and dynamic fluids. The reason for this may be due to the complexity of predicting the behavior of a nanofluid by considering it as a multi-component fluid. (Xuan and Roetzel, 2000).

Regardless of the hysteresis phenomenon in the viscosity of nanofluids, a few theoretical models can predict the viscosity of nanofluids themselves. Most, if not all, of these models, originated from the pioneering work of Einstein (1906), which is based on the assumption of a linearly viscous fluid containing dilute, suspended, and spherical particles. Several studies argued the possibility of using two-phase flow theory in nanofluids, but no proper models had been developed yet (Nguyen et al., 2007; Xuan and Roetzel, 2000). For more details about nanofluid viscosity, readers are referred to previous related studies (Batchelor, 1977; Brinkman, 1952; Einstein, 1906; Frankel and Acrivos, 1967; Graham, 1981; Lundgren, 1972).

3.6.2. Experimental Observations of Hysteresis in Viscosity

Murshed and Estellé (2017) and Nguyen et al. (2007) reported hysteresis experimentally in the viscosity of nanofluids. The experiment was conducted using mainly two water-based nanofluids: water-Al_2O_3 and water-CuO mixtures under different temperatures, particle concentration, and particle size. The measurement of nanofluid dynamic viscosities was completed using a 'piston-type' calibrated viscometer based on the Couette flow inside a cylindrical measurement chamber. The study clearly revealed that when nanofluids reached a critical temperature, the viscosity becomes dramatically altered. For example, for intermediate to high particle concentration, a jump in nanofluid viscosity was observed when the temperature exceeded the critical temperature, and once the nanofluid was cooled, a hysteresis on viscosity was observed (Nguyen et al., 2008, 2007). The reason for this phenomenon is the irreversible damage that may occur to the suspended particles when nanofluid temperature overrides the critical temperature (Nguyen et al., 2007). It is worth mentioning that the hysteresis was observed for both nanofluids, water-Al_2O_3 (36 and 47 nano-meters particles) and water-CuO (29 nano-meters particles) mixtures, only at a high-volume fraction (e.g. 7% of concentration for water-Al_2O_3 and 4.5% of concentration for water-CuO). It becames more noticeable with the increasing concentration of nanofluid particles (Murshed and Estellé, 2017; Nguyen et al., 2007).

Figure 3.9 illustrates the hysteresis phenomenon in nanofluid viscosity based on data obtained for both Al_2O_3 and CuO with different particle sizes and concentrations versus temperature (Nguyen et al., 2007). When the fluid was heated beyond 60 ^{0}C for Al_2O_3 and 55 ^{0}C for CuO and then cooled slowly, a hysteresis phenomenon occurred. Therefore,

measuring the viscosities at any points on the cooling phase gave higher values than those measured on the heating phase. The same studies (Nguyen et al., 2008, 2007) proved that unless the heating exceeded the critical temperature, hysteresis would never occur during the cooling phase. For the sake of clarity of **Figure 3.9**, it does not show the behaviour of hysteresis when concentration increased more than 7% nanoparticles for Al_2O_3 and 4.5% nanoparticles for CuO. But the studies demonstrated that hysteresis was more noticeable as the concentration increased. It is worth noting that for lower concentrations such as 1%, no hysteresis was obtained during the cooling phase. Another interesting point is that the critical temperature depends strongly on the particle's concentration and size.

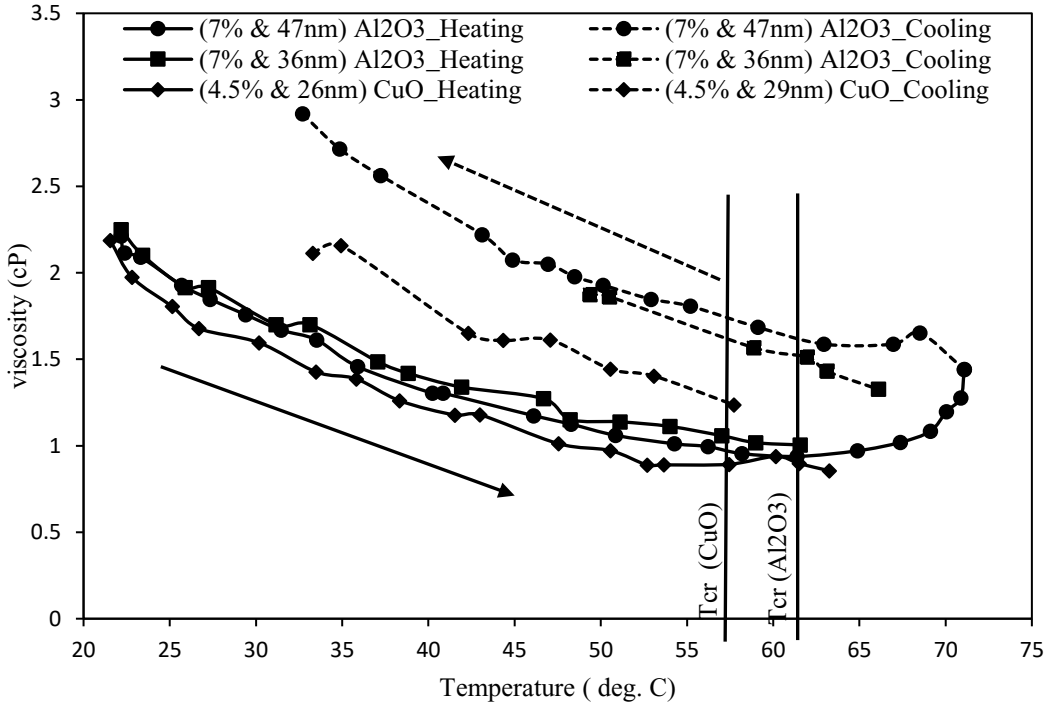

Figure 3. 9. Nanofluid Viscosity Hysteresis for Al_2O_3 and CuO (Nguyen et al., 2007)

Nguyen et al. (2008, 2007) showed the existence of hysteresis phenomena in nanofluid viscosity and that each nanofluid behaved differently depending on concentration and size

of particles. But there are several open questions: the study was the first attempt and did not have support the previous study, which means more studies need to investigate the hysteresis phenomenon in nanofluid viscosity. Moreover, the study raised concerns about the use of nanofluids for heat transfer purposes. In addition, the conditions of the study are not realistic in reservoir conditions, such as the range of temperature which is far away from the reservoir temperature. Furthermore, two nanofluids were investigated, and both were water-based, which indicates the limitations of this study.

The viscosity of nanofluids was investigated for the hysteresis phenomenon in low temperature, low concentration, and shearing time (Aladag et al., 2012). Two types of nanofluids were chosen for this experimental study, Al_2O_3-water and Carbone nanotube (CNT)-water-based. A stress-controlled rheometer equipped with a parallel plate geometry under up and down shear stress ramping was used for collecting viscosity data. The main goal of the study was to investigate the effect of temperature on the viscosity of these two nanofluids at low concentrations and a low range of temperatures from 2 ^{0}C to 10 ^{0}C. The apparent viscosities of nanofluids were discussed in terms of shear rate and temperature effects.

At a low temperature, 5 ^{0}C, and low concentration for different shearing time (120s, 180s, and 240s), both nanofluids, CNT-water and Al_2O_3-water, showed the hysteresis behaviour during increasing and decreasing shear stress. The shape and area of the hysteresis curves were different depending on the nanofluid type and shearing time. This behaviour is generally observed in thixotropic materials (Mewis and Wagner, 2009), which can be defined as time-dependent structured materials (Aladag et al., 2012). As reported, this

behaviour of hysteresis can be explained based on a nanofluid's microstructure and the attractive force between the particles. Therefore, during the increase of shear stress, the structure of nanofluids breaks down until the reverse phase started, which can rebuild and return to the initial structure; but depends on the shearing time. Retrieval of the initial structure depends on shearing time, not shear rate. Between the two types of nanofluids, CNT-water showed less hysteresis behaviour than Al_2O_3, because in CNT-water nanofluids, the destruction and rebuild of nanosuspension structures are only shear-dependent.

This study was the first study that was conducted at low concentration and low temperature for nanofluids to investigate hysteresis behaviour. But it fails to mention what percentage of concentration was used. In addition, the size of the particles was missing in this study. This study does not align with Nguyen et al. (2008, 2007), where at low concentration, there was no hysteresis observed, and no mention of critical temperature in Aladag et al. (2012) study. This was the key reason for hysteresis to happen, and the reason for hysteresis to occur was explained differently in these studies.

3.7. Summary

The focus of this chapter has been on the effects of hysteresis phenomena on EGM experimentally and theoretically in petroleum engineering, especially fluid properties, capillary pressure, viscosity, and rock properties, mainly, permeability and porosity, and relative permeability. The discussion and investigation of each property revealed a gap in which, generally, can be highlighted as the limitations of the experimental studies, such as special conditions which made it inapplicable for others. The data collected from the

experiments may have several errors because experiments were done in lab conditions, not actual reservoir conditions. Most of the developed mathematical models that represent hysteresis originated from empirical models, which, have made them limited and need experimental validation prior to usage. Physical laws that described fluid velocity and gravity are missing in the models that represent hysteresis, and the analytical solution for most of the models is complex.

Both techniques, centrifuge and porous plate, can be used in different conditions such as temperature, stress, or with different fluid systems, which means these techniques can be used to test hysteresis under reservoir conditions except when using different fluid systems. Porous plate measurements under reservoir conditions are not reliable. The main focus of most past studies of hysteresis of wettability was to allow an indication of surface hydrophobicity. Numerous methods in measuring the contact angle hysteresis were discussed and analyzed, such as the conventional telescope-goniometer method, capillary penetration methods for particles, and the Wilhelmy balance method. The applications and setbacks of these techniques were discussed.

The hysteresis phenomenon was extensively studied by many authors, either experimental, mathematical, or simulation studies, as discussed in this chapter. Capillary pressure is one of the most common fluid properties that has received attention in investigating the hysteresis phenomenon, according to the literature, compared to other properties such as viscosity, wettability and interfacial tension. In the next chapter, entropy and other thermodynamic aspects of these transport phenomena will be presented and discussed.

Chapter 4: Entropy Generation for Single-Phase Flow

4.1. Introduction

Even though previous models for fluid flow in porous media can predict the recovery factor for hydrocarbon reservoirs, this chapter aims to further analyze the recovery by considering dissipative processes and effects of well conditions on the Entropy Generation Minimization (EGM) and recovery factor. The governing equations and second law of thermodynamics are used to address: (i) the primary reservoir energy loss; (ii) the effect of production rate on EGM; (iii) the impact of well conditions on the recovery factor as well as EGM; and (iv) the influence of rock and fluid properties on EGM.

The mathematical models developed by Civan and Tiab (1989) are extended in this chapter. The following simplifying assumptions will be made in the analysis: the reservoir is cylindrical; radial flow exists toward the well; the well is vertical and/or deviated; fluid flow is one-dimensional; the fluid is either a single-phase or a two-phase fluid system; an isothermal condition is maintained; production occurs under a pseudo-steady state condition; the flow regime is non-Darcy; and a constant flow rate is assumed in the well.

Figure 4. 1 displays a sketch of a reservoir that includes three systems: the reservoir, near-wellbore (damaged or stimulated region), and the wellbore. In **Figure 4. 1**, P refers to the reservoir pressure; r_w, r_d, and r_e are the wellbore radius, radius of the damaged region, and reservoir radius, respectively; k and k_d stand for the reservoir permeability and damaged region permeability, respectively; and h designates the reservoir's formation thickness.

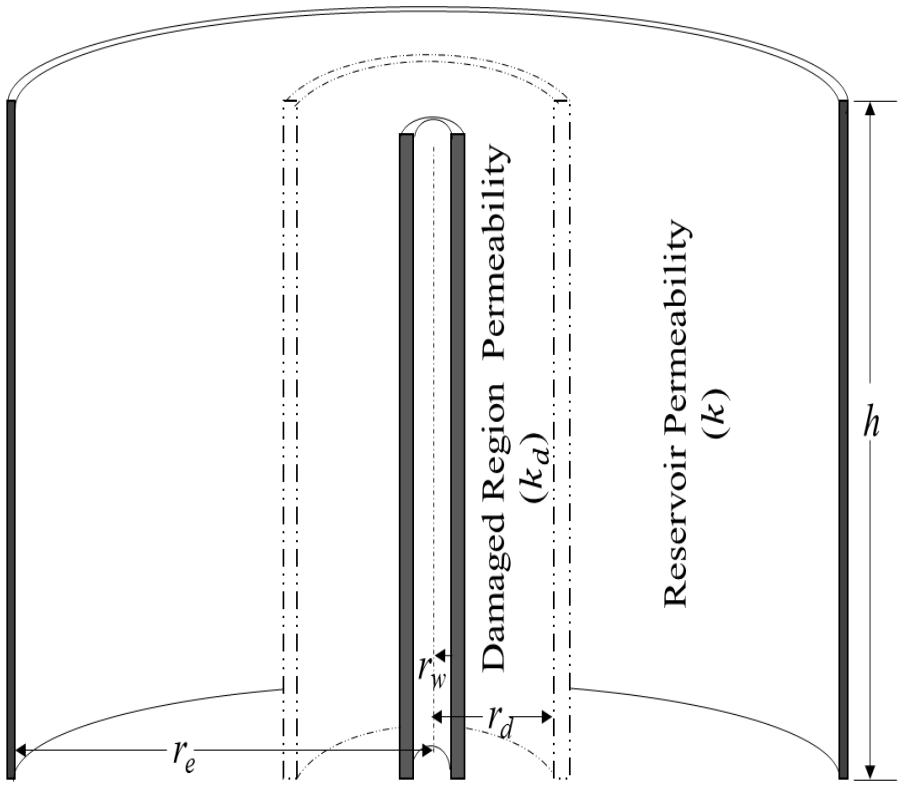

Figure 4. 1. Side view of a reservoir with three sections: reservoir, near-wellbore, and wellbore.

The derivations of the pressure profiles and total entropy production are discussed in detail in this chapter.

4.2. Formulation of Pressure Profiles

Reservoir Pressure Profile. During pseudo-steady state flow (defined as a flow regime where the pressure at any point in the reservoir declines at the same constant rate over time), the governing equation for fluid motion and Darcy's law for the rate of pressure change for a time at a constant production rate is given below (Dake, 1998):

$$\frac{\partial P}{\partial t} = -\frac{q_{sc} B}{\pi \phi c_T h r_e^2} \tag{4.1}$$

where the subscript sc refers to the standard conditions; h represents the reservoir formation thickness; q_{sc} is the flow rate at standard conditions; B is the fluid formation volume factor; ϕ represents the formation porosity; c_T is the total compressibility; and r_e symbolizes the reservoir radius.

The continuity equation with total compressibility (c_T) is expressed as follows:

$$\frac{1}{r}\frac{\partial}{\partial r}(q\rho) = 2\pi h \phi \frac{\partial \rho}{\partial t} \tag{4.2}$$

where ρ is the fluid density. Substituting $c_T = \frac{1}{\rho}\frac{\partial \rho}{\partial P}$ into Equation (4.1) and using the chain rule, the following expression is obtained:

$$\frac{\partial \rho}{\partial t} = -\frac{q_{sc} B \rho}{\pi \phi h r_e^2} \tag{4.3}$$

Substituting Equation (4.3) into Equation (4.2) yields:

$$\frac{\partial}{\partial r}\left(\frac{q}{B}\right) = -\frac{2r}{r_e^2} q_{sc} \tag{4.4}$$

The volumetric flow rate, q, at the reservoir condition is determined by integrating Equation (4.4).

To obtain the pressure distribution in the reservoir, Forchhiemer's equation is used as follows (Forchheimer, 1901; Lee and Wattenbarger, 1996):

$$\frac{\partial P}{\partial r} = \frac{\mu}{k} u + \beta \rho u^2 \tag{4.5}$$

where k is the permeability and β is the non-Darcy coefficient. Substituting the volumetric flow rate, integrating Equation (4.4), and using the Darcy velocity ($u = \frac{q}{2\pi r h}$) in Equation (4.5), the following equation is obtained:

$$\frac{\partial P}{\partial r} = \frac{\mu}{k} B \left(\frac{C - \left(\frac{r}{r_e}\right)^2 q_{sc}}{2\pi r h} \right) + \beta \rho_{sc} \left(B \frac{C - \left(\frac{r}{r_e}\right)^2 q_{sc}}{2\pi r h} \right)^2 \tag{4.6}$$

where C is a constant of integration. For a volumetric reservoir, $\partial P / \partial r = 0$ at $r = r_e$. Equation (4.6) gives two possible expressions:

$$C = q_{sc} \tag{4.7}$$

$$C = q_{sc} - \frac{2\pi r h \mu}{k \beta \rho_{sc}} \tag{4.8}$$

Equation (4.8) yields a negative pressure gradient with respect to the radius so that the first solution can be used, and the following result is obtained:

$$\frac{\partial P}{\partial r} = B \left[\frac{\mu}{k} \frac{q_{sc}}{2\pi h} \left(\frac{1}{r} - \frac{r}{r_e^2} \right) + \beta \rho_{sc} B \left(\frac{q_{sc}}{2\pi h} \right)^2 \left(\frac{1}{r} - \frac{r}{r_e^2} \right)^2 \right] \tag{4.9}$$

Equation (4.9) represents the pressure distribution in the bulk reservoir system along the radial direction.

Near-Wellbore Pressure Profile. Similar steps can be taken to develop the pressure distribution in the damaged region around the wellbore. The reservoir and near-wellbore

systems differ based on their permeabilities. The pressure profile of the damaged region becomes:

$$\frac{\partial P}{\partial r} = B\left[\frac{\mu}{\mathbf{k_d}}\frac{q_{sc}}{2\pi h}\left(\frac{1}{r_w} - \frac{r}{r_d^2}\right) + \beta\rho_{sc}B\left(\frac{q_{sc}}{2\pi h}\right)^2\left(\frac{1}{r_w} - \frac{r}{r_d^2}\right)^2\right] \tag{4.10}$$

where $\mathbf{k_d}$ represents the permeability of the damaged zone.

Pucknell and Clifford (1991) reported several methods based on well-testing measurements and correlations/models to determine the damaged region's permeability. Hawkins (1956) presented the following model to predict the skin factor of a damaged region:

$$k_d = \frac{k}{s\ \ln(r_d/r_w) - 1} \tag{4.11}$$

where s is the skin factor; r_d refers to the radius of the damaged region; and r_w is the well radius.

At the pseudo-steady state condition, the average pressure ($\overline{P}$) of a reservoir is defined as follows:

$$\overline{P} = \frac{2}{r_e^2}\int_{r_w}^{r_e} P\ r\ dr \tag{4.12}$$

Then the average pressure over the two regions becomes:

$$\overline{P} = \frac{2}{r_d^2 - r_w^2}\int_{r_w}^{r_d} P\ r\ dr + \frac{2}{r_e^2 - r_d^2}\int_{r_d}^{r_e} P\ r\ dr \tag{4.13}$$

The average pressure equation (4.13) yields the production time as upon the integration

$$t = t_i + \frac{\pi r_e^2 h}{q_{sc}} \int_{\bar{P}}^{\bar{P}_i} \frac{\phi(\bar{P}) c_t(\bar{P})}{B(\bar{P})} d\bar{P} \tag{4.14}$$

where t_i for pseudo-steady state is given by

$$t_i = t_{pss} = 1200 \frac{\phi \mu c_t r_e^2}{k} \tag{4.15}$$

Flowing Well Pressure. The governing equation for the well pressure is based on the integration of the mechanical energy equation along a streamline within a well at a constant flow rate (Ikoku, 1984; Naterer, 2018):

$$\frac{1}{\rho} \frac{dP}{d\ell} + v \frac{dv}{d\ell} + g_c \sin\theta + \frac{dW}{d\ell} = 0 \tag{4.16}$$

where ℓ is the axial coordinate; v is the velocity; g_c is the gravitational conversion constant; W represents the work, and θ symbolizes the inclination angle.

The following relationship determines the pressure loss due to friction along the well length:

$$\frac{dw}{d\ell} = \frac{f_M v^2}{2D} \tag{4.17}$$

where f_M is the Moody friction factor, and D is the wellbore diameter.

Taking the derivative of the fluid velocity ($v = \frac{4 q_{sc} B}{\pi D^2}$) with respect to pressure leads to:

$$\frac{dv}{dp} = \frac{4 q_{sc}}{\pi D^2} \frac{dB}{dp} \tag{4.18}$$

Using the chain rule and substituting Equations (4.17) and (4.18) into Equation (4.16), the following expression is obtained:

$$\frac{dp}{d\ell} = \frac{g\frac{H}{L} + \frac{f_M}{2D}\left(\frac{4q_{sc}}{\pi D^2}\right)^2 B^2}{\frac{B}{\rho_{sc}} + \left(\frac{4q_{sc}}{\pi D^2}\right)^2 B\frac{dB}{dp}} \tag{4.19}$$

where H represents the wellbore depth, L is the wellbore length, and g stands for the acceleration due to gravity. Equation (4.19) can be used to determine the pressure distribution in a flowing well.

4.3. Formulation of Entropy Production

Reservoir System – Undamaged Region. The rate of entropy production per unit volume $\langle \dot{s} \rangle$ in a porous medium can be written as follows (Slattery, 1972):

$$\langle \dot{s} \rangle = \frac{E_{vp}}{T} \tag{4.20}$$

where E_{vp} is the dissipation rate of mechanical energy in a porous medium, and T stands for the reservoir temperature.

The following equation presents the rate of dissipation of mechanical energy in a porous medium (E_{vp}) (Civan and Tiab, 1989):

$$E_{vp} = \frac{\rho_{sc} f_p \beta u^3}{\phi(1 - s_{wc})B} \tag{4.21}$$

where f_p is the porous medium friction factor and s_{wc} denotes the connate water saturation.

Substituting Equation (4.21) into Equation (4.20) yields:

$$\langle \dot{s} \rangle = \frac{\rho_{sc} f_p \beta u^3}{\phi(1 - s_{wc})TB} \tag{4.22}$$

The total entropy production rate of a radial flow system (S_T) is expressed in the following form:

$$\frac{\partial}{\partial r}\left(\frac{\partial S_T}{\partial t}\right) = 2\pi h \langle \dot{s} \rangle r \tag{4.23}$$

Rearranging Equation (4.23) and substituting Equation (4.22) into Equation (4.23) leads to:

$$\left.\frac{\partial S_T}{\partial t}\right]_{Undamaged} = 2\pi h \int_{r_d}^{r_e} \frac{\rho_{sc} f_p \beta u^3}{\phi(1 - s_{wc})TB} r \, dr \tag{4.24}$$

Equation (4.24) represents the total rate of entropy production in an undamaged region of a reservoir.

Reservoir System – Damaged Region. The only difference between the entropy production rates of the undamaged region and the damaged region is the range of the radius. The radius in the damaged region varies between r_w and r_d, whereas in an undamaged region, the radius changes from r_d to r_e. Thus, for the damaged zone, Equation (4.24) becomes:

$$\left.\frac{\partial S_T}{\partial t}\right]_{Damaged} = 2\pi h \int_{r_w}^{r_d} \frac{\rho_{sc} f_p \beta u^3}{\phi(1 - s_{wc})TB} r \, dr \tag{4.25}$$

Equation (4.25) is used to determine the total rate of entropy production in the damaged region of a reservoir.

Flowing Well System. Under the isothermal condition, the entropy production rate in a flowing well $\langle \dot{s} \rangle$ can be expressed as follows:

$$\langle \dot{s} \rangle = \frac{E_{vp}}{T} = \frac{\rho_{sc} f_M v^3}{2DTB} \tag{4.26}$$

The total entropy production rate in a flowing well can be written as:

$$\frac{\partial}{\partial \ell}\left(\frac{\partial S_T}{\partial t}\right) = \langle \dot{s} \rangle \tag{4.27}$$

Integrating Equation (4.27) gives the following expression for the total rate of entropy production in a flowing well:

$$\left(\frac{\partial S_T}{\partial t}\right) = \int_0^L \frac{\rho_{sc} f_M}{2DTB}\left[\frac{4 q_{sc} B}{\pi D^2}\right]^3 d\ell \tag{4.28}$$

Total Entropy Generation. Using the previous results, the total entropy production rate over a time interval from an initial time t_i to a final time t_f, where the pressure changes from an initial pressure P_i to a final pressure P_f, or spatially averaged $\overline{P}_i$ and $\overline{P}_f$, becomes:

$$S_T = \frac{\pi r_e^2 h}{q_{sc}} \int_{\overline{P}_f}^{\overline{P}_i} \left(\frac{\partial S_T}{\partial t}\Big|_{well} + \frac{\partial S_T}{\partial t}\Big|_{undamaged} + \frac{\partial S_T}{\partial t}\Big|_{damaged} \right) \frac{\phi(\overline{P}) c_t(\overline{P})}{B(\overline{P})} d\overline{P} \tag{4.29}$$

It should be noted that $B(\overline{P})$, $c_t(\overline{P})$, and $\phi(\overline{P})$ are functions of the average pressure. Substituting Equations (4.24), (4.25), and (4.28) into Equation (4.29), the following equation is obtained:

$$\mathbf{S_T} = \frac{\pi h r_e^2}{q_{sc}} \left[\int_{\overline{P}_i}^{\overline{P}_f} \frac{\partial S_T}{\partial t}\Big|_{well} + \int_{\overline{P}_{id}}^{\overline{P}_{fd}} \frac{\partial S_T}{\partial t}\Big|_{res} dr + \int_{\overline{P}_{iu}}^{\overline{P}_{fu}} \frac{\partial S_T}{\partial t}\Big|_{res} dr \right] \frac{\phi(\overline{p}) c_t(\overline{p})}{B(\overline{p})} d\overline{p} \tag{4.30}$$

Here $\overline{P}_{id}$ is the initial average pressure in the damaged area, $\overline{P}_{fd}$ is the final average pressure in the damaged area, $\overline{P}_{iu}$ is the initial average pressure in the undamaged area, $\overline{P}_{fu}$ is the final average pressure in the undamaged area, and the subscript "res" refers to a reservoir with both areas: damaged and undamaged.

4.4. Optimum Recovery

It has been shown in the previous sections that the magnitude of reservoir energy losses is determined by the history of the fluid flow behaviour in the porous medium, which depends on pressure depletion characteristics. Furthermore, the ultimate reservoir recovery is dependent on these two factors: the reservoir pressure and fluid flow behaviour in porous media. Based on previous studies, the permeability and non-Darcy coefficient, which affect the pressure profile in a single-phase flow reservoir, are dependant on the Reynolds number and the reservoir geometry. These parameters also affect the reservoir energy loss (Blick and Civan, 1988; Civan and Tiab, 1989).

To design an optimum production system in the reservoir, all properties and variables that have a vital effect on the total entropy production are identified and considered. In this chapter, three key variables are considered: production rate, recovery factor, and entropy production for each system.

To generalize the optimal conditions for various scales (and systems), a normalization approach is employed to estimate the dimensionless numbers. The dimensionless entropy (S_T^*) is defined as follows:

$$S_T^* = \frac{S_T}{S_{T_{max}}} \tag{4.31}$$

where S_T^* represents the normalized and dimensionless entropy production and $S_{T_{max}}$ refers to the maximum value of entropy production.

The recovery factor is another non-dimensional property, as defined below (Dake, 1998):

$$RF = \frac{q_{sc}t}{G_i} \tag{4.32}$$

where G_i introduces the initial gas in place, RF is the recovery factor, and t denotes the total production time.

For the reservoir as a thermodynamic system, a new variable called the Coefficient of Performance (COP) is introduced using the following definition (Al-Salem et al., 2019):

$$COP = S_T^* RF \tag{4.33}$$

In general, the COP is a ratio that describes the thermodynamic efficiency of a system (Al-Salem et al., 2019). In this study, the entropy production occurs by irreversible conversion of mechanical energy to internal energy of the fluid in the reservoir, and the recovery factor is the production capability of a reservoir. To have a lower reservoir energy loss, the COP should be maximized. Hence, the production rate that gives the maximum COP is the optimum production rate.

To consider the economic aspect of the optimization, the operating costs will be calculated. The Net Present Value (NPV) is then obtained and plotted versus the production rate. The correlation to determine the variable operating expenses is given below (Mian, 2011; Pashakolaie et al., 2015):

$$\text{varOPEX} = 0.7714\text{Q}^{-0.2423} \tag{4.34}$$

where varOPEX introduces the variable operational costs in USD/bbl, and Q denotes the production rate in MMbbl/year.

The total profits are calculated using the following formula:

$$\text{Total Profit}(\$) = \text{qsc} \times \text{t} \times \text{profit/bbl} \tag{4.35}$$

The Net Present Value (NPV) is also estimated as follows (Gaspars-Wieloch, 2019):

$$\text{NPV} = \frac{\text{FV}}{(1+\text{i})^{\text{n}}} \tag{4.36}$$

where FV is the future value; n is the number of years; and i indicates the interest rate.

4.5. Solution Procedure

To simulate the fluid flow behavior in the reservoir and wellbore, a computer program is created in the MATLAB environment. The reservoir and wellbore models appear in the form of nonlinear partial differential equations that cannot be solved analytically. Hence, it is necessary to use numerical solution methods. The solution of the reservoir models is determined in terms of pressure and entropy, while the solution of the wellbore models is obtained in terms of pressure, mixture entropy, and mixture density.

The only parameter that can be controlled at the surface after choosing the appropriate production rate (q_{sc}) is the wellhead pressure (P_{wh}). Therefore, to calculate the total entropy production for both reservoir and wellbore, the average reservoir pressure ($\overline{P}$) should be calculated first. Pressure at the wellhead is assumed (P_{wh}) and the wellbore pressure profile equation (Equation (4.19)) is used to calculate the Bottom Hole Pressure

(BHP). The BHP as calculated from the wellbore pressure profile equation is considered the final pressure value (abandon pressure P_{wf}) at the reservoir pressure profile.

Using the BHP value as a start point to calculate the whole reservoir pressure profile from the reservoir pressure profile equation (Equation (4.9)) is the next step of the solution procedure. By this stage, the final reservoir pressure is achieved and to get the reservoir pressure profile, the last value estimated from Equation (4.9) would be checked with the initial reservoir pressure value, which is known and given. In case the last value estimated is less than the initial reservoir pressure, then increase P_{wh} by some amount (ΔP) and repeat the process. Once the last value is estimated using Equation (4.9) and equal to the initial pressure value, the average reservoir pressure must be calculated using Equation (4.12).

It is worth mentioning that the average pressures in calculating the total entropy production are the initial and final average pressures. The total entropy production rate for the wellbore and reservoir is estimated by solving the wellbore entropy production rate equation (Equation 4.28) and the reservoir entropy production rate equation (Equation 4.24) simultaneously. The Recovery Factor (RF) will then be calculated and plotted versus the total entropy production rate. The effect of the damaged zone around the wellbore is incorporated in one zone reservoir case by using Hawkin's model (Equation 4.11), while in the two-zone reservoir case, the actual value of the damaged permeability is used. The results of these two cases are compared and discussed in Chapter 6.

One of the challenges encountered while developing the program and solution was finding an accurate increment (ΔP) to be added to the wellhead pressure P_{wh} as there are different

solutions found when using different incremental values. However, to overcome this challenge, an uncertainty assessment was carried out until the smallest and most accurate increment was achieved. Another challenge was to find the correct value of the damaged or stimulated region around the wellbore zone's radius and permeability without experiments. To overcome this challenge, in the absence of experiments, the CMG was initially used in its default conditions, by inserting the value of skin factor in the well data. Afterward, the skin factor was removed and different values for the damaged radius and permeability for the area around the wellbore were assumed. After several attempts of tuning these two parameters (radius and permeability of around wellbore area), an excellent match with the initial case (when skin factor was used) was attained. The radius and permeability that offered the perfect match were used as the given data for the mathematical models.

A summary of solution steps is shown in the flowchart in **Figure 4.2**. This provides a step-by-step procedure to estimate the total entropy production and the optimal production rate. The non-Darcy coefficient is calculated as follows (Tiss and Evans, 1989):

$$\beta = \frac{x\left[\sqrt{k\rho P_{ob}}/\mu\right]^{m}}{\phi(1-S_w)\sqrt{k}} \tag{4.37}$$

where P_{ob} denotes the overburden pressure, and x and m are constants as given below:

$$x = 2.7708 \times 10^{15} \;;\; m = -1.70594 \tag{4.38}$$

The following equation is used to calculate the gas viscosity (μ_g) (Lee and Wattenbarger, 1996):

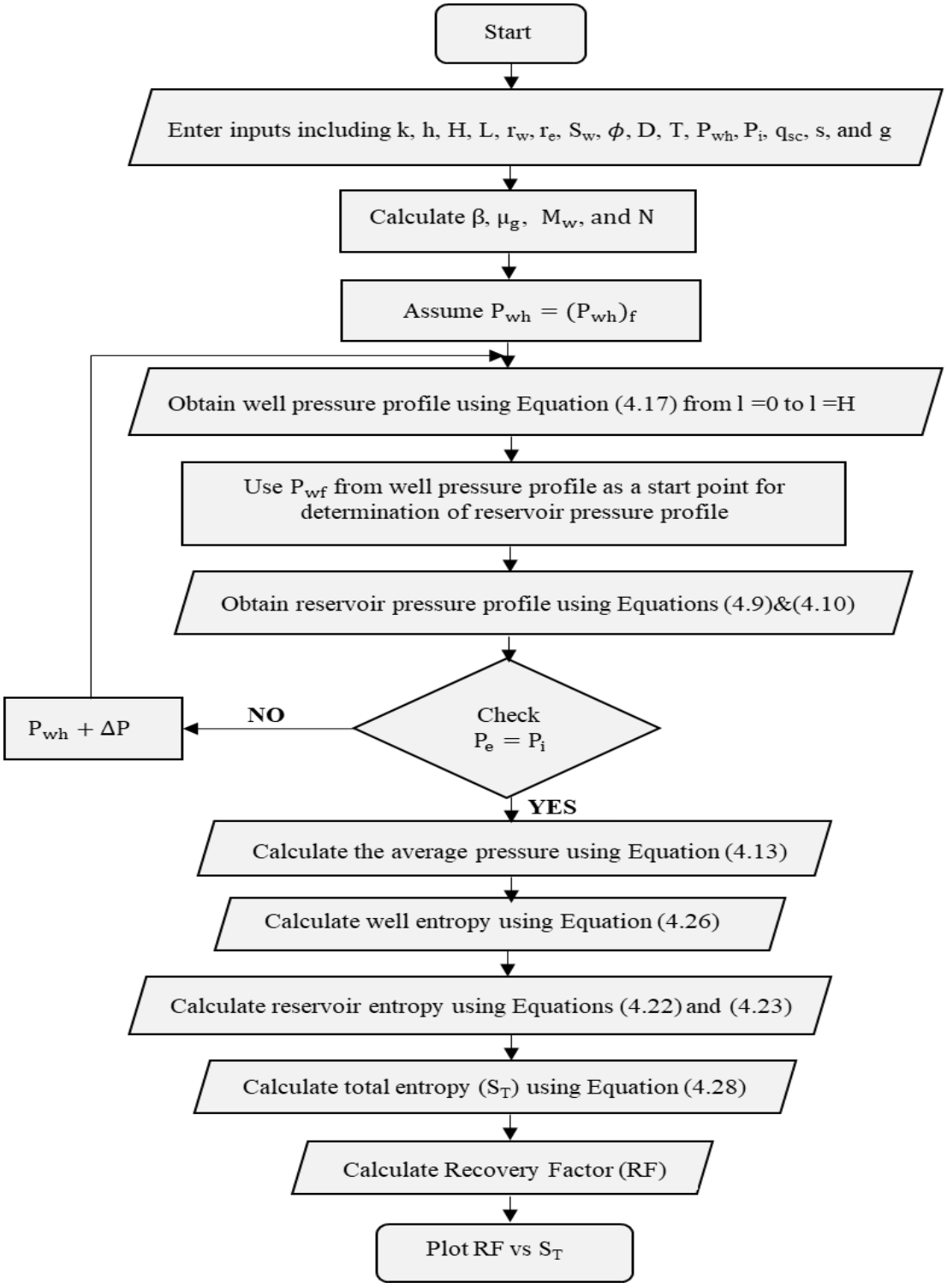

Figure 4.2. Flowchart for the modelling approach

$$\mu_g = 10^{-4} K e^{X \rho^Y} \tag{4.39}$$

where

$$\rho = 1.4935 \times 10^{-3} \frac{PM}{z\,T} \tag{4.40}$$

In Equation (4.38), z is the gas compressibility factor, and M introduces the apparent molecular weight of the mixture (Lee and Wattenbarger, 1996).

$$K = \frac{(9.379 + 0.01607M)T^{1.5}}{209.2 + 19.26M + T} \tag{4.41}$$

$$X = 3.448 + \frac{986.4}{T} + 0.01009\,M \tag{4.42}$$

$$Y = 2.447 - 0.222\,X \tag{4.43}$$

The fluid/gas molecular weight (M) is determined as follows:

$$M = \gamma\, M_a \tag{4.44}$$

In Equation (4.42), γ refers to the gas specific gravity and M_a is the molecular weight of the air.

The original hydrocarbon in place (G_i for gas) is calculated by the following expression (Dake, 1998):

$$G_i = \frac{43{,}560 A h \phi (1 - Sw)}{Bg} \tag{4.45}$$

Numerical and analytical solutions are used to predict the cumulative entropy production in a reservoir. The proposed models are first applied in two systems, reservoir and well, such that the accuracy and reliability of the current and previous studies can be examined. Then the models are extended to include the third system, near-wellbore, or damaged region.

The skin effect is incorporated into the reservoir system (with a single zone) and the wellbore system by considering the apparent wellbore radius correlation given by Ikoku (1984):

$$r'_w = r_w e^{-s} \tag{4.46}$$

where r'_w is the apparent wellbore radius.

4.6. Summary

From a thermodynamic point of view, the second law helps to assess the practical limits of operating systems. Within these limits, the optimum performance can be found. As shown in this chapter, the reservoir and porous media can be treated as a thermodynamic system; however, different mathematical equations and fundamentals are used for such a case. The main difference between the reservoir and other typical thermodynamic systems is the variables involved. In a reservoir, the controllable variables are limited, which include wellhead pressure and production flow rates.

In this chapter, it was shown how EGM can be used mathematically as a guideline for selecting the conditions that lead to better ultimate recovery as well as a better production plan that can extend a reservoir production life for a longer time. This may be accomplished by determining the conditions minimizing the total entropy generation in both reservoir and wellbore.

The goal derived governing equations to address the dissipative loss of the primary reservoir energy availability during the production using reservoir mechanisms. Furthermore, to investigate the effect of the production rate, as well as selected fluid and

rock properties on the total entropy production rate, a sensitivity analysis was performed. In addition, a new zone area is added to capture the effect of either damage or stimulation on the area around the wellbore. Detailed optimum production rate calculations were addressed in the chapter by introducing a new performance criterion, COP.

The mathematical models in this chapter are applicable for single-phase only, dry gas or oil. The models are developed for single-phase, radial flow, one-dimensional, volumetric and isothermal reservoirs under pseudo-steady state conditions. General mathematical models that describe the fluid flow in both porous media and wellbores were developed. Mass, momentum, energy and entropy equations are the main governing equations used in developing the fluid flow models. The developed models were solved by an existing numerical scheme programmed in the MATLAB environment with a new algorithm. For validation purposes, a commercial simulator, Computer Modeling Group (CMG), will verify the predicted results in a subsequent chapter.

Appendix A shows the MATLAB program code as written for the purpose of solving the one-zone reservoir models. The computer program code is simplified, and the values of parameters in this code are subject to change depending on the units and the method used. Also, **Appendix B** shows the CMG code written for validation. In the next chapter, the concepts and formulations presented in this chapter will be extended to consider two-phase flows.

Chapter 5: Entropy Generation for Two-Phase Flow

5.1. Background

Two-phase flows are more complicated than a single-phase flow in the previous chapter due to the existence of moving and deformable interfaces and their interactions with the two phases. Two-phase flow is considered as a heterogeneous mixture of multiple fluids or phases, which are not homogeneously mixed at a molecular level, but can be identified by macroscopic structures, such as solid particles, droplets, and/or bubbles, in a certain region. One can classify them according to the state of the two phases or components (e.g., gas-liquid, gas-solid, liquid-liquid and liquid-solid). Of the four types of two-phase flow systems, liquid-liquid (oil-water) flows will be discussed in this chapter.

Two-phase flow has an increasing importance in various engineering systems for optimum design and safe operations. It also can be observed in several biological systems and natural phenomena that require a better understanding of transport processes. Several important fluid dynamic and energy loss aspects of the prevailing two-phase flow are not well understood. The difficulty lies in the modelling of fluid-particle interactions and interfacial phenomena occurring between the two phases, while the mathematical difficulty lies in the formulation of the two-phase flow as two separate phases coupled with moving boundaries that could deform over time.

These challenges motivate further work to analyze the entropy generation in porous media as well as the wellbore as there are few or limited studies that shed light on two-phase flow

with entropy generation. The rest of this chapter will address the development of the pressure equations and total entropy for both systems, reservoir and wellbore.

The pressure equations and total entropy production for the reservoir and wellbore for oil-water flow will be discussed. Important quantities will be introduced in two-phase flow. For instance, saturation is defined as the fraction of the void volume of a porous medium filled with the corresponding phase. The capillary pressure is defined as the pressure difference between the wetting and nonwetting phases, and the relative permeability is the ratio of the effective permeability of the phase to the absolute permeability.

A semi-transient model will be used to describe the fluid flow in both the reservoir and wellbore. The properties of hydrocarbon mixtures are assumed to be constant as both systems are assumed to be under isothermal conditions. **Figure 5.1** shows a schematic diagram of a production volumetric reservoir. Two parts will be considered for simulation purposes: a wellbore model and a reservoir model. The primary equations governing the fluid flow in both systems are the continuity equation (conservation of mass), momentum balance equation, energy balance equation, and entropy balance equation (second law of thermodynamics).

The appropriate governing equations for the wellbore and reservoir will include the total EGM in both systems. The wellbore and reservoir equations will be solved simultaneously. A one-dimensional, pseudo-steady state and two-phase flow model will be developed for the wellbore, while a radial two-phase flow of oil and water is assumed for the reservoir system.

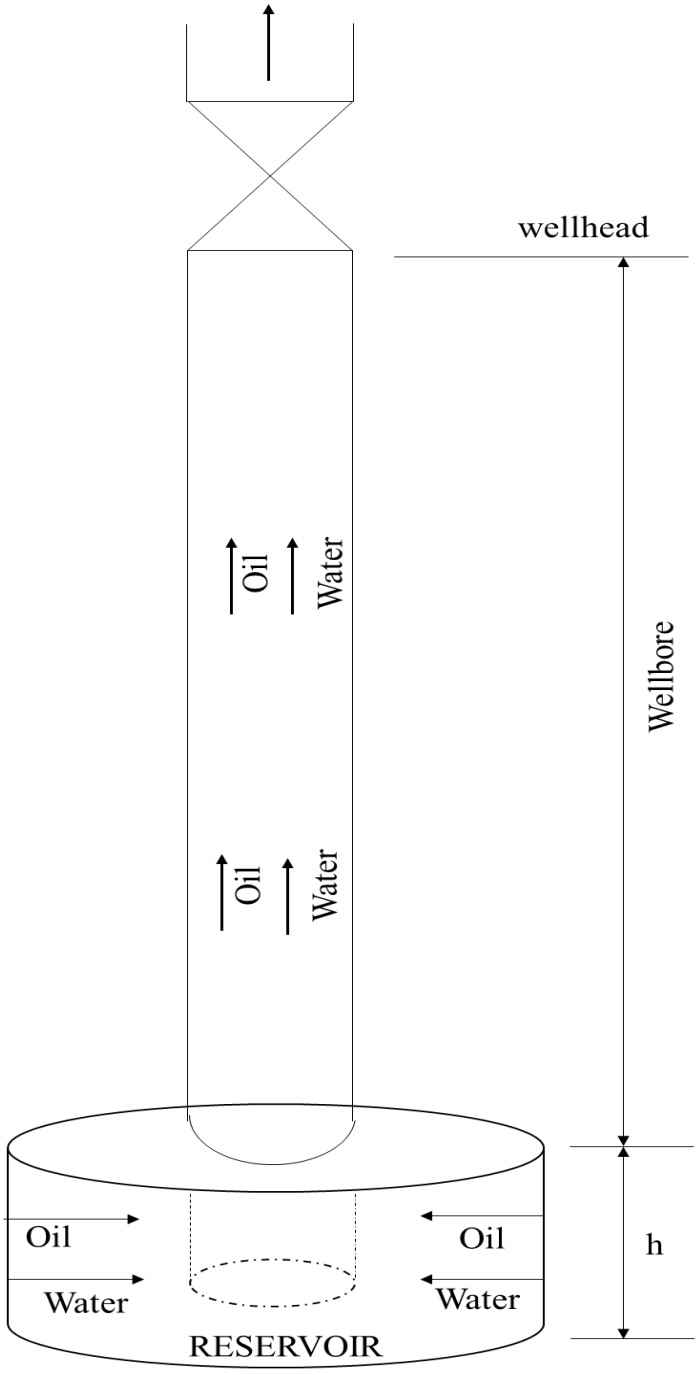

Figure 5. 1. Schematic of a production volumetric reservoir for two-phase flow

5.2. Formulation of Pressure Profiles

It is known that for pseudo-steady state flow, the rate of change of pressure with respect to time is constant and is given for a reservoir operating at a constant total terminal rate of q_{tsc} (Dake, 1998). This type of flow occurs if the outer boundary is completely closed. Therefore, the pressure will decline when fluids are removed from the reservoir since fluids cannot flow across the reservoir boundaries.

Reservoir Pressure Profile. The constitutive relations for fluid and rock properties for two-phase flow in porous media are given below (Aziz and Settari, 2002; Dake, 1998; Lee and Wattenbarger, 1996):

$$s_o + s_w = 1 \tag{5.1}$$

$$P_{cow} = P_o - P_w \tag{5.2}$$

$$c_o = -\frac{1}{B_o}\frac{\partial B_o}{\partial P} \tag{5.3}$$

$$c_w = -\frac{1}{B_w}\frac{\partial B_w}{\partial P} \tag{5.4}$$

$$c_r = \frac{1}{\emptyset}\frac{\partial \emptyset}{\partial P} \tag{5.5}$$

$$c_T = c_o s_o + c_w s_w + c_r \tag{5.6}$$

$$k_o(s_o) = kk_{ro} \tag{5.7}$$

$$k_w(s_w) = kk_{rw} \tag{5.8}$$

where P_{cow} is the oil-water capillary pressure; P_o and P_w introduce the nonwetting and wetting pressures; $c_o, c_w, c_r,$ and c_T refer to the oil, water, rock and total compressibility, respectively; k is the absolute permeability; k_o and k_w represent the oil and water effective permeability; and k_{ro} and k_{rw} are the oil and water relative permeability.

To find the value of $\frac{\partial P}{\partial t} = \text{costant}$ for two-phase flow, the material balance equations are used for both fluids as follows. The mass equation for the oil phase is given by Aziz and Settari (2002):

$$m_o = V_b \phi \rho_o s_o \tag{5.9}$$

where m_o is the oil mass in porous media; V_b stands for the bulk volume; ϕ is the porosity; ρ_o introduces the oil density; and s_o refers to oil saturation.

The mass flow rate of the oil phase is given below:

$$\frac{\partial m_o}{\partial t} = \rho_o q_o \tag{5.10}$$

where q_o is the oil volumetric flow rate.

Substituting Equation (5.9) in Equation (5.10) yields:

$$\frac{\partial}{\partial t}(V_b \phi \rho_o s_o) = \rho_o q_o \tag{5.18}$$

Taking the partial derivative of Equation (5.11) gives the following expression:

$$V_b \left[\rho_o s_o \frac{\partial \phi}{\partial t} + \phi \rho_o \frac{\partial s_o}{\partial t} + \phi s_o \frac{\partial \rho_o}{\partial t}\right] = \rho_o q_o \tag{5.12}$$

Taking the constants ($\phi \rho_o$) out of the brackets in Equation (5.12) yields:

$$V_b\phi\left[\frac{s_o}{\phi}\frac{\partial\phi}{\partial t}+\frac{\partial s_o}{\partial t}+\frac{s_o}{\rho_o}\frac{\partial\rho_o}{\partial t}\right]=q_o \tag{5.13}$$

Following the same steps, the water mass equation will be given as follows:

$$V_b\phi\left[\frac{s_w}{\phi}\frac{\partial\phi}{\partial t}+\frac{\partial s_w}{\partial t}+\frac{s_w}{\rho_w}\frac{\partial\rho_w}{\partial t}\right]=q_w \tag{5.14}$$

Adding Equations (5.13) and (5.14) leads to:

$$V_b\phi\left[(s_o+s_w)\frac{1}{\phi}\frac{\partial\phi}{\partial t}+\frac{\partial}{\partial t}(s_o+s_w)+\frac{s_o}{\rho_o}\frac{\partial\rho_o}{\partial t}+\frac{s_w}{\rho_w}\frac{\partial\rho_w}{\partial t}\right]=q_t \tag{5.15}$$

Using the chain rule, Equation (5.15) gives the following expression:

$$V_b\phi\left[(s_o+s_w)\frac{1}{\phi}\frac{\partial\phi}{\partial P_o}+\frac{\partial}{\partial t}(s_o+s_w)+\frac{s_o}{\rho_o}\frac{\partial\rho_o}{\partial P_o}+\frac{s_w}{\rho_w}\frac{\partial\rho_w}{\partial P_o}\right]\frac{\partial P_o}{\partial t}=q_t \tag{5.16}$$

Using the constitutive relationships, Equations (5.11) to (5.16) and $V_b=h\pi r_e^2$, the following equation is obtained:

$$\frac{\partial P_o}{\partial t}=\frac{q_{tsc}B}{\phi c_T h\pi r_e^2} \tag{5.17}$$

Equation (5.17) represents the rate of pressure change with respect to time for the pseudo-steady state flow.

The continuity equations for oil and water phases are given by Lee and Wattenbarger (1996) – oil phase:

$$\frac{1}{r}\frac{\partial}{\partial r}\left(r\frac{k_o}{\mu_o B_o}\,\rho_{os}\frac{\partial P}{\partial r}\right)=\frac{\partial}{\partial t}\left(\phi\frac{s_o}{B_o}\rho_{os}\right) \tag{5.18}$$

Water phase:

$$\frac{1}{r}\frac{\partial}{\partial r}\left(r\frac{k_w}{\mu_w B_w}\,\rho_{ws}\frac{\partial P}{\partial r}\right)=\frac{\partial}{\partial t}\left(\phi\frac{s_w}{B_w}\rho_{ws}\right) \tag{5.19}$$

where r is the radius; ϕ refers to the porosity; P represents the pressure; μ_o and μ_w are the viscosities for oil and water; s_o and s_w are the oil and water saturation, respectively; ρ_{os} and ρ_{ws} symbolize the densities at standard conditions for the oil and water; and B_o and B_w stand for the formation volume factors for oil and water.

For slightly compressible fluids, Equations (5.18) and (5.19) become – oil phase:

$$\frac{1}{r}\frac{\partial}{\partial r}\left(r\frac{k_o}{\mu_o B_o}\,\frac{\partial P}{\partial r}\right)=\frac{\partial}{\partial t}\left(\phi\frac{s_o}{B_o}\right) \tag{5.20}$$

Water phase:

$$\frac{1}{r}\frac{\partial}{\partial r}\left(r\frac{k_w}{\mu_w B_w}\,\frac{\partial P}{\partial r}\right)=\frac{\partial}{\partial t}\left(\phi\frac{s_w}{B_w}\right) \tag{5.21}$$

Using the product rule on the left-hand side in Equations (5.20) and (5.21) leads to – oil phase:

$$\frac{1}{r}\left(\frac{k_o}{\mu_o B_o}\right)\frac{\partial}{\partial r}\left(r\,\frac{\partial P}{\partial r}\right)+\frac{\partial P}{\partial r}\frac{\partial}{\partial r}\left(\frac{k_o}{\mu_o B_o}\right)=\phi\frac{\partial}{\partial t}\left(\frac{s_o}{B_o}\right) \tag{5.22}$$

Water phase:

$$\frac{1}{r}\left(\frac{k_w}{\mu_w B_w}\right)\frac{\partial}{\partial r}\left(r\,\frac{\partial P}{\partial r}\right)+\frac{\partial P}{\partial r}\frac{\partial}{\partial r}\left(\frac{k_w}{\mu_w B_w}\right)=\phi\frac{\partial}{\partial t}\left(\frac{s_w}{B_w}\right) \tag{5.23}$$

It is known that the formation volume factor and viscosity are a function of pressure, while the permeability is a function of oil and water saturation, not pressure. Using the chain rule in the second term of Equations (5.22) and (5.23) on the left side results in – oil phase:

$$\left[\frac{1}{r}\left(\frac{k_o}{\mu_o B_o}\right)\frac{\partial}{\partial r}\left(r\,\frac{\partial P}{\partial r}\right)\right]+\left[\frac{\partial P}{\partial r}\left(\frac{1}{\mu_o B_o}\right)\frac{\partial k_o}{\partial s_o}\frac{\partial s_o}{\partial r}\right]+\left[\frac{\partial P}{\partial r}\left(\frac{1}{\mu_o B_o}\right)\frac{\partial k_o}{\partial s_w}\frac{\partial s_w}{\partial r}\right]+\left[\left(\frac{\partial P}{\partial r}\right)^2 k_o\frac{\partial}{\partial t}\left(\frac{1}{\mu_o B_o}\right)\right]=\phi\frac{\partial}{\partial t}\left(\frac{s_o}{B_o}\right) \quad (5.24)$$

Water phase:

$$\left[\frac{1}{r}\left(\frac{k_w}{\mu_w B_w}\right)\frac{\partial}{\partial r}\left(r\,\frac{\partial P}{\partial r}\right)\right]+\left[\frac{\partial P}{\partial r}\left(\frac{1}{\mu_w B_w}\right)\frac{\partial k_w}{\partial s_o}\frac{\partial s_o}{\partial r}\right]+\left[\frac{\partial P}{\partial r}\left(\frac{1}{\mu_w B_w}\right)\frac{\partial k_w}{\partial s_w}\frac{\partial s_w}{\partial r}\right]+\left[\left(\frac{\partial P}{\partial r}\right)^2 k_w\frac{\partial}{\partial t}\left(\frac{1}{\mu_w B_w}\right)\right]=\phi\frac{\partial}{\partial t}\left(\frac{s_w}{B_w}\right) \quad (5.25)$$

Assuming $\left(\frac{\partial P}{\partial r}\right)^2$, $\left[\frac{\partial P}{\partial r}\frac{\partial s_o}{\partial r}\right]$, and $\left[\frac{\partial P}{\partial r}\frac{\partial s_w}{\partial r}\right]$ are negligible, the oil Equation (5.24) and water Equation (5.25) become the following forms – oil phase:

$$\frac{1}{r}\frac{\partial}{\partial r}\left(r\,\frac{\partial P}{\partial r}\right)=\phi\frac{\mu_o B_o}{k_o}\frac{\partial}{\partial t}\left(\frac{s_o}{B_o}\right) \quad (5.26)$$

Water phase:

$$\frac{1}{r}\frac{\partial}{\partial r}\left(r\,\frac{\partial P}{\partial r}\right)=\phi\frac{\mu_w B_w}{k_w}\frac{\partial}{\partial t}\left(\frac{s_w}{B_w}\right) \quad (5.27)$$

After using the chain rule and applying the partial derivative of the right-hand side of Equations (5.26) and (5.27), the following expressions are obtained:

Oil phase:

$$\frac{1}{r}\frac{\partial}{\partial r}\left(r\,\frac{\partial P}{\partial r}\right)=\phi\frac{\mu_o B_o}{k_o}\left[\frac{1}{B_o}\frac{\partial s_o}{\partial P}\frac{\partial P}{\partial t}+s_o\frac{\partial}{\partial P}\left(\frac{1}{B_o}\right)\frac{\partial P}{\partial t}\right] \quad (5.28)$$

Water phase:

$$\frac{1}{r}\frac{\partial}{\partial r}\left(r\,\frac{\partial P}{\partial r}\right)=\phi\frac{\mu_w B_w}{k_w}\left[\frac{1}{B_w}\frac{\partial s_w}{\partial P}\frac{\partial P}{\partial t}+s_w\frac{\partial}{\partial P}\left(\frac{1}{B_w}\right)\frac{\partial P}{\partial t}\right] \quad (5.29)$$

It is also known that:

$$\frac{\partial}{\partial P}\left(\frac{1}{B}\right) = -\frac{1}{B^2}\frac{\partial B}{\partial P} \tag{5.30}$$

Combination and rearrangement of Equations (5.28) and (5.29) to (5.30) results in:

Oil phase:

$$\frac{1}{r}\frac{\partial}{\partial r}\left(r\,\frac{\partial P}{\partial r}\right) = \phi\frac{\mu_o}{k_o}\left[\frac{\partial s_o}{\partial P} - \frac{s_o}{B_o}\frac{\partial B_o}{\partial P}\right]\frac{\partial P}{\partial t} \tag{5.31}$$

Water phase:

$$\frac{1}{r}\frac{\partial}{\partial r}\left(r\,\frac{\partial P}{\partial r}\right) = \phi\frac{\mu_w}{k_w}\left[\frac{\partial s_w}{\partial P} - \frac{s_w}{B_w}\frac{\partial B_w}{\partial P}\right]\frac{\partial P}{\partial t} \tag{5.32}$$

The fluid mobility is introduced as follows:

$$\lambda_o = \frac{k_o}{\mu_o} \tag{5.33}$$

$$\lambda_w = \frac{k_w}{\mu_w} \tag{5.34}$$

The total compressibility for two-phase flow in porous media can be given by the following model of Lee and Wattenbarger (1996):

$$c_t = \left(\frac{\partial s_w}{\partial P} - \frac{s_w}{B_w}\frac{\partial B_w}{\partial P}\right)\left(\frac{\lambda_t}{\lambda_o}\right) \tag{5.35}$$

Substituting Equation (5.35) in Equations (5.31) and (5.32) gives the following expressions – oil phase:

$$\frac{1}{r}\frac{\partial}{\partial r}\left(r\,\frac{\partial P}{\partial r}\right)=\frac{\phi c_t}{\lambda_o}\frac{\partial P}{\partial t} \tag{5.36}$$

Water phase:

$$\frac{1}{r}\frac{\partial}{\partial r}\left(r\,\frac{\partial P}{\partial r}\right)=\frac{\phi c_t}{\lambda_w}\frac{\partial P}{\partial t} \quad \text{or} \quad \frac{1}{r}\frac{\partial}{\partial r}\left(r\,\frac{\partial P}{\partial r}\right)-\frac{1}{r}\frac{\partial}{\partial r}\left(r\,\frac{\partial P_c}{\partial r}\right)=\frac{\phi c_t}{\lambda_w}\frac{\partial P}{\partial t} \tag{5.37}$$

Equation (5.36) describes fluid flow through porous media for slightly compressible fluids. Equation (5.37) includes the capillary pressure as a variable in the fluid flow.

Substituting Equation (5.17) in Equation (5.36) leads to:

$$\frac{1}{r}\frac{\partial}{\partial r}\left(r\,\frac{\partial P}{\partial r}\right)=\frac{1}{\lambda_o}\frac{q_{sc}B}{h\pi r_e^2} \tag{5.38}$$

Using the Darcy equation, Equation (5.38) turns to:

$$\frac{d}{dr}\left(\frac{q}{B}\right)=-\left(\frac{2r}{r_e}\right)q_{sc} \tag{5.39}$$

Integration of Equation (5.39) gives the volumetric flow rate in the reservoir as shown below:

$$\left(\frac{q}{B}\right)=C-\left(\frac{r}{r_e}\right)^2 q_{sc} \tag{5.40}$$

where C is an integration constant. Using the volumetric flux and substituting Equation (5.40) in the Darcy equation, the pressure distribution in the reservoir is obtained as follows:

$$\frac{\partial P}{\partial r}=B_l\frac{\mu_l}{k_l}\left(\frac{C-\left(\frac{r}{r_e}\right)^2 q_{sc}}{2\pi r h}\right) \tag{5.41}$$

For a volumetric reservoir $\partial P/\partial r = 0$ at $r = r_e$. Equation (5.41) gives one possible solution $C = q_{sc}$. Equation (5.41) becomes:

$$\frac{\partial P}{\partial r} = B_l \frac{\mu_l}{k_l} \frac{q_{sc}}{2\pi h} \left(\frac{1}{r} - \frac{r}{r_e^2} \right) \tag{5.42}$$

Equation (5.42) represents the pressure distribution in the reservoir for a two-phase flow, which is similar to a single-phase flow except that k_l is the effective liquid permeability; μ_l is the liquid viscosity; and B_l is the liquid formation volume factor.

Flowing Well Pressure. For the fluid flow in a wellbore, a pseudo-steady state is assumed. Furthermore, a one-dimensional two-phase flow is assumed for the flow in the wellbore with a constant cross-sectional area. In addition, no heat exchange between oil and water (thermal equilibrium condition) is assumed.

The mechanical energy equation (Equation (4.16)) can also be used for developing the flowing well pressure where there is a two-phase flow in a wellbore. The procedure is similar to the case of the single-phase flow. The main difference will be in the production rate, density, and formation volume factor.

Equation (4.19) is changed to the following forms for two-phase flow in a wellbore – oil phase:

$$\frac{dp_o}{d\ell} = \frac{g\frac{H}{L} + \frac{f_M}{2D}\left(\frac{4q_{osc}}{\pi D^2}\right)^2 B_o^2}{\frac{B_o}{\rho_{osc}} + \left(\frac{4q_{osc}}{\pi D^2}\right)^2 B_o \frac{dB_o}{dp}} \tag{5.43}$$

Water phase:

$$\frac{dp_w}{d\ell} = \frac{g\frac{H}{L} + \frac{f_M}{2D}\left(\frac{4q_{wsc}}{\pi D^2}\right)^2 B_w^2}{\frac{B_w}{\rho_{wsc}} + \left(\frac{4q_{wsc}}{\pi D^2}\right)^2 B_w \frac{dB_w}{dp}} \tag{5.44}$$

For both fluids flowing simultaneously, Equations (5.43) and (5.44) will become:

$$\frac{dp}{d\ell} = \frac{g\frac{H}{L} + \frac{f_M}{2D}\left(\frac{4q_{tsc}}{\pi D^2}\right)^2 B_t^2}{\frac{B_t}{\rho_{tsc}} + \left(\frac{4q_{tsc}}{\pi D^2}\right)^2 B_t \frac{dB_t}{dp}} \tag{5.45}$$

The total formation volume factor (B_t) is expressed as follows:

$$B_t = B_o \tag{5.46}$$

As the water formation factor under most process conditions has a value of 1, and it is a weak function of pressure and temperature, it is assumed that the oil formation volume factor has the main influence. Hence, the total density is determined as follows:

$$\rho_t = (1 - f_w)\rho_o + f_w\rho_w \tag{5.47}$$

where f_w stands for the water volume fraction or quality as given below (Duruewuru, 1985):

$$f_w = \frac{q_{water}}{q_{oil}} \tag{5.48}$$

5.3. Formulation of Entropy Production

Reservoir System. Equation (4.24) for single-phase is also valid for each individual phase in the two-phase (oil – water) system; however, different parameters and conditions should

be considered. Thus, the total entropy production for both oil and water phases are given by the following equations:

$$\left.\frac{\partial S_T}{\partial t}\right]_{total} = \left.\frac{\partial S_T}{\partial t}\right]_{oil} + \left.\frac{\partial S_T}{\partial t}\right]_{water} \tag{5.49}$$

$$\left.\frac{\partial S_T}{\partial t}\right]_{total} = 2\pi h\left[\int_{r_w}^{r_e}\left|\frac{\rho_{osc} f_p \beta u_o^2}{\phi s_{or} T B_o} r\, dr\right|_{oil} + \int_{r_w}^{r_e}\left|\frac{\rho_{wsc} f_p \beta u_w^2}{\phi(1-s_{wc}) T B_w} r\, dr\right|_{water}\right] \tag{5.50}$$

Flowing well System. Also, Equation (4.28) can be used to calculate the total entropy change with time for a flowing well as given below:

$$\left.\frac{\partial S_T}{\partial t}\right]_{total} = \int_0^L \left|\frac{\rho_{sc} f_M}{2DTB}\left[\frac{4q_{sc}B}{\pi D^2}\right]^3 d\ell\right|_{oil} + \int_0^L \left|\frac{\rho_{sc} f_M}{2DTB}\left[\frac{4q_{sc}B}{\pi D^2}\right]^3 d\ell\right|_{water} \tag{5.51}$$

Total Entropy Generation. The total entropy production rate for two-phase flow in the reservoir and wellbore systems over a time interval from the initial time to the final time in the pseudo-steady state is given by the following equation:

$$S_T = \frac{\pi r_e^2 h}{q_{sc}} \int_{\bar{P}_f}^{\bar{P}_i} \left(\left.\frac{\partial S_T}{\partial t}\right]_{well} + \left.\frac{\partial S_T}{\partial t}\right]_{reservoir}\right) \frac{\phi(\bar{P}) c_t(\bar{P})}{B_t(\bar{P})} d\bar{P} \tag{5.52}$$

Note that $B_t(\bar{P})$, $c_t(\bar{P})$, and $\phi(\bar{P})$ are functions of the average pressure. Substituting Equations (5.50) and (5.51) into Equation (5.52), the following equation is obtained:

$$S_T = \frac{\pi r_e^2 h}{q_{sc}} \int_{\bar{P}_f}^{\bar{P}_i} \left(\left.\frac{\partial S_T}{\partial t}\right]_{\substack{well \\ (o+w)}} + \left.\frac{\partial S_T}{\partial t}\right]_{\substack{reservoir \\ (o+w)}}\right) \frac{\phi(\bar{P}) c_t(\bar{P})}{B_t(\bar{P})} d\bar{P} \tag{5.53}$$

5.4. Solution Procedure

A computer program was also developed to simulate and solve the flow of two-phase (oil-water) equations in both the reservoir and wellbore simultaneously. Both models are nonlinear equations that can be solved by a numerical solution method. As it is assumed there is no change in temperature of the reservoir nor wellbore but only the spatial change, the finite-difference approximation or grid construction is not used as a solution method; but Euler's method is used as the solution method. The solution of both models is obtained in terms of pressure and entropy.

The equations derived in the previous section for two-phase flow in porous media and wellbore are not sufficient to fully describe the fluid flow behavior. Additional supplementary equations needed in this modelling phase are given below. The Original Hydrocarbon In Place (OHIP) is given by Dake (1998) as follows:

$$N = \frac{7758Ah\phi(1 - S_{wi})}{B_{oi}} \tag{5.54}$$

where N is the Original Hydrocarbon In Place; A is the reservoir area; h refers to the reservoir thickness; ϕ represents the porosity; S_{wi} is the initial water saturation; and B_{oi} denotes the initial oil formation volume factor.

The capillary pressure as a function of saturation in field units is given by Aziz and Settari (2002):

$$P_c = P_{nw} - P_w \tag{5.55}$$

where P_c is the capillary pressure; ρ_w stands for the density of water; ρ_o is the density of oil, and h introduces the height of the capillary rise.

Effective water saturation is expressed as follows (Brooks and Corey, 1966):

$$S_{ew} = \left[\frac{S_w - S_{wr}}{1 - S_{wr} - S_{or}}\right] \tag{5.56}$$

where S_{ew} is the effective water saturation; S_{wr} is the residual water saturation; S_{or} refers to the residual oil saturation; and S_w symbolizes the water saturation at a different P_c.

The fractural oil and water flow are given by the following expression (Dake, 1998; Lee and Wattenbarger, 1996):

$$f_w = \left[\frac{q_w}{q_t}\right] \;\&\; f_o = \left[\frac{q_o}{q_t}\right] \tag{5.57}$$

where f_w and f_o represent the water and oil fractional flow, respectively; q_w and q_o introduce the water and oil production rate, respectively; and $q_t = q_w + q_o$ is the total production rate.

The relative permeability equation as a function of saturation is given by the following expression (Brooks and Corey, 1966):

$$k_{rw} = (s_{we})^{\left(\frac{2+3\lambda}{\lambda}\right)} \tag{5.58}$$

where k_{rw} is the water relative permeability, and λ characterizes the pore size distribution of the porous medium (values range from 0.2 – 5). Higher values of λ are used for highly homogeneous porous media for which the pore size distribution is narrow (Mahmoodi et al., 2020):

$$k_{ro} = (1 - s_{we})^2 (1 - s_{we})^{\left(\frac{2+\lambda}{\lambda}\right)} \quad (5.59)$$

where k_{ro} denotes the oil relative permeability.

The solution of the two-phase model is different than the single-phase model in many factors, such as relative permeability and pressure profiles. There is a difficulty of controlling each phase's production at the surface as the pseudo-steady state is required. It is well known that control can be done for the total production rate (oil and water) that reaches the surface. In this chapter, an assumption of the fractional flow of each phase was made based on past studies of Tillero and Mogollon (2020).

In the absence of capillary pressure, both oil and water pressure will be the same at the bottom of the wellbore; however, the reservoir profiles will be slightly different according to Equation (5.42). An assumption of λ (which characterizes the pore size distribution of the porous medium) is made, followed by a calculation of relative permeability of each phase using Equations (5.58) and (5.59). The calculated relative permeabilities for both phases is used to determine the final pressure profiles of the reservoir from r_w to r_e using Equation (5.42). The initial relative permeabilities are used to calculate the initial reservoir pressure profiles. Then the average pressure is calculated. The average reservoir pressure is then used to calculate the total entropy production for both phases using Equation (5.53).

In the presence of the capillary pressure, a pressure of one phase is assumed, while the other phase is calculated using the capillary pressure equation. The next steps to calculate the total entropy production rate will be the same as the scenario of the capillary pressure's absence.

A flow chart is shown in **Figure 5.2**. This indicates a step-by-step plan to determine the total entropy production and recovery factor for two-phase flow.

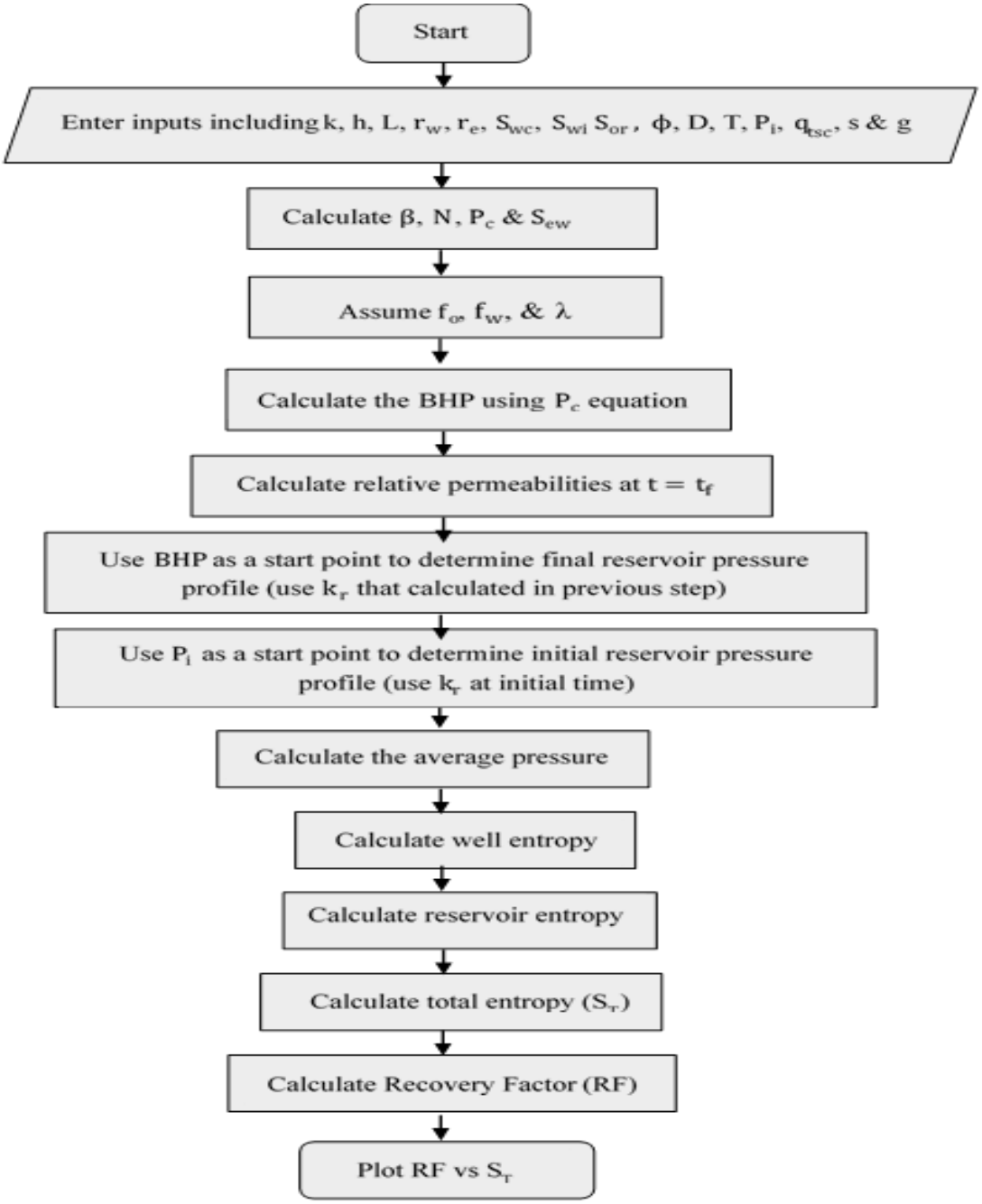

Figure 5.2. Flowchart for the approach used in two-phase flow.

5.5. Limitations of Proposed Models

Despite the effort towards developing models that describe the entropy production in both the reservoir and wellbore for both cases, single-phase and two-phase flow, there are still limitations that prevent these models from being applied in various scenarios. Due to the complexity of the fluid flow equations, some simplifying assumptions are made. Limitations of the proposed models, single-phase or two-phase, can be summarised as follows. The volumetric reservoir under pseudo-steady state conditions is the only reservoir type used in these models for entropy generation calculations. In addition, the proposed models are only applicable to isothermal conditions as the change of reservoir temperature is not considered.

The heat transfer from the fluid to the surrounding environment is not considered while developing these models. The only considered energy conversion is the energy dissipated from fluid expansion and friction. The two-phase models are only applicable to oil-water systems, not oil-gas systems. The form of equations will differ from the proposed models in terms of total compressibility, diffusivity equation, and total density while dealing with oil-gas systems.

The reservoir should be homogenous and isotropic. All physical properties of the fluid and rock are assumed uniform and do not vary in different directions. The gravitation effects in the reservoir are assumed negligible. In the Darcy equation, the gravity term is thus neglected. The models consider only the loss of the mechanical energy of the reservoir. There are no external sources of energy, such as thermal recovery, water flooding, or any form of enhanced oil recovery techniques.

5.6. Summary

It is common in petroleum engineering to have a two fluids flow in a reservoir, either oil-gas or oil-water. Therefore, for more realistic generalization, the single-phase models are extended to two-phase models in this chapter. Most of the previous studies are focused on the oil-gas system due to its common existence in reservoirs; however, the oil-water system is also common in undersaturated reservoirs. There is limited published work on this system, especially in the EGM field. For this reason, this chapter aims to fill this gap and enrich the literature on this topic.

Significant changes were made in single-phase models to address two-phase flow in both the reservoir and wellbore. For pressure profiles, important quantities need to be introduced, such as saturation, relative permeabilities, and capillary pressure. The same assumptions that are made in single-phase models are valid in two-phase models as well. It is also important to highlight that hydrocarbon mixture properties are assumed to be constant, and the fractional flow of each phase is constant for the entire production time.

The primary equations to develop the two-phase flow models are the continuity equation (conservation of mass), momentum balance equation, energy balance equation, and entropy balance equation (second law of thermodynamics). To ensure no gas phase in a reservoir or wellbore, the reservoir pressure, as well as BHP, are kept above the bubble point. It is important to note that the reservoir is under the influence of natural energy exchange mechanisms; no secondary or tertiary enhanced oil recovery technique is used.

The final pressure profiles for both reservoir and wellbore for two-phase flow models are similar to single-phase flow models except in the relative permeability, viscosity, and formation volume factor. Similarly for the total entropy production rate, except in two-phase models, both phases are flowing simultaneously in the reservoir and wellbore.

A computer program using MATLAB was developed to solve the two-phase models for both the reservoir and wellbore simultaneously. To validate the accuracy of the results, CMG simulation software is used and discussed for the two-phase flow models in the next chapter.

Chapter 6: Results and Discussion

6.1. Introduction

As discussed earlier, a comprehensive computer program using MATLAB was developed to solve the mathematical models for both single-phase and two-phase flow and to simulate the fluid flow problems. Computer Modelling Group (CMG) simulation software was also used to validate the results of the proposed models. It is mainly used in the validation of pressure profiles and the recovery factor in the reservoir. Both CMG-GEM and CM-IMEX were used to simulate the single-phase (dry gas) and two-phase (oil-water), respectively. To simulate the pesedo-steady state in CMG for both scenarios (single-phase and two-phase), only the data that represent the time period with a constant production rate were considered for validation phase. Once the production rate decreases, a deviation is observed. This will be explained with more details in this chapter.

This chapter contributes to existing knowledge of EGM applications in porous media by providing a comprehensive investigation of the three main hydrocarbon reservoir systems: reservoir, wellbore, and near-wellbore. Additionally, an economic analysis is conducted to validate the optimum production rate estimations. These two contributions bring us a step closer to have a more accurate, reliable, and comprehensive model for entropy generation in sub-surface and surface systems of single-phase and two-phase fluid flow reservoirs. Having comprehensive models that can be used to reduce the loss of reservoir energy and consequently obtain a high recovery factor is one of the research objectives. Furthermore,

filling research knowledge gaps in the petroleum industry is another motivation for conducting this research.

A one-dimensional flow is assumed in the wellbore, while a radial flow is assumed in the reservoir. Mass, momentum, energy, and entropy balance equations are utilized to address the fluid flow behaviour and energy loss in wellbore and reservoir systems. Numerical methods are employed to solve the fluid flow and entropy equations. The models are solved by an existing numerical scheme programmed in the MATLAB environment with a new algorithm. For validation purposes, a commercial simulator, Computer Modeling Group (CMG), is employed.

The main assumptions in this analysis are: (i) the reservoir is assumed to be volumetric, (ii) there is a radial flow in the reservoir, while one dimensional in the wellbore, (iii) the reservoir is isotropic and homogenous, (iv) the reservoir is under isothermal conditions, and (v) the fluid flow is under the influence of pseudo-steady state flow conditions. The models that are developed in this study are capable of handling single-phase flow (dry gas or oil) and two-phase flow (oil-water). The models in this study give a more rigorous formulation of the momentum equation for flow in porous media. Furthermore, a step-by-step solution is provided for pseudo-steady state radial flow problems for single-phase and two-phase flow. In addition, the pressure distribution equation is derived from the energy balance equation for the wellbore system.

6.2. Single-Phase Models

The models in this study for single-phase flow are based on a dry gas reservoir. However, they are also capable of handling dead oil reservoirs. In this study, the second law of thermodynamics addresses EGM in a porous system during fluid production. Appropriate models based on thermodynamics fundamentals are used to investigate the EGM of three systems: a reservoir, a near-wellbore, and a wellbore.

Numerical and analytical methods are used to predict the cumulative entropy production in a reservoir and obtain the optimum production rate. The proposed models are first developed in two systems only, reservoir and wellbore, to examine their accuracy and reliability compared to a previous study (Civan and Tiab, 1989). The models are then extended to include the third system, the near-wellbore or the damaged region.

As shown in **Figure 6.1**, the skin affects the total entropy production rate as well as the recovery factor of the reservoir. For example, at a positive skin factor, the reservoir will be at its lowest recovery factor with less energy consumption. On the contrary, at a negative skin factor, a high recovery factor is obtained with a high energy loss. Additionally, at a positive skin factor, the entropy generation reaches its maximum value earlier compared to a negative skin. The distance between the start and endpoints of the entropy generation for the positive skin is shorter compared to the negative skin case.

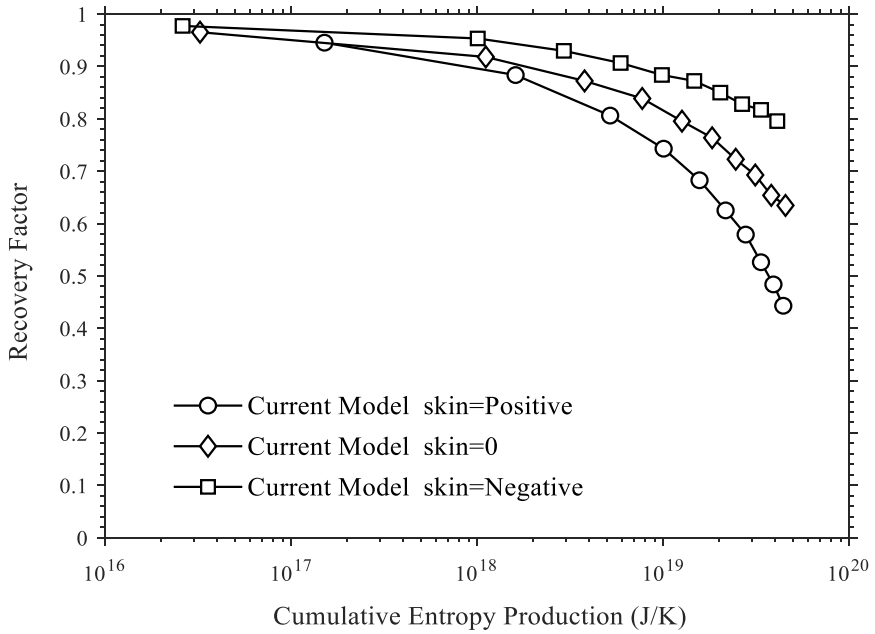

Figure 6. 1. Recovery factor versus cumulative entropy production as a function of production rate and skin factor.

6.2.1. Model Validation

For validation purposes, the single-phase models are compared to previous results of other studies. To verify accuracy and precision, the data used in the comparison are the same as those reported in Civan and Tiab (1989). **Table 6.1** shows the details of these data points in both SI and field units.

Figure 6.2 compares the current models and previous models (Civan and Tiab, 1989). The research findings in **Figures 6.2a** to **6.2c** are consistent with the results of the study conducted by Civan and Tiab (1989). According to **Figure 6.2b,** a large discrepancy is noticed due to unrealistic data/conditions in the study of Civan and Tiab (1989). It is found

that as the cumulative entropy production is increased, the recovery factor is reduced. Generally, all panels of **Figure 6.2** show the same trend as Civan and Tiab (1989), while there is an inconsistency in numerical values between them due to using different solution methods. **Table 6.2** lists the specifications of the current research model.

As the reservoir pressure profile is an essential input variable for EGM calculations, CMG simulation software is used to validate the initial and final pressure profiles estimated with the proposed model. There is a good match between the CMG simulator results and the current model, based on **Figure 6.3**. It is worth mentioning that the profiles are obtained at a constant production rate.

Table 6. 1. Data for dry gas well and reservoir systems

Parameter	**SI Unit**	**Field Unit**
D	0.0508 m	2 in
H	1524 m	5000 ft
h	7.3152 m	24 ft
L	2438.4 m	8000 ft
k	5.0E-15 D	5 mD
ϕ	0.15	0.15
r_w	0.0508 m	2 in
r_e	908.304 m	2980 ft
S_{wc}	0.20	0.20
P_i	2.7579E+7 Pa	4000 psia
$(P_{wh})_f$	1.379E+7 Pa	2000 psia
P_{ob}	1.0E+10 Pa	1.45E+6 psi

Table 6. 2. Comparison between the current model and Civan and Tiab (1989).

Approach	Current Model	Civan and Tiab's Model
Well pressure profile	Using corrected Equation (3.17)	Different model Equation (21) in their paper
Reservoir pressure profile	Using the corrected Equation (3.9)	Different model Equation (C7) in their paper
Total compressibility	Function of pressure	Independent of pressure
Gas density	Varies with pressure	Constant at various pressures
Gas composition	C1 98%, C2 1.5%, and C3 0.5%	Unknown

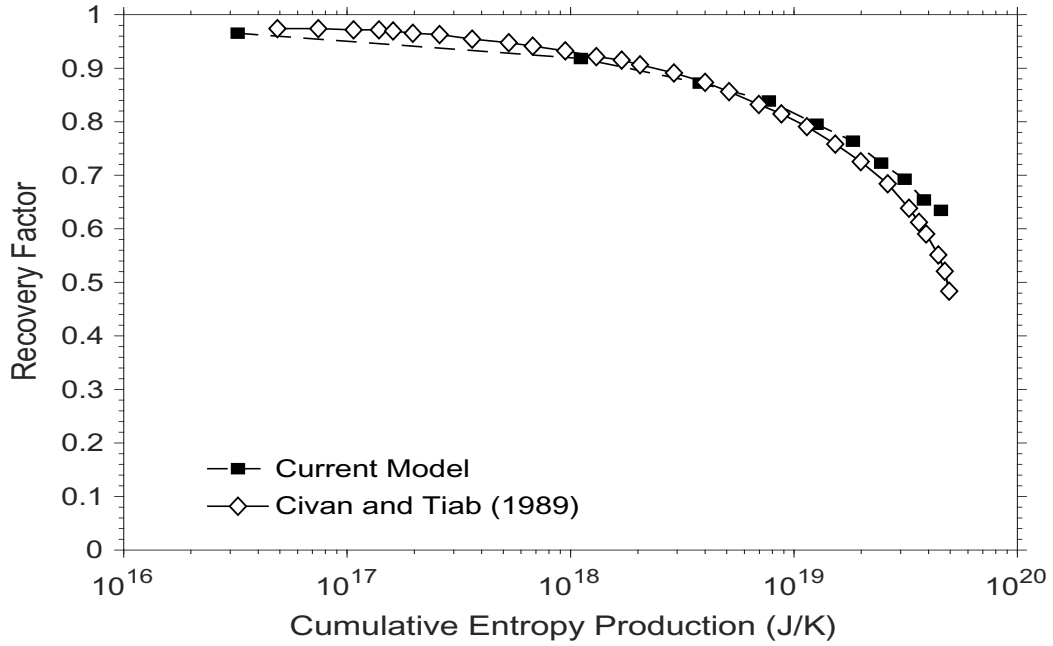

(a) No Skin Factor Effect

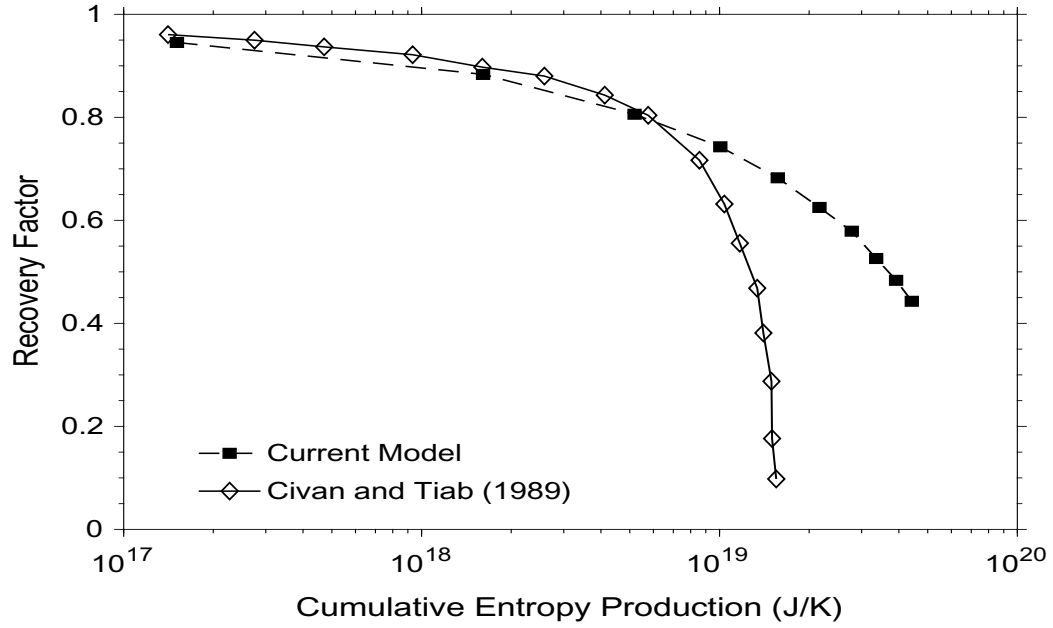

(a) Positive Skin Factor Effect

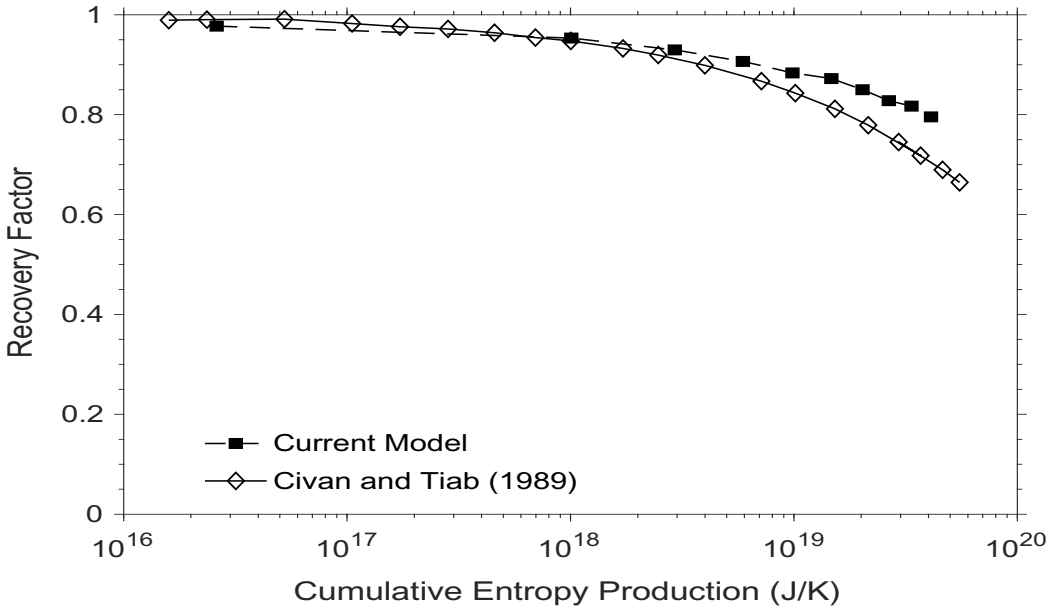

(b) Negative Skin Factor Effect

Figure 6.2. Recovery factor versus cumulative entropy production based on the results of the current model and Civan and Tiab (1989) with / without of skin factors.

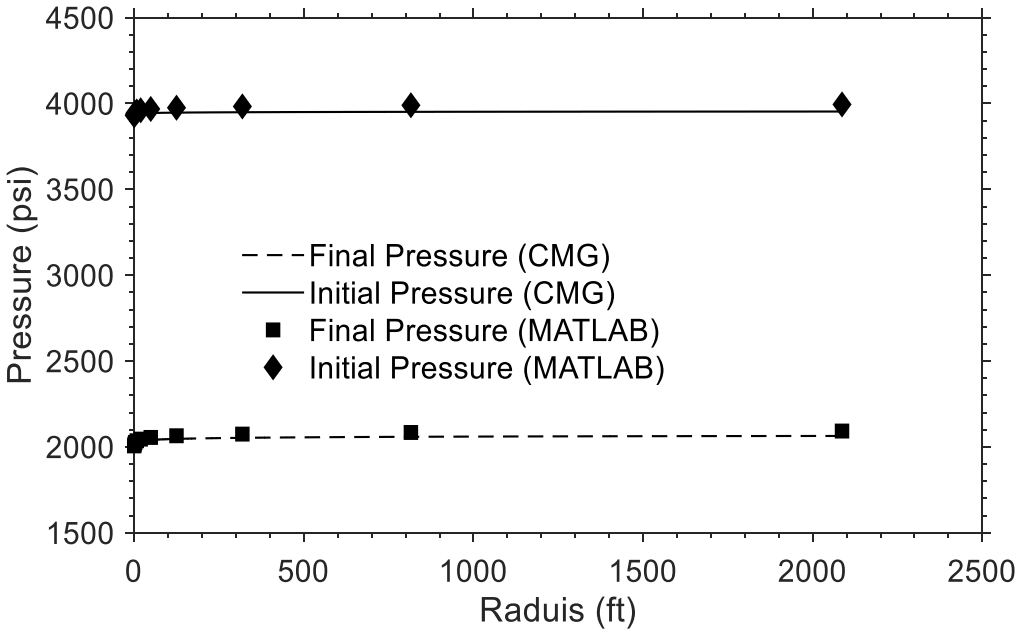

Figure 6. 3. Pressure versus radius based on the results of the current model and CMG.

The CMG is used again as a validation tool for the recovery data obtained from the current models. Recovery factors at different Bottom Hole Pressures (BHP) calculated by the current models are compared with the data obtained from CMG at a constant production rate. The result of this comparison is shown in **Figure 6.4**. As the difference between the reservoir pressure and BHP is increased (lower BHP), an increase in the recovery factor is noticed. This observation is well known in the oil and gas industry during petroleum production. **Figure 6.4** displays a good match between the current models and CMG results at high BHP. As the BHP decreases, the agreement will be less due to the incapability of CMG to maintain a constant production rate for the entire time. As shown in **Figure 6.4**, when the BHP reaches 3000 psi and lower, more deviation is noticed, resulting in a considerable discrepancy.

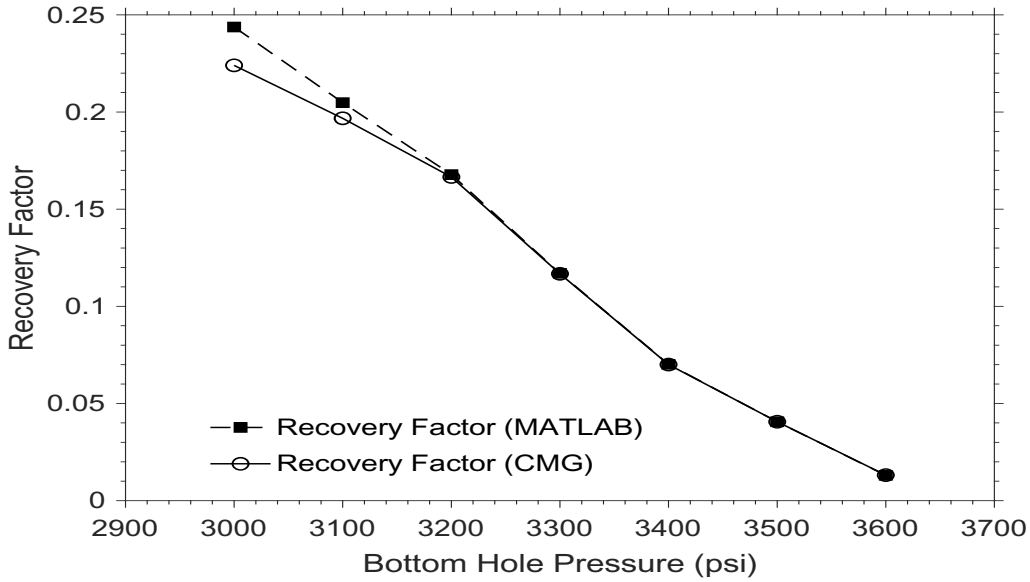

Figure 6. 4. Recovery factor versus BHP using the current model and CMG results at 0.1 m^3/s production rate.

6.2.2. Skin Effect and Comparison of Two-Zone Model with One-Zone Model

The model is extended to incorporate the three systems (refer to Equation (3.28)). The results obtained for three systems are also compared to those for two systems while using the proposed model, as shown in **Figure 6.5**. Adding a new region around the wellbore, an increase in recovery factor is noticed, while there is no significant change in the cumulative entropy production (see **Figure 6.5**). The reason for no appreciable change in the cumulative entropy production is that adding a near wellbore system does not affect the average reservoir pressure, which has a considerable impact on entropy generation. In

addition to the previous finding, the present research reveals that a substantial increase in the recovery factor occurs when increasing the production rate.

In contrast, at lower production rates, an increase in the recovery factor is unnoticeable for both damaged and stimulation scenarios. It is clear that there will be no change in the recovery factor when there is no skin effect. Adding a new region around a wellbore allows the model to incorporate two permeability values: reservoir permeability and new region permeability. Therefore, the actual value of the new region's permeability will improve the accuracy of recovery factor calculations. The CMG is also employed to verify the actual value of a new region radius that corresponds to the skin factor.

The results indicate that a substantial increase in the recovery factor occurs when increasing the production rate. In contrast, at lower production rates, an increase in the recovery factor is not noticeable for both damaged and stimulation scenarios.

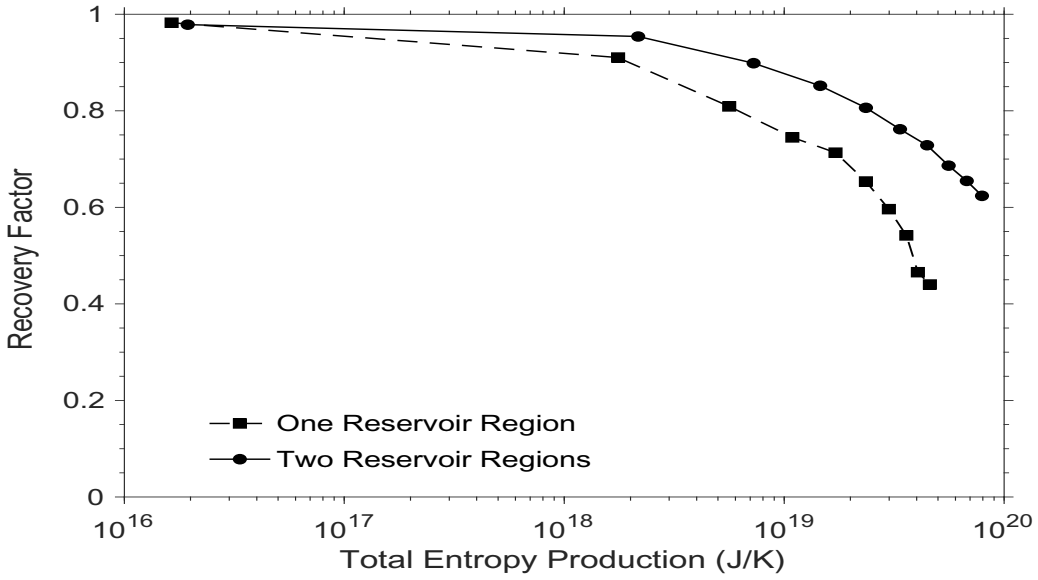

(a) Positive Skin Factor Effect

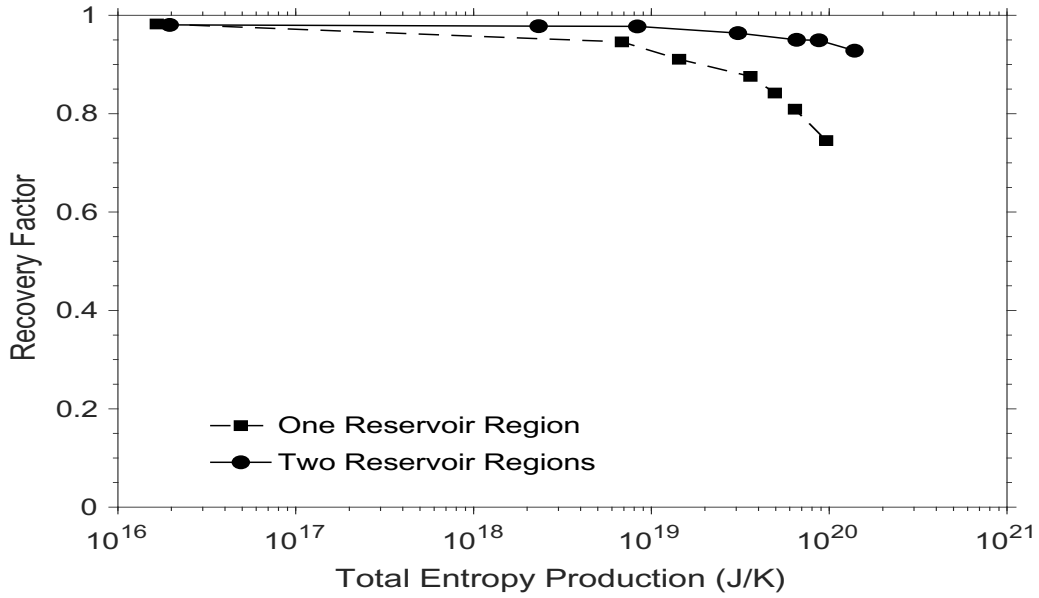

(b) Negative Skin Factor Effect

Figure 6. 5. Impact of recovery factor on total entropy production for one and two region cases.

Adding a new region around a wellbore involves two values of permeabilities in the model, reservoir permeability and new region permeability. The actual value of the permeability for the new region will improve the accuracy of recovery factor calculations.

The effect of the production rate on the EGM is clearly depicted in **Figure 6.6**. Increasing the production rate leads to an increase in entropy production. It is apparent that the increase in the total entropy production is significant at a low production rate, compared to a high production rate. To justify this behavior, the total entropy production dramatically increases when the production rate ranges between 0.01 m^3/s and 0.4 m^3/s. In comparison, the increase in entropy production is less significant beyond the production rate of 0.4 m^3/s.

At a high production rate, a reservoir uses a considerable amount of energy, especially if the reservoir is volumetric to maintain a high production rate. This reason explains entropy production maximization while increasing the production rate. The reason for having less increase in entropy production at high production rates compared to low production rates is that at high production rates, the reservoir most likely reaches its maximum energy loss level. Hence, as the production rate increases, there will not be enough energy left to be lost. In other words, at a specific production rate, the reservoir reaches its maximum energy loss. This particular production rate is referred to as an optimum production rate.

6.2.3. Sensitivity Analysis

The effects of different parameters such as porosity, temperature, viscosity, BHP, and permeability on cumulative entropy production are investigated. The viscosity, porosity, and temperature do not have a significant effect on the cumulative entropy generation.

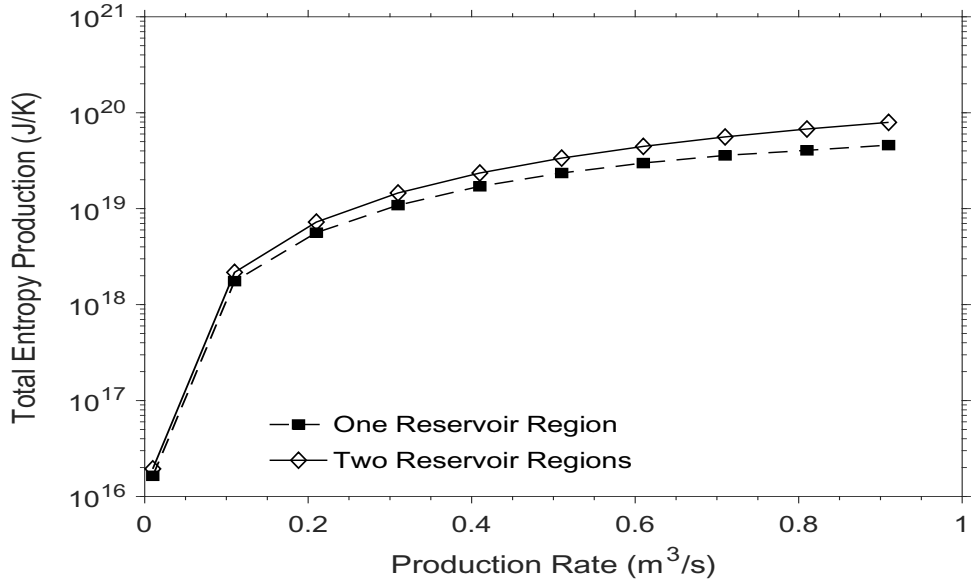

(a) Positive Skin Factor Effect

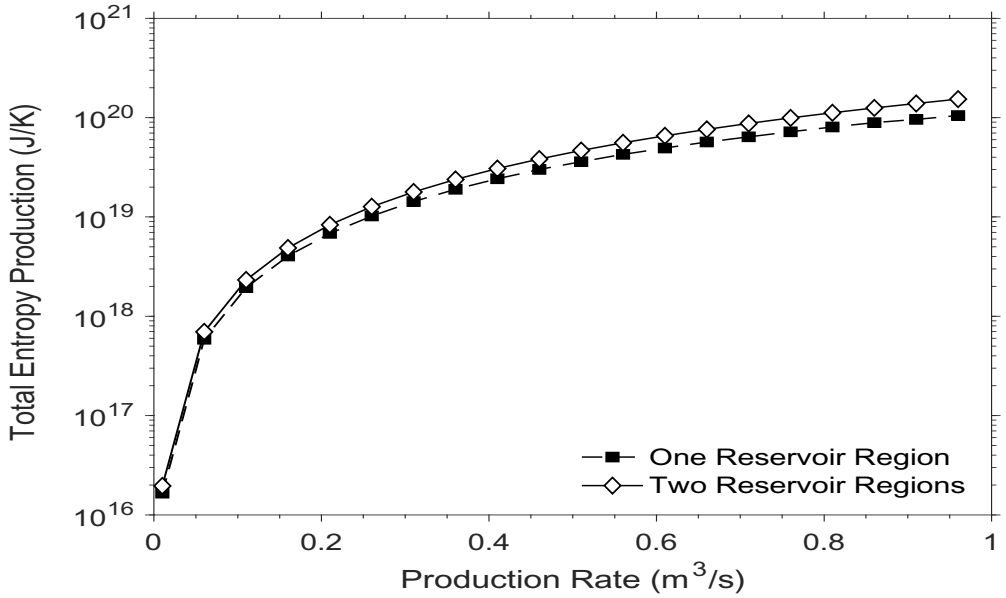

(b) Negative Skin Factor Effect

Figure 6. 6. Effect of production rate on cumulative entropy production for one-region and two-region cases

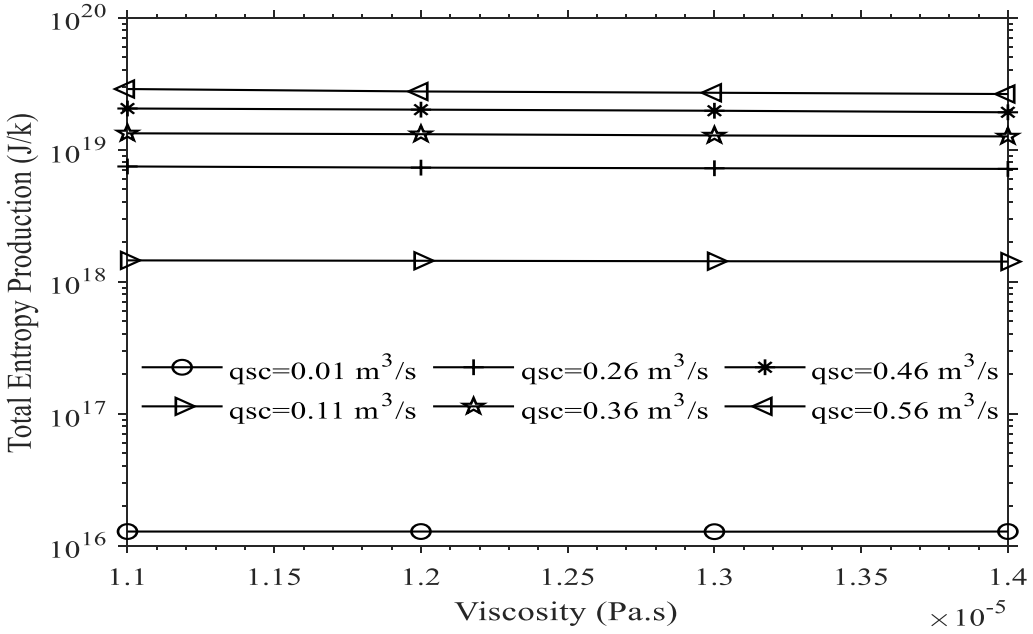

Figure 6. 7. Effects of viscosity on total entropy production at different production rates.

Results are shown in **Figure 6.7** to **Figure 6.9**. The justification of these phenomena for gas viscosity and formation porosity is understandable as the change of gas viscosity is not considerable if it is a dry gas. Also, the porosity does not change appreciably as it is a function of average pressure. As it is clear that the direct change in porosity does not have a direct effect on permeability. However, the temperature influence on entropy can be justified based on the second law of thermodynamics; however, in a porous system filled with dry gas, the change in temperature is not important despite the slight change in entropy generation minimization.

On the other hand, BHP and permeability exhibit a noticeable impact on the cumulative entropy production (see **Figure 6.10** and **Figure 6.11**). **Figure 6.10** illustrates that at the same production rate, there is a slight change in the total entropy production with BHP. To justify this finding, when the BHP increases, a decrease in pressure drop occurs, leading to less total entropy production. In addition, at a high BHP, the energy loss in the reservoir will be lower compared to a low BHP; therefore, the entropy production is less at a high BHP.

Figure 6.11 displays an increase in the total entropy production with increasing permeability at different production rates. The increase in the total entropy production is significant at low permeability values (within the range of 1E-15 m^2 and 1E-13 m^2), compared to high permeability values. These results are consistent with the preliminary results, implying that in the stimulated region (high permeability), the entropy production is high, while in the damaged region (low permeability), the entropy production is low.

When the permeability increases, the production rate increases as well and consequently, the entropy generation increases as described in **Figure 6.11**.

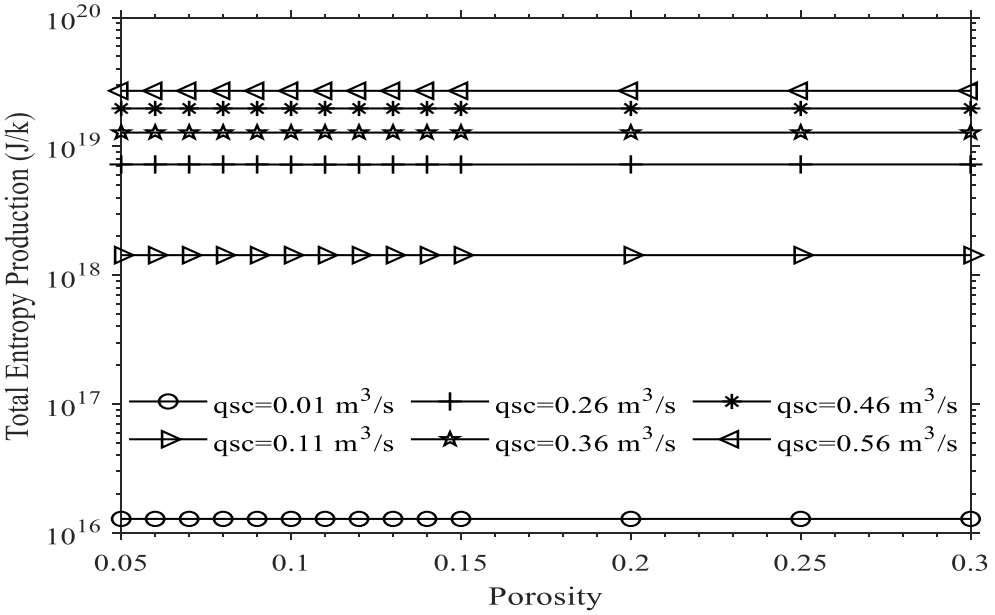

Figure 6. 8. Effects of porosity on total entropy production at different production rates.

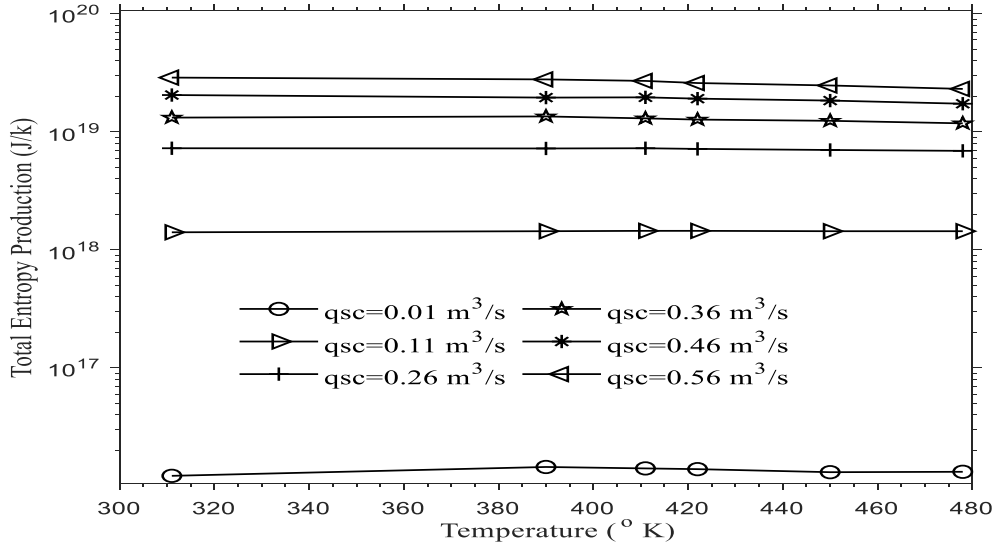

Figure 6. 9. Effects of temperature on total entropy production at different production rates.

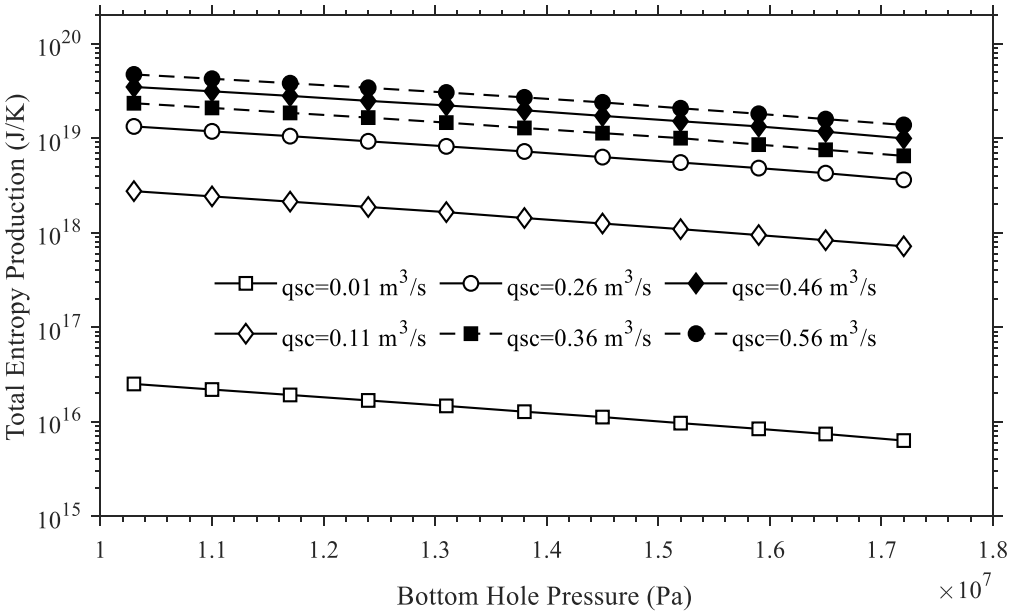

Figure 6. 10. Effects of BHP on total entropy production at different production rates

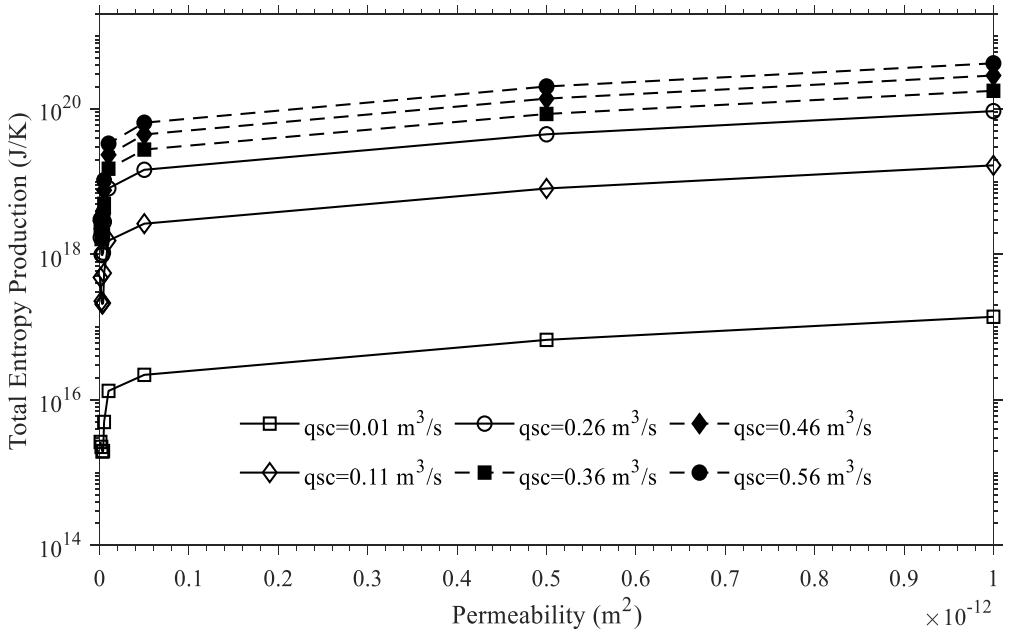

Figure 6. 11. Influence of permeability on total entropy production at different production rates.

6.3. Production Optimization Using Entropy Generation

To obtain the optimal production rate, the normalized cumulative entropy production is calculated from Equation (4.29). There is an optimal production rate that leads to a reasonable loss of reservoir energy availability but keeps the recovery factor at a high level. The entropy production is a function of the production rate and, consequently, the recovery factor. **Figure 6.12** illustrates the effect of the production rate on both the recovery factor and entropy production. The Coefficient Of Performance (COP) is estimated by Equation (4.31) to obtain the maximum value, which corresponds to a specific production rate. This production rate is the optimal rate that should be obtained for the entire production duration to have less energy loss. This result is aligned with a study conducted by Khan et al. (2016) in which they concluded that by decreasing the system duty, the energy-savings of that system is increased. In the absence of skin effects, it is found that the optimal production rate is 1.26 m^3/s (3.843 MMScf/D), within the range of the production rates in this study, as shown in **Figure 6.13**.

According to Equation (4.31), as the maximum entropy production varies, a substantial change will occur in the normalized entropy production, causing a variation in the optimal production rate, as indicated in **Figures 6.13** and **6.14**.

The COP is compared with the model results for the Net Present Value (NPV). The total operational costs corresponding to production, total profits, and NPV are calculated using Equations (4.32), (4.33), and (4.34), respectively.

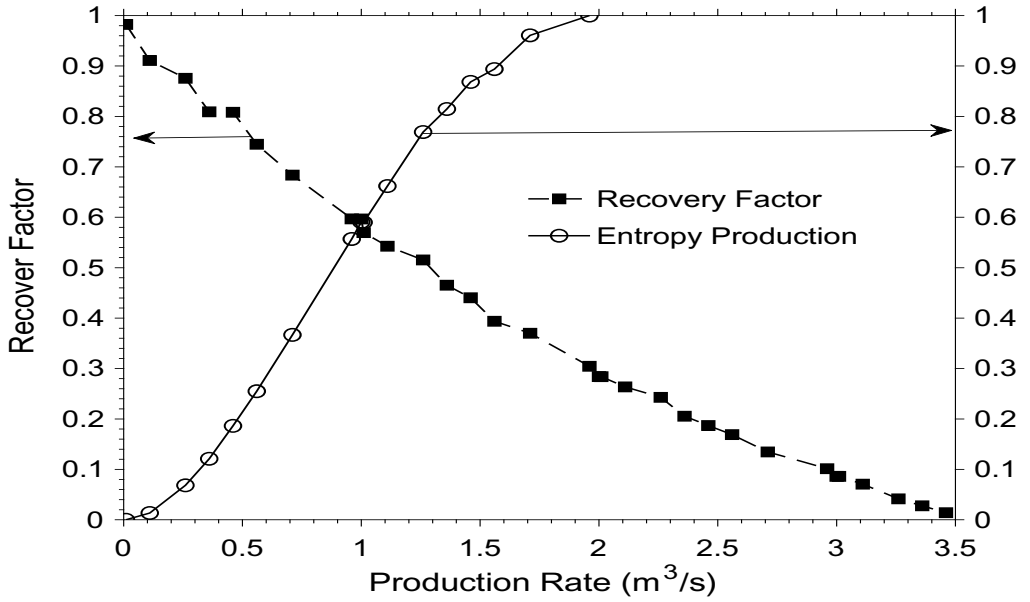

Figure 6. 12. Cumulative entropy (normalized) and recovery factor versus production rate.

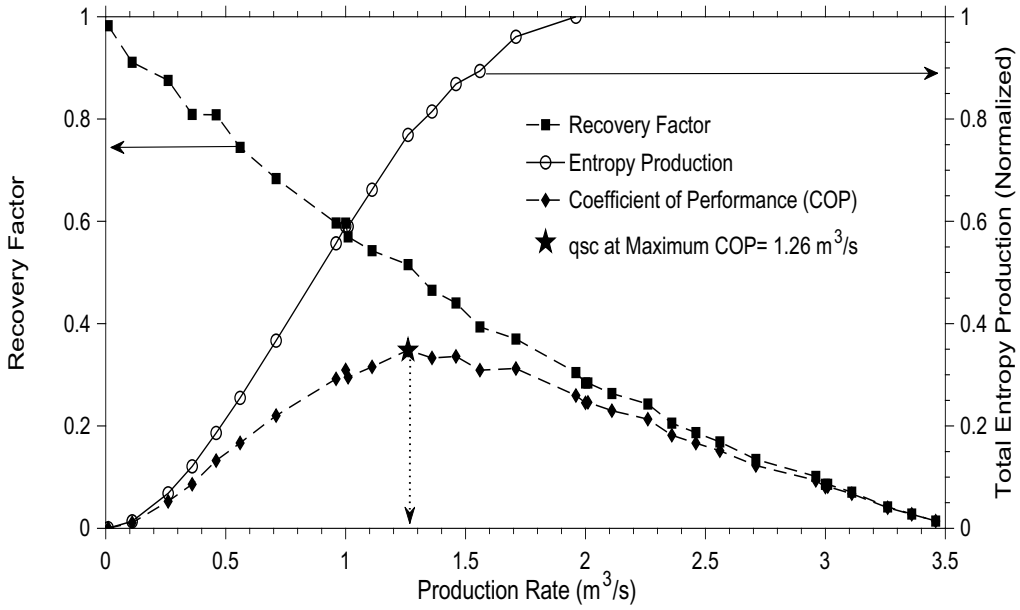

Figure 6. 13. Maximum coefficient of performance and optimum production rate based on recovery factor and entropy production data.

The production rates range from 1.98 to 686.31 MMbbl/year (0.01 to 3.46 m^3/s) and are evaluated in this study. The NPV, along with the COP, results against the production rate are shown in **Figure 6.14**. According to **Figure 6.14**, the optimal production rate from the COP is close to the value obtained from an NPV consideration.

As only two parameters (BHP and permeability) from among the five studied in this research show a considerable contribution to the total entropy production, the effect of these two parameters on the optimal production rate is investigated (see **Figure 6.15** and **Figure 6.16**). The importance of permeability and BHP in the optimal production rate is further highlighted in **Figure 6.15** and **Figure 6.16**. For example, a reservoir with a higher permeability can achieve a higher optimum production rate compared to a less permeable reservoir. In addition, the BHP needs to be kept as low as possible to attain a high optimum production rate.

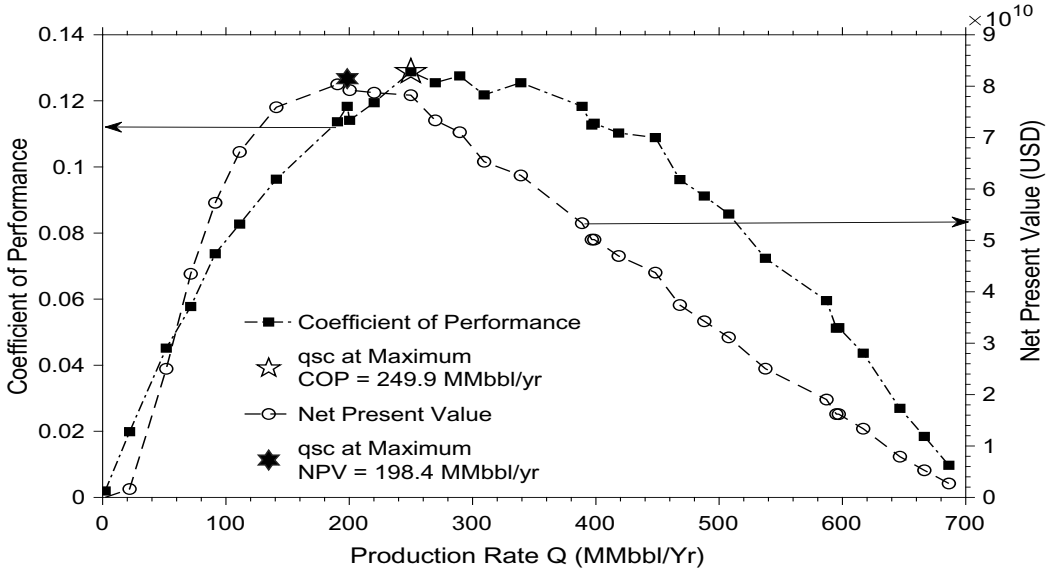

Figure 6. 14. Coefficient of performance and net present value as a function of production rate

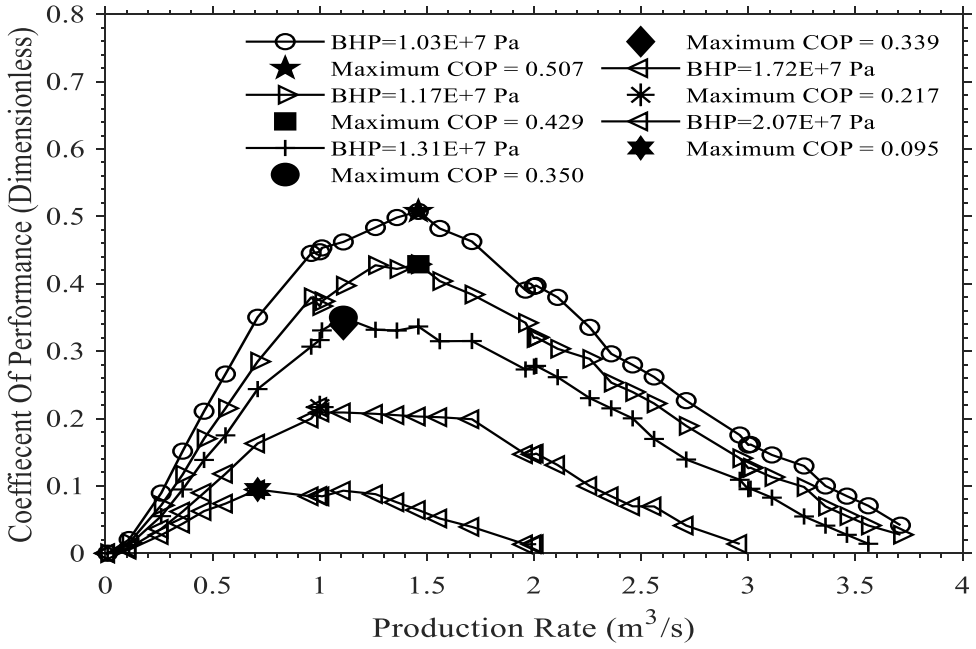

Figure 6. 15. Effect of BHP on the optimum production rate.

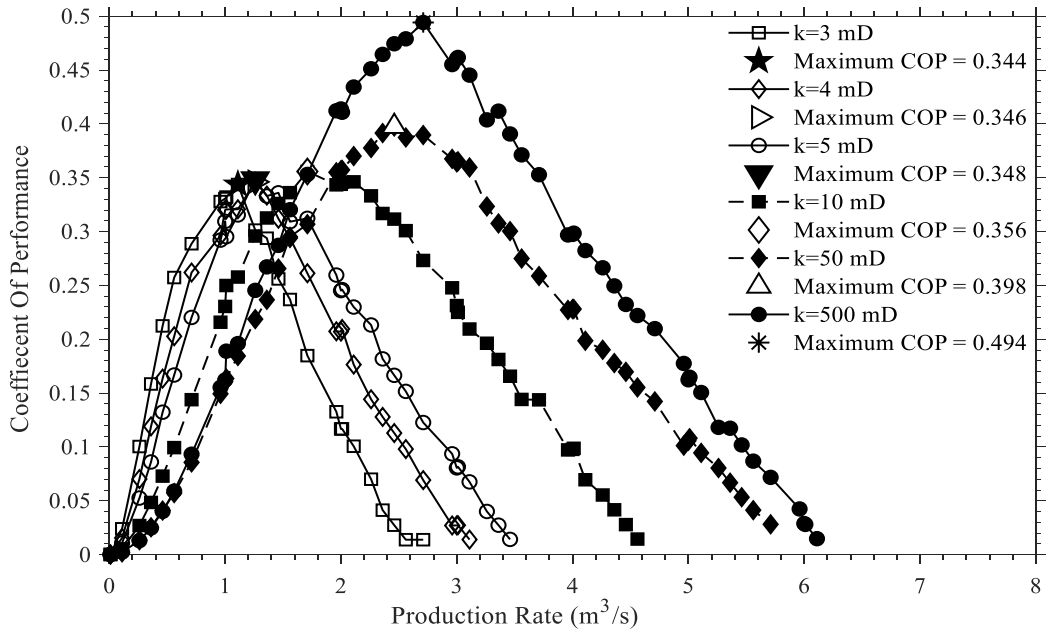

Figure 6. 16. Effect of permeability on the optimum production rate.

6.4. Two-Phase Models

The single-phase dry gas models are extended to two-phase oil-water fluid flow models. Significant changes in the mathematical equations are made to obtain the reservoir pressure profiles for both fluids, oil and water. It was found that the two-phase reservoir pressure profile is similar to that for a single-phase except in the total compressibility, viscosity, and permeability models. The same assumptions for single-phase are applied in the two-phase flow models.

To maintain the production rate constant for both fluids, oil and water, the fractional flow of water is assumed to be fixed for the entire period of time. The reservoir pressure, as well as BHP, are kept above the bubble point to prevent gas production; in this case, only two fluids are flowing in the reservoir and wellbore. It is important to note that the reservoir is under the influence of natural energy mechanisms; no secondary or tertiary enhanced oil recovery technique is used.

The results of two-phase models follow the same trend as observed based on the single-phase models. The two-phase models show that as the recovery factor increases, the total entropy production decreases at low production rates. The skin factor effect is significant in the recovery factor, while slight changes happen in total entropy generation. For validation purposes, the models are tested using real reservoir data, and the outcomes are compared to the results of the CMG. As the entropy production cannot be measured or estimated using CMG, the recovery factor and production rate data are used while comparing the two-phase models and CMG. Good agreement is noticed in the production

rate versus time, while there is an excellent match between the recovery factors at constant BHP as shown in **Figures 6.17 and 6.18**.

Table 6.3 summarizes the formation and fluid property data, while **Table 6.4** lists the saturation data.

Table 6. 3. Data for two-phase flow (oil-water system)

Parameter	Symbol	Value	Unit
Reservoir radius	r_e	2050	ft
Wellbore radius	r_w	0.25	ft
Wellbore depth	h	1000	ft
Pore compressibility	C_r	0.000004	psi^{-1}
Water compressibility	C_w	0.000003	psi^{-1}
Oil compressibility	C_o	0.00001	psi^{-1}
Oil density	ρ_o	45	$\text{lb}_\text{m}/\text{ft}^3$
Water density	ρ_w	63.02	$\text{lb}_\text{m}/\text{ft}^3$
Initial reservoir pressure	P_i	4000	psi
Capillary pressure at water/oil contact	P_c	0	psi
Bubble point pressure	P_b	1000	psi
Absolute permeability	k	265	mD
Porosity	ϕ	0.13	
Reservoir temperature	T	180	F
Initial water formation factor	B_{wi}	1.003875	bbl/STB
Initial oil formation factor	B_{oi}	1.103875	bbl/STB
Water viscosity	μ_w	0.9975	cp
Oil viscosity	μ_o	0.96	cp

Table 6. 4. Saturation data

S_w	k_{rw}	k_{ro}	P_{cow} (psia)
0.22	0	1	7
0.3	0.07	0.4	4
0.4	0.15	0.125	3
0.5	0.24	0.0649	2.5
0.6	0.33	0.0048	2
0.8	0.65	0	1
0.9	0.83	0	0.5
1	1	0	0

6.4.1. Model Validation

For the validation of two-phase flow model's results, CMG-IMEX was used. As CMG-IMEX models primary and secondary oil recovery processes in the conventional and unconventional reservoirs, it can be used to validate the production rate values from the experimental data that will be used later in the developed models. Additionally, the CMG-IMEX was used to validate the recovery factor values obtained from the developed models.

To validate the accuracy of the results, CMG simulation software is used. **Figure 6.17** shows good agreement between the real data and predictions obtained from CMG; the same trend is also noticed for both predictions and real data. An excellent match is achieved between the results of the proposed models and CMG based on **Figure 6.18**, showing the recovery factor versus time at a constant BHP.

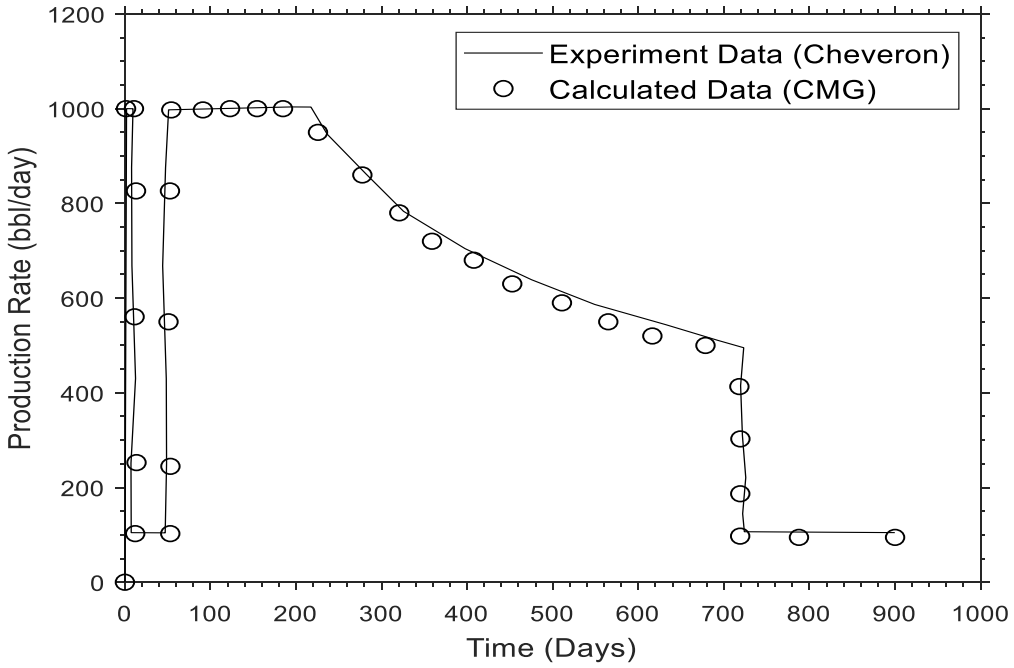

Figure 6. 17. Oil production rate versus time based on the results of the field data and CMG in the absence of skin factor.

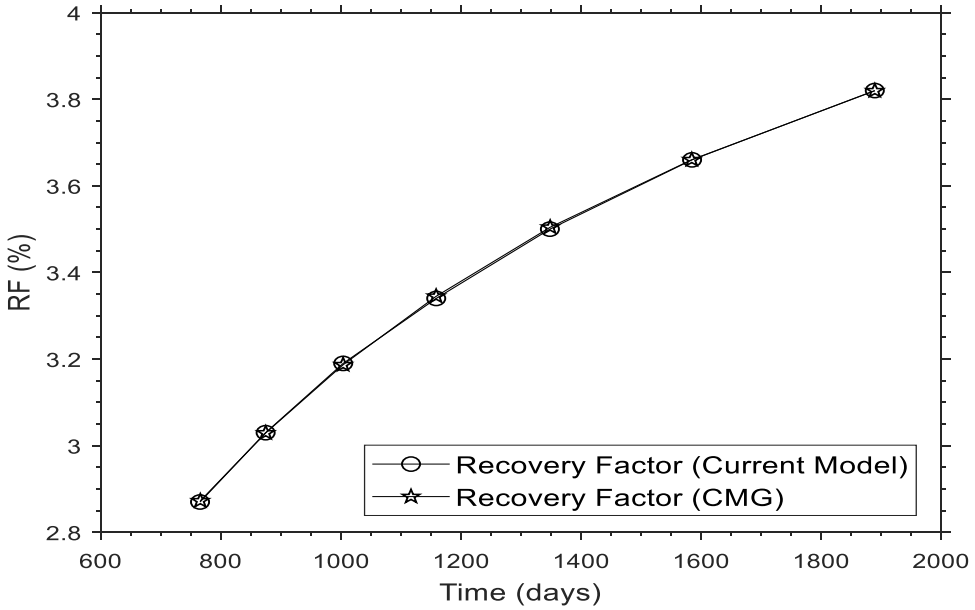

Figure 6. 18. Recovery factor versus time based on the results of the current model and CMG at constant BHP.

6.4.2. Models Results

The results from the models are divided into two scenarios: in the absence and presence of capillary pressure. The results of oil and water phase are display in **Figures 6.19** and **6.20**. To satisfy the assumption of a constant production rate in pseudo-steady state flow conditions for two-phase flow, the fractional flow for oil and water is assumed to be constant for the entire production time.

The total entropy production increases as the production rate increases for both oil and water despite the skin effect, as shown in **Figure 6.19** and **Figure 6.20** for oil and water, respectively. **Figure 6.19** and **Figure 6.20** are obtained at $P_c = 0$. The general trend of total entropy production versus recovery factor for two-phase flow is similar to that of the

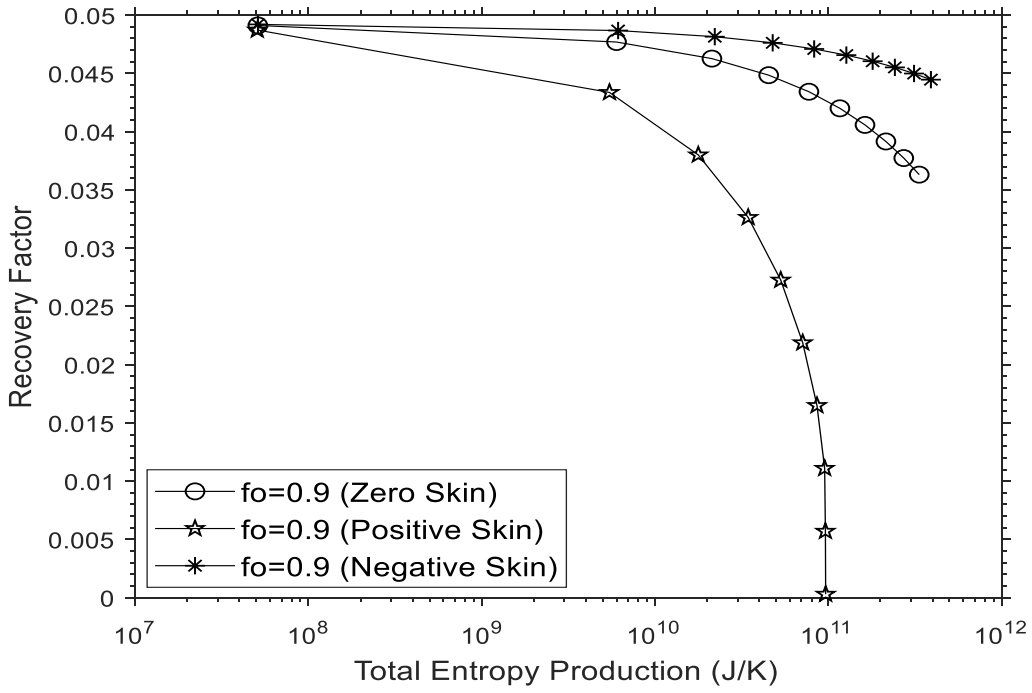

(a) Oil Fractional Flow (f_o) = 0.9

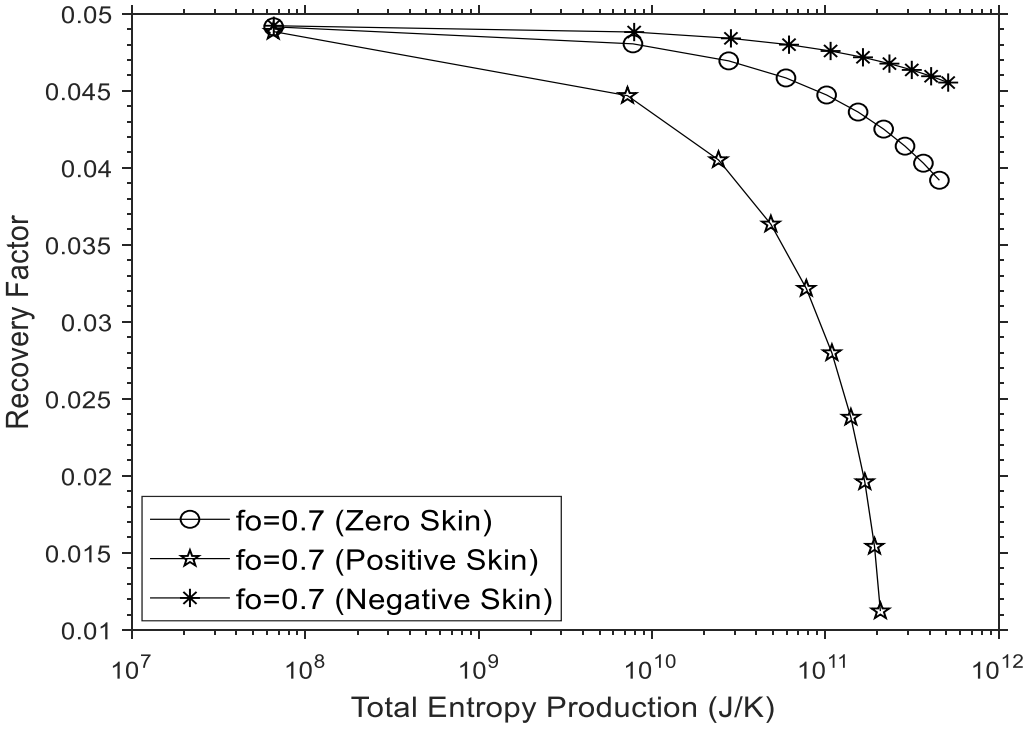

(b) Oil Fractional Flow (f_o) = 0.7

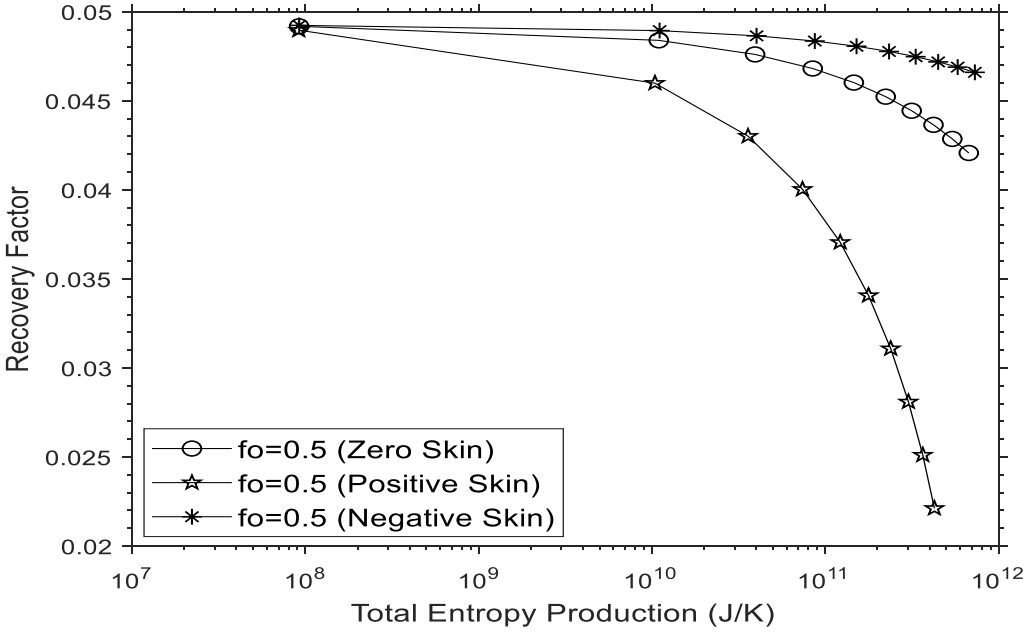

(c) Oil Fractional Flow (f_o) = 0.5

Figure 6. 19. Recovery factor versus cumulative entropy production based on the results of different oil fractional flow at $P_c = 0$.

single-phase flow. The skin factor does not affect the total entropy production significantly. However, it influences the recovery factor. This effect is more pronounced in oil, as shown in **Figure 6.19**. The skin has no considerable impact on total entropy due to high oil viscosity as well as the low values of effective permeabilities for both oil and water phases. In the water phase, the effect is not appreciable in both entropy production and recovery factor (See **Figure 6.20**).

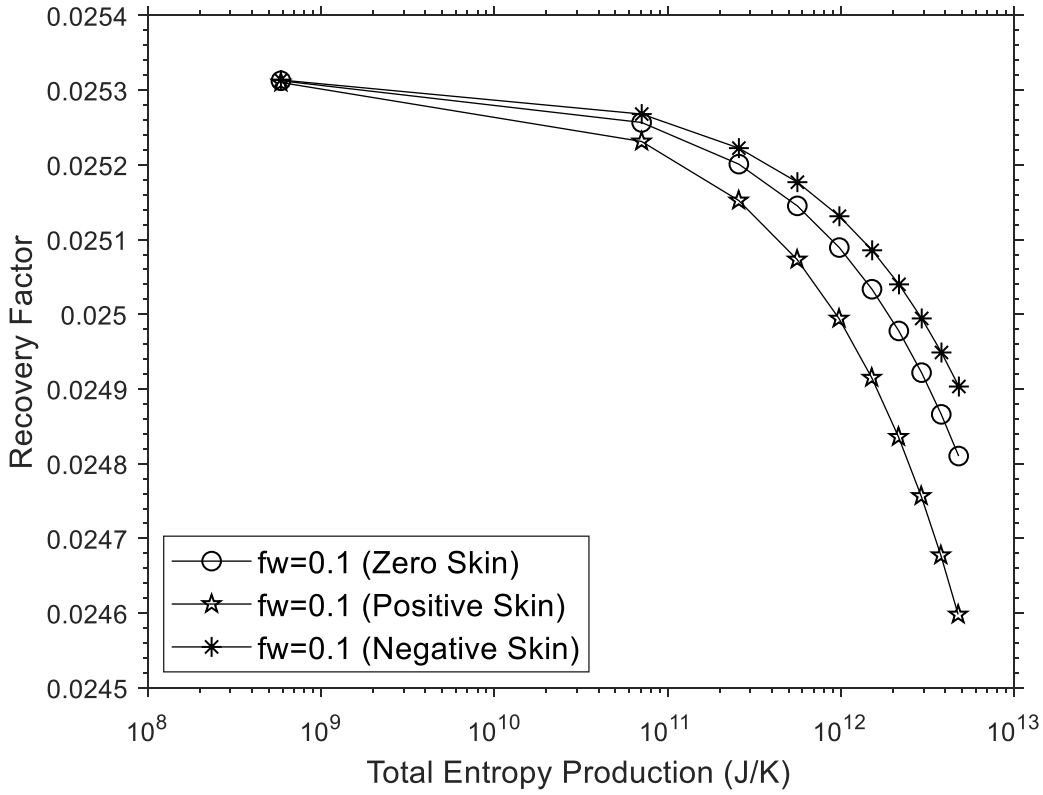

(a) Water Fractional (f_w) Flow = 0.1

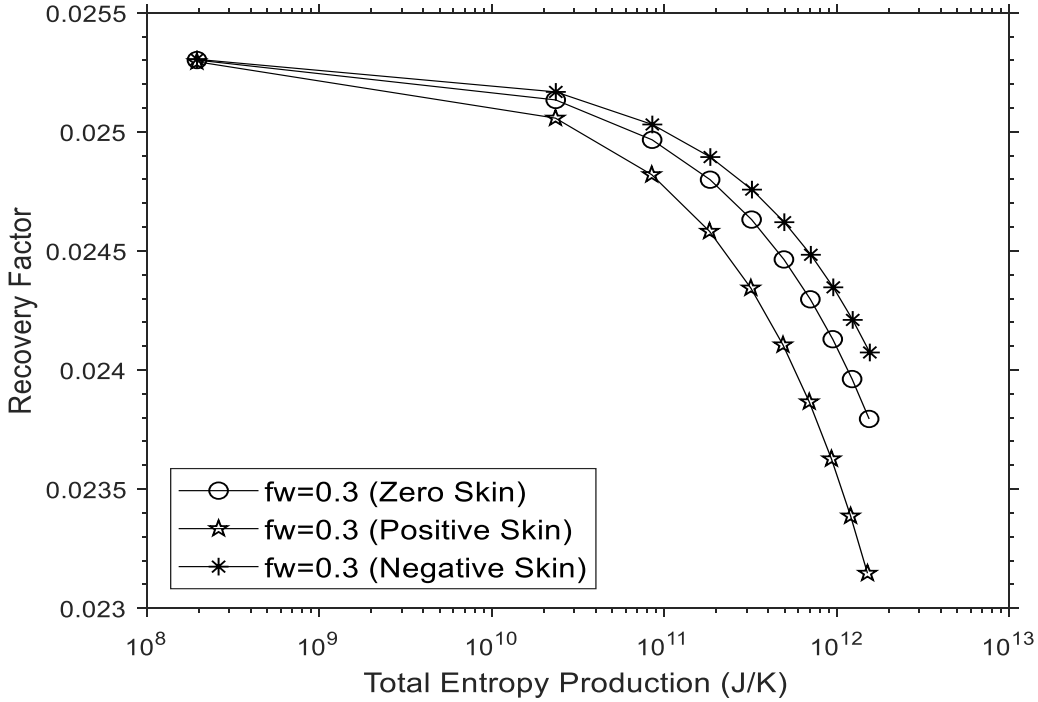

(b) Water Fractional (f_w) Flow = 0.3

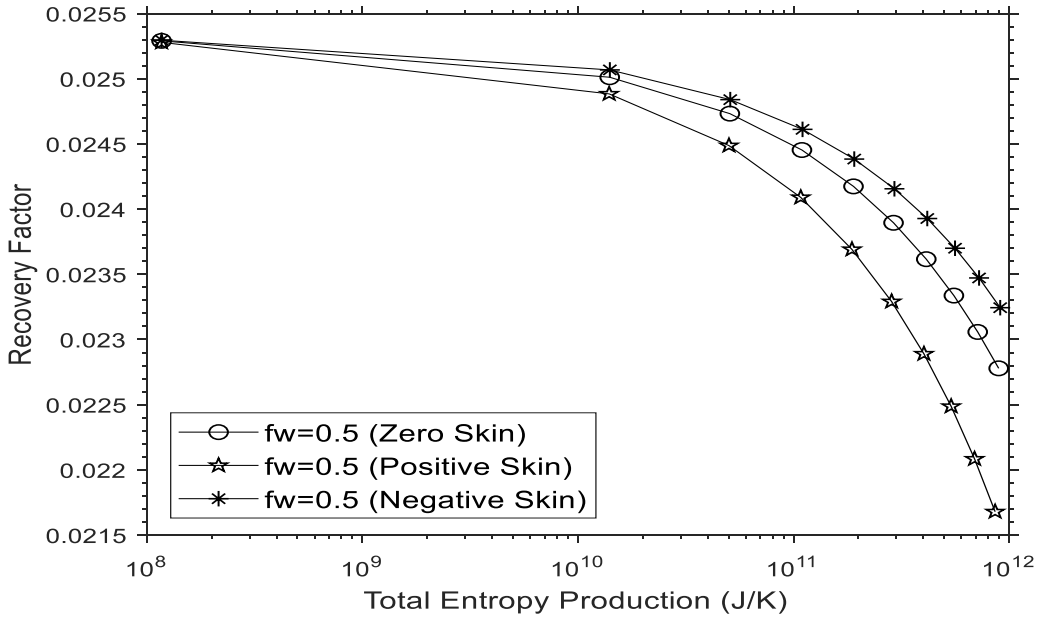

(c) Water Fractional (f_w) Flow = 0.5

Figure 6. 20. Recovery factor versus cumulative entropy production based on the results of different water fraction flow at $P_c = 0$.

Furthermore, the recovery factor and total entropy production for a water change slightly with an increasing water fractional flow, as depicted in **Figure 6.20**. This might occur due to the low water production rate (low water fraction) and the low value of water relative permeability, compared to the oil phase.

As the reservoir is under a natural energy mechanism, and no Enhanced Oil Recovery (EOR) technique is used, the recovery factors for both oil and water are relatively low. The BHP is kept equal or above the bubble point pressure, 1000 psi, to avoid any gas production at the surface.

Different fractional flows for both oil and water at the same skin effect are obtained, as depicted in **Figure 6.21** and **Figure 6.22**. As the oil fractional flow increases at the same skin effect, both the recovery factor and the total entropy production increase (**Figure 6.21**). However, if production rate decrease, the production time of the reservoir increases, which is not always favorable due to high money investment for less production. For the water phase, the opposite behaviour is observed. Both the recovery factor and total entropy production decrease when the water fractional flow increases, as shown in **Figure 6.22**. The production time decreases as water production increases.

At a zero skin effect and capillary pressure ($P_c = 0$), when a high oil production rate and low water production rate are experienced, the total entropy production is higher in water than in oil, as depicted in **Figure 6.23**.

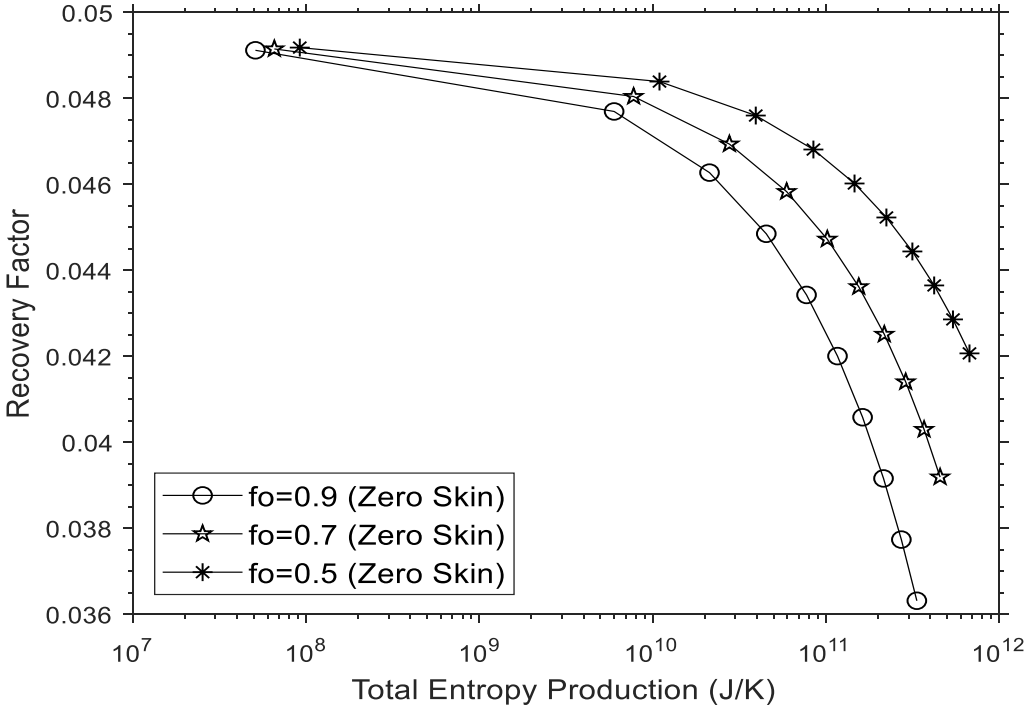

(a) No Skin Factor Effect

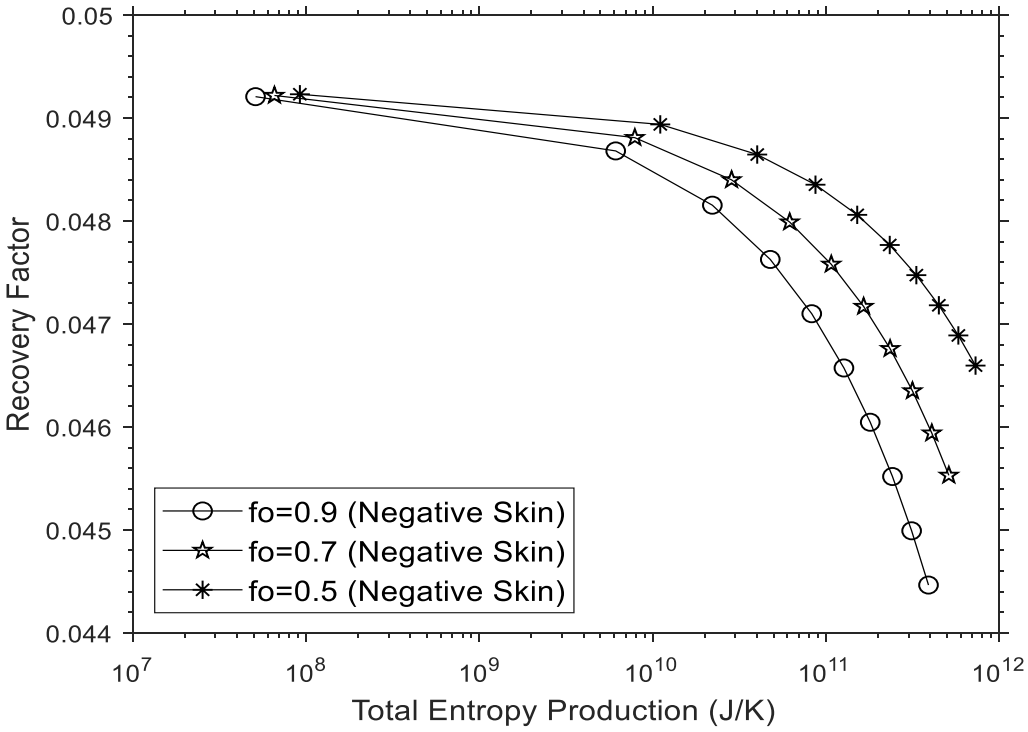

(b) Negative Skin Factor Effect

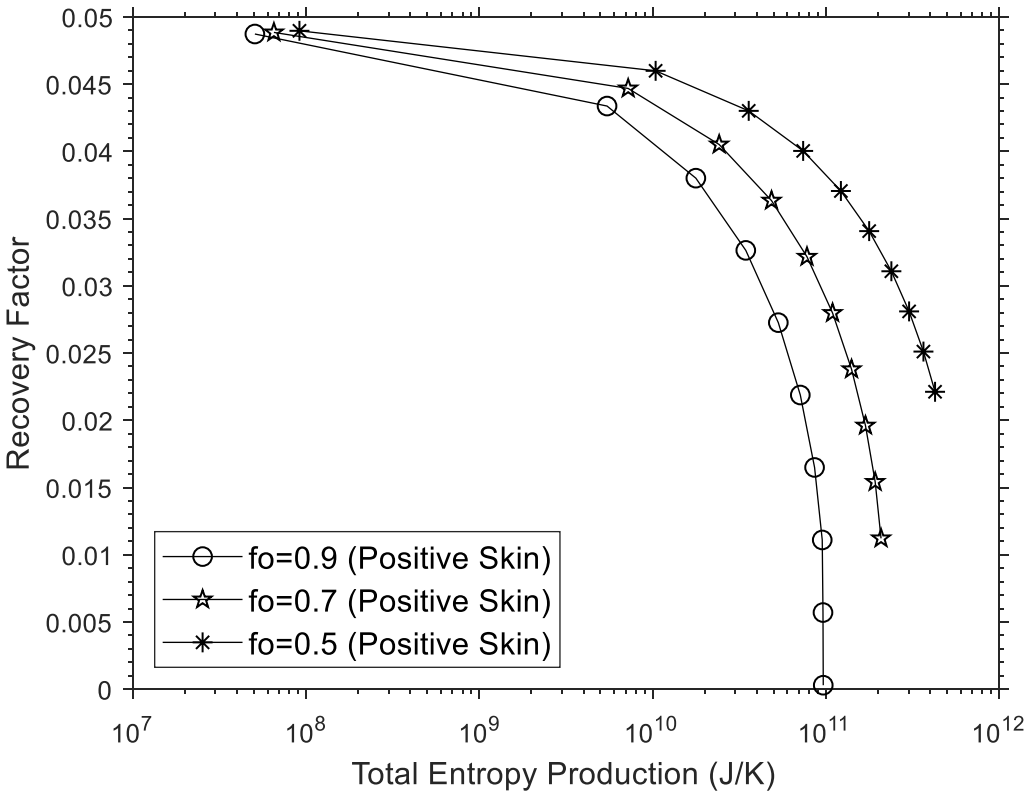

(c) Positive Skin Factor Effect

Figure 6. 21. Recovery factor versus cumulative entropy production based on different values of oil fractional flow for the same skin factor at $P_c = 0$.

This phenomenon occurs due to the low water production rate. It is worth mentioning that the water production time is significantly higher than oil production time in this case. On the other hand, when the production rates of water and oil are the same, the total entropy production is almost similar, as shown in **Figure 6.24**.

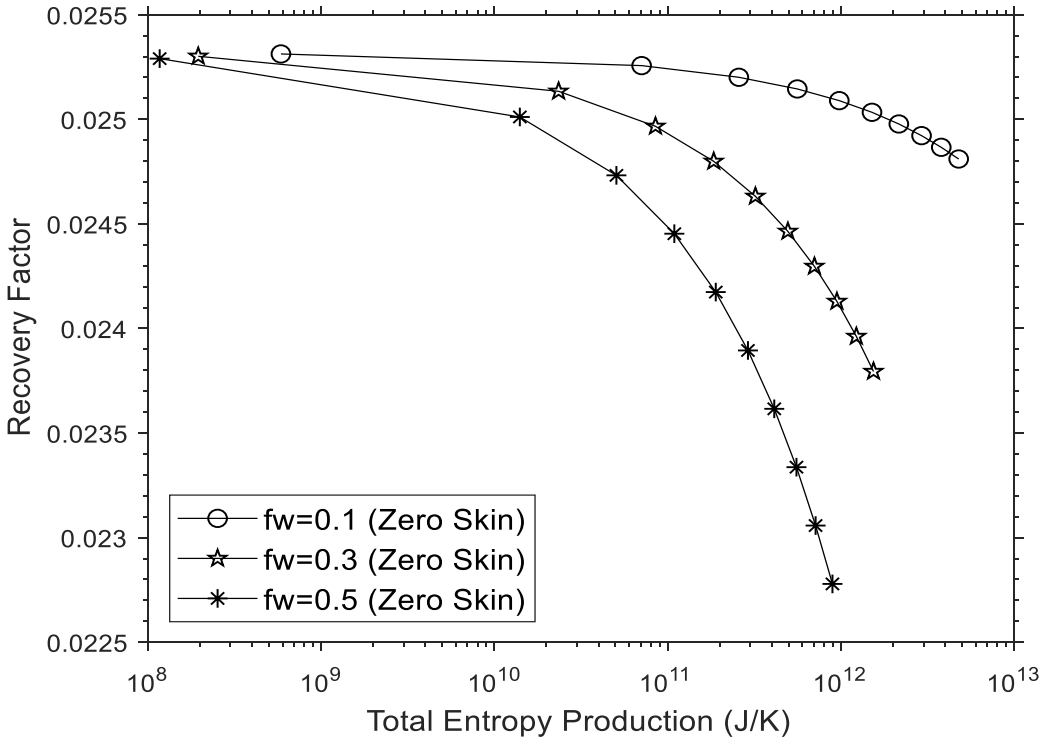

(a) No Skin Factor Effect

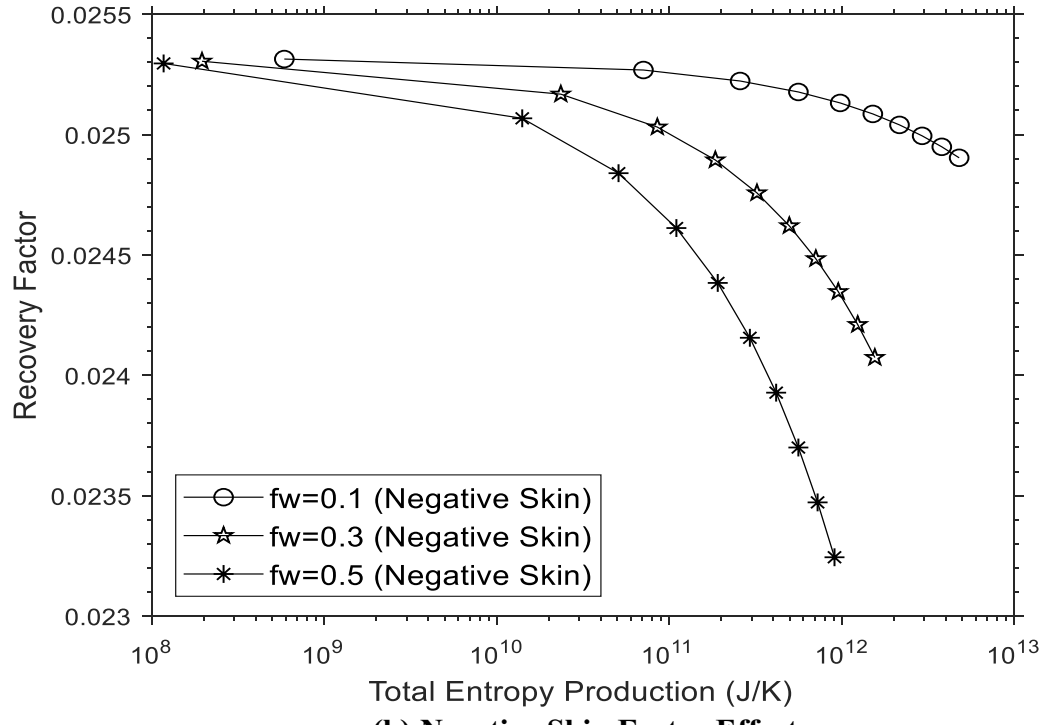

(b) Negative Skin Factor Effect

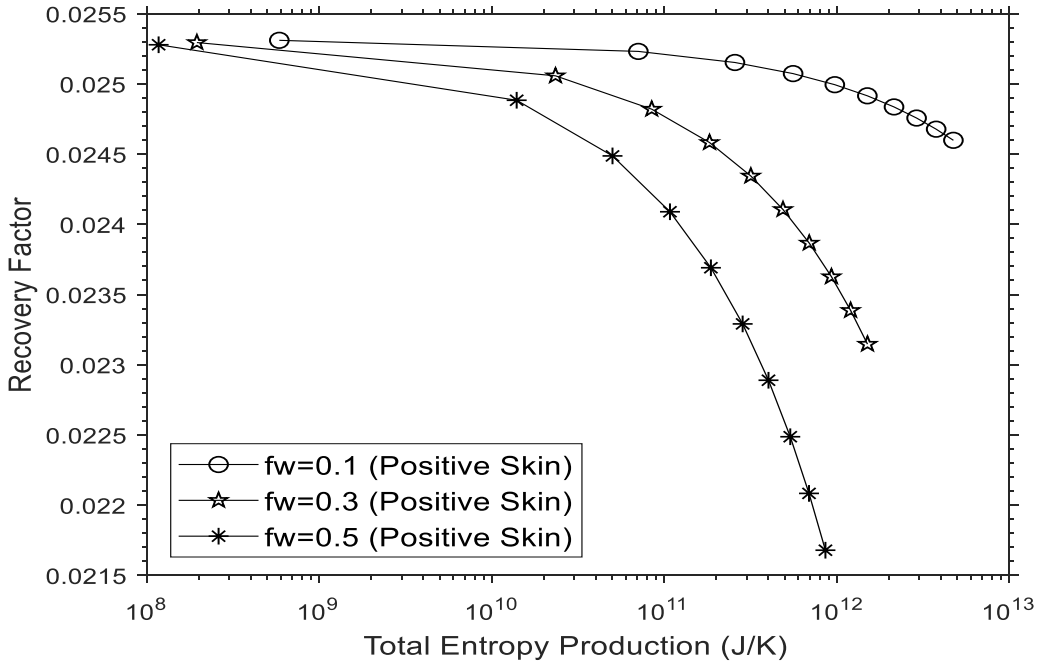

(c) Positive Skin Factor Effect

Figure 6. 22. Recovery factor versus cumulative entropy production based on different values of water fractional flow for the same skin factor at $P_c = 0$.

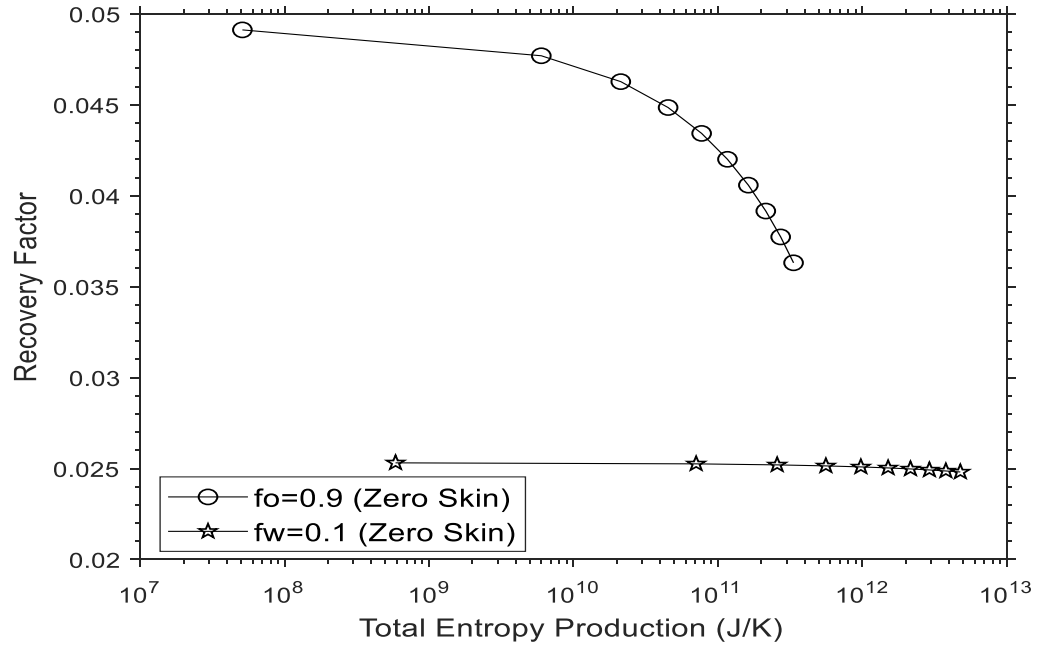

Figure 6. 23. Comparison between $f_o = 0.9$ and $f_w = 0.1$ at the same no skin effect when $P_c = 0$

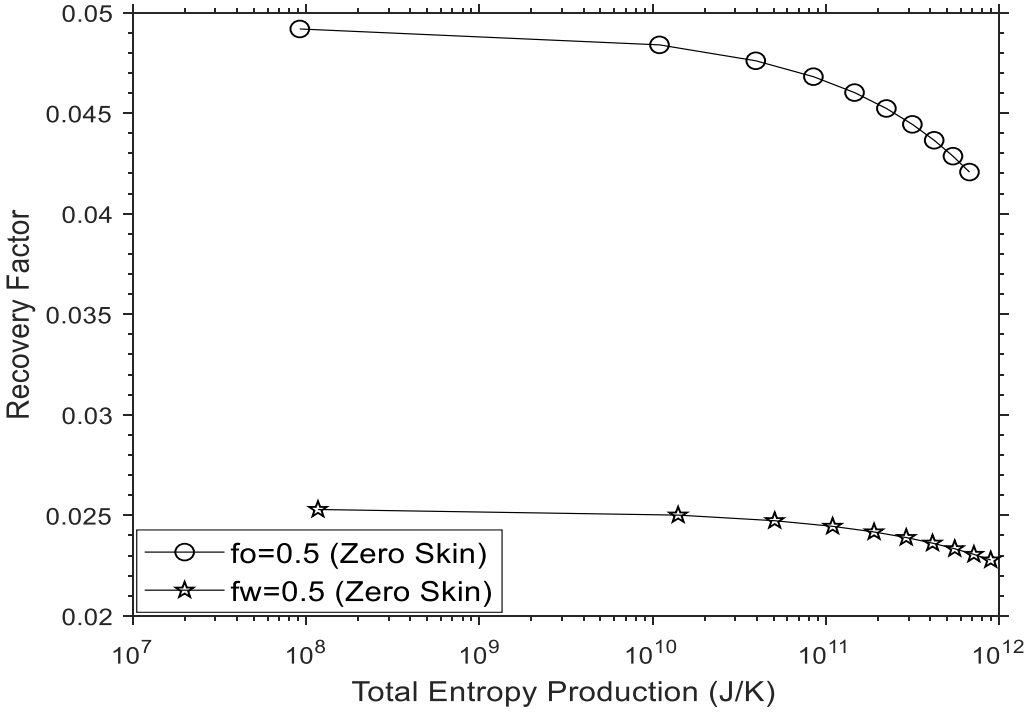

Figure 6. 24. Comparison between $f_o = 0.5$ and $f_w = 0.5$ at the no skin effect when $P_c = 0$.

The results of the models also reveal that the capillary pressure has a significant impact on both the oil and water recovery factor and total entropy production. **Figure 6.25** displays an example of the effect of capillary pressure on the recovery factor and total entropy production when $f_w = 0.1$. It can be observed that the change in recovery factor (from 2.5% to 5.5%) is more significant compared to the change in the total entropy production (from 4.7E12 J/s to 1.0E13 J/s). The capillary pressure will affect the reservoir pressure profiles, leading to variations in both recovery factor and total entropy production.

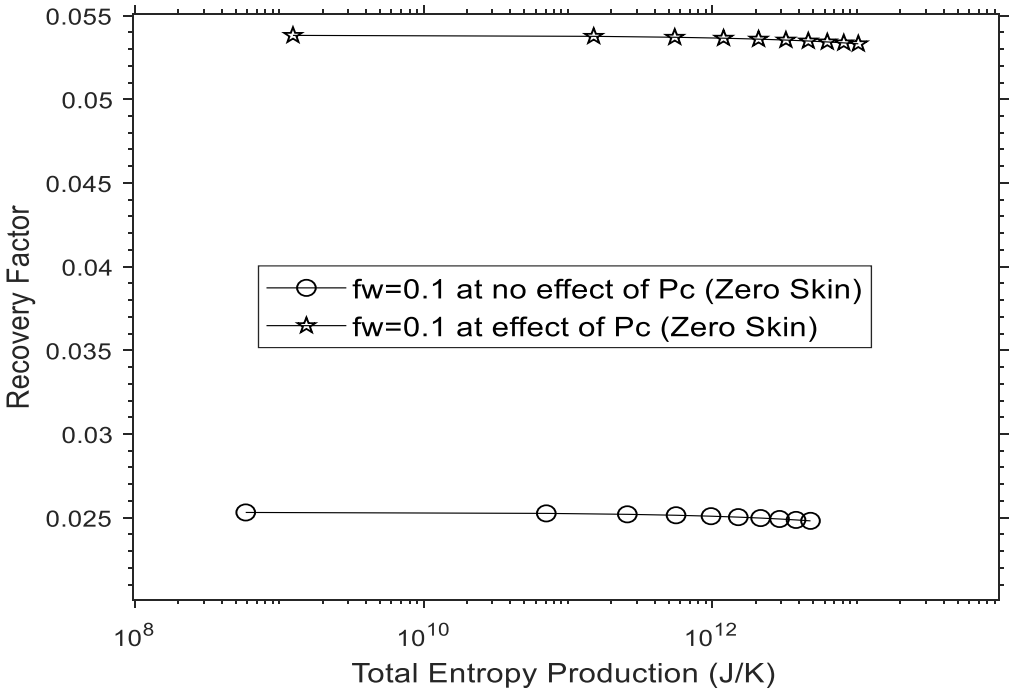

(a) No Skin Factor Effect

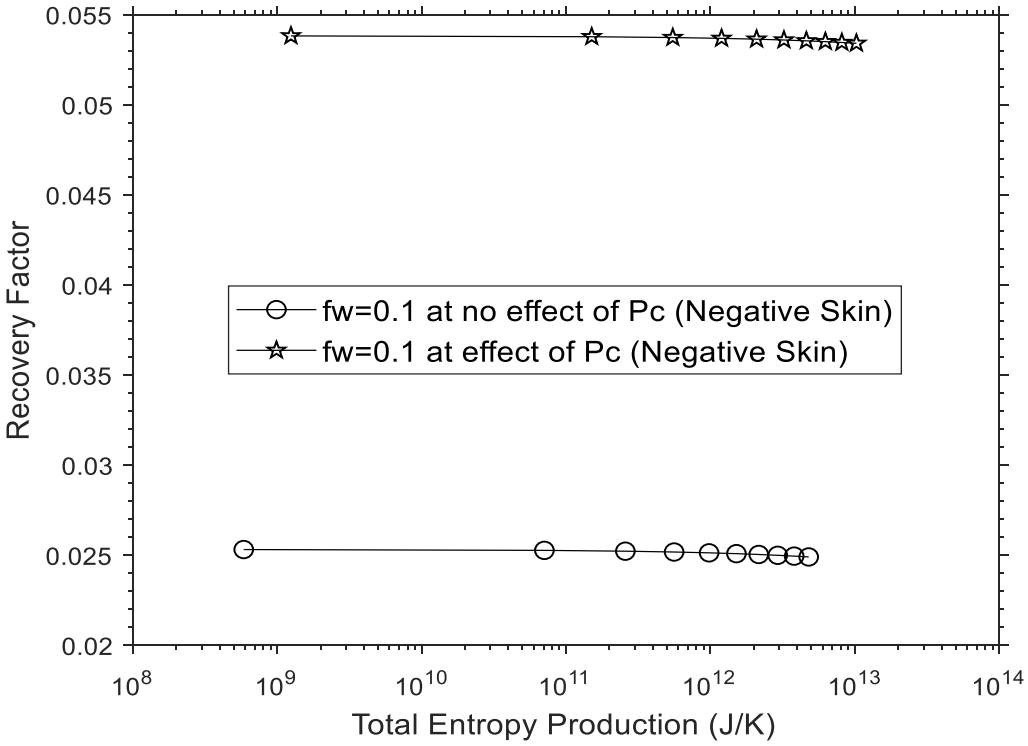

(b) Negative Skin Factor Effect

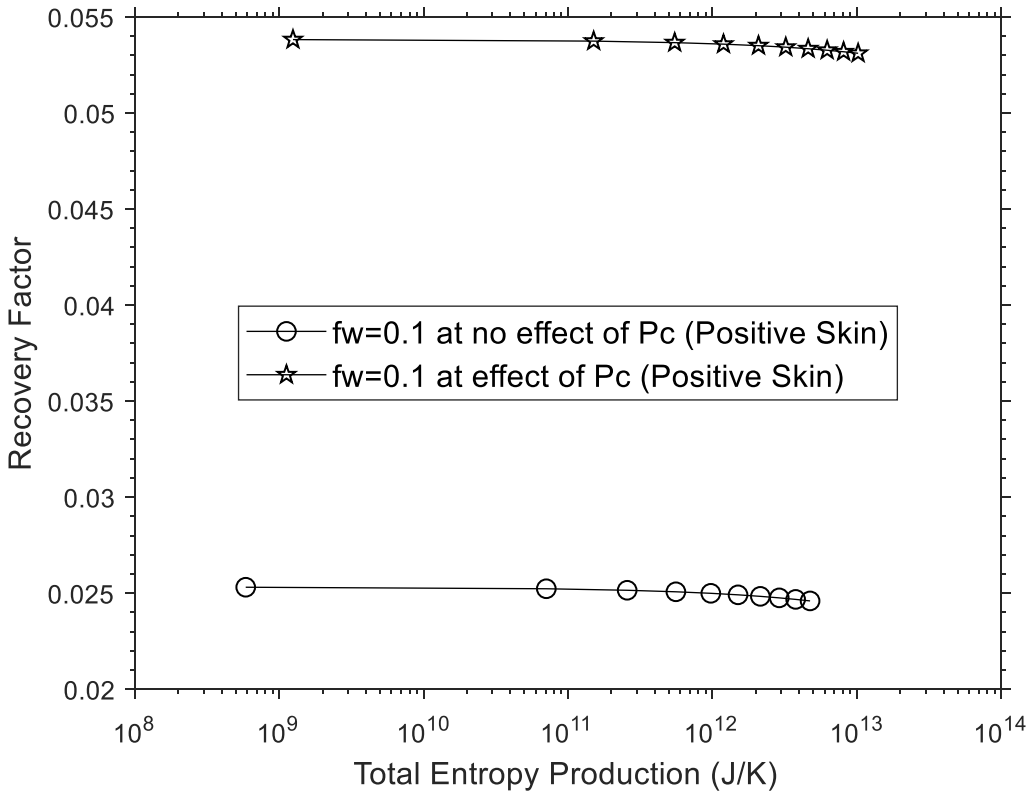

(c) Positive Skin Factor Effect

Figure 6. 25. Effects of capillary pressure on water production Recovery Factor at the same skin effect.

At the same skin effect, the oil production time required to have a higher recovery factor increases as the oil production rate decreases, as shown in **Figure 6.26**. However, at the same oil flow rate and different skin effects, the oil production time for the positive skin scenario is less than that for both negative and zero skin cases. **Figure 6.26** also depicts that there is not much difference at the same production rate for the negative and zero skin effects.

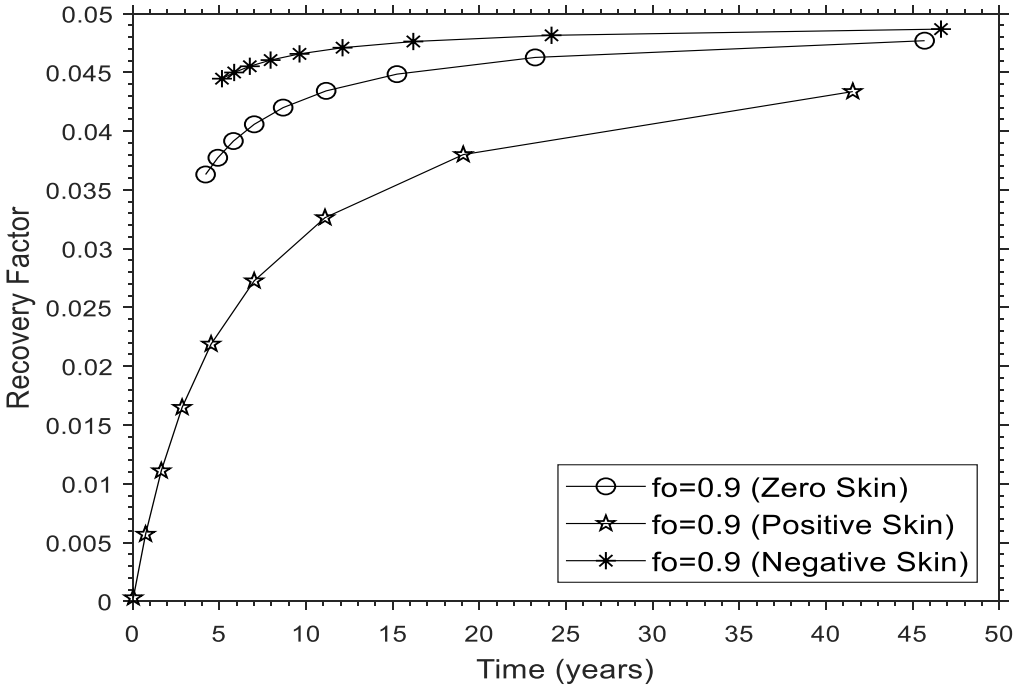

(a) Oil Fractional (f_o) Flow =0.9

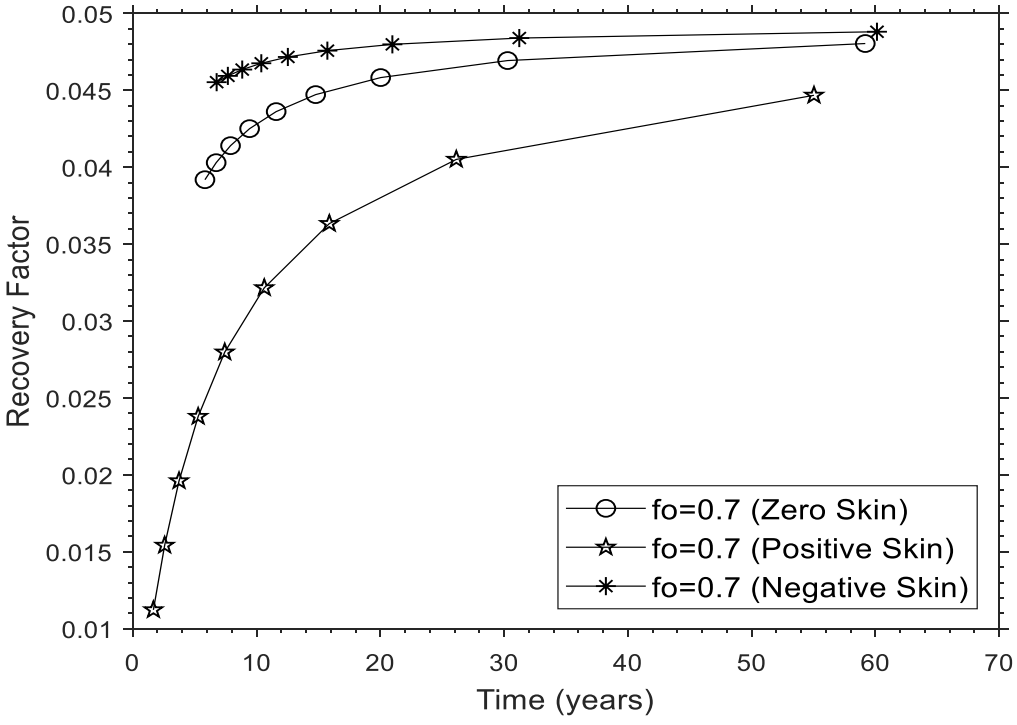

(b) Oil Fractional (f_o) Flow =0.7

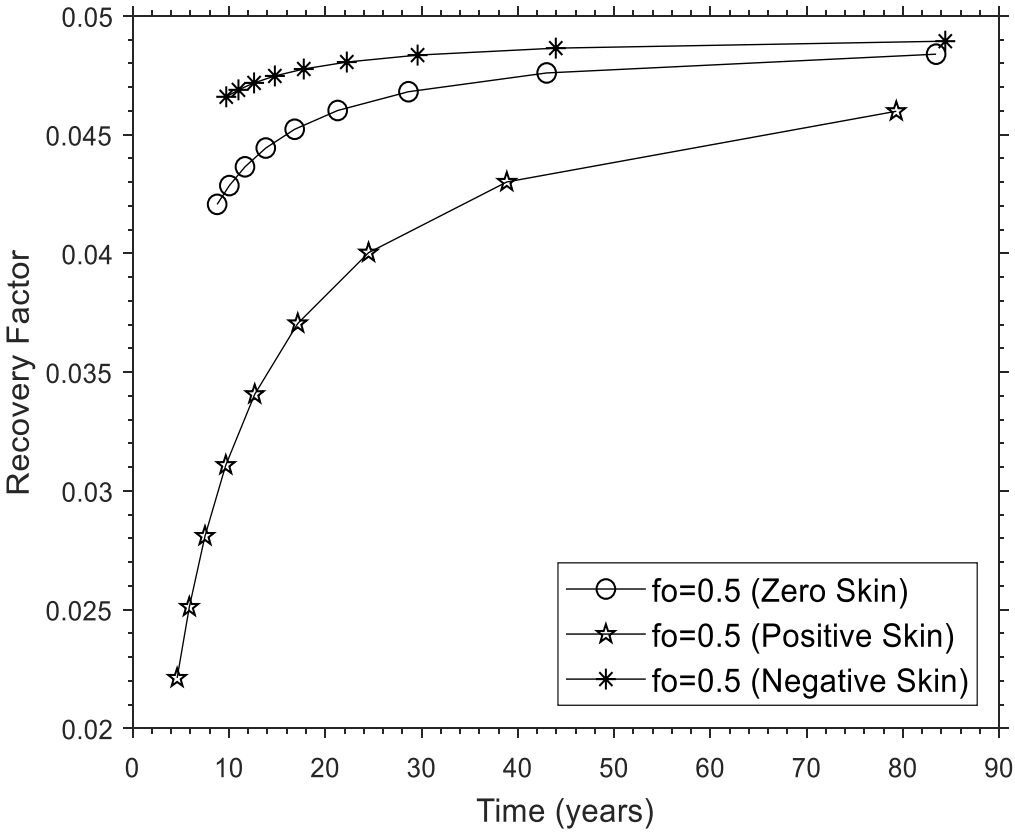

(c) Oil Fractional (f_o) Flow =0.5

Figure 6. 26. Recovery Factor versus time based on the same value of f_o for different values of skin factor at $P_c = 0$ psi.

The capillary pressure has a strong influence on the reservoir production life. For example, at a water fractional flow of 0.5, the recovery factor is much higher when the capillary pressure is considered compared to assuming no capillary pressure effect. However, the time needed to achieve this result is much higher in the case of capillary pressure, as can be seen in **Figure 6.27**.

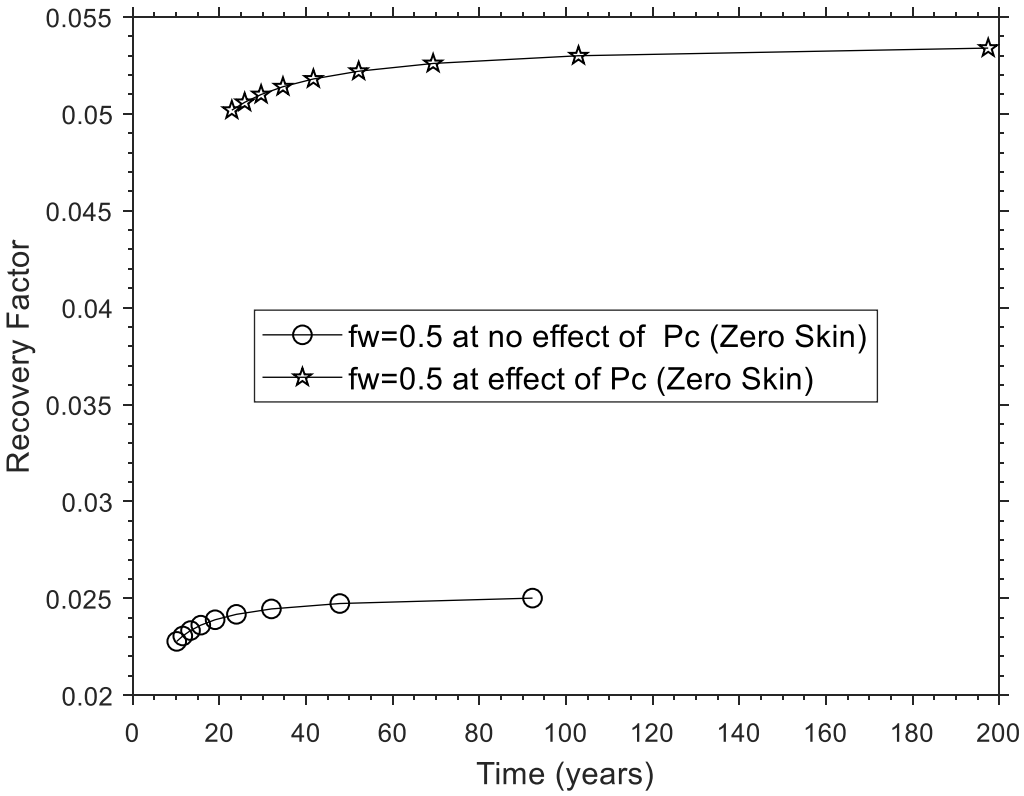

Figure 6. 27. Effect of capillary pressure on recovery factor versus time based on the same value of f_w and the same effect of skin factor.

6.4.3. Sensitivity Analysis

Effect of Viscosity. Most, if not all, of the methods to investigate the effect of temperature on oil viscosity are empirical, such as Beal's correlation, Beggs-Robinson's correlation, and Glaso's correlation (Ahmed, 2016). Sutton and Farshad (1990) concluded that Glaso's correlation gives better accuracy than Beals's and Beggs-Robinson's correlations. Thus, Glaso's correlation is used in this study to explore the temperature effect on viscosity (μ_{od}) and the American Petroleum Institute (API) gravity, as given below:

$$\mu_{od} = [3.141(10^{10})](T - 460)^{-3.444}[\log(API)]^{A} \quad (6.1)$$

The temperature is in R (Rankine), and the coefficient A is expressed as follows:

$$A = 10.313[\log(T - 460)] - 36.447 \quad (6.2)$$

The effect of reservoir temperature is investigated over a wide range, from 120^{o}F to 200^{o}F. It is well known that viscosity is a function of temperature and density. Therefore, any temperature change will considerably affect viscosity. In this research, it was found that as the temperature increases, the recovery factor increases and the entropy production is also increased. From **Figure 6.28**, the recovery factor versus entropy production in a semi-log scale for different viscosity is plotted. **Figure 6.29** shows a semi-log scale for entropy production versus viscosity. At low production rates, there is no appreciable change in entropy production when the viscosity changes. Simultaneously, at higher production rates, there is a noticeable decrease in entropy production as viscosity increases. In addition, **Figure 6.30** displays the same results on a standard scale for beter clarity. Observing more changes in high production rate compard to low production rate is due to the higher entropy production when high production rate occurs. The effect of viscosity on the recovery factor at a constant production rate is also investigated. It is concluded that as the viscosity increases, the recovery factor decreases at a constant production rate based on **Figure 6.31**. This increase is more noticeable at high production rates compared to low production rates.

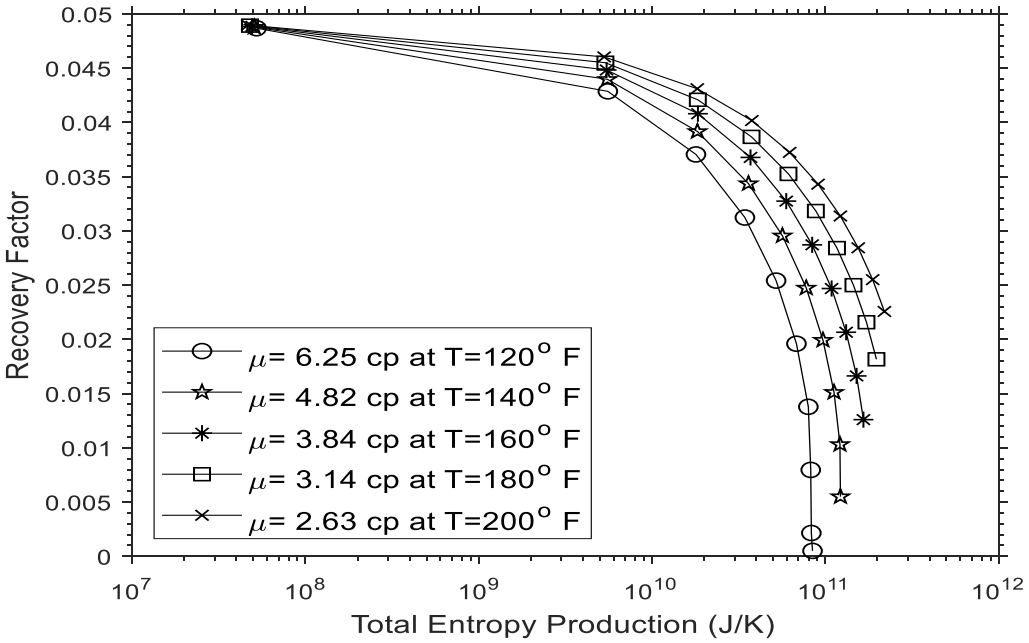

Figure 6. 28. Effect of viscosity on entropy production and recovery factor as a function of production rates.

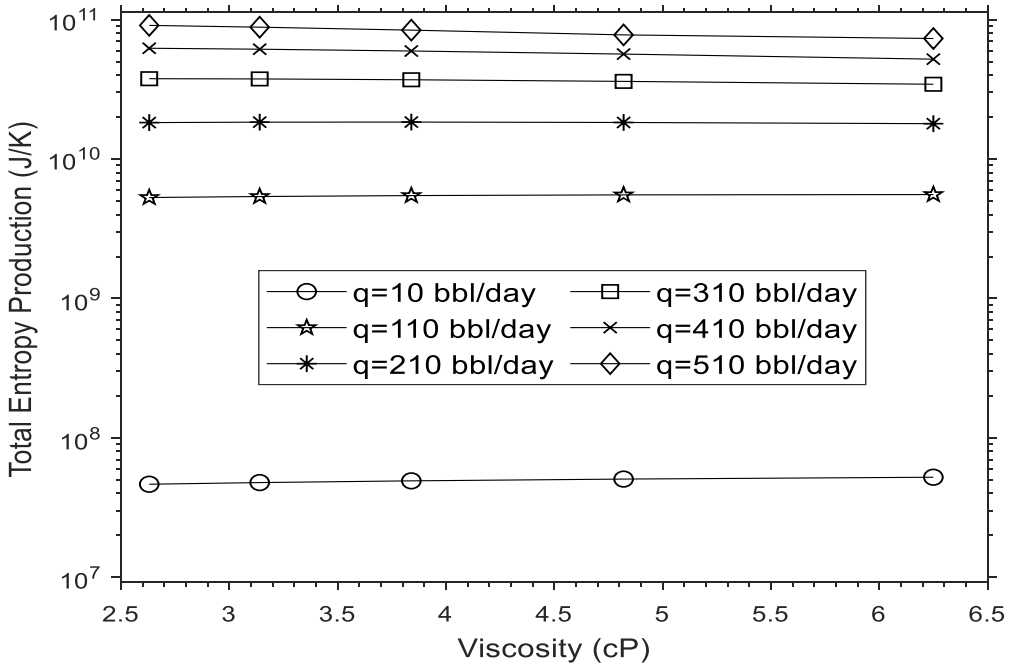

Figure 6. 29. Entropy production versus viscoity at a constant flow rate on a semi-log scale.

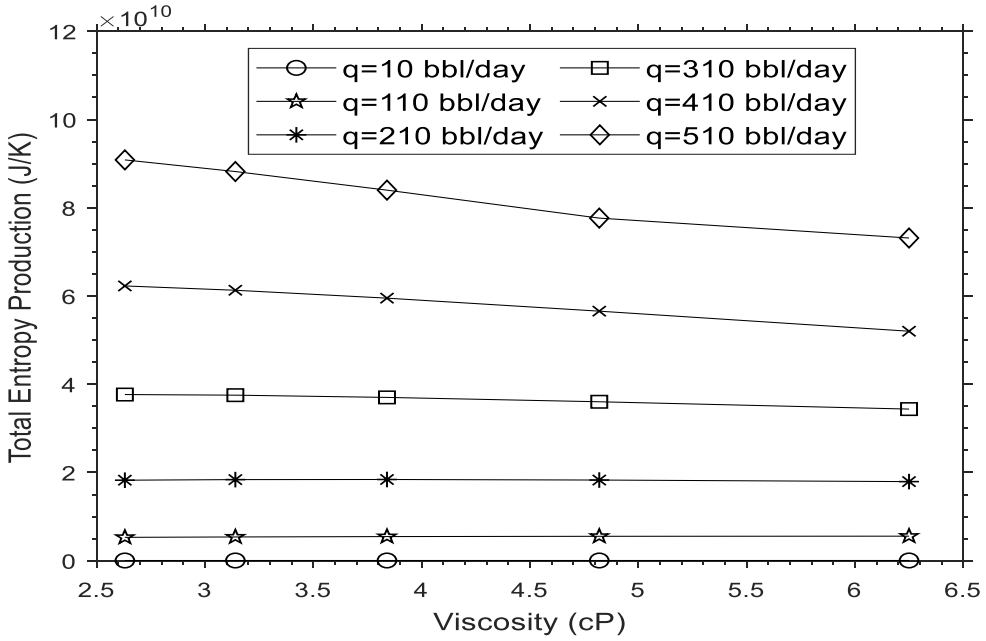

Figure 6. 30. Entropy production versus temperature at a constant flow rate on a non-log scale.

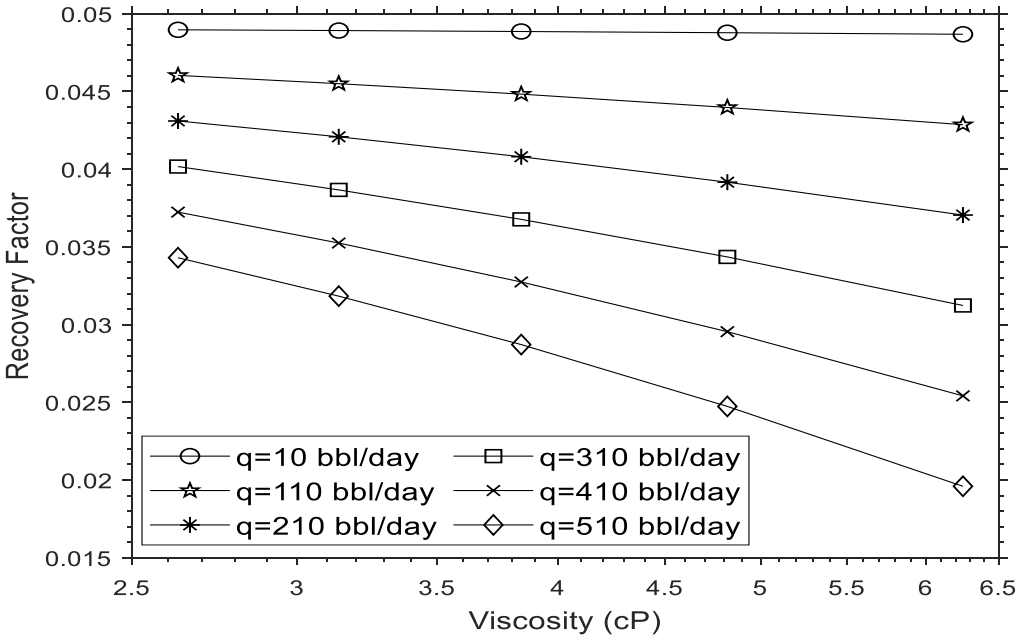

Figure 6. 31. Recovery factor versus temperature at a constant flow rate.

Effect of API. As indicated before, the API gravity is also affected by temperature. In this study, the effect of temperature on API is discussed. A broad range of API values (20 – 60) is examined in this research. As depicted in **Figure 6.32**, as the API increases, both recovery factors and entropy production increase. The effect of API on recovery factor and entropy production is more noticeable than the effect of viscosity. For example, at 200^{o}F, the recovery factor in the case of viscosity is 2.25%, and entropy production is 2.19E11 J/s compared to 3.62% and 3.3E11 J/s for API. Entropy production versus API at constant production rates is demonstrated in **Figure 6.33**.

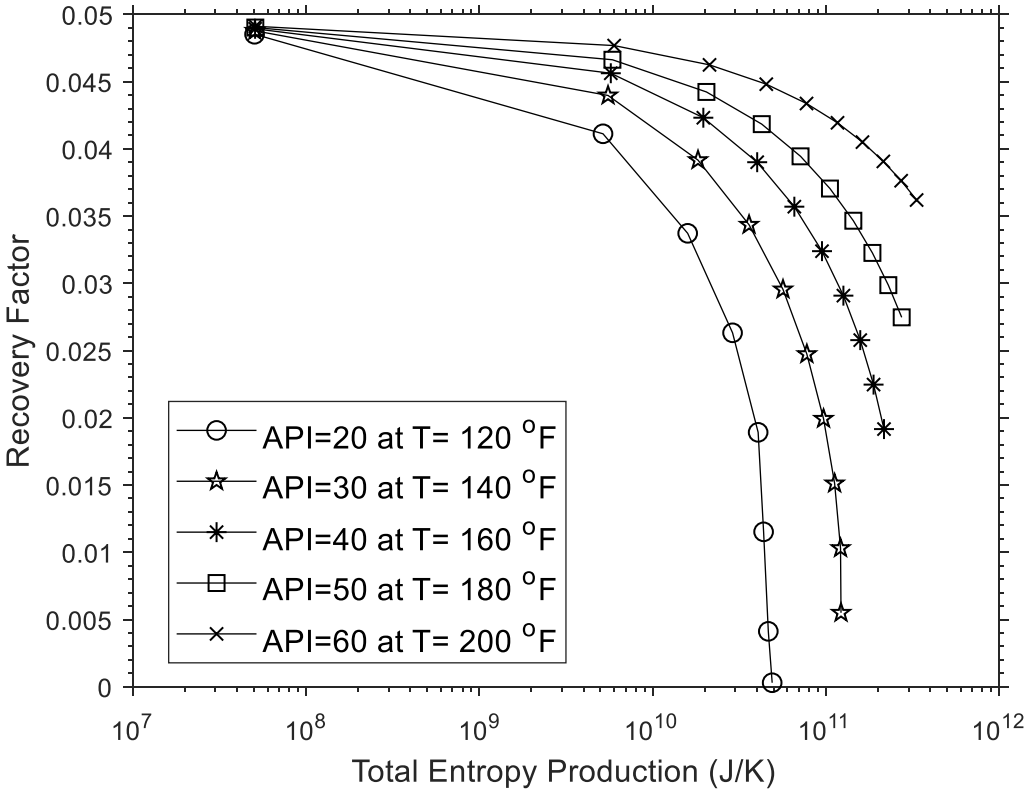

Figure 6. 32. Effect of API on entropy production and recovery factor as a function of production rate.

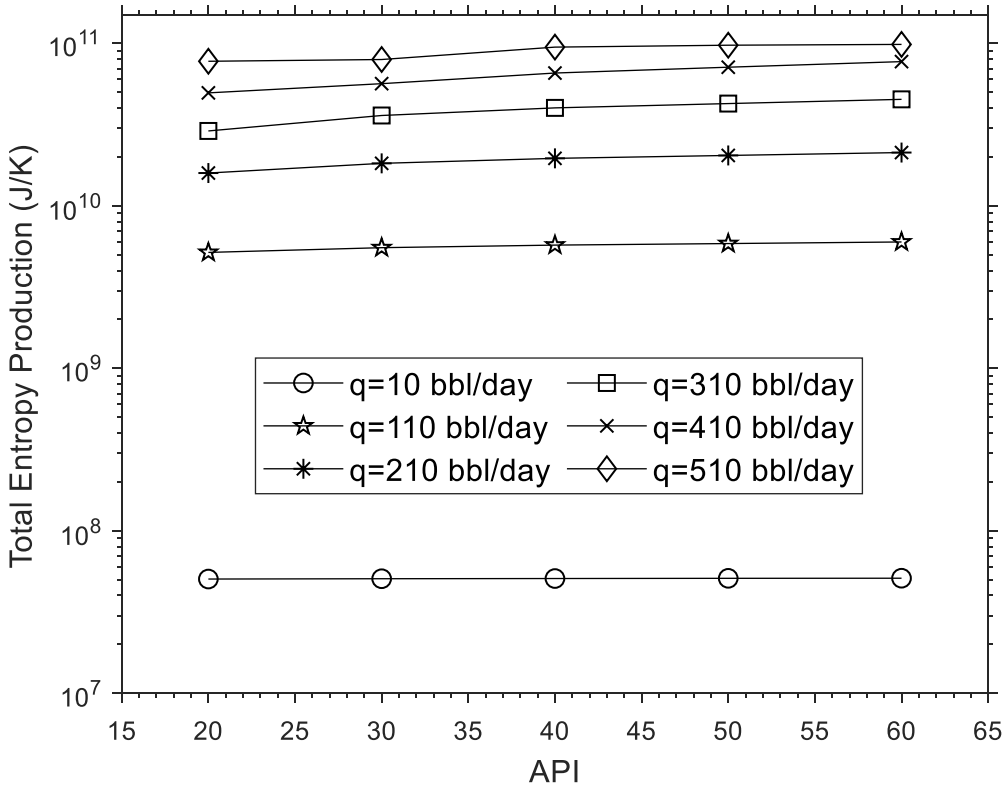

Figure 6. 33. Entropy production versus API as a constant flow rate on a semi-log scale.

It is observed that as the API increases, there is an increase in entropy production, especially at high production rates. A crude oil's density is an important measure of its overall quality. This is because lighter oils are generally easier to produce and refine than heavy oils, and therefore tend to have higher enery loss. **Figure 6.34** shows the same results but on a non-log scale. The effect of production rate and API on the recovery factor is also investigated as a function of different production rates. The results are shown in **Figure 6.35** below.

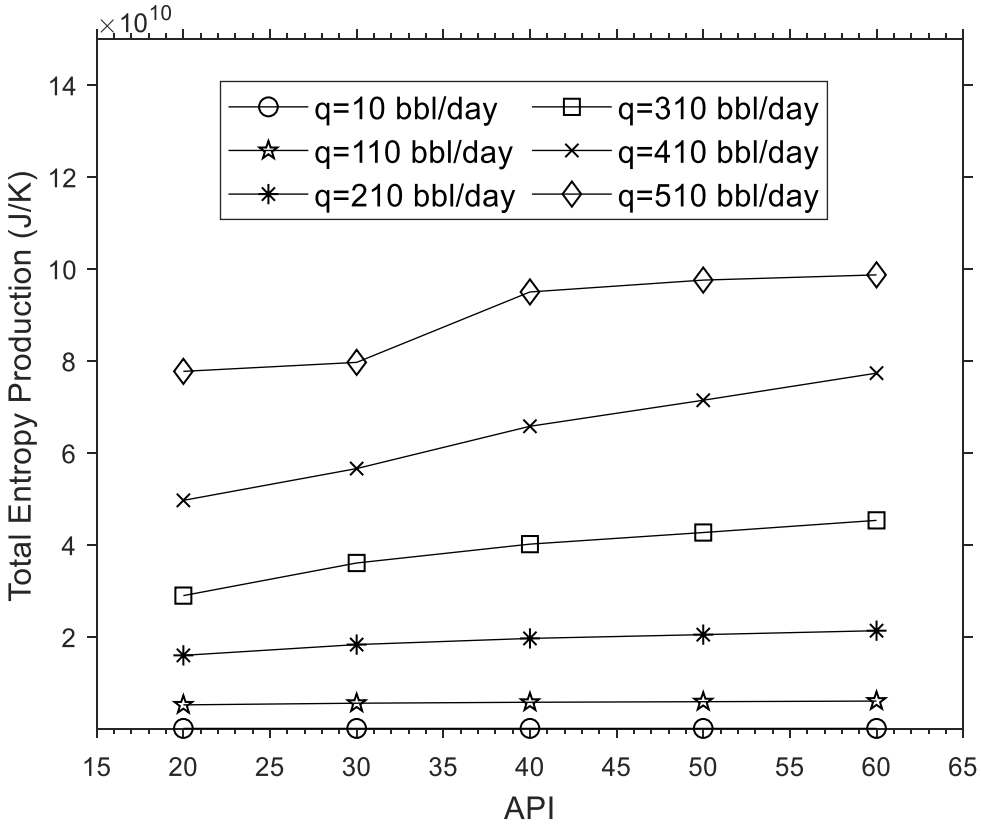

Figure 6. 34. Entropy production versus API as a constant flow rate on a standard scale.

According to **Figure 6.35**, the recovery factor increases as the API increases. This increase is more pronounced at higher production rates. It is found that both viscosity and API affect the total entropy production and recovery factor. However, the influence of viscosity on entropy production is the opposite of the impact of API on total entropy production. This is in agreement with the literature. When the viscosity increases, the oil will be heavier. On the other hand, when the density increases, the oil becomes lighter, resulting in higher production rate.

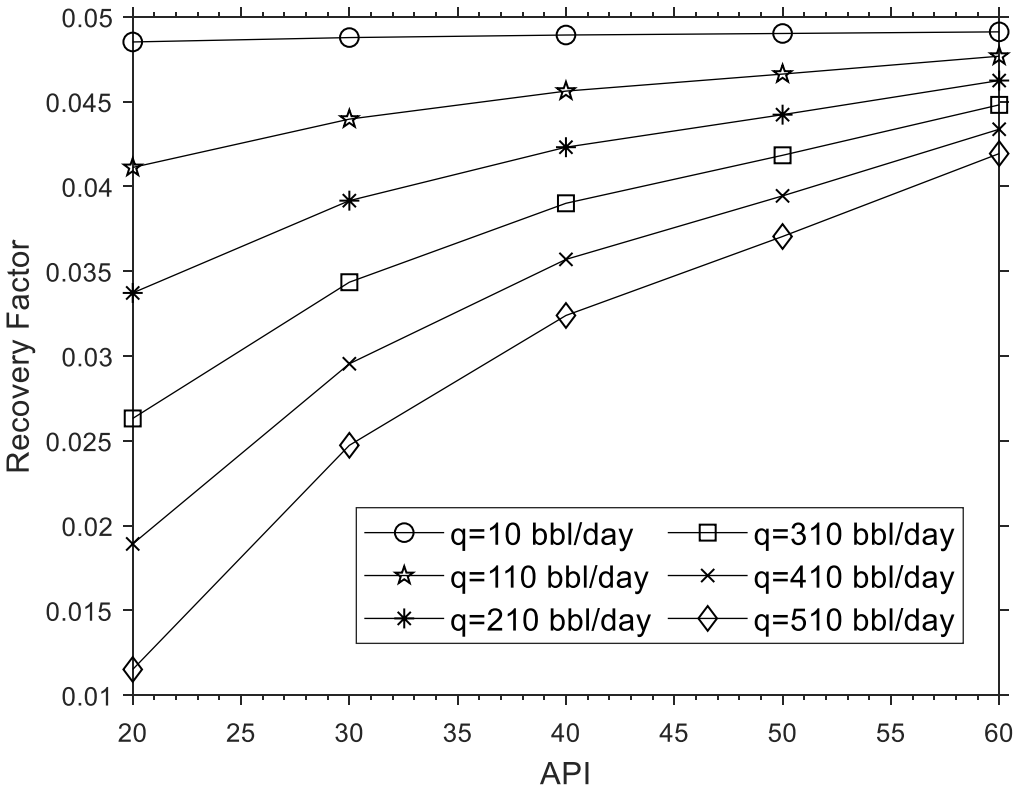

Figure 6. 35. Recovery factor versus API at a constant production rate.

Effect of Wettability/Relative Permeability. The effect of wettability on the fluid location and distribution in porous media is well known, which leads to the belief that the effect of wettability on relative permeability is essential. The data used in this study to investigate the effect of wettability on relative permeability (Anderson, 1987) is reported in **Table 6.5**. It is worth mentioning that the reservoir is water-wet oil reservoir.

Table 6. 5. Oil saturation as a function of contact angle

Effective Oil Permeability (mD)	Contact Angle (degrees)
561	0 (water-wet)
472	47
459	90
380	138
357	180 (oil-wet)

Wettability is a tendency of fluid to stick to the surface of formation when other types of fluid are present. Wettability of rock is measured by a core analysis in a laboratory and typically a laboratory measure contact angle between the fluid and the rock. Rock wettability is one of the factors whose effect on entropy production is also analyzed. As the relative permeability and capillary pressure are affected by rock wettability, both variables are studied. It was reported in past literature that as the water contact angle increases, the effective oil permeability decreases (Anderson, 1986b). It was found that the effect of wettability in terms of relative permeability is apparent, as indicated in **Figure 6.36**. At 100% water-wet, both the recovery factor and entropy production are at their maximum values, which is in agreement with past literature.

On the other hand, when the rock is 100% oil-wet, the recovery factor and entropy are at their minimum. Both cases, fully water-wet and fully oil-wet, are examined under different flow rates. At a constant flow rate, the wettability effect on entropy production is investigated. It was found that as the contact angle increases, the entropy production decreases only for higher production rates based on **Figure 6.37,** showing entropy production versus effective permeability on a semi-log scale. **Figure 6.38** also demonstrates the entropy production versus the effective permeability on a linear scale. At a constant flow rate, it was found that as the effective permeability increases, the recovery factor increases. This phenomenon is clearly observable at a higher production rate, as indicated in **Figure 6.39**.

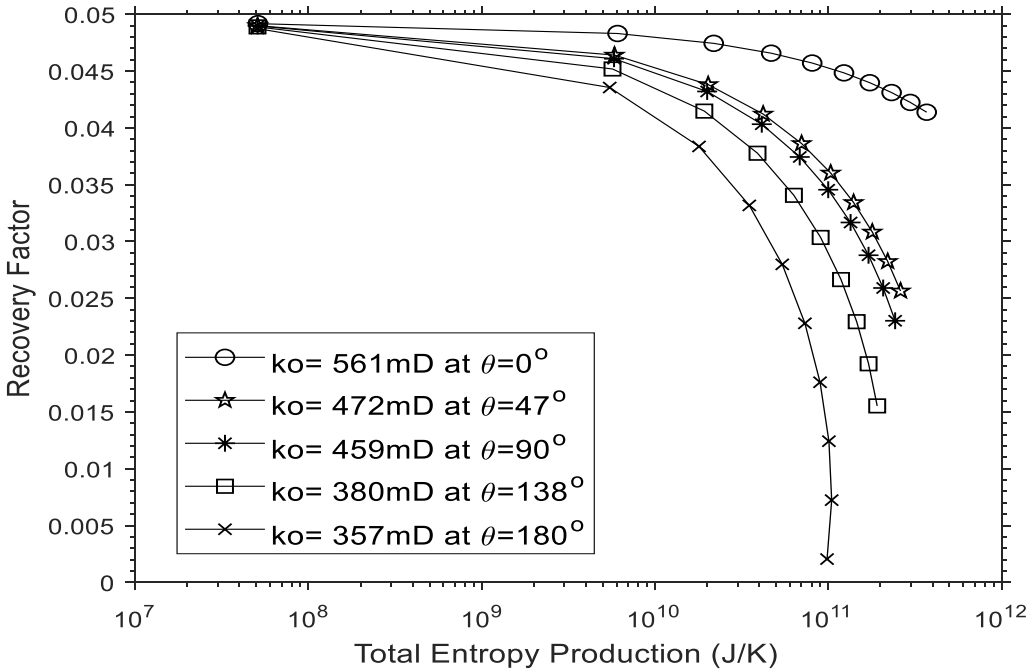

Figure 6. 36. Effect of effective permeability as a function of relative permeability on entropy production and recovery factor.

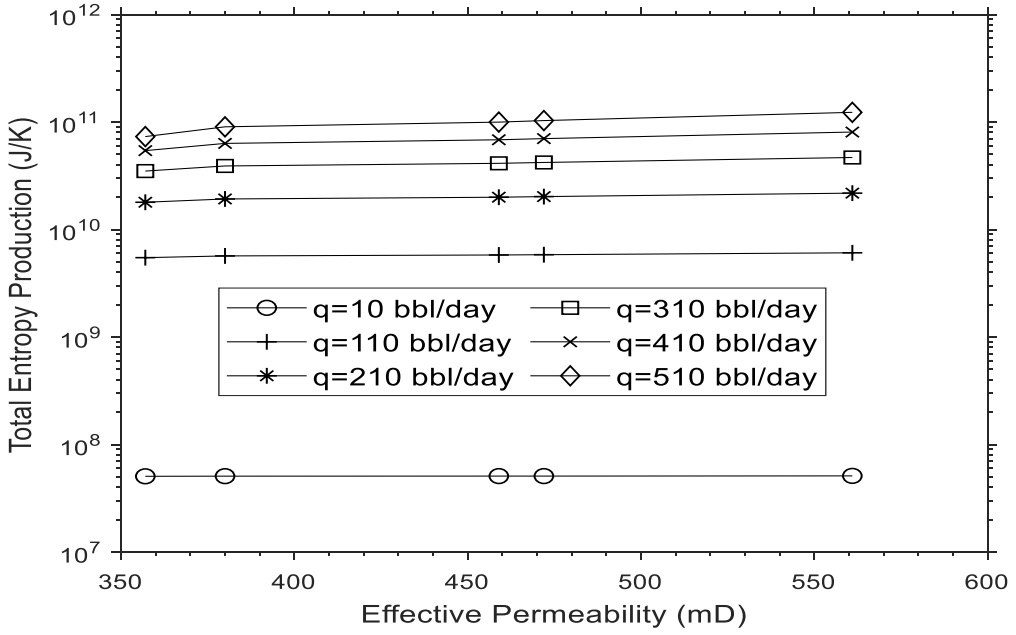

Figure 6. 37. Entropy versus effective permeability at a constant flow rate on a semi-log scale.

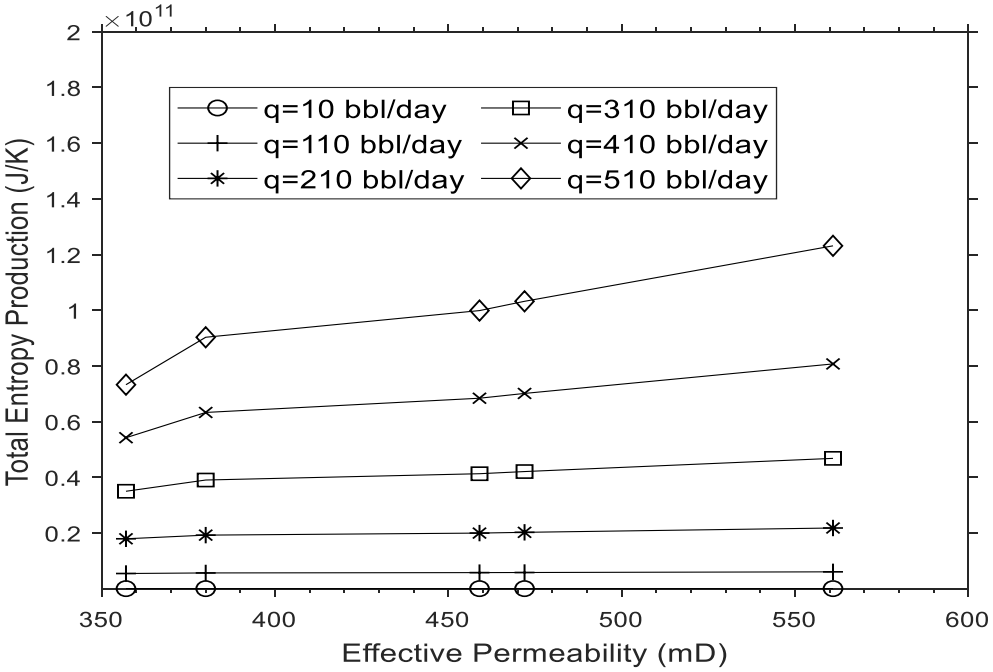

Figure 6. 38. Entropy versus wettability at a constant flow rate on a non-log scale.

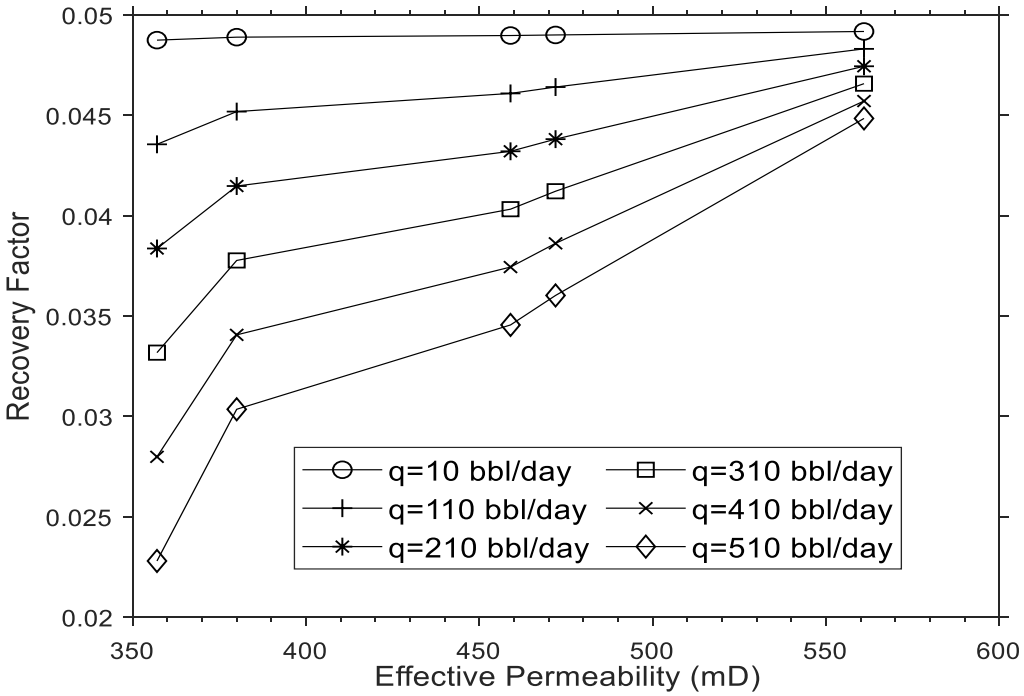

Figure 6. 39. Recovery factor versus contact angle at a constant production rate.

Effect of Wettability and Capillary Pressure. The capillary pressure is dependent on the interfacial tension, pore size, and wetting angle. Capillary pressure is the most fundamental rock/fluid property in multiphase flow, just as porosity and permeability are for single phase flow in oil and gas reservoirs. Capillary pressure curves directly determine the irreducible water saturation, residual oil saturation, and rock wettability and can be used to determine water oil contact point and approximate oil recovery. Wettability, pore structure, initial saturation, and saturation history are the most important factors that affect the capillary pressure and relative permeability (Anderson, 1987a). No direct or simple relationship correlates capillary pressure and wettability. However, cores with reservoir wettability give the most accurate measurements for capillary pressure and wettability.

Capillary pressure strongly influences the model, as discussed earlier, when two cases are studied: with and without the capillary pressure. However, the capillary pressure shows no significant change with a change of the contact angle from 0 to 90^{o} in this study. The impact of contact angle variations is significant in relative permeability rather than capillary pressure (Anderson, 1987a). As the influence of relative permeability on the entropy production and recovery factor is studied, they are also tested against wettability as a function of capillary pressure (see **Figures 6.40 to 6.43**). It worth noting that there is a slight reduction in recovery factor upon an increase in the contact angle based on **Figure 6.43**.

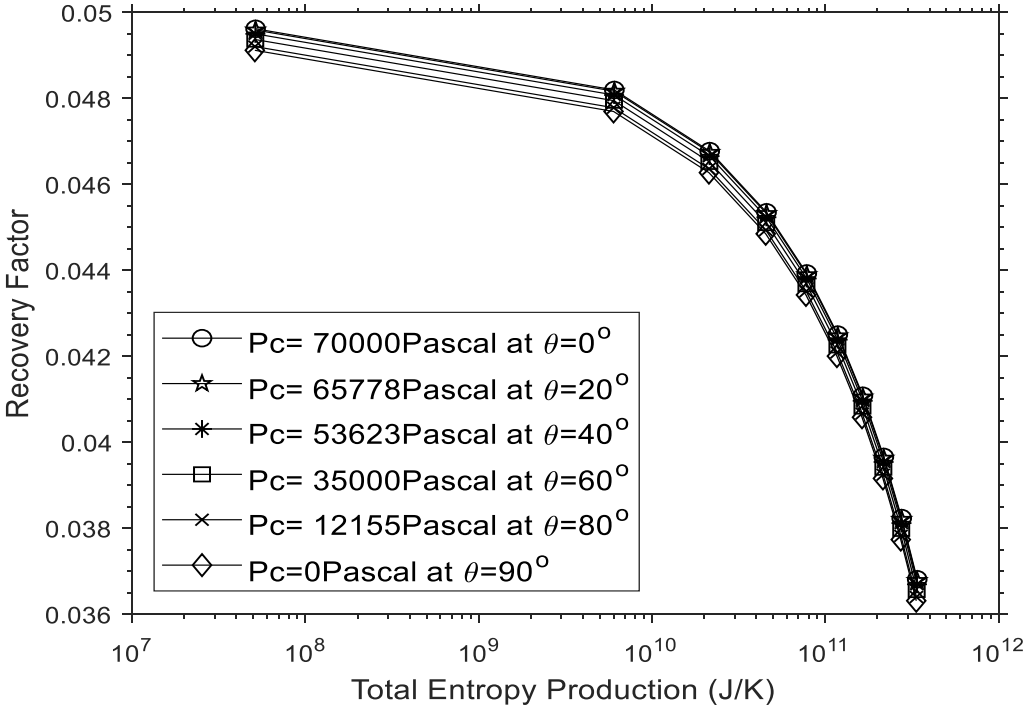

Figure 6. 40. Effect of wettability as a function of capillary pressure on entropy production and recovery factor

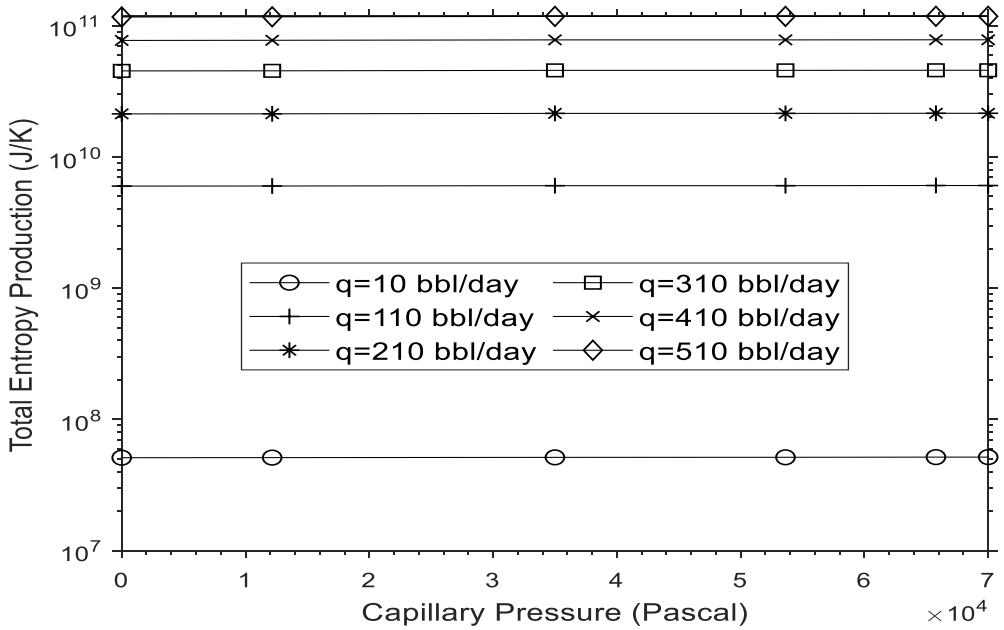

Figure 6. 41. Entropy versus wettability at a constant flow rate on a semi-log scale.

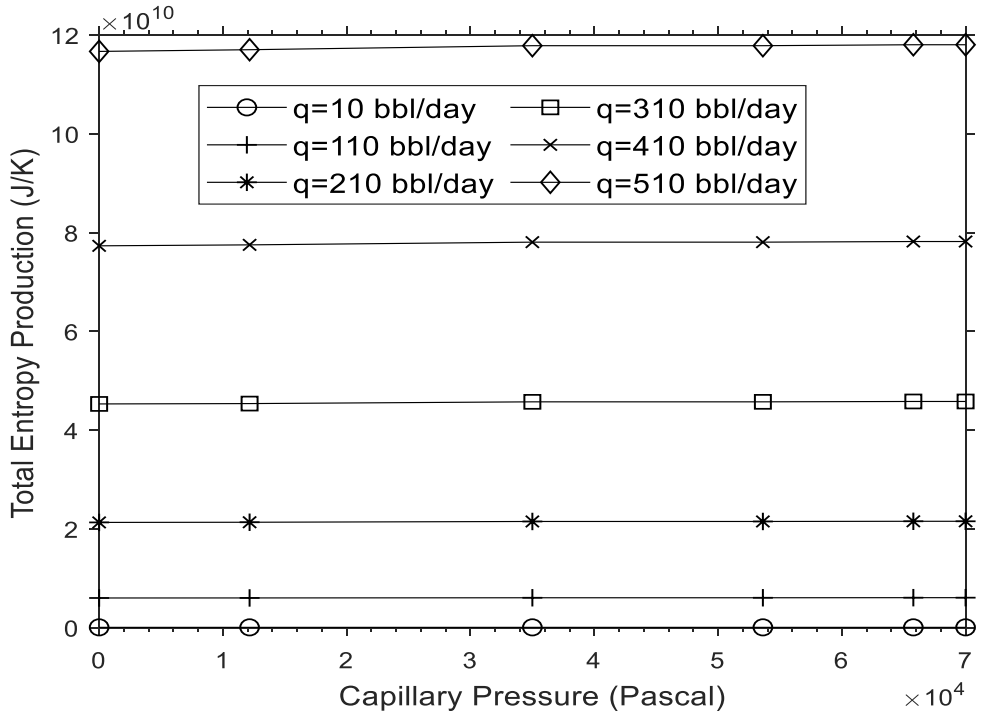

Figure 6. 42. Entropy versus wettability at a constant flow rate on a non-log scale.

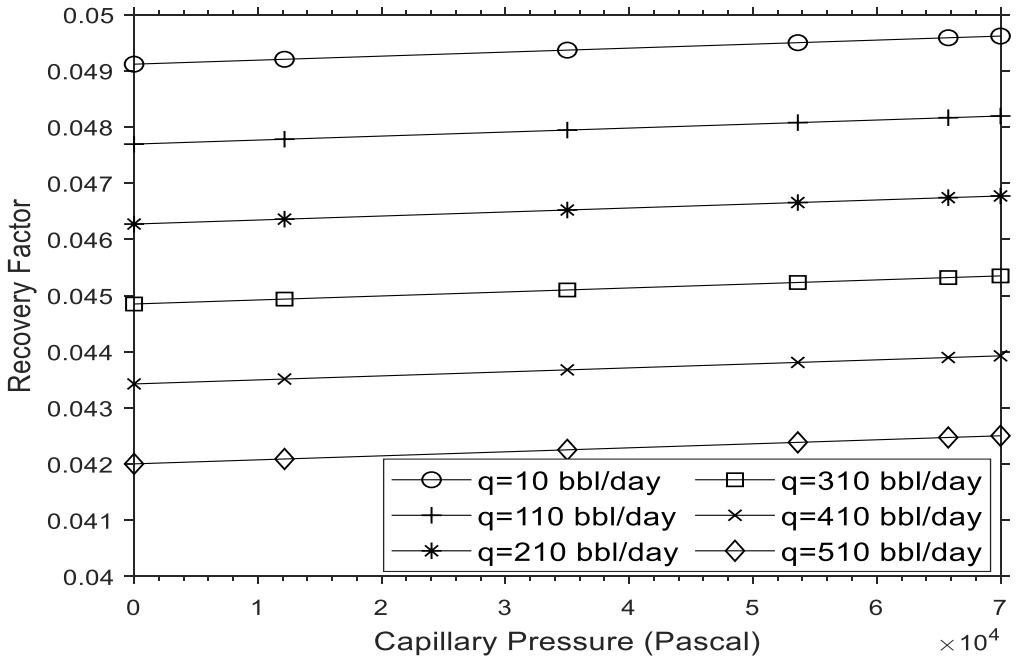

Figure 6. 43. Recovery factor versus contact angle at a constant production rate.

6.5. Summary

This chapter showed the benefits of Entropy Generation Minimization (EGM) as a useful design tool for achieving a higher recovery factor. The second law of thermodynamics was applied with the EGM in a wellbore and porous system during fluid production. The models were used to investigate the EGM of three systems: a reservoir, a near-wellbore, and a wellbore.

The results showed how EGM can be used as an effective design tool for investigating reservoir energy loss at the various process and thermodynamic conditions, which may lead to a higher hydrocarbon recovery factor. General mathematical models that describe the fluid flow in both porous media and wellbores are developed. Mass, momentum, energy and entropy equations are the main governing equations that are used in developing the fluid flow models. The effect of the near-wellbore zone on entropy generation and the recovery factor is included mathematically in the single-phase models.

The results of this research show how the production rate affects the cumulative entropy production and the recovery factor in a reservoir. At the same production rate, the entropy generation reaches a maximum in a shorter time when the skin factor is positive, while it reaches a maximum in a longer time when the skin factor is negative. Moreover, adding the skin factor of a new region (damaged or stimulated) around a wellbore to the mathematical models enhances the recovery factor.

For single-phase flow models. An optimum production rate is estimated to decrease dissipative energy losses, resulting in an optimum recovery factor. In the absence of a skin

effect, it is found that the optimum production rate is 1.26 m^3/s (3.843 MMScf/D). At this production rate, the recovery factor is 51.54%, while the cumulative entropy production is 1.05E+20 J/K.

To design an optimum production system in a reservoir, all properties and variables that have a significant effect on total entropy production are identified and considered. In this study, only three main variables - production rate, recovery factor, and entropy production for each system - are considered. To generalize the optimal conditions for various scales, the normalization approach is employed to obtain dimensionless numbers by combining the variables. It is evident that the production rate has an essential role in entropy production minimization of hydrocarbon reservoirs.

The single-phase models are extended to incorporate the wellbore condition effect. The results from the three-system models are compared to those for two-system models. Adding a new region around the wellbore increases the recovery factor, while there is no significant change in the cumulative entropy production. The reason for no significant change in cumulative entropy production is because adding a near wellbore system does not affect the average reservoir pressure, which has a considerable effect on entropy. The present results also show that a substantial increase in the recovery factor occurs with increasing the production rate, while at lower production rates, an increase in the recovery factor is not significant in both damaged and stimulated scenarios. This could occur because adding a new region around a wellbore allows the model to incorporate two permeability values: reservoir permeability and new region permeability. Therefore, the actual value of the new region's permeability will improve the accuracy of recovery factor calculations. There will

be no changes in the recovery factor when there is no skin effect. The CMG is also employed to verify the actual value of a new region radius that corresponds to the skin factor.

The effects of different parameters such as porosity, temperature, viscosity, BHP, and permeability on cumulative entropy production are investigated. It was found that viscosity, porosity, and temperature have no considerable influence on cumulative entropy production. However, BHP and permeability exhibit a noticeable impact on cumulative entropy production. It is concluded that at a constant production rate, there is a slight change in the total entropy production with BHP. A possible explanation is that when the BHP increases, a decrease in pressure drop occurs, leading to lower total entropy production. Additionally, at a high BHP, the dissipative energy loss in the reservoir will be lower compared to a low BHP.

Furthermore, an increase in the total entropy production with increasing permeability at different production rates was observed. The increase in the total entropy production is significant at low permeability (within the range of 1E-15 m^2 and 1E-13 m^2), compared to high permeability values. These results are consistent with the preliminary results, implying that at the stimulated region (high permeability), the entropy production is high, while at the damaged region (low permeability), the entropy production is low. When the permeability increases, the production rate increases as well and consequently, the entropy generation increases.

The wellbore models for single-phase flow that were developed are capable of being used in new wells, exploration wells, or wells that have been shut down to determine the potential of the well flow. Past models of Civan and Tiab (1989) have been modified and extended in this study so that they apply to three-system hydrocarbon reservoirs. Furthermore, this study employed newly developed algorithm for solving the modified flow conditions and two-phase conditions.

Two-phase flow models. The skin effect has more influence in the curve's trend of recovery factor versus total entropy production of the oil phase compared to the water phase. This behavior might be due to the lower water production rate (low water fraction) and the low value of water relative permeability, compared to the oil phase. At the same skin factor effect, as the oil production rate decreases, the recovery factor and total entropy production increase. However, the reservoir production lifetime increases with a decrease in the production rate. On the contrary, the recovery factor and total entropy production decrease as the water production rate increases.

The effect of capillary pressure is important in two-phase flow models. However, the change of capillary pressure value does not have a significant impact on the two-phase flow results. The strong impact of the existence of capillary pressure on the model is due to the change of BHP; when the capillary pressure is assumed to be zero, the BHPs for the oil and water are presumed equal. In the absence of capillary pressure, the only scenario that the total entropy production is the same for oil and water is when the fractional flow of

water is 0.5. At $f_w = 0.1$ and $P_c \neq 0$, the change in the recovery factor is more noticeable compared to a change in the total entropy production.

The effect of temperature and rock wettability is investigated in the models. The viscosity and API are both functions of temperature, while the relative permeability and capillary pressure are a function of rock wettability. Therefore, viscosity, API, relative permeability, and the capillary factor as a function of wettability are investigated and analyzed in this study. As the temperature increases, the total entropy production increases as well at high production rates. This occurs because when the temperature increases, the viscosity decreases, leading to a reduction in the recovery factor and consequently an increase in the total entropy production. Various API and viscosity values are used in this study to investigate the impact of temperature on the two-phase model results.

As the water contact angle increases, the oil effective permeability increases. At 100% water saturation, both the recovery factor and entropy production are at their maximum. On the other hand, when the rock is fully oil-wet, the recovery factor and entropy production are at their minimum. Both cases, fully water-wet and fully oil-wet, are investigated under different flow rates. It was found that as the contact angle increases, the entropy production decreases, especially for higher production rates. In this study, it is concluded that the impact of contact angle change is significant in relative permeability rather than in the capillary pressure. No appreciable change in either recovery factor, or total entropy production, is observed when a range of capillary pressure is tested in the two-phase models.

Chapter 7: Conclusions and Recommendations

7.1. Conclusions

In the modeling, a one-dimensional flow was assumed in the wellbore, while a radial flow was assumed in the reservoir. Mass, momentum, energy, and entropy balance equations, particularly with Entropy Generation Minimization (EGM), were used to address the fluid flow behavior and energy loss in wellbore and reservoir systems. Numerical methods were used in solving the fluid flow and entropy equations. The models were solved by a new numerical scheme programmed in the MATLAB environment with a new algorithm. For validation purposes, a commercial simulator, Computer Modeling Group (CMG), verified the predicted results.

This study contributes to existing knowledge of EGM applications in porous media for both academic and industrial purposes by providing a comprehensive entropy investigation of the three main sections of hydrocarbon reservoir system: reservoir, wellbore, and near-wellbore. The model was modified to explicitly near wellbore to account for skin effect explicitly on entropy generation. At a constant production rate, a positive skin factor causes a reservoir to consume mechanical energy faster than for the case with a negative skin factor. In addition, the purpose of considering the new near well region is to capture the effect of damage or stimulation on the area around the wellbore.

Single-phase models were used to study the effects of different parameters on entropy generation. It was observed that the Bottom Hole Pressure (BHP) and permeability have the most influence on entropy generation. The influence of relative permeability, viscosity,

API, and capillary pressure on total entropy production rate were investigated in two-phase flow models. It was found that capillary pressure changes had no effect on the total entropy rate, while the decrease or increase of total entropy production on the other parameters was more noticeable. The general trend of total entropy production versus recovery factor for two-phase flow is similar to single-phase flow. The total entropy production increases as the production rate increases for both oil and water phases despite the skin effect. As the reservoir is under the natural energy mechanism and no Enhanced Oil Recovery (EOR) technique is used, the recovery factor for both oil and water are relatively low, less than 5%. The BHP is kept equal to or above the bubble point pressure, 1000 psi, to avoid any gas production at the surface.

For the water phase, both the recovery factor and total entropy production change slightly with increasing water fraction flow. This might have occurred due to the low water production rate (low water fraction) and the low magnitude of water relative permeability compared to the oil phase.

Capillary pressure has moderate influence on the production rate. In the single phase model a 2.5% increase in the water recovery factor was observed compared to the “no capillary pressure” case when the capillary pressure is considered. However, the change of capillary pressure value does not have a significant impact on the two-phase flow model results. Pressure profiles and recovery factor outcomes of the proposed models are validated with CMG in terms of accuracy and consistency. However, CMG does not have the feature to confirm the EGM calculations.

These contributions bring the state of knowledge closer to a more accurate, reliable, and comprehensive model for entropy generation in sub-surface and surface systems of single-phase and two-phase flow reservoirs. Having comprehensive models that can be used to reduce the loss of reservoir mechanical energy and consequently achieve a higher recovery factor is one of the research motivations. A new performance index based on entropy generation called COP was developed which can be used to optimize the production rate. Additionally, an economic analysis was used to validate the optimum production rate estimations. Furthermore, enriching/ filling the research knowledge gaps is another strong motivation for conducting this research.

7.2. Recommendations

Despite considerable efforts to develop comprehensive models that can predict the energy losses in porous media and wellbores, there are still some areas that could not be explored fully. As the fluid flow equations are complex, simplified assumptions were made, which may limit the applicability of the proposed models. Therefore, the following recommendations are made for more accurate models and widespread application of EGM as a design tool for hydrocarbon reservoir.

A one-dimensional flow under isothermal conditions was the main assumption of developing the proposed models in this study. Naturally, fluid flow is three-dimensional, which means the flow parameters, such as velocity and pressure, vary in all three coordinate directions. Therefore, extending the model to two or three dimensions, as well as non-isothermal conditions, is recommended for a better representation.

The focus of this study was to investigate the natural reservoir energy generated from the reservoir mechanisms, which, as shown previously, are not an effective production technique for most of the existing reservoirs. Thus, having a three-phase model instead of a two-phase flow model in a reservoir with an external energy provider, such as EOR techniques, would be beneficial.

The current models were developed with the assumptions of reservoir homogenously, and simple capillary pressure and relative permeability models. Thus, having a heterogeneous reservoir with recent relative permeability and capillary pressure models would strongly recommend for better presentations.

Developing non-dimensional variables for the models is useful for generalization purposes. In addition, techniques and methods, such as pore-scale modelling for more complex structures and stability analysis for the entire system, could be introduced in the proposed models, as well as including the gravity effect in the governing equations. Also, further effort could be made to include EGM analysis as a feature for commercial simulators, such as CMG and Eclipse.

References

A, Smithwich, R.W., 1988. Contact-angle studies of microscopic mercury droplets on glass. J. Colloid Interface Sci. 123, 482–485. https://doi.org/10.1016/0021-9797(88)90269-X

Ahmed, T., 2019. Reservoir Engineering Handbook, Fifth Edit. ed. Gulf Professional Publishing. https://doi.org/10.1016/C2016-0-04718-6

Ahmed, T., 2016. Equations of State and PVT Analysis Applications for Improved Reservoir Modeling. Elsevier Inc. https://doi.org/10.1016/C2014-0-00119-0

Akbarabadi, M., Piri, M., 2013. Relative permeability hysteresis and capillary trapping characteristics of supercritical CO2/brine systems: An experimental study at reservoir conditions. Adv. Water Resour. 52, 190–206. https://doi.org/10.1016/j.advwatres.2012.06.014

Al-Salem, K., Hosseini, E., Nohesara, A., Mehri, M., Ali, M., Almuzaiqer, R., Alimoradi, A., Tlili, I., 2019. Suggestion of New Correlations for the Exergy Efficiency and Coefficient of Exergy Performance of Annulus Section of Conically Coiled Tube-in-Tube Heat Exchangers. Chem. Eng. Res. Des. 152, 309–319. https://doi.org/10.1016/j.cherd.2019.10.002

Aladag, B., Halelfadl, S., Doner, N., Maré, T., Duret, S., Estellé, P., 2012. Experimental investigations of the viscosity of nanofluids at low temperatures. Appl. Energy 97, 876–880. https://doi.org/10.1016/j.apenergy.2011.12.101

Alemayehu, C., Verda, V., Sciubba, E., 2015. Entropy Generation Analysis as a Design Tool—A review. Renew. Sustain. Energy Rev. 43, 1167–1181. https://doi.org/10.1016/j.rser.2014.11.104

Amaefule, J.O., Handy, L.L., 1982. The Effect of Intetfacial Tensions on Relative Oil / Water Penneabilities of Consolidated Porous Media. Soc. Pet. Eng. J. 22, 371–381. https://doi.org/10.2118/9783-PA

Anderson, W.G., 1987a. Wettability Literature Survey- Part 4: Effects of Wettability on Capillary Pressure. J. Pet. Technol. 39. https://doi.org/10.2118/15271-PA

Anderson, W.G., 1987b. Wettability Literature Survey-Part 6: The Effects of Wettability on Waterflooding. J. Pet. Technol. 39. https://doi.org/10.2118/16471-PA

Anderson, W.G., 1987c. Wettability Literature Survey Part 5: The Effects of Wettability on Relative Permeability. J. Pet. Technol. 39. https://doi.org/10.2118/16323-PA

Anderson, W.G., 1986a. Wettability Literature Survey- Part 1: Rock/Oil/Brine Interactions and the Effects of Core Handling on Wettability. J. Pet. Technol. 38. https://doi.org/10.2118/13932-PA

Anderson, W.G., 1986b. Wettability Literature Survey-Part 3: The Effects of Wettability on the Electrical Properties of Porous Media. J. Pet. Technol. 38. https://doi.org/10.2118/13934-PA

Archer, J.S., Wall, C.G., 1986. Petroleum Engineering Principles and Practice. https://doi.org/10.1007/978-94-010-9601-0

Aziz, A., Khan, W.A., 2012. Minimum Entropy Generation Design of a Convectively Heated Pin Fin with Tip Heat Loss. Int. J. Exergy 10, 44–60. https://doi.org/10.1504/IJEX.2012.045060

Aziz, K., Settari, A., 2002. Petroleum Reservoir Simulation. Applied Science Publishers LTD.

Azoumah, Y., Neveu, P., Mazet, N., 2006. Constructal Design Combined With Entropy Generation Minimization for Solid–Gas Reactors. Int. J. Therm. Sci. 45, 716–728. https://doi.org/10.1016/j.ijthermalsci.2005.10.006

Bartell, F.E., Cardwell, P.H., 1942. Reproducible Contact Angles on Reproducible Metal Surfaces. I. Contact Angles of Water against Silver and Gold. J. Am. Chem. Soc. 64, 494–497. https://doi.org/10.1021/ja01255a007

Batchelor, G.K., 1977. The effect of Brownian motion on the bulk stress in a suspension of spherical particles. J. Fluid Mech. 83, 97–117. https://doi.org/10.1017/S0022112077001062

Batycky, J.P., McCaffery, F.G., Hodgins, P.K., Fisher, D.B., 1981. Interpreting Relative Permeability and Wettability From Unsteady-State Displacement Measurements. Soc. Pet. Eng. J. 21, 296–308. https://doi.org/10.2118/9403-pa

Bejan, A., 1996. Entropy Generation Minimization: The New Thermodynamics of Finite-Size Devices and Finite-Time Processes. J. Appl. Phys. 79, 1191–1218. https://doi.org/10.1063/1.362674

Bejan, A., 1995. Entropy Generation Minimization: The Method of Thermodynamic Optimization of Finite-Size Systems and Finite-Time Processes. CRC Press. Inc. Boca Raton, Boca Raton. https://doi.org/10.1201/9781482239171

Bendix, P.B., Henninger, S.K., Henning, H.M., 2016. Temperature and mechanical stabilities and changes in porosity of silicone binder based zeolite coatings. Ind. Eng. Chem. Res. 55, 4942–4947. https://doi.org/10.1021/acs.iecr.6b00558

Benner, F.C., Dodoo, C.G., Bartell, F.E., 1942. Evaluation of Effective Displacement Pressures for Petroleum Oil-Water Silica Systems, in: Drilling and Production Practice, 1 January, New York, New York.

Bennett, C.H., 1982. The Thermodynamics of Computation—A Review. Int. J. Theor. Phys. Vol. 21, 905–940. https://doi.org/10.1007/BF02084158

Bernabe, Y., 1987. The effective pressure law for permeability during pore pressure and confining pressure cycling of several crystalline rocks. J. Geophys. Res. 92, 649. https://doi.org/10.1029/JB092iB01p00649

Bidi, M., Nobari, M.R.H., Saffar-Avval, M., 2010. A Numerical Evaluation of Combustion in Porous Media by EGM (Entropy Generation Minimization). Energy 35, 3483–3500. https://doi.org/10.1016/j.energy.2010.04.053

Bigelow, W.C., Pickett, D.L., Zisman, W.A., 1946. Oleophobic monolayers: I. Films adsorbed from solution in non-polar liquids. J. Colloid Sci. 1, 513–538. https://doi.org/10.1016/0095-8522(46)90059-1

Bikerman, J.J., 1950. Sliding of drops from surfaces of different roughnesses. J. Colloid Sci. 5, 349–359. https://doi.org/10.1016/0095-8522(50)90059-6

Biot, M.A., 1941. General Theory of Three-Dimensional Consolidation. J. Appl. Phys. 12, 155–164. https://doi.org/10.1063/1.1712886

Blick, E.F., Civan, F., 1988. Porous-Media Momentum Equation for Highly Accelerated Flow. SPE Reserv. Eng. 3. https://doi.org/10.2118/16202-PA

Bouchard, A.J., Hawkins, J.T., 1992. Reservoir-Engineering Implications of Capillary-Pressure and Relative-Permeability Hysteresis. Log Anal. 33, 415–420.

Bouvier, L., Maquignon, S.M., 1991. Reconciliation of Log and Laboratory Derived Irreducible Water Saturations in a Double Porosity Reservoir, Gordon and Breach publishers, Philadelphia.

Brandon, S., Haimovich, N., Yeger, E., Marmur, A., 2003. Partial wetting of chemically patterned surfaces: The effect of drop size. J. Colloid Interface Sci. 263, 237–243. https://doi.org/10.1016/S0021-9797(03)00285-6

Brandon, S., Marmur, A., 1996. Simulation of Contact Angle Hysteresis on Chemically Heterogeneous Surfaces. J. Colloid Interface Sci. 183, 351–355. https://doi.org/10.1006/jcis.1996.0556

Brandon, S., Wachs, A., Marmur, A., 1997. Simulated Contact Angle Hysteresis of a Three-Dimensional Drop on a Chemically Heterogeneous Surface: A Numerical Example. J. Colloid Interface Sci. 191, 110–116. https://doi.org/10.1006/jcis.1997.4912

Braun, E.M., Blackwell, R.J., 1981. A Steady-State Technique for Measuring Oil-Water Relative Permeability Curves at Reservoir Conditions. 56th Annu. Fall Tech. Conf. Exhib. San Antonio, Texas, Oct. 5 - 7. SPE 10155. https://doi.org/10.2118/10155-MS

Braun, E.M., Holland, R.F., 1995. Relative Permeability Hysteresis: Laboratory Measurements and a Conceptual Model. SPE Reserv. Eng. 10, 222–228. https://doi.org/10.2118/28615-PA

Brinkman, H.C., 1952. The viscosity of concentrated suspensions and solution. J. Chem. Phys. 20, 571–581. https://doi.org/10.1063/1.1700493

Brockway, L.O., Jones., R.L., 1964. Electron Microscopic Investigation of the Adsorption of Long-Chain Fatty Acid Monolayers on Glass. Adv. Chem. 43, 275–294. https://doi.org/10.1021/ba-1964-0043.ch019

Brooks, R.H.., Corey, A.T., 1966. Properties of Porous Media Affecting Fluid Flow. J. Irrig. Drain. Div. 92, 61–90.

Brown, H., 1951. Capillary Pressure Investigations. J. Pet. Technol. 3, 67–74. https://doi.org/10.2118/951067-G

Bruce, W.., Welge, H., 1947. The restored-state method for determination of oil in place and connate water. Oil Gas J. 46, 223–238.

Bruce, Welge, H.J., 1947. The restored-state method for determination of oil in place and connate water. Oil Gas J. 46, 223–238.

Budziak, C.J., Neumann, A.W., 1990. Automation of the capillary rise technique for measuring contact angles. Colloids and Surfaces 43, 279–293. https://doi.org/10.1016/0166-6622(90)80293-D

Bull-D-14, 1984. Statistical Analysis of Crude Oil Recovery and Recovery Efficiency. American Petroleum Institute.

Buongiorno, J., 2005. Convective Transport in Nanofluids. J. Heat Transf. 128, 240–250. https://doi.org/doi:10.1115/1.2150834

Burdine, N.T., 1953. Relative Permeability Calculations From Pore Size Distribution Data. J. Pet. Technol. 5, 71–78. https://doi.org/10.2118/225-G

Cano Barrita, P.F.D.J., Balcom, B.J., McAloon, M.J., Green, D.P., Dick, J., 2008. Capillary Pressure Measurement on Cores by MRI. J. Pet. Technol. 60, 63–66.

Carlson, F.M., 1981. Simulation of Relative Permeability Hysteresis to the Nonwetting Phase. SPE Annu. Tech. Conf. Exhib. https://doi.org/10.2118/10157-ms

Carnot, L., 1803. Principes fondamentaux del' equilibre et du mouvement.

Carnot, L., 1786. Essai sur les machines en general.

Carnot, S., 1824. Reflections on the Motive Power of Heat. Paris, France.

Cassie, A.B.D., 1948. Contact angles. Discuss. Faraday Soc. 3, 11–16.

Cassie, A.B.D., Baxter, S., 1944. Wettability of porous surfaces. Trans. Faraday Soc. 40, 546–551.

Chandlereng, 2017. Formation Response Tester [WWW Document]. Web. URL http://www.chandlereng.com (accessed 5.8.17).

Charles, R., Crawford, P.B., 1975. Factors Affecting Solution Gas Drive Recovery, in: Annual Technical Meeting. https://doi-org.qe2a-proxy.mun.ca/10.2118/75-14

Chau, T.T., 2009. A review of techniques for measurement of contact angles and their applicability on mineral surfaces. Miner. Eng. 22, 213–219. https://doi.org/10.1016/j.mineng.2008.07.009

Cheng, B.K., Naccarato, B., Kim, K.J., Kumar, A., 2016. Theoretical consideration of contact angle hysteresis using surface-energy-minimization methods. Int. J. Heat Mass Transf. 102, 154–161. https://doi.org/10.1016/j.ijheatmasstransfer.2016.06.014

Chierici, G., 1984. Novel Relations for Drainage and Imbibition Relative Permeabilities. Soc. Pet. Eng. J. 24, 275–276. https://doi.org/10.2118/10165-PA

Christensen, J.R., Stenby, E.H., Skauge, A., 1998. Compositional and Relative Permeability Hysteresis Effects on Near-Miscible WAG. SPE/DOE Improv. Oil Recover. Symp. https://doi.org/10.2118/39627-MS

Civan, F., 2017. Phenomenological Correlation of Pressurization/Depressurization Hysteresis of Stress-Dependent Porosity and Permeability of Shale Reservoirs, in: SPE Annual Technical Conference and Exhibition, 9-11 October, San Antonio, Texas, USA. Society of Petroleum Engineers. https://doi.org/10.2118/187041-MS

Civan, F., Tiab, D., 1989. Second Law Analysis of Petroleum Reservoirs for Optimized Performance, in: SPE Production Operations Symposium,. Society of Petroleum Engineers, Oklahoma City. https://doi.org/10.2118/18855-MS

Coleman, S., Wilde, H.D., Moore, T.W., 1930. Quantitative Effect of Gas-oil Ratios on Decline of Average Rock Pressure. Trans. AIME 86. https://doi.org//10.2118/930174-G

Colonna, J., Brissaud, F., Millet, J.L., 1972. Evolution of Capillarity and Relative Permeability Hysteresis. Soc. Pet. Eng. J. 12, 28–38. https://doi.org/10.2118/2941-PA

Corey, A.T., 1954. Interrelation of Gas and Oil Relative Permeabilities. Prod. Mon. 19, 38–41.

Craft, B., Hawkins, M., 1991. Applied Petroleum Reservoir Engineering. Prentice Hall.

crawford, f. w., and hoover, g. m., 1966. Flow of fluids through porous mediums. J. Geophys. Res. 71, 2911–2917. https://doi.org/10.1029/JZ071i012p02911

Cui, X., Bustin, A.M.M., Bustin, R.M., 2009. Measurements of gas permeability and diffusivity of tight reservoir rocks: Different approaches and their applications. Geofluids 9, 208–223. https://doi.org/10.1111/j.1468-8123.2009.00244.x

Cutler, J.M.., Rees, W.A., 1970. A Study of Water Coning in the Oil Creek Reservoir, North Antioch Field, Oklahoma. Soc. Pet. Eng. https://doi.org/10.2118/2814-MS

Dake, L.P., 1998. Fundamentals of Reservoir Engineering. Elsevier.

Daungthongsuk, W., Wongwises, S., 2007. A critical review of convective heat transfer of nanofluids. Renew. Sustain. Energy Rev. 11, 797–817. https://doi.org/10.1016/j.rser.2005.06.005

David, C., Wong, T.-F., Zhu, W., Zhang, J., 1994. Laboratory measurement of compaction-induced permeability change in porous rocks: Implications for the generation and maintenance of pore pressure excess in the crust. Pure Appl. Geophys. 143, 425–456. https://doi.org/10.1007/BF00874337

De Gennes, P.G., 1985. Wetting: statics and dynamics. Rev. Mod. Phys. 57, 827. https://doi.org/10.1103/RevModPhys.57.827

Delshad, M.., Lenhard, R.J.., Oostrom, M.., Pope, G.A., 2003. A Mixed-Wet Hysteretic Relative Permeability and Capillary Pressure Model for Reservoir Simulations. SPE Reserv. Eval. Eng. 6. https://doi.org/10.2118/86916-PA

Denoyelle, L.C., Lemonnier, P., 1987. Simulation of C02 Huff 'n' Puff Using Relative Permeability Hysteresis, in: The 62nd Annual Technical Conference and Exhibition of the Society of Petroleum Engineers Held.

Derjaguin, B.V., 1946. On the Dependence of the Contact Angle on the Microrelief or Roughness of a Wetted Solid Surface. J. Appl. Chemsitry 51.

Dernaika, M.R., Kalam, M.Z., Basioni, M., Dawoud, A., Skjæveland, S.M., 2011a. Hysteresis Effects in Capillary Pressure, Relative Permeability and Resistivity Index Of North Sea Chalk, in: The International Symposium of the Society of Core Analysts. pp. 1–12.

Dernaika, M.R., Kalam, M.Z., Basioni, M., Dawoud, A., Skjæveland, S.M., 2011b. Hysteresis of Capillary Pressure, Resistivity Index and Relative Permeability in Carbonate Rock Types. Int. Symp. Soc. Core Anal. 1–12.

Dettre, R.H., Johnson Jr, R.E., 1965. Contact Angle Hysteresis. IV. Contact Angle Measurements on Heterogeneous Surfaces. J. Phys. Chem. 69, 1507–1515. https://doi.org/10.1021/j100889a012

Dixit, A., McDougall, S., Sorbie, K., 1997. A pore-level investigation of relative permeability hysteresis in water-wet systems. SPE Int. Symp. … 115–123. https://doi.org/10.2118/37233-PA

Dong, J.-J., Hsu, J.-Y., Wu, W.-J., Shimamoto, T., Hung, J.-H., Yeh, E.-C., Wu, Y.-H., Sone, H., 2010. Stress-dependence of the permeability and porosity of sandstone and shale from TCDP Hole-A. Int. J. Rock Mech. Min. 47, 1141–1157. https://doi.org/10.1016/j.ijrmms.2010.06.019

Dullien, F.A.L., 1992. Porous Media: Fluid Transport and Pore Structure, 2ed Editio. ed. Elsevier Inc, NY/Boston, London, London. https://doi.org/10.1016/C2009-0-26184-8

Dumore, J.M., 1970. Development of Gas-Saturation During Solution-Gas Drive in an Oil Layer Below a Gas Cap. Soc. Pet. Eng. J. 10. https://doi.org//10.2118/2508-PA

Dumore, J.M., Schols, R.S., 1974. Drainage capillary-pressure functions and the influence of connate wate. Soc. Pet. Eng. https://doi.org/10.2118/4096-PA

Duruewuru, A.U., 1985. Thermodynamics Analysis of Transient Two Phase Flow In Oil And Gas Reservoirs. University of Oklahoma.

Eick, J.D., Good, R.J., Neumann, A.W., 1975. Thermodynamics of contact angles. II. Rough solid surfaces. J. Colloid Interface Sci. 53, 235–248. https://doi.org/10.1016/0021-9797(75)90010-7

Einstein, A., 1906. Eine neue Bestimmung der Moleküldimensionen. Ann. Phys. 324, 289–306. https://doi.org/10.1002/andp.19063240204

Elhaj, M., Barri, A., Hashan, M., Hossain, M.E., 2018a. State of the Art on Porosity and Permeability Hysteresis: Useful Techniques for Hydrocarbon Recovery. Society of Petroleum Engineers, SPE Kingdom of Saudi Arabia Annual Technical Symposium and Exhibition, 23-26 April, Dammam, Saudi Arabia. https://doi.org/10.2118/192409-MS

Elhaj, M., Hashan, M., Hossain, M.E., 2018b. A Critical Review and Future Trend on Relative Permeability Hysteresis, in: Society of Petroleum Engineers - SPE Trinidad and Tobago Section Energy Resources Conference 2018. https://doi.org/10.2118/191260-ms

Elhaj, M., Imtiaz, S.A., Naterer, G.F., Zendehboudi, S., 2020. Production Optimization of Hydrocarbon Reservoirs by Entropy Generation Minimization. J. Nat. Gas Sci. Eng. 83. https://doi.org/10.1016/j.jngse.2020.103538

Elhaj, M.A., Hossain, M.E., Imtiaz, S.A., Naterer, G.F., 2020. Hysteresis of Wettability in Porous Media: A Review. J. Pet. Explor. Prod. Technol. 10, 1897–1905. https://doi.org/10.1007/s13202-020-00872-x

Evans, E.T.., Geurrero, C.E., 1979. Theory and Application of Capillary Pressure, in: SPWLA 20th Annual Logging Symposium.

Evrenos, A.I., 1969. Numerical Simulation in Porous of Hysteretic Media Flow. SPE J.

Extrand, C.W., 2004. Contact angles and their hysteresis as a measure of liquid-solid adhesion. Langmuir 20, 4017–4021. https://doi.org/10.1021/la0354988

Extrand, C.W., 2003. Contact angles and hysteresis on surfaces with chemically heterogeneous islands. Langmuir 19, 3793–3796. https://doi.org/10.1021/la0268350

Extrand, C.W., 2002. Model for contact angles and hysteresis on rough and ultraphobic surfaces. Langmuir 18, 7991–7999. https://doi.org/10.1021/la025769z

Extrand, C.W., 1998. A Thermodynamic Model for Contact Angle Hysteresis. J. Colloid Interface Sci. 207, 11–19. https://doi.org/10.1006/jcis.1998.5743

Extrand, C.W., Kumagai, Y., 1997. An Experimental Study of Contact Angle Hysteresis. J. Colloid Interface Sci. 191, 378–383. https://doi.org/10.1006/jcis.1997.4935

Extrand, C.W., Kumagai, Y., 1995. Liquid drops on an inclined plane: the relation between contact angles, drop shape, and retentive force. J. Colloid Interface Sci. 170, 515–521. https://doi.org/10.1006/jcis.1995.1130

Fenrick, W.J., 1964. Simple Tangentometer. Rev. Sci. Instrum. 35, 1616. https://doi.org/10.1063/1.1719236

Forchheimer, P., 1901. Wasserbewegung Durch Boden. Z. Ver. Deutsch, Ing 45, 1782–1788.

Frankel, N.A., Acrivos, A., 1967. On the viscosity of a concentrate suspension of solid spheres. Chem. Eng. Sci. 22, 847–853. https://doi.org/10.1016/0009-2509(67)80149-0

Gaines, G.L., 1960. Some observations on monolayers of carbon-14 labeled stearic acid. J. Colloid Sci. 15, 321–339. https://doi.org/10.1016/0095-8522(60)90036-2

Gao, L., McCarthy, T.J., 2006. Contact angle hysteresis explained. Langmuir 22, 6234–6237. https://doi.org/10.1021/la060254j

Garg, S.K., Pritchett, J.W., 1977. Simulation Of Drive Mechanisms In Geopressured Reservoirs, in: The 18th U.S. Symposium on Rock Mechanics (USRMS).

Gaspars-Wieloch, H., 2019. Project Net Present Value Estimation Under Uncertainty. Cent. Eur. J. Oper. Res. 27, 179–197. https://doi.org/10.1007/s10100-017-0500-0

Giangaspero, G., Sciubba, E., 2013. Application of the Entropy Generation Minimization Method to a Solar Heat Exchanger: A Pseudo-Optimization Design Process Based on the Analysis of the Local Entropy Generation Maps. Energy 58, 52–65. https://doi.org/10.1016/j.energy.2013.01.069

Gibbs, W., 1948. The Collected Works. NY: Longmans, New York.

Good, R.J., 1952. A Thermodynamic Derivation of Wenzel's Modification of Young's Equation for Contact Angles; Together with a Theory of Hysteresis1. J. Am. Chem. Soc. 74, 5041–5042. https://doi.org/10.1021/ja01140a014

Good, R.J., Kotsidas, E.D., 1979. Contact angles on swollen polymers: the surface energy of crosslinked polystyrene. J. Adhes. 10. https://doi.org/10.1080/00218467908544608

Graham, A.L., 1981. On the viscosity of suspensions of solid spheres. Appl. Sci. Res. 37, 275–286. https://doi.org/10.1007/BF00951252

Gray, W.G., 1982. Derivation of Vertically Averaged Equations Describing Multiphase Flow in Porous Media. Water Resour. Res. 18, 1705–1712. https://doi.org/10.1029/WR018i006p01705

Greder, H.N.., Gallato, V.., Cordelier, P.., Laran, L.., Munoz, F.., D'Abrigeon, O., 1997. Forty Comparisons of Mercury Injection Data with Oil/Water Capillary Pressure Measurements by the Porous Plate Technique. Soc. Core Anal.

Green, D.P., Dick, J.R., Mcaloon, M., Burger, J., Balcom, B., 2008. Oil / Water Imbibition and Drainage Capillary Pressure Determined by MRI on a Wide Sampling of Rocks. Int. Symp. Soc. Core Anal. 1–12.

Habte, A.D., Onur, M., Saaid, I.M.B., 2015. Pressure transient behavior of immiscible water alternating gas (IWAG) injection well with and without relative permeability

hysteresis and capillary pressure effects. J. Pet. Sci. Eng. 127, 169–178. https://doi.org/10.1016/j.petrol.2015.01.025

Haines, W.B., 1930. Studies in the physical properties of soil. V. The hysteresis effect in capillary properties, and the modes of moisture distribution associated therewith. J. Agric. Sci. 20, 97–116. https://doi.org/10.1017/S002185960008864X

Hall, H.N., 1961. Analysis of Gravity Drainage. J. Pet. Technol. 13. https://doi.org//10.2118/1517-G-PA

Hamon, G., & Pellerin, F.M., 1997. Evidencing Capillary Pressure and Relative Permeability Trends for Reservoir Simulation, in: SPE Annual Technical Conference and Exhibition, 5-8 October, San Antonio, Texas. https://doi.org/10.2118/38898-MS

Hansen, R.S., Miotto, M., 1957. Relaxation phenomena and contact angle hysteresis. J. Am. Chem. Soc. 79, 1765–1765. https://doi.org/10.1021/ja01564a067

Hassler, G.L.., Brunner, E., 1945. Measurement of Capillary Pressures in Small Core Samples. Trans. AIME 160. https://doi.org/10.2118/945114-G

Hatsopoulos, G.N., Keenan, J.H., Butler, H.W., 1966. Principles of General Thermodynamics. J. Appl. Mech. 33, 479–480. https://doi.org/10.1115/1.3625109

Hawkins, M.F., 1956. A Note on the Skin Effect. J. Pet. Technol. 8. https://doi.org/10.2118/732-G

Heller, R., Vermylen, J., Zoback, M., 2014. Experimental investigation of matrix permeability of gas shales. Am. Assoc. Pet. Geol. Bull. 98, 975–995. https://doi.org/10.1306/09231313023

Herwig, H., Kock, F., 2007. Direct and Indirect Methods of Calculating Entropy Generation Rates in Turbulent Convective Heat Transfer Problems. Heat Mass Transf. 43, 207–215. https://doi.org/10.1007/s00231-006-0086-x

Hicks, A.L., Weber, A.G., Ledbetter, R.L., 1959. Computing Techniques for Water-Drive Reservoirs. J. Pet. Technol. 11. https://doi-org/10.2118/1122-G

Hirasakl, G.J., 1991. Wettability : Fundamentals and Surface Forces. SPE J. 6. https://doi.org/10.2118/17367-PA

Hirasawa, S., Tsubota, R., Kawanami, T., Shirai, K., 2013. Reduction of Heat Loss From Solar Thermal Collector by Diminishing Natural Convection with High-Porosity Porous Medium. Sol. Energy 97, 305–313. https://doi.org/10.1016/j.solener.2013.08.035

Hoholick, J.D., Metarko, T., Potter, P.E., 1984. Regional variations of porosity and cement; St. Peter and Mount Simon sandstones in Illinois Basin. AAPG Bull. 68, 753–764.

Howell, J.R., Hall, M.J., Ellzey, J.L., 1996. Combustion of Hydrocarbon Fuels Within Porous Inert Media. Prog. Energy Combust. Sci. 22, 121–145. https://doi.org/10.1016/0360-1285(96)00001-9

Huh, C., Mason, S.G., 1977. Effects of surface roughness on wetting (theoretical). J. Colloid Interface Sci. 60, 11–38. https://doi.org/10.1016/0021-9797(77)90251-X

Hunter, R.J., 2001. Foundations of colloid science, 2nd ed. ed. Oxford University Press.

Ikoku, C., 1984. Natural Gas Production Engineering. John Wiley & Sons, New York, New Y or.

Institute, A.P., 1998. Recommended Practices for Core Analysis Section 1- Planning a Coring Program. API Recomm. Pract. 40.

Ivakhnenko, O.P., Potter, D.K., 2008. The Use of Magnetic Hysteresis And Remanence Measurements For Rapidly And Non-Destructively Characterizing Reservoir Rocks And Fluids. Petrophysics 49, 47–56.

Ivakhnenko, O.P., Potter, D.K., 2004. Magnetic susceptibility of petroleum reservoir fluids. Phys. Chem. Earth, Parts A/B/C 29, 899–907. https://doi.org/10.1016/j.pce.2004.06.001

Johnson Jr, R.E., Dettre, R.H., 1966. The Wettability of Low-Energy Liquid Surfaces. J. Colloid Interface Sci. 21, 610–622. https://doi.org/10.1016/0095-8522(66)90021-3

Johnson Jr, R.E., Dettre, R.H., 1964. Contact Angle Hysteresis. III. Study of an Idealized Heterogeneous Surface. J. Phys. Chem. 68, 1744–1750. https://doi.org/10.1021/j100789a012

Johnson Jr, R.E., Dettre, R.H., Brandreth, D.A., 1977. Dynamic contact angles and contact angle hysteresis. J. Colloid Interface Sci. 62, 205–212. https://doi.org/10.1016/0021-9797(77)90114-X

Johnson, K.A., Shah, D.O., 1985. Effect of oil chain length and electrolytes on water solubilization in alcohol-free pharmaceutical microemulsions. J. Colloid Interface Sci. 107, 269–271. https://doi.org/10.1016/0021-9797(85)90172-9

Jones, F.O., Owens, W.W., 1980. A Laboratory Study of Low-Permeability Gas Sands. J. Pet. Technol. 32. https://doi.org/10.2118/7551-PA

Jr., R. a., Ertekin, T., Stahl, C.D., 1985. Effect of Capillary Number and Its Constituents on Two-Phase Relative Permeability Curves. J. Pet. Technol. 37, 249–260. https://doi.org/10.2118/12170-PA

Kadet, V. V., Galechyan, A.M., 2014. Percolation modeling of relative permeability hysteresis. J. Pet. Sci. Eng. 119, 139–148. https://doi.org/10.1016/j.petrol.2014.05.001

Kantzas, A., Nikakhtar, B., Pow, M., 1998. Principles of three phase capillary pressures. J. Can. Pet. Technol. 37, 48–54. https://doi.org/10.2118/98-07-05

Keelan, D.K., Pugh, V.J., 1975. Trapped-Gas Saturations in Carbonate Formations. Soc. Pet. Eng. 149–160. https://doi.org/doi:10.2118/4535-PA

Khan, N.B.N., Barifcani, A., Tade, M., Pareek, V., 2016. A Case Study: Application of Energy and Exergy Analysis for Enhancing the Process Efficiency of a Three Stage

Propane Pre-Cooling Cycle of the Cascade LNG Process. J. Nat. Gas Sci. Eng. 29, 125–133. https://doi.org/10.1016/j.jngse.2015.12.034

Killough, J.E., 1976. Reservoir Simulation With History-Dependent Saturation Functions. Soc. Pet. Eng. J. 16, 37–48. https://doi.org/10.2118/5106-PA

Kleppe, J., Delaplace, P., Lenormand, R., Hamon, G., Chaput, E., 1997. Representation of Capillary Pressure Hysteresis in Reservoir Simulation. Proc. SPE Annu. Meet. https://doi.org/10.2118/38899-MS

Kocamustafaogullari, G., 1971. Thermo-Fluid Dynamics of Separated Two-Phase Flow. Georgia Institure of Technology.

Kokkedee, J.., Boutkan, V., 1995. Towards measurement of capillary pressure and relative permeability at representative wettability. Geol. Soc. Spec. Publ. 84, 43–50. https://doi.org/10.1144/GSL.SP.1995.084.01.05

Kool, J.B., Parker, C.J., 1987. Development and evaluation of closed-form expressions for hysteretic soil hydraulic properties. Water Resour. Res. 23, 105–114.

Kossack, C. a, 2000. Comparison of Reservoir Simulation Hysteresis Options. SPE Annu. Tech. Conf. Exhib. https://doi.org/10.2118/63147-ms

Kranzz, R.L., Frankel, A.D., Engelder, T., Scholz, C.H., 1979. The permeability of whole and jointed Barre Granite. Int. J. Rock Mech. Min. Sci. 16, 225–234. https://doi.org/10.1016/0148-9062(79)91197-5

Krasovitski, B., Marmur, A., 2005. Drops Down the Hill: Theoretical Study of Limiting Contact Angles and the Hysteresis Range on a Tilted Plate. Langmuir 21, 3881–3885. https://doi.org/10.1021/la0474565

Kulchanyavivat, S., 2005. The Effective Approach for Predicting Viscosity of Saturated And Under-saturated Reservoir Oil. Texas A&M University.

Kwok, D.Y., Budziak, C.J., Neumann, A.W., 1995. Measurements of static and low rate dynamic contact angles by means of an automated capillary rise technique. J. Colloid Interface Sci. 173, 143–150. https://doi.org/10.1006/jcis.1995.1307

Kwok, D.Y., Lin, R., Mui, M., Neumann, A.W., 1996. Low-rate dynamic and static contact angles and the determination of solid surface tensions. Colloids Surfaces A Physicochem. Eng. Asp. 116, 63–77. https://doi.org/10.1016/0927-7757(96)03590-X

Land, C.S., 1968. Calculation of Imbibition Relative Permeability for Two- and Three-Phase Flow From Rock Properties. Soc. Pet. Eng. J. 8, 149–156. https://doi.org/10.2118/1942-PA

Langmuir, I., 1938. Overturning and anchoring of monolayers. Science (80-.). 87, 493–500.

Langmuir, I., Schaefer, V.J., 1937. The Effect of Dissolved Salts on Insoluble Monolayers. J. Am. Chem. Soc. 59, 2400–2414. https://doi.org/10.1021/ja01290a091

Larachi, F., Cassanello, M., Laurent, A., 1998. Gas−Liquid Interfacial Mass Transfer in Trickle-Bed Reactors at Elevated Pressures. Ind. Eng. Chem. Res. 37, 718–733.

https://doi.org/10.1021/ie960903u

Lee, J., Wattenbarger, R.A., 1996. Gas Reservoir Engineering.

Leja, J., Poling, G.W., 1960. On the interpretation of contact angle. Proc. 5th Miner. Process. Congr. (IMM, London) 325.

Lenhard, R.J., 1992. Measurement and modeling of three-phase saturation-pressure hysteresis. J. Contam. Hydrol. 9, 243–269. https://doi.org/10.1016/0169-7722(92)90007-2

Lenhard, R.J., Oostrom, M., 1998. A Parametric Model for Predicting Relative Permeability-Saturation-Capillary Pressure Relationships of Oil–Water Systems in Porous Media with Mixed Wettability. Transp. Porous Media 31, 109–131. https://doi.org/10.1023/A:100650340

Lenhard, R.J., Parker, J.C., Kaluarachchi, J.J., 1989. A Model for Hysteretic Constitutive Relations Governing Multiphase Flow 3. Refinements and Numerical Simulations. Water Resour. Res. 25, 1727–36.

Lerk, C.F., Lagas, M., Boelstra, J.P., Broersma, P., 1977. Contact angles of pharmaceutical powders. J. Pharm. Sci. 66, 1480–1481. https://doi.org/10.1002/jps.2600661034

Lester, G.R., 1961. Contact angles of liquids at deformable solid surfaces. J. Colloid Sci. 16, 315–326. https://doi.org/10.1016/0095-8522(61)90032-0

Letellier, P., Mayaffre, A., Turmine, M., 2007. Drop size effect on contact angle explained by nonextensive thermodynamics. Young's equation revisited. J. Colloid Interface

Sci. 314, 604–614. https://doi.org/10.1016/j.jcis.2007.05.085

Leverett, M.C., 1941. Capillary behavior in porous solids. Trans. AIME 152–169. https://doi.org/10.2118/941152-G

Li, D., Wang, H., Qin, Y., Han, L., Wei, X., Qin, D., 2017. Entropy Production Analysis of Hysteresis Characteristic of a Pump-Turbine Model. Energy Convers. Manag. 149, 175–191. https://doi.org/10.1016/j.enconman.2017.07.024

Lin, Y.-W., Chang, K.-H., Chen, C.-K., 2017. A Modified Differential Transform Method (DTM) for Analyzing Irreversibility of Heat Transfer in Flow Through a Moving Plate with Variable Temperature. Commun. Theor. Phys. 68, 647. https://doi.org/10.1088/0253-6102/68/5/647

Lindeloff, N., Pedersen, K.S., Ronningsen, H.P., Milter, J., 2004. The Corresponding States Viscosity Model Applied to Heavy Oil Systems. J. Can. Pet. Technol. 43. https://doi.org/10.2118/04-09-04

Longeron, D.G.., Argaud, M.J.., Bouvier, L., 1989a. Resistivity Index and Capillary Pressure Measurements Under Reservoir Conditions Using Crude Oil, in: SPE Annual Technical Conference and Exhibition, 8-11 October, San Antonio, Texas. Society of Petroleum Engineers. https://doi.org/10.2118/SPE-19589-MS

Longeron, D.G.., Argaud, M.J.., Feraud, J.-P., 1989b. Effect of Overburden Pressure and the Nature and Microscopic Distribution of Fluids on Electrical Properties of Rock Samples. Soc. Pet. Eng. 4. https://doi.org/10.2118/15383-PA

Luffel, D.L., Guidry, F.K., 1992. New Core Analysis Methods for Measuring Reservoir Rock Properties of Devonian Shale. SPE Annu. Tech. Conf. Exhib. 1184–1190. https://doi.org/10.2118/20571-PA

Luffel, D.L., Hopkins, C.W., Schettler Jr., P.D., 1993. Matrix Permeability Measurement of Gas Productive Shales. 68th Annu. Tech. Conf. Exhib. 261–266. https://doi.org/10.2523/26633-MS

Lund, A., Dyke, S.J., Song, W., Bilionis, I., 2019. Global Sensitivity Analysis for The Design of Nonlinear Identification Experiments. Nonlinear Dyn. 98. https://doi.org/10.1007/s11071-019-05199-9

Lundgren, T.S., 1972. Slow flow through stationary random beds and suspensions of spheres. J. Fluid Mech. 51, 273–299. https://doi.org/10.1017/S002211207200120X

Lv, Q., Liu, X., Wang, E., Wang, S., 2013. Analytical Solution to Predicting Gaseous Mass Flow Rates of Microchannels in a Wide Range of Knudsen Numbers. Phys. Rev. E 88. https://doi.org/10.1103/PhysRevE.88.013007

Macdougall, G., Ockrent, C., 1942. Surface energy relations in liquid/solid systems. I. The adhesion of liquids to solids and a new method of determining the surface tension of liquids. Proc. R. Soc. London A Math. Phys. Eng. Sci. 180, 151–173. https://doi.org/10.1098/rspa.1942.0031

Mahdavi, M., Saffar-Avval, M., Tiari, S., Mansoori, Z., 2014. Entropy Generation and Heat Transfer Numerical Analysis in Pipes Partially Filled with Porous Medium. Int. J.

Heat Mass Transf. 79, 496–506. https://doi.org/10.1016/j.ijheatmasstransfer.2014.08.037

Mahmoodi, M., Rezaei, N., Zendehboudi, S., Heagle, D., 2020. Fluid Dynamic Modeling of Multiphase Flow in Heterogeneous Porous Media with Matrix, Fracture, and Skin. J. hyroglogy 583. https://doi.org/10.1016/j.jhydrol.2019.124510

Maïga, S.E.B., Nguyen, C.T., Galanis, N., Roy, G., Maré, T., Coqueux, M., 2006. Heat transfer enhancement in turbulent tube flow using Al2O3 nanoparticle suspension. Int. J. Numer. Methods Heat Fluid Flow 16, 275–292. https://doi.org/10.1108/09615530610649717

Maiti, R., Atta, A., Nigam, K., 2008. Effect of particle porosity on hysteresis in trickle-bed reactors. Ind. Eng. Chem. Res. 47, 8126–8135. https://doi.org/10.1021/ie8003539

Maiti, R.N., Nigam, K.D.P., 2007. Gas−Liquid Distributors for Trickle-Bed Reactors: A Review. Ind. Eng. Chem. Res. 46, 6164–6182. https://doi.org/10.1021/ie070255m

Marmur, A., 1994. Contact Angle Hysteresis on Heterogeneous Smooth Surfaces. J. Colloid Interface Sci. 168, 40–46. https://doi.org/10.1006/jcis.1994.1391

Masalmeh, S.K., 2001. Experimental Measurements of Capillary Pressure and Relative Permeability Hysteresis. Pap. SCA 23, 17–19.

McCullough, J.J.., Albaugh, F.W.., Jones, P.H., 1944. Determination Of The Interstitial-Water Content Of Oil And Gas Sand By Laboratory Tests Of Core Samples. Am. Pet. Inst. 180.

Melrose, J.C.., Brander, C.F., 1974. Role of Capillary Forces in Determining Microscopic Discplacement Effeciency for Oil Recovery by Water Flooding. Can. Pet. Technol. 13. https://doi.org/10.2118/74-04-05

Melrose, J.C., 1990. Valid Capillary Pressure Data at Low Wetting-Phase Saturations. SPE Reserv. Eng. 5. https://doi.org/10.2118/18331-PA

Melrose, J.C., 1965. Wettability as Related to Capillary Action in Porous Media. Soc. Pet. Eng. J. 5. https://doi.org/10.2118/1085-PA

Mewis, J., Wagner, N.J., 2009. Thixotropy. Adv. Colloid Interface Sci. 147–148, 214–227. https://doi.org/10.1016/j.cis.2008.09.005

Mian, M.A., 2011. Project Economics and Decision Analysis: Deterministic models, 2nd Revise. ed. PennWell Books.

Michaels, A.S., Lummis, R.C., 1959. Contact Angle Hysteresis on Aquagels, in: AIChE/SPE Joint Symposium on Wetting and Capillarity in Fluid Displacement Processes, 17-20 May, Kansas City, Missouri, USA. https://doi.org/10.2118/1274-G

Miller, C., 1979. Numerical Model of Transient Two-Phase Flow in a Wellbore. California.

Miller, Christakos, G., Imhoff, P.T., McBride, J.F., Pedit, J.A., Trangenstein, J.A., 1998. Multiphase Flow and Transport Modeling in Heterogeneous Porous Media: Challenges and Approaches. Adv. Water Resour. 21, 77–120. https://doi.org/10.1016/S0309-1708(96)00036-X

Monnery, W.D., Svrcek, W.Y., Mehrotra, A.K., 1995. Viscosity: A critical review of practical predictive and correlative methods. Can. J. Chem. Eng. 73, 3–40. https://doi.org/10.1002/cjce.5450730103

Moore, T.F.., Slobod, R.L., 1956. The Effect of Viscosity and Capillarity on the Displacement of Oil by Water. Prod. Mon. 20–30.

Morita, N., Gray, K.E., Sroujl, F., Jogi, P.N., 1992. Rock-Property Changes During Reservoir Compaction. SPE Form. Eval. 7, 197–205. https://doi.org/10.2118/13099-PA

Morrow, N.R., 1990. Wettability and Its Effect on Oil Recovery. J. Pet. Technol. 42. https://doi.org/10.2118/21621-PA

Morrow, N.R., 1970. Physics and Thermodynamics of Capillary Action in Porous Media. Ind. Eng. Chem. 62, 32–56. https://doi.org/10.1021/ie50726a006

Murshed, S.M.S., Estellé, P., 2017. A state of the art review on viscosity of nanofluids. Renew. Sustain. Energy Rev. 76, 1134–1152. https://doi.org/10.1016/j.rser.2017.03.113

Murshed, S.M.S., Leong, K.C., Yang, C., 2008. Thermophysical and electrokinetic properties of nanofluids – A critical review. Appl. Therm. Eng. 28, 2109–2125. https://doi.org/10.1016/j.applthermaleng.2008.01.005

Naterer, G.F., 2018. Advanced Heat Transfe. CRC Press, Boca Raton.

Naterer, G.F., Camberos, J.A., 2008. Entropy Based Design and Analysis of Fluids Engineering Systems. CRC Press. Inc. Boca Raton, Boca Raton. https://doi.org/10.1201/9781420006919

Natural Resources Canada, 2019. Energy Fact Book. Ottawa.

Nelson, R.A., Handin, J., 1977. An Experimental Study of Fracture Permeability in Porous Rock. Am. Assoc. Pet. Geol. Bull. 61, 227–236.

Neumann, A.W., 1964. Über die Meßmethodik zur Bestimmung grenzflächenenergetischer Größen. Zeitschrift für Phys. Chemie 41, 339–352. https://doi.org/10.1524/zpch.1964.41.5_6.339

Neumann, A.W., Good, R.J., 1972. Thermodynamics of contact angles. I. Heterogeneous solid surfaces. J. Colloid Interface Sci. 38, 341–358. https://doi.org/10.1016/0021-9797(72)90251-2

Nguyen, C.T., Desgranges, F., Galanis, N., Roy, G., Mar??, T., Boucher, S., Angue Mintsa, H., 2008. Viscosity data for Al2O3-water nanofluid-hysteresis: is heat transfer enhancement using nanofluids reliable? Int. J. Therm. Sci. 47, 103–111. https://doi.org/10.1016/j.ijthermalsci.2007.01.033

Nguyen, C.T., Desgranges, F., Roy, G., Galanis, N., Maré, T., Boucher, S., Angue Mintsa, H., 2007. Temperature and particle-size dependent viscosity data for water-based nanofluids - Hysteresis phenomenon. Int. J. Heat Fluid Flow 28, 1492–1506. https://doi.org/10.1016/j.ijheatfluidflow.2007.02.004

Nield, D.A., 2007. The Modeling of Viscous Dissipation in a Saturated Porous Medium. J. Heat Transfer 129, 1459–1463. https://doi.org/10.1115/1.2755069

Nigam;, A.K.K.D.P., Duquenne;, A.M., Delmas, H., 2011. RECENT DEVELOPMENTS ON HYDROPROCESSING REACTORS. Rev. Chem. Eng. 19, 531– 603. https://doi.org/10.1515/REVCE.2003.19.6.531

Nooruddin, H.A., Hossain, M.E., Al-Yousef, H., Okasha, T., 2014. Comparison of permeability models using mercury injection capillary pressure data on carbonate rock samples. J. Pet. Sci. Eng. 121, 9–22. https://doi.org/10.1016/j.petrol.2014.06.032

Odukoya, A., Naterer, G.F., Dincer, 2011. Entropy Generation of Droplet Motion with Surface Tension Hysteresis in a Closed Microchannel. J. Micromechanics Microengineering 21. https://doi.org/10.1088/0960-1317/21/9/095022

Ogolo, N.A., Isebor, J.O., Onyekonwu, M.O., 2014. Feasibility Study of Improved Gas Recovery by Water Influx Control in Water Drive Gas Reservoirs, in: SPE Nigeria Annual International Conference and Exhibition. https://doi.org/10.2118/172364-MS

Ogulata, R.T., Doba, F., 1998. Experiments and Entropy Generation Minimization Analysis of a Cross-Flow Heat Exchanger. Int. J. Heat Mass Transf. 41, 373–381. https://doi.org/10.1016/S0017-9310(97)00129-4

Omoregle, Z., 1988. Factors Affecting the Equivalency of Different Capillary Pressure Measurement Techniques. SPE Form. Eval. 3, 147–155.

Öpik, U., 2000. Contact-Angle Hysteresis Caused by a Random Distribution of Weak Heterogeneities on a Solid Surface. J. Colloid Interface Sci. 223, 143–166. https://doi.org/10.1006/jcis.1999.6637

Parker, J.C., Lenhard, R.J., 1987a. A Model for Hysteretic Constitutive Relations Governing Multiphase Flow 1. Saturation-Pressure Relations. Water Resour. Res. 23, 2187–2196.

Parker, J.C., Lenhard, R.J., 1987b. A parametric model for constitutive properties governing multiphase flow in porous media. Water Resour. Res. 23, 618–624.

Parvazdavani, M., Masihi, M., Ghazanfari, M.H., 2014. Monitoring the influence of dispersed nano-particles on oil-water relative permeability hysteresis. J. Pet. Sci. Eng. 124, 222–231. https://doi.org/10.1016/j.petrol.2014.10.005

Pashakolaie, V.G., Khaleghi, S., Mohammadi, T., Khorsandi, M., 2015. Oil production cost function and oil recovery implementation- Evidence from an Iranian oil field. Energy Explor. Exploit. 33, 459–470. https://doi.org/10.1260/0144-5987.33.4.459

Pease, D.C., 1945. The Significance of the Contact Angle in Relation to the Solid Surface. J. Phys. Chem. 49, 107–110. https://doi.org/10.1021/j150440a007

Phillips, M.C., Riddiford, A.C., 1972. Dynamic contact angles. II. Velocity and relaxation effects for various liquids. J. Colloid Interface Sci. 41, 77–85. https://doi.org/10.1016/0021-9797(72)90088-4

Pickell, J.J.., Swanson, B.F.., Hickman, W.B., 1966. Application of Air-Mercury and Oil-Air Capillary Pressure Data In the Study of Pore Structure and Fluid Distribution. Soc. Pet. Eng. 6, 55–61. https://doi.org/doi:10.2118/1227-PA

Pierce, E., Carmona, F.J., Amirfazli, A., 2008. Understanding of sliding and contact angle results in tilted plate experiments. Colloids Surfaces A Physicochem. Eng. Asp. 323, 73–82. https://doi.org/10.1016/j.colsurfa.2007.09.032

Pooladi-Darvish, M., Firoozabadi, A., 1999. Solution-gas Drive In Heavy Oil Reservoirs. J. Can. Pet. Technol. 38. https://doi-org./10.2118/99-04-06

Potter, D.K., 2007. Magnetic Susceptibility As a Rapid, Nondestructive Technique For Improved Petrophysical Parameter Prediction1. Petrophysics 48, 191–201.

Potter, D.K., Alghamdi, T.M., Ivakhnenko, O.P., 2008. Sensitive Carbonate Reservoir Rock Characterisation From Magnetic Susceptibility : Mineral Quantification , Correlation With Petrophysical Properties , and Anisotropy. Middle East 52, 1–12.

Preisach, F., 1935. Über die magnetische Nachwirkung. Z. Phys. 94. https://doi.org/10.1007/BF01349418

Profice, S., Lasseux, D., Jannot, Y., 2011. Permeability, porosity and Klinkenberg coefficient determination on crushed porous media. Soc. Core … 53, 1–12.

Pucknell, J.K., Clifford, P.J., 1991. Calculation of Total Skin Factors, in: Offshore Europe, Aberdeen, United Kingdom. Society of Petroleum Engineers, Aberdeen, United Kingdom. https://doi.org/10.2118/23100-MS

Purcell, W.R., 1950. Interpretation of Capillary Pressure Data. J. Pet. Technol. 2, 369–371. https://doi.org/10.2118/950369-G

Purcell, W.R., 1949. Capillary Pressures - Their Measurement Using Mercury and the Calculation of Permeability Therefrom. Soc. Pet. Eng. 39–48. https://doi.org/10.2118/949039-G

Puthenveettil, B.A., Senthilkumar, V.K., Hopfinger, E.J., 2013. Motion of Drops on Inclined Surfaces in The Inertial Regime. J. Fluid Mech. 726, 26–61. https://doi:10.1017/jfm.2013.209

Quiñones-Cisneros, S., 2000. The friction theory (f-theory) for viscosity modeling. Fluid Phase … 169, 249–276. https://doi.org/10.1016/S0378-3812(00)00310-1

Ralston, J., Newcombe, G., 1992. Static and Dynamic Contact Angles, in: Colloid Chemistry in Mineral Processing. ELSEVIER SCIENCE PUBLISHERS B.V, p. 173.

Rohmer, J., Loschetter, A., Raucoules, D., 2017. Global Sensitivity Analysis for Supporting History Matching of Geomechanical Reservoir Models Using Satellite InSAR Data: A Case Study at the CO2 Storage Site of In Salah, Algeria, in: Sensitivity Analysis in Earth Observation Modelling. pp. 145–159. https://doi.org/10.1016/B978-0-12-803011-0.00008-2

Rose, W.., Bruce, W.A., 1949. Evaluation Of Capillary Character In Petroleum Reservoir Rock. J. Pet. Technol. 1. https://doi.org/10.2118/949127-G

Ruch, R.J., Bartell, L.S., 1960. Wetting of Solids by Solutions as a Function of Solute Adsirption, 2. J. Phys. Chem. 64, 513–519. https://doi.org/10.1021/j100834a001

Sabatier, L., 1994. Comparative Study of Drainage Capillary Pressure Measurements Using Different Techniques and For Different Fluid Systems. Soc. Core Anal.

Sage, B.H., Lacey, W.N., 1935. Energy Relations in a Flowing Well, in: Drilling and Production Practice. American Petroleum Institute.

Saidur, R., Leong, K.Y., Mohammad, H.A., 2011. A review on applications and challenges of nanofluids. Renew. Sustain. Energy Rev. 15, 1646–1668. https://doi.org/10.1016/j.rser.2010.11.035

Salim, A., Sausse, J., Pironon, J., Fourar, M., Veslud, C.L.C. de, 2008. 3D Confocal Scanning Laser Microscopy to Quantify Contact Angles in Natural Oil-Water Mixtures. Oil Gas Sci. Technol. 63, 645–655. https://doi.org/10.2516/ogst:2008011

Salter, G.R.J.J., 1990. The effect of pore-structure on hysteresis in relative permeability and capillary pressure: Pore-level modeling. Transp. Porous Media 5, 103–151. https://doi.org/10.1007/BF00144600

San, J.Y., Worek, W.M., Lavan, Z., 1985. Entropy Generation in Convective Heat Transfer and Isothermal Convective Mass Transfer. J. Heat Transfer 109, 647–652. https://doi.org/doi:10.1115/1.3248137

Sangi, R., Müller, D., 2019. Application of the Second Law of Thermodynamics to Control: A review. Energy 174, 938–953. https://doi.org/10.1016/j.energy.2019.03.024

Santos, I.C.V.M., Oliveira, P.F., Mansur, C.R.E., 2017. Factors That Affect Crude Oil Viscosity and Techniques To Reduce It: A Review. BRAZILIAN J. Pet. GAS 11, 115–130.

Santoso, R., Hoteit, H., Vahrenkamp, V., 2019. Optimization of Energy Recovery from Geothermal Reservoirs Undergoing Re-Injection: Conceptual Application in Saudi Arabia, in: SPE Middle East Oil and Gas Show and Conference. Society of Petroleum Engineers. https://doi.org/10.2118/195155-MS

Sarathi, P.S., Tiab, D., 1981. Effects of Production Rate on The In Situ Energy Utilization of Dry and Condensate Gas Reservoirs, in: Middle East Technical Conference and Exhibition,. Society of Petroleum Engineers, Bahrain. https://doi.org/10.2118/9642-MS

Schilthuis, R.J., 1936. Active Oil and Reservoir Energy. Trans. AIME 118. https://doi.org/10.2118/936033-G

Schwartz, A.M., Minor, F.W., 1959. A simplified thermodynamic approach to capillarity: I. Application to flow in capillary channels. J. Colloid Sci. 14, 572–583. https://doi.org/10.1016/0095-8522(59)90024-8

Sciacovelli, A., Verda, V., Sciubba, E., 2015. Entropy Generation Analysis as a Design Tool—A Review. Renew. Sustain. Energy Rev. 43, 1167–1181. https://doi.org/10.1016/j.rser.2014.11.104

Selvadurai, A.P.S., 2015. Normal stress-induced permeability hysteresis of a fracture in a granite cylinder. Geofluids 15, 37–47. https://doi.org/10.1111/gfl.12107

Shi, Y., Wang, C., 1986. Pore pressure generation in sedimentary basins: Overloading versus aquathermal. J. Geophys. Res. 91, 2153–2162. https://doi.org/10.1029/JB091iB02p02153

Shimokawa, M., Takamura, T., 1973. Relation between interfacial tension and capillary liquid rise on polished metal electrodes. J. Electroanal. Chem. Interfacial Electrochem. 41, 359–366. https://doi.org/10.1016/S0022-0728(73)80414-0

Shuttleworth, R., Bailey, G.L.J., 1948. The spreading of a liquid over a rough solid. Discuss. Faraday Soc. 3, 16–22.

Sinha, S., Braun, E.M., Determan, M.D., Passey, Q.R., Leonardi, S.A., Boros, J.A., Wood III, A.C., Zirkle, T., Kudva, R.A., 2013. Steady-state permeability measurements on intact shale samples at reservoir conditions - Effect of stress, temperature, pressure, and type of gas. SPE Middle East Oil Gas Show Conf. March 10-13 SPE 164263. https://doi.org/10.2118/164263-MS

Slattery, J.C., 1972. Momentum, Energy, and Mass Transfer in Continua. McGraw-Hill Book Co., New York. https://doi.org/10.1002/aic.690180446

Spelt, J.K., Absolom, D.R., Neumann, A.W., 1986. olid surface tension: The interpretation of contact angles by the equation of state approach and the theory of surface tension components. Langmuir 2, 620–625. https://doi.org/10.1021/la00071a017

Spiteri, E.J., Juanes R., B.M.J., Orr Jr., F.M., 2005. Relative-Permeability Hysteresis: Trapping Models and Application to Geological CO2 Sequestration. SPE Annu. Tech. Conf. Exhib. Dallas. https://doi.org/10.2118/96448-MS

Stegemeier, G.L., 1977. Mechanisms of Entrapment and Mobilization Of Oil In Porous Media. Improv. Oil Recover. by Surfactant Polym. Flooding 55–91. https://doi.org/10.1016/B978-0-12-641750-0.50007-4

Stegemeier, G.L., 1974. Relationship of Trapped Oil Saturation to petrophysical Properties of Porous Media. Soc. Pet. Eng. https://doi.org/10.2118/4754-MS

Stodola, A., 1898. Die kreisprozesse der gasmaschine (Gas engine Cycles). Zeistschrift der 23, 1089–1091.

Sun, P.J., Wu, J.Y., Zhang, P., Xu, L., Jiang, M.L., 2009. Experimental Study of the Influences of Degraded Vacuum on Multilayer Insulation Blankets. Cryogenics (Guildf). 49, 719–726. https://doi.org/10.1016/j.cryogenics.2009.09.003

Sutton, R.P., Farshad, F., 1990. Evaluation of Empirically Derived PVT Properties for Gulf of Mexico Crude Oils. SPE J. 5. https://doi.org/10.2118/13172-PA

Swanson, B.F., 1985. Microporosity In Reservoir Rocks - Its Measurement And Influence On Electrical Resistivity, in: SPWLA 26th Annual Logging Symposium, 17-20 June. Society of Petrophysicists and Well-Log Analysts, Dallas, Texas.

Szabo, M.T., 1974. New Methods for Measuring Imbibition Capillary Pressure and Electrical Resistivity Curves by Centrifuge. Soc. Pet. Eng. 243252. https://doi.org/10.2118/3038-PA

Taggart, A.F., Taylor, T.C., Ince, C.R., 1930. Experiments with flotation reagents. Trans. Am. Inst. Min. Metall. Eng. 87, 285–386.

Talsma, T., 1970. Hysteresis in two sands and the independent domain model. Water Resour. Res. 6, 964–970. https://doi.org/10.1029/WR006i003p00964

Tan, T., 1990. Representation Of Hysteresis In Capillary Pressure For Reservoir Simulation Models. Pet. Soc. Canada 29. https://doi.org/10.2118/90-04-07

Taylor, R., Coulombe, S., Otanicar, T., Phelan, P., Gunawan, A., Lv, W., Rosengarten, G., Prasher, R., Tyagi, H., 2013. Small particles, big impacts: A review of the diverse applications of nanofluids. J. Appl. Phys. 113. https://doi.org/10.1063/1.4754271

Teklu, T., Li, X., Zhou, Z., Cui, Q., Abass, H., 2016a. Fracture and Matrix Permeability Hysteresis in Organic Rich Mudrocks. Unconv. Resour. Technol. Conf. https://doi.org/10.15530-urtec-2016-2431080

Teklu, T., Zhou, Z., Li, X., Abass, H., 2016b. Experimental Investigation on Permeability and Porosity Hysteresis in Low-Permeability Formations, in: The SPE Low Perm

Symposium Held in Denver, Colorado, USA,. https://doi.org/10.2118/180226-MS

Teklu, T., Zhou, Z., Li, X., Abass, H., 2016c. Cyclic Permeability and Porosity Hysteresis in Mudrocks – Experimental Study. 50th US Rock Mech. / Geomech. Symp. 1–12.

Thornton, O.F.., Marshall, D.L., 1947. Estimating Interstitial Water by the Capillary Pressure Method. Trans. AIME 170. https://doi.org/10.2118/947069-G

Tiab, D., Duruewuru, A.U., 1988. Thermodynamic Analysis of Transient Two-Phase Flow in Petroleum Reservoirs. SPE Prod. Eng. 3, 495–507. https://doi.org/10.2118/16203-PA

Tiab, D., Sarathie, S.P., Chichlow, H.., 1980. Thermodynamic Analysis of Gas Reservoirs, in: ASME Proceedings, Energy Tech. Conf. and Exhibition. The American Society of Mechanical Engineering, New Orleans, LA.

Tillero, E., Machado, F.T.F., Romero, D., 2011. From Volumetric Energy Balance to the Entropy Generation: The Evolution of the State of the Art in Thermodynamic Concepts in Petroleum Production Systems, in: SPE Production and Operations Symposium, 27-29 March, Oklahoma City, Oklahoma, USA. https://doi-org.qe2a-proxy.mun.ca/10.2118/139913-MS

Tillero, E., Mogollon, J.L., 2020. Unified Oil and Water Fractional-Flow Functions: Improving Waterflood Performance Analytical Modeling Technique, in: The SPE Latin American and Caribbean Petroleum Engineering Conference. https://doi.org//10.2118/199055-MS

Timmons, C.O., Zisman, W.A., 1966. The effect of liquid structure on contact angle hysteresis. J. Colloid Interface Sci. 22, 165–171. https://doi.org/10.1016/0021-9797(66)90080-4

Tinni, A., Fathi, E., Agarwal, R., Sondergeld, C., Akkutlu, Y., Rai, C., 2012. Shale permeability measurements on plugs and crushed samples. SPE Can. … 1–14. https://doi.org/10.2118/162235-MS

Tiss, M., Evans, R.D., 1989. Measurement and Correlation of non-Darcy Flow Coefficient in Consolidated Porous Media. J. Pet. Sci. Eng. 3. https://doi.org/10.1016/0920-4105(89)90030-2

Torabi, Mohsen, Karimi, N., Peterson, G.P., Yee, S., 2017a. Challenges and Progress on The Modelling of Entropy Generation in Porous Media: A Review. Int. J. Heat Mass Transf. 114, 31–46. https://doi.org/10.1016/j.ijheatmasstransfer.2017.06.021

Torabi, M., Karimi, N., Zhang, K., 2015a. Heat Transfer and Second law Analyses of Forced Convection in a Channel Partially Filled by Porous Media and Featuring Internal Heat Sources. Energy 93, 106–127. https://doi.org/10.1016/j.energy.2015.09.010

Torabi, Mohsen, Zhang, K., Karimi, N., Peterson, G.P., 2016. Entropy Generation in Thermal Systems with Solid Structures – A Concise Review. Int. J. Heat Mass Transf. 97, 917–931. https://doi.org/10.1016/j.ijheatmasstransfer.2016.03.007

Torabi, M., Zhang, K., Mahmud, S., 2015b. Temperature and Entropy Generation Analyses Between and Inside Rotating Cylinders Using Copper–Water Nanofluid. J. Heat Transfer 137, 051701. https://doi.org/10.1115/1.4029596

Torabi, Mohsen, Zhang, Z., Peterson, G.P., 2017b. Interface Entropy Generation in Micro Porous Channels with Velocity Slip and Temperature Jump. Appl. Therm. Eng. 111, 684–693. https://ddoi.org/10.1016/j.applthermaleng.2016.09.148

Torabi, Mehrdad, Peterson, G.P., Torabi, Mohsen, Karimi, N., 2016. A Thermodynamic Analysis of Forced Convection Through Porous Media using Pore ScaleModeling. Int. J. Heat Mass Transf. 99, 303–316. https://doi.org/10.1016/j.ijheatmasstransfer.2016.03.127

Torabi, Mehrdad, Torabi, Mohsen, Peterson, G.P., 2017. Heat Transfer and Entropy Generation Analyses of Forced Convection Through Porous Media Using Pore Scale Modeling. J. Heat Transfer 139, 012601. https://doi.org/10.1115/1.4034181

Torabzadeh, S.J., Handy, L.L., 1984. The Effect of Temperature and Interfacial Tension on Water/Oil Relative Permeabilities of Consolidated Sands. SPE Enhanc. Oil Recover. Symp. 15-18 April. Tulsa, Oklahoma. https://doi.org/10.2118/12689-MS

Vafai, K., 2015. Handbook of Porous Media. CRC Press, Boca Raton.

Van Genuchten, M.T.A., 1980. A Closed Form Equation for Predicting The Hydraulic Conductivity of Unsaturated Soils. Soil Sci. Soc. Am. J. 44, 892–898. https://doi.org/10.2136/sssaj1980.03615995004400050002x

Van Spronsen, E., 1982. Three-phase relative permeability measurements using the centrifuge method. SPE Enhanc. Oil Recover. Symp. 0. https://doi.org/10.2118/10688-MS

Vergelati, C., Perwuelz, A., Vovelle, L., Romero, M.A., Holl, Y., 1994. Poly (ethylene terephthalate) surface dynamics in air and water studied by tensiometry and molecular modelling. Polymer (Guildf). 35, 62–270. https://doi.org/10.1016/0032-3861(94)90689-0

Versluys, J., 1934. Energy Relationships in the Oil Bearing Formation. Oil Wkly. 38–46.

Wang, C., Liu, M., Zhao, Y., Qiao, Y., Yan, J., 2018. Entropy Generation Analysis on a Heat Exchanger with Different Design and Operation Factors During Transient Processes. Energy 158, 330–342. https://doi.org/10.1016/j.energy.2018.06.016

Wang, F.H.L., 1988. Effect of Wettability Alteration on Water-Oil Relative Permeability, Dispersion, and Flowable Saturation in Porous Media. SPE Reserv. Eng. 3. https://doi.org/10.2118/15019-PA

Wang, X., Alvarado, V., 2016a. Analysis of capillary pressure and relative permeability hysteresis under low-salinity waterflooding conditions. Fuel 180, 228–243. https://doi.org/10.1016/j.fuel.2016.04.039

Wang, X., Alvarado, V., 2016b. Effects of Low-Salinity Waterflooding on Capillary Pressure Hysteresis. SPE Improv. Oil Recover. Conf. 1–16. http://doi.org/10.2118/179562-MS

Wardlaw, N.C.., Taylor, R.P., 1976. Mercury capillary pressure curves and the interpretation of pore-structure and capillary behavior in reservoir rocks. Bull. Can. Pet. Geol. 24, 225–262.

Wark, S.I., Cox, A.B., 1932. Principles of Flotation: an Experimental Study of the Effect of Xanthates on Contact Angles at Mineral Surfaces, American Institute of Mining & Metallurgical Engineers. American Institute of Mining & Metallurgical Engineers.

Warpinski, N.R., Teufel, L.W., 1992. Determination of the effective-stress law for permeability and deformation in low-permeability rocks. SPE Form. Eval. 7. https://doi.org/10.2118/20572-PA

Washburn, E.W., 1921. The dynamics of capillary flow. Phys. Rev. 17, 273–283. https://doi.org/10.1103/PhysRev.17.273

Wilhelmy, L., 1863. Ueber die Abhängigkeit der Capillaritäts-Constanten des Alkohols von Substanz und Gestalt des benetzten festen Körpers. Ann. Phys. 195, 177–217. https://doi.org/10.1002/andp.18631950602

Witherspoon, P.A., Wang, J.S.Y., Iwai, K., Gale, J.E., 1980. Validity of Cubic Law for fluid flow in a deformable rock fracture. Water Resour. Res. 16, 1016–1024. https://doi.org/10.1029/WR016i006p01016

Wunderlich, R.W., 1985. Imaging of Wetting and Nonwetting Phase Distributions: Application to Centrifuge Capillary Pressure Measurements. Soc. Pet. Eng. https://doi.org/10.2118/14422-MS

Wunnik;, J.N.M. van, Oedai;, S., Masalmeh, S., 1999. Capillary Pressure Probe For Scal Applications. SCA9908, USA.

Xuan, Y., Roetzel, W., 2000. Conceptions for heat transfer correlation of nanofluids. Int. J. Heat Mass Transf. 43, 3701–3707. https://doi.org/10.1016/S0017-9310(99)00369-5

Yuan, Y., Lee, T.R., 2013. Contact Angle and Wetting Properties. Surf. Sci. Tech. 3–34. https://doi.org/10.1007/978-3-642-34243-1_1

Zhang, H., Falcone, G., Teodoriu, C., 2010. Relative permeability hysteresis effects in the near-wellbore region during liquid loading in gas wells. SPE Lat. Am. Caribb. Pet. Eng. Conf. Proc. 2.

Zhang, W., Wahlgren, M., Sivik, B., 1989. Membrane Characterization by the Contact Angle Technique: II. Characterization of UF-Membranes and Comparison between the Captive Bubble and Sessile Drop as Methods to obtain Water Contact Angles. Desalination 72, 263–273. https://doi.org/10.1016/0011-9164(89)80011-6

Zisman, W.A., 1968. The Solid/Liquid Interface—An Essential and Active Frontier of Science. Adv. Chem. 87, 1–9. https://doi.org/10.1021/ba-1968-0087.ch001

Zisman, W.A., 1964. Relation of the Equilibrium Contact Angle to Liquid and Solid Constitution. Am. Chem. Soc. Publ. 43, 1–51. https://doi.org/10.1021/ba-1964-0043.ch001

Zografi, G., Tam, S.S., 1976. Wettability of pharmaceutical solids: estimates of solid surface polarity. J. Pharm. Sci. 65, 1145–1149. https://doi.org/10.1002/jps.2600650805

Appendices

Appendix A: MATLAB Computer Program

In this appendix, a brief description of the MATLAB code to solve the equations and models is presented. The program contains the following major components: main file and functions. The main file has the general and main commands, and it also can contain more than one function. For the sake of brevity, the function, which contains operations on the variable within the function workplace, is created separately and then called in the main file.

Single-zone reservoir model code

Main file

```
clc
clear
close all
format long
mu=0.013E-3;  % Gas Viscosity
k=5E-15;      % Gas Permeability
h=7.32;       % Formation Thickness
beta=2.031e3; % Non-Darcy Coefficient
Mw=0.021725;  % molecular Weight
R=8.314;      % Universal Gas Constant
SG=0.75;      % Specific Gravity
re=914.14;    % Reservoir Radius
s=[5 0 -5];   % Skin Factor
g=9.81;       % Gravity
H=1524;       % Well Depth
Phi=0.15;     % Porosity
Sw=0.2;       % Water Saturation
D=0.0508;     % Diameter
T=390;        % Reservoir Temperature
N=5.17E8;     % Original Gas in Place

delta_l=10;
```

```
L=1:delta_l:H;

Pe=2.76e7;     % Initial Reservoir Pressure
Pwhf=1.38e7;   % Bottom Hole Pressure

%%%%%%%%%%%%%%%%%%%%%%%%%%%%%%%%%%%%%%%%%%%%%%%%%%%%%%%%%%%%%%%%%%%%%%%

P_hat=Pwhf:300000:Pe;
qsc=[0.01 0.1 1];
a=0;
LLL=2438.4;    % Wellbore Length
X=[];
ST=[];
RF=[];
for kk=1:length(s)
rw=0.0508*exp(-s(kk));

delta_r=0.001;
r=rw:delta_r:re;

P_difference=[];
t=[];
P_avgi=[];
P_avgf=[];


t0=149616.9792; tpss=t0=1200*Phi*mu*Ct*re^2/k (in Field
Units)

for j=1:length(qsc)
    I=[];
    PP=[];

for n=1:length(P_hat)
    PPP=[];

PPP=Pwelli(P_hat(n),qsc(j),T,SG,R,delta_l,D,H,g,L,LLL);



PP(n,:)=Preservoiri(PPP(end),qsc(j),T,R,SG,mu,k,h,re,beta,
r);

    if (PP(n,end)>Pe)
```

```
        PP(n,:)=[];

        break;

    end

    I(n)=Calculate_I(re,r,PP(n,:));

figure(j^2+kk)
subplot(1,2,1)
plot(L,PPP,'r-','MarkerSize',1,'LineWidth',0.1);
title('Well','FontSize',10,'FontWeight','bold')
xlabel('Depth (m)','FontSize',10,'FontWeight','bold')
xlim([0 H])
ylabel('Pressure, Pa','FontSize',10,'FontWeight','bold')
ylim([1.38e7 2.8e7])
grid on
hold on
subplot(1,2,2)
plot(r,PP,'r-','MarkerSize',1,'LineWidth',0.1);

title('Reservoir','FontSize',10,'FontWeight','bold')
        xlabel('Raduis
(m)','FontSize',10,'FontWeight','bold')
ylim([1e7 3e7])
        ylabel('Pressure,
Pa','FontSize',10,'FontWeight','bold')
xlim([rw re])
grid on
hold on
plot(r,I(n)*ones(1,length(r)),'LineWidth',0.1)
hold on
legend('Pressure Distribution','Average Pressure')

P_avgi(j)=I(end);
P_avgf(j)=I(1);
delta_P=100000;
P=P_avgf(j):delta_P:P_avgi(j);
P_difference(j)=P_avgi(j)-P_avgf(j);

%%%%%%%%%%%%%%%%%%%%%%%%%%%%%%%%%%%%%%%%%%%%%%%%%%%%%%%%%%%%%%%%%%%%%%%%

 Ct=[];
 z=[];
```

```
 dzdp=[];
 rau=[];
 rausc=[];
 X=[];
for i=1:length(P)

    z(i)=equationz(P(i));
    B_g(i,j)=350.958*T*z(i)/P(i);
    dzdp(i)=dz(P(i));
    Ct(i)=1/P(i)-(1/z(i))*dzdp(i);
    rau(i)=P(i)*(0.02897*SG)/(z(i)*R*T);
    rausc(i)=rau(i)*B_g(i,j);


X(i)=((EntropyTotal(P(i),qsc(j),LLL,h,H,D,T,B_g(i,j),rausc
(i),P_difference(j),rau(i),beta,Phi,Sw,re,delta_l,r,rw)*Ph
i*Ct(i))/B_g(i,j));
end

t(j)=t0+(pi*re^2*h/qsc(j))*delta_P*sum(Phi.*Ct./B_g(find(B
_g(:,j),1,'last'),j));


ST(j,kk)=((pi*re^2*h)/qsc(j))*sum(X)*delta_P;
RF(j,kk)=((t(j))*qsc(j)/N);

end
end

figure(2)
    plot(ST(:,kk),RF(:,kk),'LineWidth',1)
    hold on
    set(gca, 'XScale', 'log')
    title('RF vs ST','FontSize',10,'FontWeight','bold')
        xlabel('Cumulative Entropy Production
(J/K)','FontSize',10,'FontWeight','bold')
%         xlim([0 H])
        ylabel('Recovery
Factor','FontSize',10,'FontWeight','bold')
        ylim([0 1])
        grid on
end
legend('Civans work s=Positive','Civans work s=0','Civans
work s=Negative')
```

Functions

Reservoir Pressure Profile

```
function [PP] =
Preservoiri(PPP,qsc,T,R,SG,mu,k,h,re,beta,r)
z=[];
B_g=[];
rau=[];
rausc=[];
PP=[];
for i=1:length(r)-1
    delta_r=r(i+1)-r(i);
    z(i)=equationz(PPP);
    B_g(i)=350.958*T*z(i)/PPP;
    rau(i)=0.02897*PPP*SG/(z(i)*R*T);
    rausc(i)=B_g(i)*rau(i);
    PP(i)=PPP;

    PPP=PPP+delta_r*B_g(i)*((mu/k)*(qsc/(2*pi*h))*(1/r(i)-
(r(i)/re^2))+(beta*B_g(i)*rausc(i)*(qsc/(2*pi*h))^2*(1/r(i
)-(r(i)/re^2))^2));
end
end
```

Wellbore Pressure profile

```
function [PPP] = Pwelli(P,qsc,T,SG,R,delta_l,D,H,g,L,LLL)

for i=1:length(L)

    z(i)=equationz(P);
    B_g(i)=350.958*T*z(i)/P;
    rau(i)=0.02897*P*SG/(z(i)*R*T);
    rausc(i)=B_g(i)*rau(i);
    v(i)=(4*qsc*B_g(i))/(pi*D^2);
    fM(i)=(D*P_delta)/(0.5*L(i)*rau(i)*v(i)^2);
    PPP(i)=P;
Y=delta_l*((rausc(i)/B_g(i))*(g*H/(LLL)+(fM/(2*D))*(qsc/(p
i*D/4))^2*B_g(i)^2));

    P=P+Y;

end
end
```

Wellbore Entropy Generation Minimization

```
function [dStdtw] =
EntropyWell(rausc,rau,H,P,B_g,D,T,P_difference,LLL,qsc,del
ta_l)

LL=linspace(0.1,LLL,100);
fM=[];
v=(qsc*B_g)/((pi*D^2)/4);
for i=1:length(LL)
    fM(i)=(D*P_difference)/(0.5*LL(i)*rau*v^2);

dStdt(i)=((rausc*fM(i)/(2*D*T*B_g))*(qsc*B_g/((pi*D^2)/4))
^3)*delta_l;
end

    dStdtw=sum(dStdt);

end
```

Total Entropy Generation Minimization

```
function [dStdtT] =
EntropyTotal(P,qsc,LLL,h,H,D,T,B_g,rausc,P_difference,rau,
beta,Phi,Sw,re,delta_l,r,rw)

dStdt=[];
u=[];
delta_r=0.001;
r=0.0508:delta_r:re;

for i=1:length(r)

    u(i)=((1-(r(i)/re)^2)*qsc*B_g)/(2*pi*r(i)*h);
    fP(i)=(1/(beta*rau*u(i)^2))*(P_difference/L);
    dStdt(i)=delta_r*(2*pi*h)*(rausc*fP*beta/(Phi*(1-
Sw)*T*B_g)*(((1-
(r(i)/re)^2)*qsc*B_g)/(2*pi*r(i)*h))^3)*r(i);

end
dStdtr=sum(dStdt);

dStdtT=dStdtr+EntropyWell(rausc,rau,H,P,B_g,D,T,P_differen
ce,LLL,qsc,delta_l);
end
```

Appendix B: Computer Modeling Group (CMG) Code

The CMG is a reservoir simulation software tool for oil and gas systems with three reservoir simulation applications: IMEX, GEM, and STARTS. As the GEM deals with compositions and equations of state, it is used in this study for a single-phase case.

Many models are developed using the GEM-CMG application to investigate all the scenarios that are possible. However, in this appendix, the default GEM-CMG model that was developed using the same data as used in MATLAB models is used for the purpose of validation and attached below.

```
** 2019-08-08, 11:42:10 AM, student
RESULTS SIMULATOR GEM 201610

INUNIT FIELD
WSRF WELL 1
WSRF GRID TIME
OUTSRF GRID SO SG SW PRES
OUTSRF RES NONE
WPRN GRID 0
OUTPRN GRID NONE
OUTPRN RES NONE

**  Distance units: ft
RESULTS XOFFSET         0.0000
RESULTS YOFFSET         0.0000

**  (DEGREES)
**  (DEGREES)
RESULTS ROTATION         0.0000  **  (DEGREES)
RESULTS AXES-DIRECTIONS 1.0 -1.0 1.0

**
**********************************************************************
*****
** Definition of fundamental cylindrical grid
```

```
**
**********************************************************************
*****
GRID RADIAL 10 3 6 *RW        0.25
KDIR DOWN
DI IVAR        0.389526       0.996448        2.54902        6.52065
       16.6805        42.6704        109.155        279.231        714.301
       1827.26
DJ JVAR            120            120            120
DK ALL
 180*24
DTOP
 30*5000
PERMI CON           5
**  0 = null block, 1 = active block
NULL CON           1
NETPAY CON           4
POR CON        0.15
PERMJ CON           5
PERMK CON         2.5
**  0 = pinched block, 1 = active block
PINCHOUTARRAY CON           1
CPOR .0000003
** new GEM requires END-GRID line for CTPOR/CPTPOR/TPPOR.
*END-GRID
CTPOR .005
CPTPOR .001
TRPOR 203
**The following is the fluid component
**property data in GEM format.
**The unit system and fluid compositions should
**be specified in the I/O control section.
**The units and compositions specified in WinProp
**are included here as comments for informational purposes.
** PVT UNITS CONSISTENT WITH *INUNIT *FIELD
**COMPOSITION *PRIMARY
**         0.0000000E+00  0.0000000E+00  0.0000000E+00  9.8000000E-01
**         1.5000000E-02  5.0000000E-03
**COMPOSITION *SECOND
**         0.0000000E+00  0.0000000E+00  0.0000000E+00  0.0000000E+00
**         0.0000000E+00  0.0000000E+00
** Model and number of components
MODEL PR
NC 6 6
```

```
COMPNAME 'N2' 'H2S' 'CO2' 'CH4' 'C2H6' 'C3H8'
TRES 203.5
VISCOR HZYT
MIXVC 1.0000000E+00
MW
2.8013000E+01  3.4080000E+01  4.4010000E+01  1.6043000E+01  3.0070000E+01
4.4097000E+01
AC
0.04 0.1 0.225 0.008 0.098 0.152
PCRIT
3.3500000E+01  8.8200000E+01  7.2800000E+01  4.5400000E+01  4.8200000E+01
4.1900000E+01
VCRIT
8.9500000E-02   9.8500000E-02   9.4000000E-02   9.9000000E-02   1.4800000E-01
2.0300000E-01
TCRIT
1.2620000E+02  3.7320000E+02  3.0420000E+02  1.9060000E+02  3.0540000E+02
3.6980000E+02
PCHOR
41 80.1 78 77 108 150.3
SG
0.809 0.801 0.818 0.3 0.356 0.507
TB
-320.35 -76.63 -109.21 -258.61 -127.57 -43.69
OMEGA
0.457236 0.457236 0.457236 0.457236 0.457236 0.457236
OMEGB
0.0777961 0.0777961 0.0777961 0.0777961 0.0777961 0.0777961
VSHIFT
0 0 0 0 0 0
VISVC
8.9500000E-02   9.8500000E-02   9.4000000E-02   9.9000000E-02   1.4800000E-01
2.0300000E-01
BIN
1.3000000E-01
0.0000000E+00 1.3500000E-01
2.5000000E-02 7.0000000E-02 1.0500000E-01
1.0000000E-02 8.5000000E-02 1.3000000E-01 2.6890022E-03
9.0000000E-02 8.0000000E-02 1.2500000E-01 8.5370405E-03 1.6620489E-03

ENTHCOEF
-6.5665000E-01  2.5409800E-01  -1.6624000E-05  1.5302000E-08  -3.0995000E-12
1.5167000E-16
```

```
-2.3279000E-01   2.3744800E-01   -2.3234000E-05   3.8812000E-08   -1.1328700E-11
1.1484100E-15
9.6880000E-02   1.5884300E-01   -3.3712000E-05   1.4810500E-07   -9.6620300E-11
2.0738320E-14
-2.8385700E+00   5.3828500E-01   -2.1140900E-04   3.3927600E-07   -1.1643220E-10
1.3896120E-14
-1.4220000E-02   2.6461200E-01   -2.4568000E-05   2.9140200E-07   -1.2810330E-10
1.8134820E-14
6.8715000E-01   1.6030400E-01   1.2608400E-04   1.8143000E-07   -9.1891300E-11
1.3548500E-14

HCFLAG
0 0 0 0 0 0
ROCKFLUID
RPT 1
**       Sg      krg     krog
**$       Sl      krg     krog
SLT
       0.21    0.784      0.0
       0.32    0.448     0.01
        0.4    0.288    0.024
      0.472    0.184    0.052
       0.58    0.086    0.152
       0.68    0.024    0.272
      0.832    0.006    0.448
      0.872      0.0      0.9
INITIAL

USER_INPUT
PRES CON        4000
SW CON         0.2
ZGLOBALC 'N2' CON          0
ZGLOBALC 'H2S' CON          0
ZGLOBALC 'CO2' CON          0
ZGLOBALC 'CH4' CON       0.98
ZGLOBALC 'C3H8' CON      0.005
ZGLOBALC 'C2H6' CON      0.015
NUMERICAL
NORM SATUR 0.015
NORM GMOLAR 0.015
NORM AQUEOUS 0.015
NEWTONCYC 30
RUN
DATE 1901 1  1.00000
```

```
**
**
WELL  'Well-1'
PRODUCER 'Well-1'
OPERATE  MAX  STG  3050000.0  CONT
OPERATE  MIN  BHP  2000.0  CONT
**         rad  geofac  wfrac  skin
GEOMETRY  K  0.167  0.37  1.0  0.0
     PERF      GEOA  'Well-1'
** UBA            ff         Status  Connection
   1 1 1         1.0  OPEN    FLOW-TO  'SURFACE'  REFLAYER
   1 1 2         1.0  OPEN    FLOW-TO  1
   1 1 3         1.0  OPEN    FLOW-TO  2
   1 1 4         1.0  OPEN    FLOW-TO  3
   1 1 5         1.0  OPEN    FLOW-TO  4
   1 1 6         1.0  OPEN    FLOW-TO  5
DATE 1901 2  1.00000
DATE 1970 1  1.00000

RESULTS SPEC 'Permeability I'
RESULTS SPEC SPECNOTCALCVAL -99999
RESULTS SPEC REGION 'All Layers (Whole Grid)'
RESULTS SPEC REGIONTYPE 'REGION_WHOLEGRID'
RESULTS SPEC LAYERNUMB 0
RESULTS SPEC PORTYPE 1
RESULTS SPEC CON 5
RESULTS SPEC SPECKEEPMOD 'YES'
RESULTS SPEC STOP


RESULTS SPEC 'Net Pay'
RESULTS SPEC SPECNOTCALCVAL -99999
RESULTS SPEC REGION 'All Layers (Whole Grid)'
RESULTS SPEC REGIONTYPE 'REGION_WHOLEGRID'
RESULTS SPEC LAYERNUMB 0
RESULTS SPEC PORTYPE 1
RESULTS SPEC CON 4
RESULTS SPEC SPECKEEPMOD 'YES'
RESULTS SPEC STOP


RESULTS SPEC 'Permeability K'
RESULTS SPEC SPECNOTCALCVAL -99999
RESULTS SPEC REGION 'All Layers (Whole Grid)'
```

```
RESULTS SPEC REGIONTYPE 'REGION_WHOLEGRID'
RESULTS SPEC LAYERNUMB 0
RESULTS SPEC PORTYPE 1
RESULTS SPEC CON 2.5
RESULTS SPEC SPECKEEPMOD 'YES'
RESULTS SPEC STOP


RESULTS SPEC 'Permeability J'
RESULTS SPEC SPECNOTCALCVAL -99999
RESULTS SPEC REGION 'All Layers (Whole Grid)'
RESULTS SPEC REGIONTYPE 'REGION_WHOLEGRID'
RESULTS SPEC LAYERNUMB 0
RESULTS SPEC PORTYPE 1
RESULTS SPEC CON 5
RESULTS SPEC SPECKEEPMOD 'YES'
RESULTS SPEC STOP


RESULTS SPEC 'Porosity'
RESULTS SPEC SPECNOTCALCVAL -99999
RESULTS SPEC REGION 'All Layers (Whole Grid)'
RESULTS SPEC REGIONTYPE 'REGION_WHOLEGRID'
RESULTS SPEC LAYERNUMB 0
RESULTS SPEC PORTYPE 1
RESULTS SPEC CON 0.15
RESULTS SPEC SPECKEEPMOD 'YES'
RESULTS SPEC STOP


RESULTS SPEC 'Pressure'
RESULTS SPEC SPECNOTCALCVAL -99999
RESULTS SPEC REGION 'All Layers (Whole Grid)'
RESULTS SPEC REGIONTYPE 'REGION_WHOLEGRID'
RESULTS SPEC LAYERNUMB 0
RESULTS SPEC PORTYPE 1
RESULTS SPEC CON 4000
RESULTS SPEC SPECKEEPMOD 'YES'
RESULTS SPEC STOP


RESULTS SPEC 'Water Saturation'
RESULTS SPEC SPECNOTCALCVAL -99999
RESULTS SPEC REGION 'All Layers (Whole Grid)'
```

```
RESULTS SPEC REGIONTYPE 'REGION_WHOLEGRID'
RESULTS SPEC LAYERNUMB 0
RESULTS SPEC PORTYPE 1
RESULTS SPEC CON 0.2
RESULTS SPEC SPECKEEPMOD 'YES'
RESULTS SPEC STOP


RESULTS SPEC 'Global Composition$C' 'C2H6'
RESULTS SPEC SPECNOTCALCVAL -99999
RESULTS SPEC REGION 'All Layers (Whole Grid)'
RESULTS SPEC REGIONTYPE 'REGION_WHOLEGRID'
RESULTS SPEC LAYERNUMB 0
RESULTS SPEC PORTYPE 1
RESULTS SPEC CON 0.015
RESULTS SPEC SPECKEEPMOD 'YES'
RESULTS SPEC STOP


RESULTS SPEC 'Global Composition$C' 'CH4'
RESULTS SPEC SPECNOTCALCVAL -99999
RESULTS SPEC REGION 'All Layers (Whole Grid)'
RESULTS SPEC REGIONTYPE 'REGION_WHOLEGRID'
RESULTS SPEC LAYERNUMB 0
RESULTS SPEC PORTYPE 1
RESULTS SPEC CON 0.98
RESULTS SPEC SPECKEEPMOD 'YES'
RESULTS SPEC STOP


RESULTS SPEC 'Grid Thickness'
RESULTS SPEC SPECNOTCALCVAL -99999
RESULTS SPEC REGION 'All Layers (Whole Grid)'
RESULTS SPEC REGIONTYPE 'REGION_WHOLEGRID'
RESULTS SPEC LAYERNUMB 0
RESULTS SPEC PORTYPE 1
RESULTS SPEC CON 24
RESULTS SPEC SPECKEEPMOD 'YES'
RESULTS SPEC STOP


RESULTS SPEC 'Global Composition$C' 'CO2'
RESULTS SPEC SPECNOTCALCVAL -99999
RESULTS SPEC REGION 'All Layers (Whole Grid)'
```

```
RESULTS SPEC REGIONTYPE 'REGION_WHOLEGRID'
RESULTS SPEC LAYERNUMB 0
RESULTS SPEC PORTYPE 1
RESULTS SPEC CON 0
RESULTS SPEC SPECKEEPMOD 'YES'
RESULTS SPEC STOP


RESULTS SPEC 'Global Composition$C' 'C3H8'
RESULTS SPEC SPECNOTCALCVAL -99999
RESULTS SPEC REGION 'All Layers (Whole Grid)'
RESULTS SPEC REGIONTYPE 'REGION_WHOLEGRID'
RESULTS SPEC LAYERNUMB 0
RESULTS SPEC PORTYPE 1
RESULTS SPEC CON 0.005
RESULTS SPEC SPECKEEPMOD 'YES'
RESULTS SPEC STOP


RESULTS SPEC 'Global Composition$C' 'N2'
RESULTS SPEC SPECNOTCALCVAL -99999
RESULTS SPEC REGION 'All Layers (Whole Grid)'
RESULTS SPEC REGIONTYPE 'REGION_WHOLEGRID'
RESULTS SPEC LAYERNUMB 0
RESULTS SPEC PORTYPE 1
RESULTS SPEC CON 0
RESULTS SPEC SPECKEEPMOD 'YES'
RESULTS SPEC STOP


RESULTS SPEC 'Global Composition$C' 'H2S'
RESULTS SPEC SPECNOTCALCVAL -99999
RESULTS SPEC REGION 'All Layers (Whole Grid)'
RESULTS SPEC REGIONTYPE 'REGION_WHOLEGRID'
RESULTS SPEC LAYERNUMB 0
RESULTS SPEC PORTYPE 1
RESULTS SPEC CON 0
RESULTS SPEC SPECKEEPMOD 'YES'
RESULTS SPEC STOP


RESULTS SPEC 'Grid Top'
RESULTS SPEC SPECNOTCALCVAL -99999
RESULTS SPEC REGION 'Layer 1 - Whole layer'
```

```
RESULTS SPEC REGIONTYPE 'REGION_LAYER'
RESULTS SPEC LAYERNUMB 1
RESULTS SPEC PORTYPE 1
RESULTS SPEC CON 5000
RESULTS SPEC SPECKEEPMOD 'YES'
RESULTS SPEC STOP
```